

The Journal of the Indian Association of Sedimentologists



The Indian Association of Sedimentologists

Volume 38

No. I

Jan - June 2021



Courtesy: G Shanumugam

Sand grain flows on lee side of an aeolian dune, Saudi Arabia

All rights reserved. No part of this publication may be reproduced, distributed, or transmitted in any form or by any means, including photocopying, recording, or other electronic or mechanical methods, without the prior written permission of the publisher, except in the case of brief quotations embodied in critical reviews and certain other non-commercial uses permitted by copyright law. For permission requests, write to the Managing Editor / s.

Editor-in-Chief

Professor Abhijit Basu, Indiana, USA

Associate Editor-in-Chief

Professor D. Rajasekhar Reddy, Vizag

Editorial Board

Dr. Ameer Ghori, Geological Survey of Western Australia

Dr. Armstrong Altrin, National Autonomous University of Mexico

Professor Atul V. Joshi M.S. Baroda University, Vadodara

Dr. Aymon Baud, Zurich Switzerland

Professor B.P. Singh, Banaras Hindu University, Varanasi

Dr. Daniel Le Heron, Vienna University, Austria

Professor Erfan Mondal, Aligarh Muslim University, Aligarh

Professor G. Shanmugam, Arlington Texas, USA

Professor G.N. Nayak, Goa University, Goa

Dr. Guido Meinhold, Keele University, UK

Dr. James Riding, British Geological Survey, UK

Professor Jon Gluyas, Durham, UK

Dr. Jonathan Craig, Eni, Milan, Italy

Professor M. E. Brookfield, University of Massachusetts at Boston, USA

Professor R. Nagendra, Anna University, Chennai

Professor S. J. Sangode, Pune University, Pune

Professor S. K. Pandita, Jammu University, Jammu

Professor Santanu Banerjee, Indian Institute of Technology, Mumbai

Professor Subir Sarkar, Jadavpur University, Kolkata

Professor Zhong Qiang-Chen, China University of Geosciences, Wuhan-China

Managing Editors

Professor G. M. Bhat, Jammu University

Dr. Bashir Ahmad Lone, Jammu University

****** Photograph showing grain avalanches (i.e., grain flows) on the lee side of an aeolian dune. Saudi Arabia. Red scale = 5 cm. Photo by G. Shanmugam. See related article: Shanmugam, G. 2020. Gravity flows: Types, definitions, origins, identification markers, and problems. Journal Indian Association of Sedimentologists, Vol. 37, Issue 2, p. 61-90***

The journal of the Indian Association of Sedimentologists

Managing Editors:
G. M. Bhat
Bashir Ahmad Lone

The Journal of the Indian Association of Sedimentologists (IAS) is both an international open access online journal and print journal and is leader in its field and publishes ground-breaking research from across the spectrum of sedimentology, sedimentary geology, sedimentary geochemistry, experimental and theoretical sediment transport, mass movement fluxes, modern and ancient sedimentary environments, sequence-, cyclo-, chrono- and chemostratigraphy, sediment-biological interaction, palaeosols, diagenesis, stable isotope geochemistry, environmental sedimentology, neotectonics, geohazards, stratigraphy, palynology, sedimentary mineral resources and hydrocarbons, and allied branches of sedimentary - stratigraphic research. It also publishes review articles, editorials, conference reports, tributes, announcements, advertisements, etc. It is currently distributed to universities and research laboratories in India and abroad. Access to the complete electronic journal archive over the past eight years comes free of cost. Subscribers also have the option to buy the printed journal at subsidized cost.



TABLE OF CONTENTS

ARTICLES	AUTHOR	PAGE NO
<i>From The Desk of the Editor-in-Chief</i>	Abhijit Basu	1
<i>Editorial</i>	G M Bhat	2 – 4
<i>Tectonic Setting and Provenance of Eocene Sandstones of Disang Group, Tirap District, Arunachal Pradesh</i>	Bijit Kumar Gogoi, R K Sarmah	5 – 12
<i>Geochemistry, Depositional and Tectonic setting of the Barail Group of the Indo-Myanmar Ranges</i>	Salam Ranjeeta Devi	13 – 22
<i>Petro-mineralogical and geochemical characteristics of Shahaba Limestone from Gogi-Kanchankayi sector, Bhima Basin, Karnataka with reference to Uranium mineralisation</i>	Debasish Roy, Dheeraj Pande, Sikta Patnaik, S K Varughese, A K Pradhan, B Saravanan, A K Bhatt	23 – 32
<i>Facies Evaluation and Depositional Environments of Carbonates of the Bagh Group, Dhar District, Madhya Pradesh, India</i>	Sreejita Chatterjee, Dhiren Kumar Ruidas	33 – 40
<i>Provenance and depositional characteristics of Lathi Formation in southern part of Jaisalmer Basin: Implications for exploration of sandstone type uranium mineralization</i>	Shijo Mathew, Pritam Karmakar, Rajeev Bidwai, S K Sharma, Navin Goyal, D K Sinha	41 – 50
<i>Legal Frame Work for Exploitation of Beach Sand Mineral Resources: Historical Perspective and Action by Government of India for conservation</i>	Rohit Jaiswal	51 – 53
<i>Architecture and Source of Alluvial Fan deposits of the Gish and Lish Rivers, Sikkim-Darjeeling Himalaya, India</i> Ananda Badekar, Uttaran Goswami, Sweta Samant	Ananda Badekar, Uttaran Goswami, Sweta Samant	55 – 64
<i>Sediment Budget and Sediment Trap efficiency of Baglihar Hydroelectric project Reservoir – a calibrated model for prediction of longevity of the Dam</i>	Romesh Kumar, AHSAN UL HAQ, G M Bhat, Yudhbir Singh, Javid Ahmed Dar	65 – 74
<i>Provenance Characterization and Palaeoenvironmental Analysis of the Meta-Sedimentary Rocks of Sonaghati Formation, Betul District, Madhya Pradesh Using Geochemical Approach</i>	Shradha Shukla	75 – 92
<i>Provenance of the Sawa Formation Sandstones, Vindhyan Super Group, Southeast Rajasthan, India</i>	JYOTI MATHUR	93 – 102
<i>On the occurrence of ichnogenera Planolites and Psilonichnus from the Jogira Formation (Lower to Middle Eocene), Bikaner Basin, Western India: Implications on depositional environment</i>	Shyam Narayan Mude, Ravindrasing Pardeshi, Manoj Memane	103 – 108
<i>Facies Architecture and Sedimentary Structures in the drill cores of Uranium Bearing Sediments of</i>	SHEKHAR GUPTA, R V Singh, Rahul Banerjee, M B Verma	109 – 118

<i>Banganapalle Formation of Palnad Sub-basin, Guntur District, Andhra Pradesh</i>		
<i>Investigation on Suitability of Argillaceous Rocks of Vindhyan Super Group as Host Rock for Deep Geological Repository using Thermal Analysis</i>	<i>T.K. Pal, R.K. Bajpai, A. Acharya, R. S. Bhatia, D. Datta</i>	<i>119 – 125</i>
<i>Acknowledgements</i>	<i>Managing Editors, IAS</i>	<i>126</i>

ABHIJIT BASU

Herman B Wells Professor Emeritus
Indiana University, U.S.A



From the desk of the Editor-in-Chief

Labour of love in the year of COVID and beyond, contributed by authors, reviewers, editors, and especially the current Managing Editors has sustained and enhanced this journal. All papers now have a "doi" and Google Scholar is listing them. Many papers are routinely available through ResearchGate. From an editor's perspective, such visibility of the journal is gratifying. We expect that appropriate keywords will also draw additional attention to the papers. The current issue has 13 papers. Their quality reflects the significant efforts and time that the authors, reviewers, and editors have put in.

The first issue of the Journal was published in 1976. Since then, i.e., in the last forty-five years, many transformative papers have adorned its pages. Scope of the papers has evolved with time keeping pace with advances in knowledge and wisdom in sedimentology *sensu lato*. The Journal has caught up with the revolution of electronic publication. The current Managing Editors, with the aid of the Editorial Board, have deftly steered and streamlined the submission, editorial, and publication process in the last 3 years. This is a remarkable feat. The complicated IT process, evolving worldwide, remains blissfully behind the scene while being continually updated. Publishers of the most widely respected journals in science are always on the lookout for improved systems. Our Managing Editors cheerfully shoulder the responsibility of such enhancement. It is time to offer a collective Vote of Thanks to all readers, authors, and editors.

I shall be looking forward to a COVID-free world and to publishing results of your zealous research in the Journal of Indian Association of Sedimentologists.

Abhijit Basu
Editor-in-chief
IAS

Is Nuclear Energy the Answer to India's Growing Energy Needs?

The sustainable development of human societies has invariably depended on energy resources. With the ever increasing population and industrial growth, the demand for energy resources has increased many folds globally. India with its current population of about 1.394 billion is also struggling to fulfill its energy needs and mostly depends upon imports of about 87% of its energy requirements. India being a continent size country with huge potential of land and oceanic natural resources is by and large unexplored. With its 26 mega sedimentary basins having proven and potential natural energy resources, the country is not in a position to meet the domestic energy requirements indigenously. Accordingly to the 'National Geographic' report presently India uses 320 billion kilowatt-hours of energy every day. Most of this energy requirement is met by burning fossil fuels. Although burning of fossil fuels have catered to our energy needs very efficiently, but they are also non-renewable and rapidly depleting on the one hand and are detrimental for climate change and global warming. These fuel sources have immensely contributed to greenhouse gas emissions and pollution. Need of the hour is to find suitable and better replacements for these natural energy resources. India has been constantly researching newer and greener sources of energy which are environment friendly and have less impact global warming. Some of the cleaner and greener energy resources which have potential to cater India's energy demand are atomic energy, solar energy, hydropower, and energy from wind and bio fuels which are promising alternatives to the existing fossil fuels. Other relatively new sources of energy which are being explored include fuel cells, geothermal energy, and ocean energy.

At present fossil fuels account for 86% of the total energy produced in the world of which petroleum accounted for 36.8%, coal 26.6% and natural gas 22.9% (according to the estimates by the Energy Information Administration). Indian energy scenarios also fit well within these estimates which need to be addressed earnestly because our heavy dependence on fossil fuels results in carbon dioxide produced during combustion which amounts to 21.3 billion tons per year. In contrary of producing carbon dioxide, the natural processes are capable of absorbing only about half of the total amount of carbon dioxide emissions released into the atmosphere. Thus every year the amount of carbon dioxide in the atmosphere is increasing by 10.65 billion tons, which is considered as the leading contributor to global warming that potentially impacts very adverse effects on the ecosystem. Natural gas is

another major source of energy in use. It is being considered as cleaner than other fossil fuels, but still been found to contribute to pollution and global warming and it is not fully clean, non-polluting alternative to fossil fuels. According to the estimates made in 2004, carbon dioxide emissions due to the use of natural gas amounted to 5,300 million tons while use of coal and oil contributed to carbon dioxide emissions of 10,600 and 10,200 million tons respectively. It has been estimated that in 2030, natural gas is likely to emit 11,000 million tons of carbon dioxide and 8,400 million tons from coal and 17,200 tons from oil. Natural gas when released directly into the atmosphere is a far more potent greenhouse gas than carbon dioxide. In such a scenario the better option is to concentrate exploring other energy options which are environment friendly and do not impact adversely on global warming and ecosystems. One of such options is to directly tap energy from the Sun which has unlimited source of energy. The earth receives about 174 billion megawatts of power at the upper atmosphere as a result of solar radiation. About 30% of the incident solar radiation is reflected back, while about 3.85×10^{24} Joules every year, is absorbed by the atmosphere, oceans and landmasses. The amount of solar energy available during an hour is more than the total amount of energy consumed worldwide during an entire year. The greatest challenge lies in harnessing this energy because this is a diffused form of energy. Other challenge of harnessing the solar energy is building cost effective solar panels/storage of energy, lacking of which at the moment costs about 3 folds higher as compared to the cost of the coal-based power per kilowatt/hour. Unless we perfect the solar harnessing technology and store solar energy in a viable and cost-effective manner, fossil fuels will continue to dominate the source of energy used and further deteriorate the environments and the ecosystems.

Perhaps a viable solution to the energy crisis of our times lies in nuclear energy even though this kind of energy is also marred by number of challenges. However, with surge in demand for power, nuclear energy is gaining increasing importance as a clean source of power which is also likely to address the global issue of climate change. At present the nuclear power reactors operational in 30 countries around the world account for 14% of the total power generation of the world. The International Atomic Energy Agency (IAEA) expects the global nuclear power generation capacity to increase to 473–748 GW by 2030 from 437–542 GW in 2020. In spite of the fact that nuclear energy gains importance, it faces several challenges in emerging as a reliable and clean source of energy. The important one that needs immediate attention include improvement in economic competitiveness, designing

safe and reliable nuclear power plants, management of disposal of radioactive waste, raising public confidence in nuclear power, and ensuring nuclear non-proliferation and security. In the process of harnessing nuclear energy usually in 'nuclear fission' uranium is used. At the current rates of consumption, the uranium reserves discovered in the Earth's crust can last for about 100 years. As per available research trends, the energy consumption will increase 3 fold during the next 100 years, which means that the available uranium resources will only last for approximately 30 years. The option of reprocessing of used uranium (residue rich in plutonium and left over uranium) can stretch the available uranium resources by a few decades more.

The main source of electricity generation in India is coal, gas, hydroelectricity and wind power. Nuclear power is the fifth important source of energy. As of November 2020, India had 22 nuclear reactors in operation in 7 nuclear power plants, with a total installed capacity of 6,780 MW. Nuclear power produced a total of 35 TWh which formed 3.22% of country's electricity supply in 2017. Seven more reactors were under construction with a combined generation capacity of 4,300 MW. India has small uranium reserves and the country is dependent on uranium imports to fuel its nuclear power plants. Since early 1990s, Russia has been a major supplier of nuclear fuel to India. Due to dwindling domestic uranium reserves, electricity generation from nuclear power plants in India declined by 12.83% from 2006 to 2008. In September 2008, the Nuclear Suppliers Group (NSG) permitted a waiver to India enabling her to sign bilateral deals on civilian nuclear energy technology cooperation with several other countries and import nuclear fuels. Kazakhstan was the largest supplier of uranium to India providing 5,000 tonnes during 2015-19. With concerted efforts by the geoscientists of the country, in March 2011 large deposits of uranium were discovered in the Tummalapalle belt in Andhra Pradesh and in the Bhima basin in Karnataka by the Atomic Minerals Directorate for Exploration and Research (AMD) of India. The Tummalapalle belt uranium reserves is one of the best 20 uranium reserves discoveries of the world. So far 44,000 tonnes of natural uranium have been discovered in the region. The natural uranium deposits of the Bhima basin are better grade of natural uranium ore as compared to the Tummalapalle belt.

On the other hand nuclear fusion could be the solution to the current energy demand. Fusion utilizes hydrogen isotopes, lithium, and boron. The estimated lithium reserves from the earth and the sea can last for more than 60 million years. Deuterium, an isotope of hydrogen, can last another 250 million years. At the moment, the process of harnessing energy from this Deuterium isotope is very complicated and the process

is in its infancy. It is expected that on acquiring knowledge how to utilize nuclear fusion (a clean process with low carbon dioxide emission and relatively short half-life) for the generation of energy in a viable manner, it could solve energy crisis of the world. These discoveries and their exploitation are likely to lessen the import of nuclear fuel and shall increase nuclear power generation in India in the near future. In recent years, India has shown increased interest in thorium fuels and fuel cycles because of large deposits of thorium (518,000 tonnes) in the form of monazite in beach sands as compared to very modest reserves of low-grade uranium (92,000 tonnes). In this direction India has been making advances in the field of thorium-based fuels and is working to design and develop a prototype for an atomic reactor using thorium and low-enriched uranium. This forms a key part of India's three stage nuclear power programme conceived under the fusion power area through the ITER initiative. India has reasonably assured resources of 319,000 tonnes of thorium – about 13% of the world total, and these are intended to fuel its nuclear power program for a longer-term. AMD claims almost 12 million tonnes of monazite which might contain 700,000 tonnes of thorium.

The nuclear fusion could also be part of the solution to the current energy demand. Fusion utilizes hydrogen isotopes, lithium, and boron. The estimated lithium reserves from the earth and the sea can last for more than 60 million years. Deuterium, an isotope of hydrogen, can last another 250 million years. At the moment, the process of harnessing energy from this Deuterium isotope is very complicated and the process is in its infancy. It is expected that on acquiring knowledge how to utilize nuclear fusion (a clean process with low carbon dioxide emission and relatively short half-life) for the generation of energy in a viable manner, it could solve energy crisis of the world. India's dependence on imported energy resources and the inconsistent development of the energy sector are the main challenges to meet the increasing energy demand. The 2019 edition of BP's Energy Outlook projected India's energy consumption increasing by 156% from 2017 and 2040. The report also shows the country's energy mix will evolve slowly by 2040, with fossil fuels consumption reducing from 92% in 2017 to 79% in 2040. In actual terms, primary energy consumption from fossil fuels is expected to increase by 120% during this period.

Early in 2019 India was set to achieve 100% household electricity connection but couldn't achieve the target. The OECD's International Energy Agency projected that India will need some \$1.6 trillion investment in power generation, transmission and distribution by 2035 including 63 GWe target. However, in March 2018, the government stated that

nuclear capacity would fall well short of its 63 GWe target and the total nuclear capacity is likely to be about 22.5 GWe by the year 2031. There are number of reasons to miss the set targets, the major among them appear to be dependence of import of the nuclear fuels and low domestic production.

The most important priority of the government of India is economic growth and to alleviate poverty. This compels the government to generate electricity by burning coal and hydrocarbons. The burning of coal for power generation means that CO₂ emission reduction is not a high priority, and the government declined to set targets ahead of the 21st Conference of the Parties on Climate Change held in Paris in 2015. “The environment minister in September 2014 said it would be 30 years before India would be likely to see a decrease in CO₂ emissions”. The geosciences fraternity of India is whole heartedly making efforts to explore more and more regions/basins of the country for nuclear energy fuels. In their pursuit they have been concentrating on newer and unexplored regions of the country. In their endeavours during the past few years, exploration activities have been concentrated in the following areas with results with fruits:

- Proterozoic Cuddapah Basin, Andhra Pradesh, and Telangana.
- Mesoproterozoic Singhbhum Shear Zone, Jharkhand.
- Mesoproterozoic North Delhi Fold Belt, Rajasthan & Haryana.
- Cretaceous Mahadek Basin, Meghalaya.
- Neoproterozoic Bhima Basin, Karnataka.
- Proterozoic Kaladgi Basin, Karnataka.
- Paleozoic – Mesozoic Satpura Gondwana Basin, Madhya Pradesh.
- Mesoproterozoic Chhotanagpur Granite Gneiss Complex, Uttar Pradesh, Madhya Pradesh, and Jharkhand.
- Cenozoic Siwalik Group, Himachal Pradesh.
- Proterozoic Aravalli Fold belt, Rajasthan.
- Other potential geological domains are under active exploration such as the: Dharmapuri Shear Zone in the Southern Granulite Terrain, Tamil Nadu; basement rocks of the Cuddapah Basin, Andhra Pradesh; Shillong Basin, Assam; basement crystallines, Arunachal Pradesh; Vindhyan and Bijwar basins, Uttar Pradesh and Madhya Pradesh; Kotri-Dongargarh belt, Chhattisgarh.
- Extensive exploration including ground and heliborne geophysical (ZTEM, TDEM, magnetic and radiometric), ground geological, radiometric and geochemical surveys and drilling are planned in other geological domains of the country that have the potential to host uranium.

India's uranium resources are modest, with 183,600 tonnes of uranium as identified resources in situ, 160,000 tU of this as reasonably assured resources in situ and 23,600 tonnes as inferred resources in situ (to \$260/kgU) on January 2015 in the OECD NEA 'Red Book'. In July 2017, 229,499 tU was claimed by the DAE. These are all in a high-cost category, and India expects to import an increasing proportion of its uranium fuel needs. In 2013 it was importing about 40% of uranium requirements. In July 2015 record annual domestic production of 1252 t U₃O₈ (1062 tU) was reported. However, 2015 production was only 385 tU.

Mining and processing of uranium is carried out by Uranium Corporation of India Ltd (UCIL), also a subsidiary of the Department of Atomic Energy (DAE), in Jharkhand near Calcutta. Common mills are near Jaduguda (2500 t/day) and Turamdih (3000 t/day, expanding to 4500 t/day). Jaduguda ore is reported to grade 0.05-0.06%U. All Jharkhand mines are in the Singhbhum shear zone, and all are underground except Banduhurang. Another mill is at Tummalapalle in AP, expanding from 3000 to 4500 t/day. Fracture/fault-controlled uranium mineralisation similar to that in Karnataka in the North Delhi Fold Belt is in the 130 km long Rohil belt in Sikar district in Rajasthan, with 6133 tU identified (March 2014). AMD reports further uranium resources in Chattisgarh state (3380 tU), Himachal Pradesh (665 tU), Maharashtra (300 tU), and Uttar Pradesh (750 tU). In Jharkhand UCIL has a small project to recover uranium from copper tailings, near Hindustan Copper's Rakha and Surda mines.

These above mentioned ongoing and future endeavours of exploration and exploitation of nuclear fuel resources in the country shall improve the nuclear power generation in future. The current issue of the JIAS contains 6 articles on the subject which were presented by the geoscientists of AMD and allied research organisations during the 37th Convention of the Indian Association of sedimentologists at AMD, Hyderabad in November 2019.

G. M. Bhat
University of Jammu, Jammu
bhat@jugaa.com

Tectonic Setting and Provenance of Eocene Sandstones of Disang Group, Tirap District, Arunachal Pradesh

B. K. Gogoi and R. K. Sarmah

Department of Applied Geology, Dibrugarh University, Assam

Abstract

The petrographic study of sandstone belonging to Disang Group of Eocene age shows that quartz and rock fragments are the main constituents among the framework grains. Feldspar percentage is low whereas plagioclase feldspar is dominant with the rare occurrence of K-feldspar. XRF-analysis reveals that SiO₂, Al₂O₃, Fe₂O₃, MnO, TiO₂, Na₂O, K₂O, CaO, MgO and P₂O₅ are the major and minor elements. SiO₂ constitutes the major proportion of the oxides in the sediments. The study reveals that the provenance of these sandstones is mainly the igneous and metamorphic rocks, and the tectonic setting was an active continental margin. The presence of higher content of chert and mafic rock fragments points towards the ophiolite zone as a provenance. Detritus were possibly derived from the uplifted fold thrust belt of the Myanmar's landmass with subordinate contribution from the Mishmi Hills region lying to the northeast of the study area.

Keywords: Disang Group, plagioclase feldspar, ophiolite zone, geochemistry, provenance

Introduction

Disang Group occupies a vast area in the Tissa and Tirap valleys. It is a thick sequence of splintery shales interbedded with sandstone and siltstone, extensively developed from the southern part to Nampong in the northeast. The present study area is confined to a part of the Tissa river section and Deomali-Khonsa road section bounded by

latitude 27°0'N-27°10'N and longitudes 95°20'-95°30' E (Fig.1A & Fig.1B). The Disang Group of rocks outcrop along the Khonsa-Longding and Wakka road sections of Tirap District, Arunachal Pradesh. They continue south westwards into Nagaland where they are subdivided into Lower Disang and Upper Disang formations (Sinha and Chatterjee, 1982). Apart from these, Disang Group

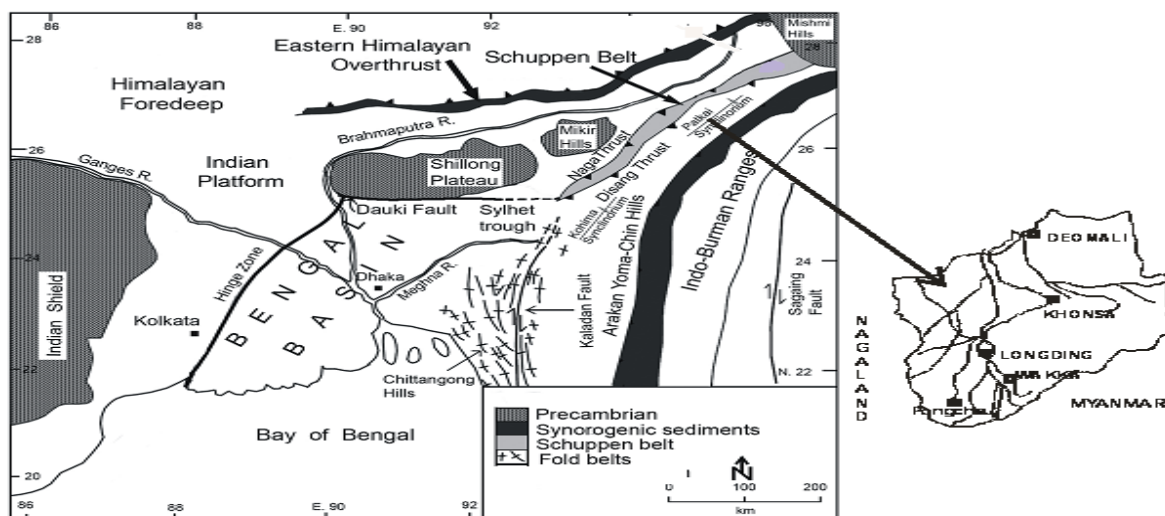


Fig.1A: Map showing the tectonic elements such as the eastern Himalaya and Indo-Burman Ranges. Samples were collected from the south eastern part of Schuppen. (after Hutchison, 1989).

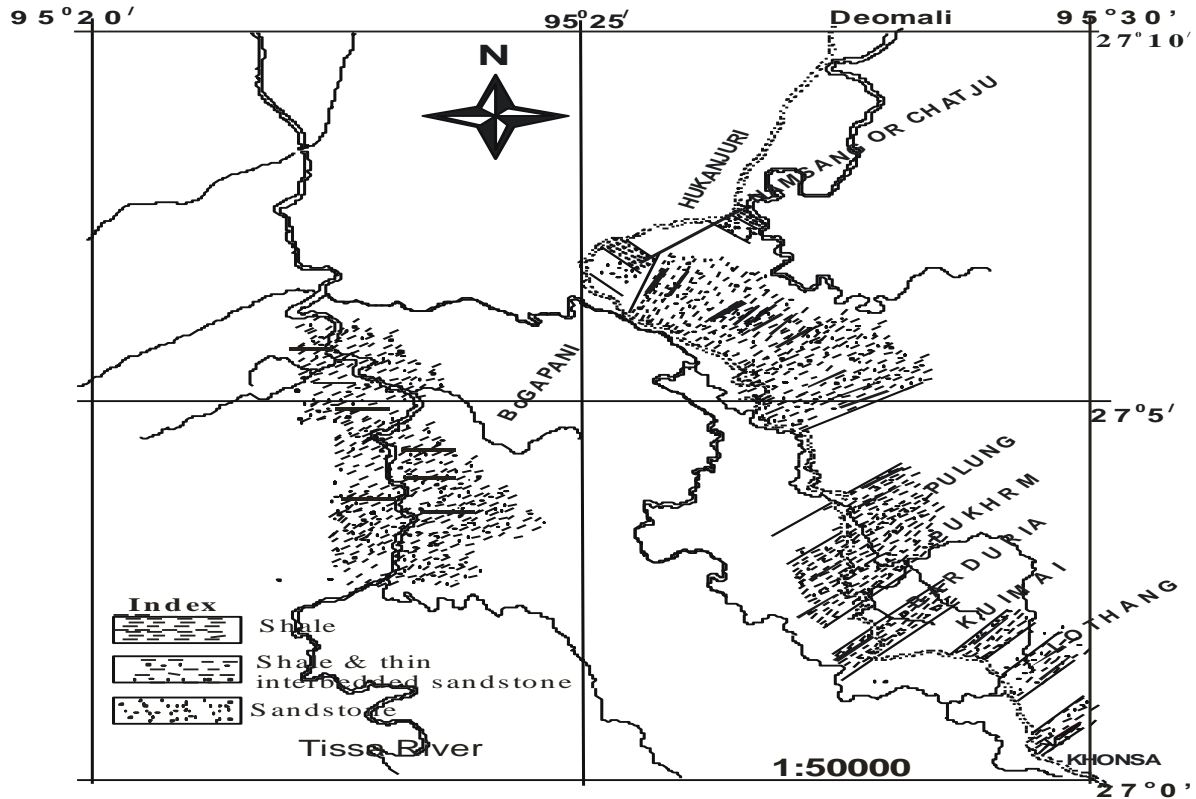


Fig.1B: Location map showing Sampling position in Tissa river section, Tirap District, Arunachal Pradesh

also occupies large areas in Changlang District of Arunachal Pradesh, Nagaland, Manipur states and in a small portion of the North Cachar Hills (Singh et al., 2008; Singh et al., 2017). The Disang Group of rocks exposed in the study area is represented by rhythmic alteration of shale, sandstone and siltstone. The sandstones are fine to medium grained and light grey in colour. The objective of the present study is to infer the provenance and tectonic setting of the sandstones based on petrography and major oxides study.

Geological setup

During the middle Eocene, collision of Indian plate with the Tibetan and central Burmese plates resulted in strong compressional forces from which the Assam-Arakan basin was formed. In this basin, the flysch type of sediments of Disang Group was deposited in a shallow but rapidly sinking basin during the Eocene period (Nandi, 2001). Kumar (2004) reported that the Disang sediments were deposited in deep marine environment close to an arc-trench system during the Eocene. The sub-flysch Barail sediments were accumulated in this basin under the coastal to fluvio-deltaic environmental set-up during Oligocene (Sinha and Chatterjee, 1982). During the Plio-Pleistocene periods due to continuing

thrusting of the Asian and Burmese plates, compressional forces acted from two directions, one from the north and the other from the southeast. As a result of this southeast directional compressional force the development of the Naga-Schuppen belt took place. In the Naga Patkai hill ranges the Tertiary sediments were affected by number of major faults and thrusts which constitute the Schuppen belt. Southwest directional forces from the Mishmi Hills resulted in the development of Mana Bhum anticline and Roing fault against which the block lying to the east was up-thrusted. These forces, possibly, also refolded the structure in the Naga- Patkai ranges from NE-SW to assume NW-SE trend along with the Mishmi thrust. On the basis of structural elements the Naga-Patkai ranges are subdivided into two belts, viz., the Schuppen belt and the Kohima Patkai synclinorium (Mathur and Evans, 1964). The Disang thrust is the dividing line between these two structural belts, the area lying to its southeast forms Patkai Synclinorium, whereas the rocks of the Disang, Barail groups and Post-Barail sediments have been folded into a number of north-easterly plunging folds which swerve to east-west and then to NW-SE trend. Of these folds, Patkai anticline exposes the Disang Group of rocks which occupy a large area of the Tirap and Tissa valleys.

Material and methods

Sandstone samples were collected from outcrops of the Tissa river section and Deomali-Khonsa road section. Major and minor geochemical elements were determined by using Philips PW 1480 sequential X-ray fluorescence spectrometer in Gauhati University, Assam. 1-2g of powdered samples (ASTM 250 mesh) were mixed with 0.5 g of grade E Merck boric acid (H_3BNO_3) and pressed in a steel mould under a pressure of 25 to 30 tons to make a pellet. A known sample of silicate rock was taken for reference. X40 software was used to calculate concentrations of oxides in weight percent. Thin-sections for the petrographic study were prepared in the Department of Dibrugarh University, Assam. Point counting of the sandstone thin sections was used for quantitative compositional analysis. The modal analysis was performed by counting more than 400 points per thin section, using the Gazzi-Dickinson point-counting method (Gazzi, 1966 in Dickinson, 1970). Crystals greater than 0.0625 mm within lithic fragments were counted as monocrystalline grains; this point counting method minimizes compositional dependence on grain size and, therefore, sandstones of different grain sizes can be compared (Ingersoll et al., 1984).

Results and Discussion

Petrography: Petrographic study reveals that sandstones under study are fine to medium grained and are moderately sorted. Framework grains constitute quartz (monocrystalline quartz and polycrystalline quartz), plagioclase feldspar and rock fragments. Among the framework grains, quartz dominates over feldspar and rock fragments. Sedimentary/metasedimentary types are the main rock fragments, followed by metamorphic lithic fragments. Volcanic fragments were identified in two studied thin sections. The feldspar percentage is low with rare potash feldspar. The result of the modal analysis is shown in (Table 1).

Quartz - Quartz is the dominant detrital framework grain in sandstone samples (54.66-66.14%; average 60.21%). Quartz grains are fine to medium grained, angular to subangular and subrounded. Elongate quartz grains are rarely observed. Grain to grain contacts are mainly concavo-convex, long and point. Monocrystalline quartz (Qm) dominate over polycrystalline quartz (Qp). The non-undulatory type monocrystalline quartz (Qnu) is more dominant than the undulatory one (Qu).

Feldspar - Feldspar percentages vary between 0.75-1.90 %, (average 1.21%). Sandstones consist mainly of plagioclase feldspar and with the rare occurrence

of K-feldspar. The grains are sub-angular and sub-rounded in habit and show clear distorted grain boundaries. Some plagioclase feldspars show bending of twin lamellae, which may be the result of the pressure effect.

Rock fragments - The percentage of rock fragments varies between 4.57-8.6 % (average 6.68 %, excluding chert). Rock fragments are mainly sedimentary (Lc) with a subordinate amount of metamorphic rock fragments. Sedimentary rock fragments are mainly chert, shale and siltstone. Metamorphic lithics (Lm) include mainly mica schist and few grains of quartz mica aggregate. Radiolarian chert is also observed in few studied samples.

Matrix - Matrix percentage is ranging from 15.58 to 22.95% (average 18.49%). Matrix occurs as crushed lithic grains, small mosaics of quartz grains, and phyllosilicates (particularly sericite, pseudomatrix) and as epimatrix.

Cement - Cement percentage varies from 6.39 – 9.86% (average 7.65 %). The quartz grains are indurated by mainly argillaceous/carbonaceous cement with a subordinate amount of ferruginous cement.

Mica - Muscovite is more abundant than biotite. Diagenetic mica is also observed within the argillaceous matrix as a layer or lenses with diffused boundaries.

Miscellaneous - Some grains of rutile and tourmaline are observed in the sandstones under the microscope and few reddish coloured altered grains occur in the sandstones which are rather difficult to identify.

Geochemistry: Results of Major and minor elements of sandstones is shown in Table 2. The results show that SiO_2 (64.03-67.89 wt. %) constitute the major portion of the oxides followed by Al_2O_3 (11.21-13.33 wt %) and Fe_2O_3 (6.09- 8.88wt %). The MgO content ranges from 1.32-2.12 wt % whereas, CaO concentrations vary from 0.11-5.08 wt %. The K_2O and Na_2O concentrations range from 1.23-3.48 wt % and 2.26-2.79 wt % respectively. MnO, TiO_2 and P_2O_5 contents are in minor amounts and their concentrations are 0.03-0.42 wt %, 1.08-1.43 wt % and 0.52-0.66 wt % respectively. The range of chemical variations depends on the absolute amount of quartz and the chemically unstable grains. A low concentration of plagioclase is corroborated in the petrographic observation and is supported by the small amount of CaO and Na_2O ; however, K_2O may be derived from mica minerals. TiO_2 values suggest that samples contain opaque minerals. High Al_2O_3 is due to the presence of clays and subordinate micas

and Fe₂O₃ may be derived from the cementing materials present in the samples at the grain boundaries.

Sandstone classification

The sandstones of the Disang Group are classified following Dott (1964) by their matrix content. Modal analysis reveals that the sandstones under study contains a high percentage of matrix (average 18.40%) for which they are classified as lithic-wacke as per Dott's classification (Fig.2) and is supported by the plot of Log Na₂O/K₂O₃ vs Log SiO₂/Al₂O₃ (Fig.3; Pettijohn, 1975). According to Folk's (1974) classification, the modal data plot in the sublitharenite field (Fig.4) while noting that our modal analysis followed the Gazzi-Dikinson method.

Provenance and Tectonic settings

Point counting parameters defined by Dickinson (1985), Ingersol and Suczek (1979) and Dorsey (1988) were considered. The main assumption behind sandstone provenance studies is that different tectonic settings contain characteristic rock types which, when eroded, produce sandstones with specific compositional ranges (Dickinson, 1985). Quartz is the dominant minerals in the present case, where non-undulatory is dominant over undulatory types. Undulatory extinction characterizes quartz derived from metamorphic source rocks; non-undulatory extinction indicates volcanic rocks or grains recycled from older sandstone (Basu, 1985). Polycrystalline grains composed of five or more crystals with straight to slightly curved inter-crystal

Table 1: Results of modal analysis of sandstone of Disang Group, Tirap District

Sample	Qm		Qp		F	Mica	chert	Rock fragments (L=Ls+Lv+Lm)	Matri x	Cement
	Undulatory (Qu)	Non undulatory (Qnu)	2 to 3	>3						
DS-1	6.27	30.47	8.42	9.50	1.08	1.79	5.38	8.60	18.64	9.86
DS-10	7.15	34.98	5.72	14.94	1.75	0.79	3.18	6.04	15.58	9.86
DS-16	5.95	32.92	7.71	9.11	0.88	1.40	6.13	8.06	19.61	8.23
DS-20	8.11	34.32	6.55	13.26	1.09	1.72	3.74	7.96	16.38	6.86
DS-29	7.54	35.79	5.61	12.98	1.40	1.23	4.56	5.79	17.37	7.72
KS-1	6.16	32.65	6.16	11.75	0.93	2.24	3.17	5.78	22.95	8.21
KS-5	8.25	32.99	5.77	11.75	1.44	1.03	3.92	7.63	20.82	6.39
KS-9	7.16	33.99	6.62	12.70	1.25	1.43	3.76	6.98	18.60	7.51
KS-17	7.96	31.65	7.59	13.38	1.63	1.81	3.07	7.41	17.36	8.14
KS-20	9.45	34.93	6.75	14.39	0.75	2.25	2.10	7.20	15.59	6.60
KS-29	7.74	33.23	6.37	15.33	0.91	1.37	3.34	5.31	18.66	7.74
KTL-1	9.50	28.50	6.04	12.44	1.90	1.04	4.32	7.77	21.59	6.91
KTL-5	7.02	30.53	6.67	14.21	0.88	1.75	3.16	8.25	18.95	8.60
KTL-12	8.03	33.86	8.03	16.22	1.26	0.94	2.99	4.57	15.59	8.50
KTL-16	9.55	31.77	6.77	13.89	1.56	1.39	3.99	6.25	17.36	7.47
KTL-25	6.15	30.92	7.54	16.77	0.92	1.23	5.85	6.31	17.85	6.46
KTL-38	7.55	31.56	7.03	14.75	1.54	0.86	4.12	4.97	20.93	6.69
KTL-41	6.17	31.49	7.63	16.40	0.81	1.79	2.92	6.82	19.32	6.66
KTL-54	7.11	31.58	7.97	17.21	1.14	1.42	2.99	5.26	18.21	7.11

Table 2: Major oxides (%) composition of studied sandstone of Disang Group

Sample no	SiO ₂	Al ₂ O ₃	Fe ₂ O ₃	MnO	MgO	CaO	Na ₂ O	K ₂ O	TiO ₂	P ₂ O ₅	LOI
DS-1	65.34	11.45	6.48	0.22	1.67	4.74	2.68	3.48	1.39	0.57	2.21
DS-3	67.89	11.59	6.15	0.16	1.72	5.08	2.61	2.7	1.41	0.52	2.11
DS-10	66.26	12.34	8.88	0.22	1.32	0.11	2.65	2.48	1.2	0.54	4.21
DS-16	64.47	12.1	6.73	0.12	1.81	2.05	2.33	3.15	1.08	0.57	5.62
DS-20	65.64	11.78	6.58	0.22	1.67	1.74	2.34	2.48	1.32	0.61	6.22
DS-29	65.15	11.55	7.15	0.16	1.47	2.18	2.26	3.14	1.43	0.54	5.5
DS-43	66.46	13.33	6.85	0.03	1.31	0.21	2.42	2.48	1.26	0.66	4.81
KS-1	64.03	12.15	7.21	0.21	2.12	2.3	2.34	1.23	1.23	0.64	6.71
KS-5	65.47	11.99	8.43	0.33	1.34	1.25	2.53	1.64	1.35	0.57	5.96
KS-9	64.22	12.12	8.29	0.42	1.61	1.09	2.79	2.12	1.24	0.58	5.87
KS-13	65.23	12.34	7.68	0.32	1.42	0.11	2.45	2.34	1.26	0.59	7.31
KS-20	65.47	11.21	6.09	0.12	1.92	2.21	2.57	2.15	1.17	0.59	6.69

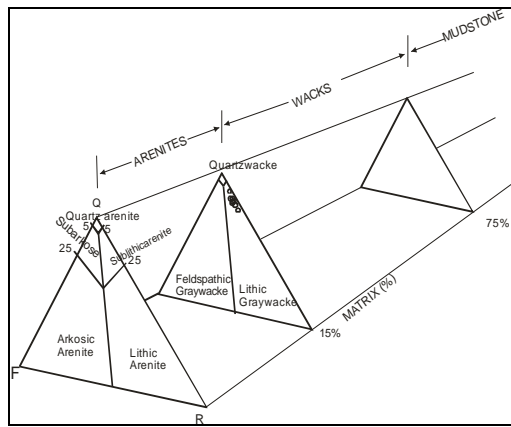


Fig. 2: Sandstone classification of Disang Group (Dott, 1964)

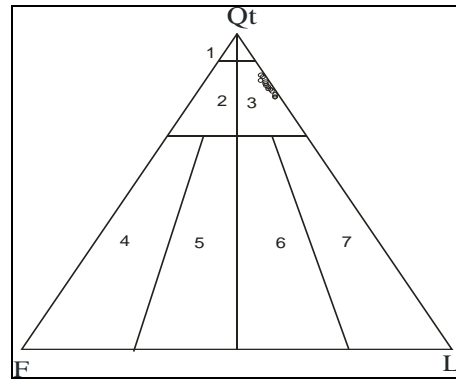


Fig.4: Triangular diagram shows mineralogical classification of the studied sandstone of Disang Group (Folk, 1974). Where, Q: Total quartz; F: Feldspar; L: rock fragments 1. Quartz arenite; 2. Subarkose; 3. Sublitharenite; 4. Arkose; 5. Lithic arkose; 6. Feldspathic litharenite; 7. Litharenite

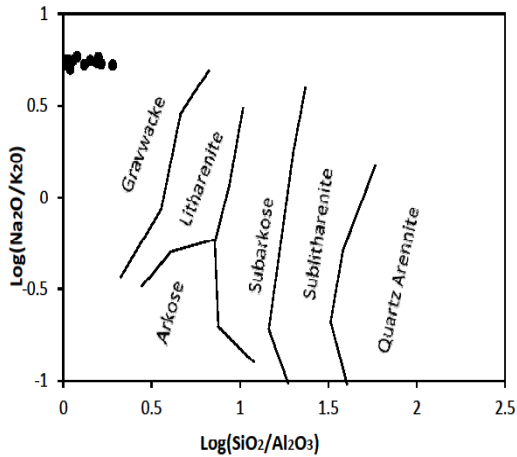


Fig.3: Chemical composition of sandstones plotted on Pettijohn scheme (after Pettijohn, 1975)

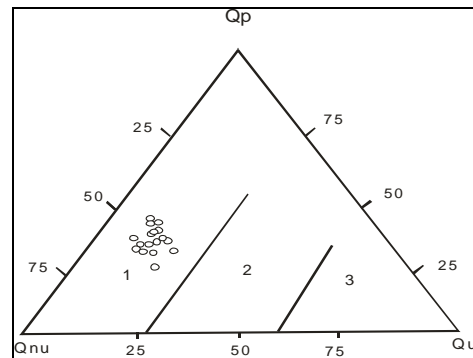


Fig.5: Ternary plot of detrital quartz types of the Disang Sandstone (after Basu et al., 1975). Open circles represent the studied samples; Qp = Quartz polycrystalline; Qnu = Quartz non-undulatory (monocrystalline); Qu=Quartz undulatory (monocrystalline).

boundaries have also been observed which suggests an origin from plutonic igneous rocks (Folk, 1974; Blatt et al., 1980). Plagioclase feldspar is of volcanic or hypabyssal origin (Pittman, 1963). The present investigation shows that the sandstones are abundant in quartz and, sedimentary and metasedimentary lithic fragment. This type of mixed character of lithic fragments is generally found in recycled orogenic sources. Source regions of recycled orogens are created by upfolding or upfaulting of sedimentary or metasedimentary terrains which mainly result from the collision of continental blocks (Boggs, 1992). Metamorphic rock fragments are present in all the studied thin sections suggesting contribution from metamorphic provenance as well.

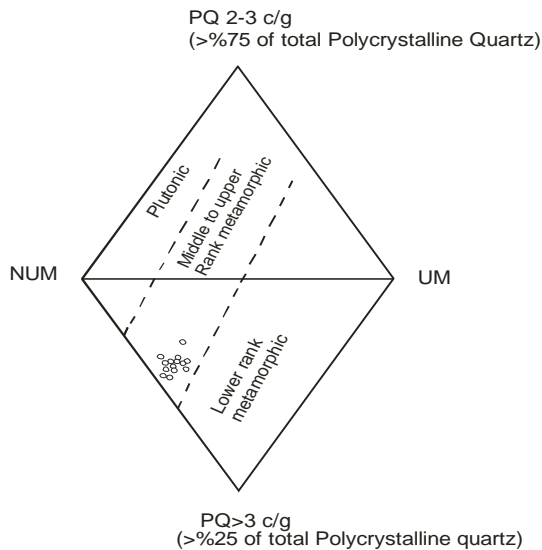


Fig. 6: Diamond diagram used to discriminate sands sourced by different types of crystalline rocks, on the basis of the extinction pattern and polycrystallinity of quartz grains of sandstone of Disang Group (after Basu et al., 1975)

The occurrence of mafic rock fragments and high chert content suggests their derivation from the ophiolite zone. A plot of Qp-Qnu-Qu (Fig.5; Basu et al., 1975), suggests that quartz grains of the studied sandstones are of plutonic origin whereas, the diamond plot shows that the sediments were derived from medium to high rank metamorphic source (Fig.6; Basu et al., 1975). In the Qt-F-L plot (L: Lv + Ls + Lm, Fig.7; Dickinson et al., 1983) samples are falling in the recycled orogen field whereas the Qm-F-Lt plot (Lt: L+ Qp, Fig.8; Dickinson and Suczek, 1979) shows that samples are dominantly from transitional recycled orogen; three samples fall in the recycled orogen field. A plot of Log K₂O/Na₂O versus Fe₂O₃+MgO also supports the recycled orogen source for the studied sandstone (Fig. 9). The discriminant functions of Roser and Korsch (1988) were used to discriminate between the four sedimentary provenance fields. In Fig. 10 (Roser and Korsch, 1988) majority of samples fall in

the mafic igneous province field whereas four samples fall in the intermediate igneous field and one sample falls in the quartzose sedimentary province field. The discriminant diagram after Roser and Korsch (1988) shows that the sandstones are scattered in the P1 (mafic igneous provenance) and P4 (quartzose sedimentary provenance) field supports the interpretation that sandstones were derived from Quartzose sedimentary provenance and mafic igneous provenance (Fig. 11). Plot adopted from Amajor (1987) indicates towards the basaltic sources (Fig. 12). A plot of Qp-Lv-Ls suggests that the sandstones were derived from collision suture and fold thrust belts (Fig. 13). Active margin (fore arc, continental arc, back arc, strike slip) sediments are characterized by a mixture of arc derived material and old upper crustal sources, whereas passive margin sediments are generally dominated by old upper crustal sources (McLennan et al., 1990). K₂O/N₂O and SiO₂ are increasing from oceanic island arc to active continental margin to passive continental margin.

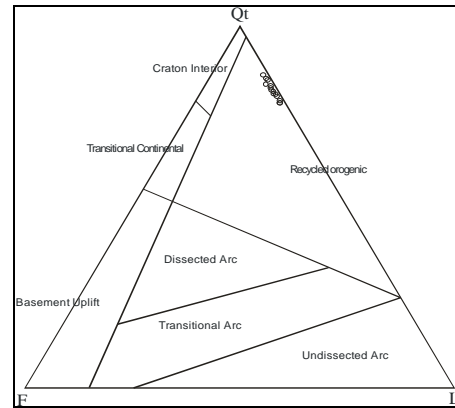


Fig.7: QtFL plot showing composition of studied sandstones of Disang Group. Provenance fields are from Dickinson (1985).

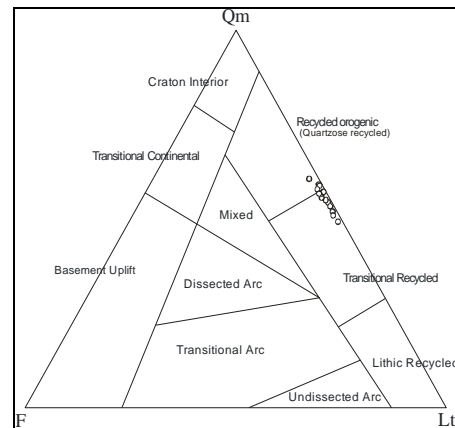


Fig.8: QmFLt plot for sandstones of Disang Group (Dickinson, 1985). Where Lt= Ls+Lv+Lm+ Qp+ Chert

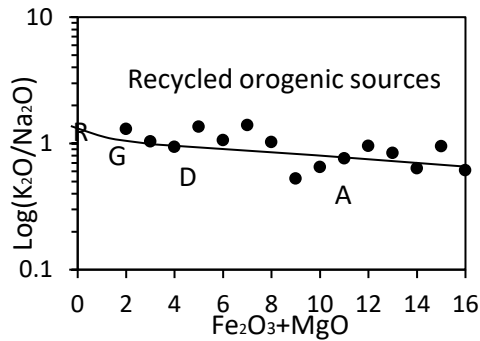


Fig. 9: Plot of K_2O/Na_2O versus Fe_2O_3+MgO . A, D, R and G Mean andesite, dacite, rhyolite and granite, respectively from developed for the Southern Welsh Basin, Edge (PM) of Continents. The Solid Line Connecting A, D, R and G is the Average Basalt. Samples above the line represent the Recycled Orogenic Sources (Roser and Korsch, 1988)

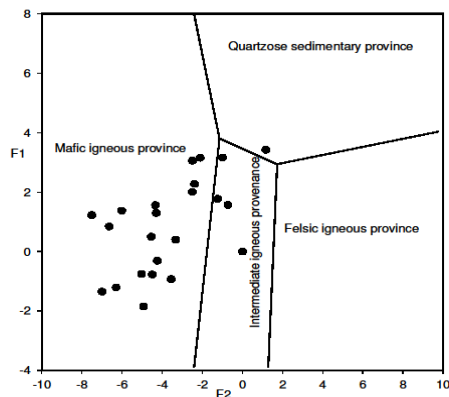


Fig. 10: Discrimination diagram for sedimentary provenance (Roser and Korsch, 1988), F1 and F2 are the Discriminating function.

$$F1 = (56.50TiO_2 - 10.879Fe_2O_3 + 30.875MgO - 5.404Na_2O + 11.112K_2O) / Al_2O_3 - 3.89$$

$$F2 = (30.638TiO_2 - 12.541Fe_2O_3 + 7.32MgO + 12.031Na_2O + 35.402K_2O) / Al_2O_3 - 6.382$$

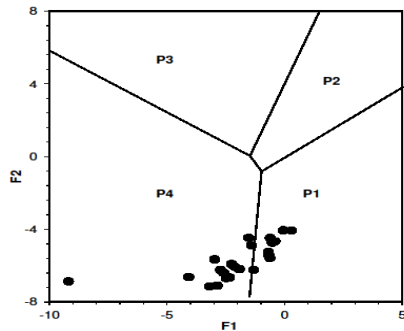


Fig. 11: Discrimination function diagram for the provenance signature of the sandstone using major elements (after Roser and Korsch, 1988)

$$DF1 = (-1.773TiO_2 + 0.607Al_2O_3 + 0.760Fe_2O_3 - 1.5MgO + 0.616CaO + 0.509Na_2O - 1.224K_2O - 9.190)$$

$$DF2 = (-0.445TiO_2 + 0.070Al_2O_3 + 0.250Fe_2O_3 - 1.142MgO + 0.438CaO + 1.475Na_2O - 1.426K_2O - 6.861)$$

P-1: Mafic igneous provenance, P-2: Intermediate igneous provenance, P-3: Felsic igneous provenance, P-4: Quartzose sedimentary provenance

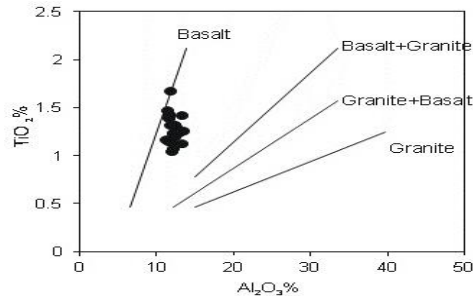


Fig.12: TiO_2 vs. Al_2O_3 binary plot (Amajor, 1987)

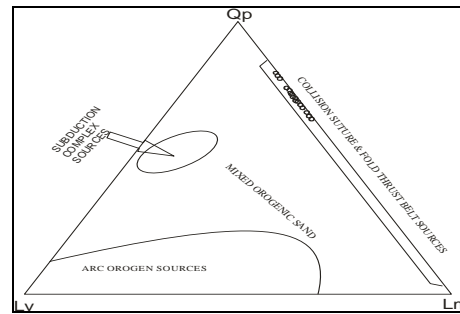


Fig.13: QpLvLs plots for framework modes of the studied sandstones showing different provenance fields after Dickinson and Suczek (1979)

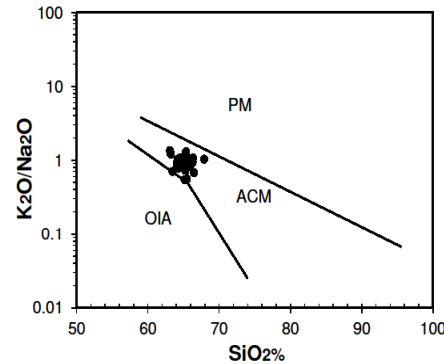


Fig. 14: K_2O/Na_2O Vs SiO_2 tectonic discrimination plot for the analyzed sandstone samples (after Roser and Korsch, 1986) OAI = Oceanic island arc; ACM=Active continental margin; PM=Passive margin

The ratio of K_2O/Na_2O Vs SiO_2 (Fig. 14) is used to discriminate the tectonic setting (Roser and Korsch, 1986). It is found that in K_2O/Na_2O Vs SiO_2 all the samples plot in the active continental margin field.

Conclusions

The results of this investigation show that sandstone of Disang Group under study can be classified as lithic wacke based on matrix content and mineralogically they are classified as sublithic arenites. Based on the integrated petrographical, major and minor elemental studies it can be concluded that these sediments were mainly derived from igneous and

metamorphic sources in an active continental margin tectonic setup. The low content of feldspar, abundance of sedimentary and metasedimentary lithics and pseudomatrix, presence of volcanic rock fragments and radiolarian chert grains suggest that the detritus were possibly derived from subduction complexes in a recycled orogens. Detritus were possibly derived from the uplifted fold thrust belt of Myanmar's landmass comprising of igneous and metamorphic basement complex with older sedimentary sequences with minor contributions of detritus from Mishmi Hills region lying to the NE of the study area.

Acknowledgement

The authors are grateful to the authorities, to the laboratory attendant of the Department of Applied Geology; Dibrugarh University for assisting in laboratory work. Anonymous reviewers are thanked for constructive suggestion for improvement of the MS

References

- Amajor, L. C. (1987). Major and trace elements geochemistry of albino and Touronian shale from the Southern Benue trough, Nigeria. *Journal of African Earth Science*, 6, 633-641.
- Basu, A., Young, S.W., Suttner, L.J., James, W.C. and Mach, G.H. (1975). Reevaluation of the use of undulatory extinction and polycrystallinity in detrital quartz for provenance interpretation. *Journal of Sedimentary Petrology*, 45, 873-882.
- Basu, A. (1985). Reading provenance from detrital quartz, G.G.ZUFFA (Ed.) *Provenance of Arenites*, 231-247.
- Blatt, H., Middleton, G. and Murray, R. (1980). Origin of Sedimentary rocks, 2nd Ed. Prentice-Hall, New Jersey, 782.
- Boggs, S. (1992). Sedimentary Petrology. Blackwell scientific Publications.
- Dickinson, W. R. (1970). Interpreting detrital modes of greywacke and arkose. *Journal of Sedimentary Petrology*, 40, 695-707.
- Dickinson, W. R. (1985). Interpreting provenance relations from detrital modes of sandstones. In: Zuffa, G. (Ed.), *Provenance of Arenites*. Reidel, Dordrecht, 333-361.
- Dickinson, W. R. and Suczek, C. A. (1979). Plate tectonic and sandstone composition. *Bulletin of American Association of Petroleum Geology*, 63, 2164-2172.
- Dickinson, W. R., Beard, L. S., Brakenridge, G. R., Erjavec, J. L., Ferguson, R. C., Inman, K. F., Knepp, R. A., Lindberg, F. A. and Ryberg, P. T. (1983). Provenance of North American Phanerozoic sandstone in relation to tectonic setting. *Geological Society of American Bulletin*, 94, 222-235.
- Dorsey, R. J. (1988). Provenance evolution and unroofing history of a modern arc continent collision: Evidence from petrography of Plio-Pleistocene sandstones, eastern Taiwan. *Journal of Sedimentary Petrology*, 58, 208-218.
- Dott, R. H. Jr. (1964). Wacke, greywacke and matrix – what approach to immature sandstone classification?. *Journal of Sedimentary Petrology*, 34, 625-632.
- Folk, R. L. (1974). Petrology of Sedimentary Rocks: Austin, TX, Hemphill Press, second edition, 182.
- Gazzi, P. (1966). Le arenarie del flysch sopracretaceo dell'Appennino modenese; correlazioni con il flysch di Monghidoro. *Mineralogicae Petrografica Acts*, 12, 69-97.
- Hutchison, C. S. (1989). Geological Evolution of South East Asia. Oxford University Press, New York.
- Ingersoll, R. V. and Suczek, C. A. (1979). Petrography and provenance of Neogene sand from Nicobar and Bengal fans. DSDP sites 211 and 218. *Journal of Sedimentary Petrology*, 49, 1217-1228.
- Ingersoll, R. V., Bullard, T. F., Ford, R. L., Grimm, J. P., Pickle, J. D. and Sares, S. W. (1984). The effect of grain size on detrital modes: a test of the Gazzi-Dickinson point-counting method. *Journal of Sedimentary Petrology*, 46, 620-632.
- Kumar, P. (2004). Provenance history of the Cenozoic sediments near Digboi-Margherita area, eastern syntaxis of the Himalayas, Assam, northeast India. Unpublished M.Sc. thesis. Auburn University, Auburn, 131.
- Mathur, L. P. and Evans. P. (1964). Oil in India, International geological Congress Twenty- Second Session, India, 7-52.
- McLennan, S. M., Taylor, S. R., McCulloch, M. T. and Maynard, J. B. (1990). Geochemical and Nd-Sr isotopic composition of deep-sea turbidities: Crustal evolution and plate tectonic associations. *Geochimica Cosmochimica Acta*, 54, 2015-2050.
- Nandi, D. R. (2001). Geodynamics of Northeastern India and its adjoining rejoin. *Abstract Publication Kolkata*, 39-49.
- Pettijohn, F. J. (1975). Sedimentary rocks, 3rd Ed.: New York, Harper & Row, 628.
- Pittman, E. D. (1963). Use of zoned plagioclase as an indicator of provenance. In: Sand and Sandstone (cd. by Pettijohn, Potter and Siever, 1987). *Journal of Sedimentary Petrology*, 33, 380-386.
- Roser, B. P. and Korsch, R. J. (1986). Determination of tectonic setting of sandstone-mudstone suites using SiO₂ content and K₂O/Na₂O ration. *Journal of Geology*, 94, 635-650.
- Roser, B. P. and Korsch, R. J. (1988). Provenance signatures of sandstone-mudstone suits determined using discriminant function analysis of major element data. *Chemical Geology*, 79, 119.
- Singh, Ch. G. and Kushwaha, R. A. S. (2008). Petrographic analysis of Tertiary Sediments between Imphal and Moreh, Manipur. *Journal of the Indian Association of Sedimentologists*, 27, 23-34.
- Singh, Y. R., Singh, B.P. and Ranjeeta Devi, S. (2017). Source Rock Characterization, Diagenesis and Depositional Environment of the Upper Disang Formation from Gelmoul Area of Manipur, NE India. *Journal of the Indian Association of Sedimentologists*, 34, 1-7.
- Sinha, N. K. and Chatterjee, B. P. (1982). Notes on the Disang Group in parts of Nagaland and its Fossil fauna. *Records of the Geological Survey of India*, 112 (4), 50-52.

(Received: 27 April 2018; Revised version Accepted: 31 May 2021)

GEOCHEMISTRY, DEPOSITIONAL AND TECTONIC SETTING OF THE BARAIL GROUP OF THE INDO-MYANMAR RANGES

Salam Ranjeeta Devi

Department of Earth Sciences, Manipur University, Imphal-795003, India

Email: ranjeeta_27@rediffmail.com

Abstract

The present paper deals with the study of the depositional environment and tectonic setting during the sedimentation of the Barail Group of rocks of the Indo-Myanmar Ranges (IMR). The Barail Group (Oligocene) consist of sandstone intercalated with shale and siltstone. Geochemical study suggests low to high degree of chemical weathering. ICV vs. CIA, Al_2O_3 vs. TiO_2 diagrams indicate that the sediments were derived from the multiple source rocks dominantly of mafic composition. Arid to semi-arid/semi-humid climate prevailed during the deposition of the Barail Group sediments. Sedimentation occurred in a tectonic setting of overlap of passive to active continental margin under marine environment.

Keywords: Geochemistry, Deposition, Tectonic setting, Barail Group, Indo-Myanmar Ranges, Marine environment.

Introduction

Geochemical studies have shown a close relationship between chemical composition of the sedimentary rocks and their provenance. Tectonism has a primary control on sedimentary rock composition (Blatt et al., 1980). Geochemical indices are most frequently used in the interpretation of depositional environment (Roaldest, 1970). Geochemistry has been widely used as an important tool to interpret chemical weathering, source rock composition, climate condition as well as tectonic during of the sediments deposition in a basin. Geochemical analysis of the sediments provides clues for provenance interpretations for sediments of all grain sizes (Bhatia, 1983; Taylor and McLennan, 1985; Armstrong-Altrin et al., 2017; Chaudhuri et al., 2020). Geochemical studies are also suitable for the interpretation of provenance of shales (Wronkiewicz and Condie, 1987; Garver and Scott, 1995; Fedo et al., 1995). Discriminant plots based on mixtures of the oxides of Ti, Al, Fe, Mg, Ca, Na and K are useful for distinguishing different provinces (Roser and Korsch, 1988; Saha et al., 2018). Being immobile, titanium oxides and alumina are particularly useful for provenance interpretations (Hayashi et al., 1997). Different binary and ternary plots of major element oxide provide significant information about palaeoweathering, palaeoclimate, nature of source rocks, tectonic setting and depositional basin (Potter et al. 2005; Suttner and Dutta, 1986; McLennan et al. 1980; Schieber 1992; Roser and Korsch, 1986; Roaldest, 1978). The Barail Group of rocks are well exposed in most part of the Indo-Myanmar Ranges (IMR). However, geochemical studies on the Barail Group of rock have remained confined to small areas with meagre data available on geochemistry of these rocks. Systematic geochemical analysis of these rocks

from different parts of the IMR can help in understanding the degree of chemical weathering, recycling and nature of source rocks, climatic variability and reconstruction of the depositional environment, and tectonic setting during their sedimentation. This paper deals with the comparison of geochemical data of the Barail Group of rocks from different areas of Assam (North Cachar Hills, Sen et al., 2015), Nagaland (Naga Hills, Srivastava, 2013), Manipur (Manipur Hills, Devi et al., 2017), Shillong Plateau (Mandal, 2009) and the Sylhet basin (Hossain and Roser, 2006) of the IMR, to work out the source rock composition, change in source area, degree of weathering, climatic changes, and to reconstruct depositional environment and tectonic setting.

Geological Setting

The Indo-Myanmar Ranges have been evolved as an accretionary prism due to subduction of the Indian plate beneath the Myanmar plate (Soibam, 1998). The IMR consist of Naga- Hills, Manipur Hills, Mizo-Chin Hills and Arakan Yoma Hills (Fig. 1). It comprises of ophiolites and associated Late Cretaceous sediments, the Disang Group of Eocene consisting of thick sequences of dark grey to black splintery shales with intercalation of siltstones and fine to medium-grained sandstones. The Disang-Barail transition strata comprises of siltstone, sandstone and shale. The contact between the sediments of Disangs and Barails, runs more or less parallel to the western margin of the Imphal valley and continues northerly towards Kohima in Naga Hills and further south along the eastern border of Mizoram Hills of the Indo-Myanmar ranges. The contact is usually gradational with some local tectonic contacts marked by a high angle reverse fault (Soibam, 1998) and in some places by conglomeratic horizon.

This gradational contact is related with a gradual change from dominantly argillaceous marine to a mainly arenaceous shallow marine depositional environment. The shale of the Upper Disang transition with Lower Barail shows relatively increasing intercalations of thin siltstone beds and fine sandstones

which are thinly to moderately thick bedded and massive in nature. Silty shale is again a very important component of the Disang-Barail transition and is found associated with many plant (leaves, barks, fruits, etc.) impressions which sometimes are weakly to moderately carbonized (Guleria et al. 2005). The Barail Group of

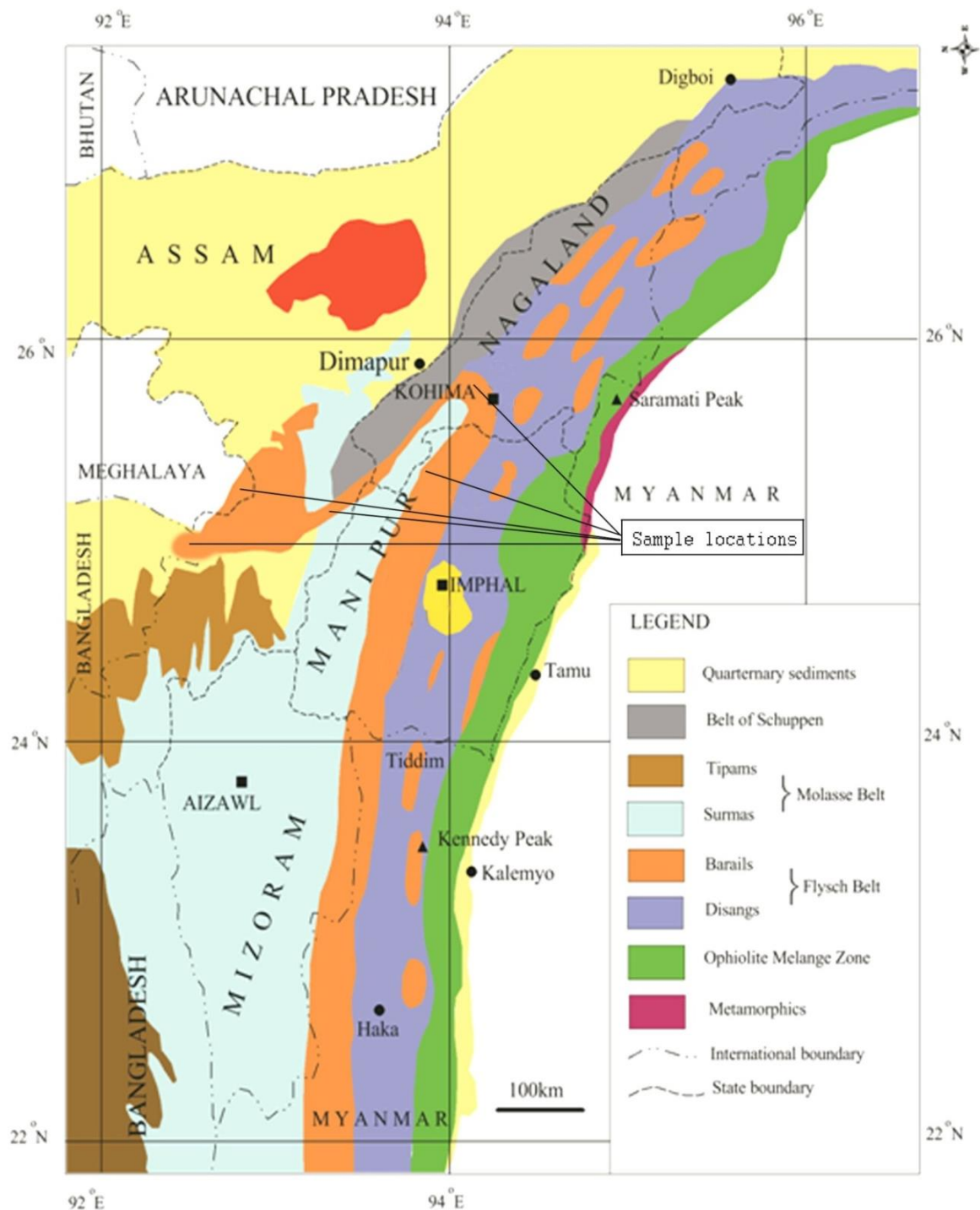


Figure 1: Geological map of NE India (Soibam, 1998) showing sample locations.

fine to medium grained multistoried thickly bedded sandstones, intercalated with siltstone and shale overlying the Disang-Barail Transition.

The Barail Group represents a thick sequence of sandstones with shale (500m) in the Barail Range of North Cachar Hills, Assam (NE India, 1932). The Barails are also well exposed along the Patkai ranges

and Dhansiri valley of Nagaland. In Meghalaya, the Barail Group is mainly exposed in the Garo Hills and consists of about 1000 m thick sandstones with minor shale and carbonaceous shale/coal sequences. In Manipur, the Barails (~3200 m) occur on the western half and are also found occurring as outliers forming capping of Disangs in the eastern part of and within the Imphal Valley. The nature of succession suggests that they were formed in flysch and sub-flysch basin and often display typical turbidite character. In Sylhet basin, Barail Group unconformably overlies the Kopilli Formation of Jaintia Group. The Jenam Formation (sandstone, siltstone, and silty shale) forms the lower part of the Barail Group and Renji Formation overlies Jenam Formation. In Tirap district of Arunachal

Pradesh, the rocks of the Barail Group occur in two different depositional environments (Anon, 2010). In Arunachal Pradesh, Barail Group is usually succeeded by the Tipam with an apparent erosional unconformity in the Schuppen belt. The age of this group of rocks may range from Oligocene to Late Eocene. The Surma Group overlies the Barail Group. The rocks of Surma Group are characterised by intercalation of massive sandstone and shales sequence comprising of thin inter bands of shales and siltstone. The Tipams are moderately coarse grained, ferruginous, massive, sometimes faulted sandstones. It overlies the Surma Group with stratigraphic break. The geological succession of the Barail Group from these areas is shown in the Table 1.

Table 1: Lithostratigraphic classification of the Barail Group of rock in NE Indian subcontinent

Age	Group	Formation and lithology				
		Assam Sen et al., 2015	Nagaland Srivastava, 2013	Manipur Soibam, 1998	Shillong Plateau, Ranga Rao, 1983, Mandal, 2009	Sylhet Reimann, 1993, Hossain and Roser, 2006
Lower Miocene	Surma	Sandstones with shale	Sandstone with shale	Sandstone intercala- ted with shale and siltstone	Fine-grained sandstone with shale	Alternation of sandstone, shale and siltstone
unconformity						
Oligocene	Barail	Fine to medium grained, massive and bedded sandstones with shale and laminated sandstones	Sandstone with minor shale	Fine to medium grained, massive and bedded sand- stones with shale and laminated sandstones	Argillaceous sandstone (Renji Fm) Medium to fine-grained, hard massive sandstone (Jenam Fm) Medium to fine sandstone within subordinate shale and conglomerate (Laisong Fm)	Yellowish brown sandstone, shale and coal lenses (Renji Fm) Grey to brownish siltstone, silty shale and sandstone (Jenam Fm)
Late Eocene to early Oligocene	Disang-Barail Transitional sequence	Base is not exposed	Shales with minor sandstones	Siltstone with plant impress- ions intercala- ted with shale and sandstone	Alternating sandstone and black shale	Shale with subordinate sandstone and thin limestone (Kopili Fm)

Sampling and Analytical Procedures

Fresh samples of the Barail sandstones and shales were collected from outcrops exposed in stream cuts, road cuts and small quarries from the NW

Manipur. Sample locations are shown in the Figure 1. After careful thin section examination under microscope, four sandstone samples of Barail Group and four shale samples were selected for geochemical analysis. Samples with significant diagenetic alteration,

especially with more than 15% secondary carbonate cement, were not considered for geochemical analysis (Devi et al., 2017). The chips of these samples were further powdered to -200 mesh size. Whole rock major elements were analysed using fused pellets glued with polyvinyl alcohol on SIEMENS SRS 3000 sequential X-ray Spectrometer at Wadia Institute of Himalayan Geology, Dehra Dun. Analytical accuracy of the major oxide data is <5% and average precision is always better than 1.5% (Saini et al. 1998). 16 representative shale samples of Barail Group from North Cachar Hills, Assam were analysed in the Department of Instrumentation and USIC by XRFS method. The results after chemical analysis have been studied (Sen et al., 2012).

Samples of the Oligocene Jenam and Renji formations of Sylhet basin were also taken from cores of hydrocarbon exploration wells (Hossain and Roser, 2006). The Jenam Formation of the lower Barail Group is encountered only in the Atgram-1X well between 4712 m and 4968 m bsl (Petrobangla, 1982), where it consists of indurated dark grey shale/silty shale. The Renji Formation (Barail Group) was intersected from 3975m to 4712m in Atgram-1X and from 4820m to 4977m in the Fenchuganj 2 well. This formation consists mainly of light to dark grey, fine to medium grained indurated sandstone with minor shale and siltstone. The base of the Barail Group was not intersected in these wells. The chipped samples (<10 mm in diameter) were washed with running tap water, after draining, the cleaned samples were then dried in an oven at 110°C for several hours. The oven-dried samples were subsequently crushed in a tungsten-carbide ring mill for 25 to 45 seconds and about 10 g of each powdered sample was then dried at 110°C in oven for 24 hours before gravimetric determination of loss on ignition (LOI). After LOI was estimated in a muffle furnace at 1020°C for at least 2 hours, the ignited materials were disaggregated by hand and gentle grinding in an agate mortar and pestle, and subsequently returned to 110°C temperature in oven for at least 24 hours. The ignited rock samples were then used for preparation of glass fusion beads for the X-ray fluorescence (XRF) analysis. The XRF analyses of the major elements were made using a Rigaku RIX 2000 instrument at Shimane University. Glass fusion beads were prepared in an automatic bead sampler (fusion 240 seconds, agitation 360 seconds), using an alkali flux (80% lithium tetraborate and 20% lithium metaborate), with a sample to flux ratio of 1:2 (Kimura and Yamada, 1996).

Samples of Shillong Plateau were dried in an oven at 50°C for nearly 24 hours (Mandal, 2009). Approximately 20 gm of dried sediment for each sample was crushed with a mortar and pestle to a grain size of <0.63 mm and homogenized to sent to ACME Laboratories Ltd., Vancouver, BC, Canada, for analysis. In the laboratory, samples were analyzed by ICP-emission spectra following lithium metaborate/tetraborate fusion and dilute nitric digestion. Loss of

Ignition (LOI) was calculated by weighing the difference after ignition at 1000° C. Geochemical analysis included 11 major oxides (SiO₂, Al₂O₃, Fe₂O₃, MgO, CaO, Na₂O, K₂O, TiO₂, P₂O₅, MnO, and Cr₂O₃).

Palaeoweathering and Paleoclimate

Weathering processes also control the composition of clastic sediments. The Chemical index of weathering (CIA, Nesbitt and Young, 1982) is one of the important weathering indices to know the degree of chemical weathering in a source area. The relation between the degree of weathering and the original source rock composition are well assessed by the combination of CIA with the index of compositional variability (ICV, Cox et al, 1995; Potter et al., 2005). The ICV can be used to discriminate source rock type based on major-elemental geochemistry. The high ICV value (ICV>1) indicates that the sediments are derived from compositionally immature source rocks whereas, low value (ICV<1) suggests compositionally mature source rocks. Thus, changes in ICV values may be the result of both variations in the source rock composition and differences in the degree of weathering (Potter et al., 2005). A trend in CIA vs. ICV diagrams (Fig. 2) suggests the source rock composition of the sediments and degree of chemical weathering. In this diagram all the samples are scattered indicating variable effect of weathering from low to high degree and originated from different sources, that is, the sediments of the Barail Group from different areas were derived from different source rocks composition.

Climate is another factor that controls the degree of chemical weathering. Major Oxide elemental data provides useful information on climatic condition that prevailed during the deposition of sedimentary rocks. The bivariate plot (Fig.3) of (Al₂O₃ +Na₂O) vs Si₂O after Suttner and Dutta (1986) differentiate the climatic conditions under which sediments were deposited. Samples plot on this diagram suggests climatic variability from arid to semi-arid/semi-humid climatic condition during deposition of the Barail sediment.

Source Rock Composition

Composition of the clastic sediment is mainly influenced by the source rock characteristics, the nature of the sedimentary processes within the depositional basin and the type of deposition paths that link sources area to the depositional basin (Dickinson and Suczek, 1979). Processes like weathering and diagenesis can influence the chemical composition of the sediments (Cullers et al., 1988) and therefore, less mobile element oxides (Al₂O₃ and TiO₂) have been widely used to determine source rocks. TiO₂ (%) and Al₂O₃ (%) bivariate plot is being used significantly for determining source rock compositions (McLennan et al., 1980; Schieber, 1992; Paikaray et al., 2008). The bivariate plot of Ti₂O vs. Al₂O₃ (Fig. 4) for the

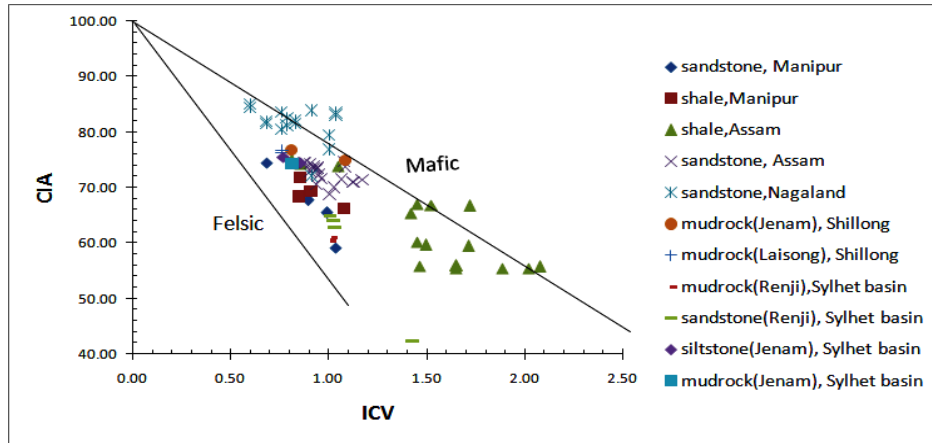


Figure 2: ICV vs. CIA diagram (Potter et al. 2005)

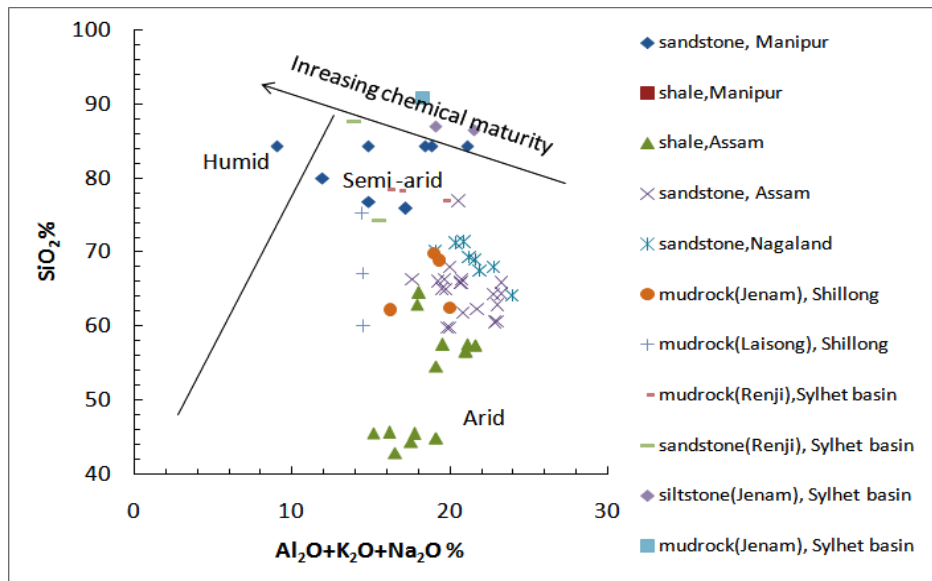


Figure 3: $Al_2O_3+K_2O+Na_2O\%$ (Suttner and Dutta. 1986).

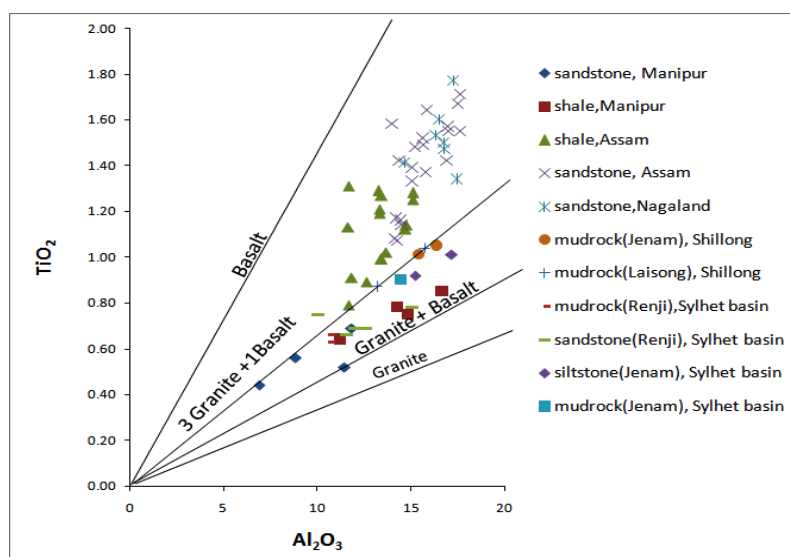
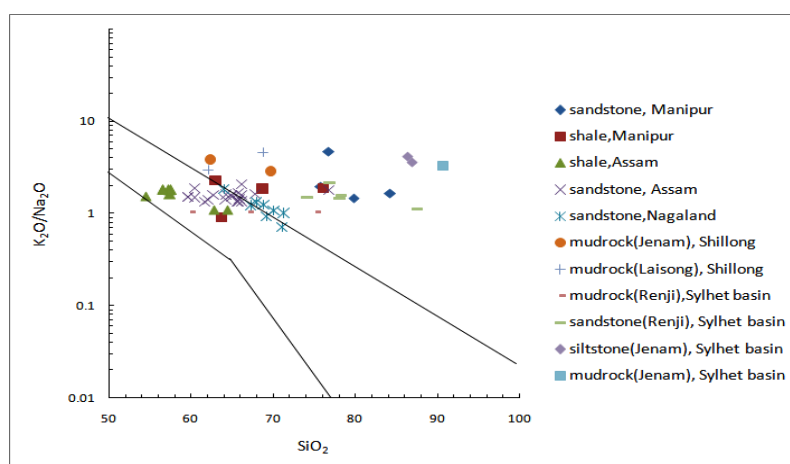
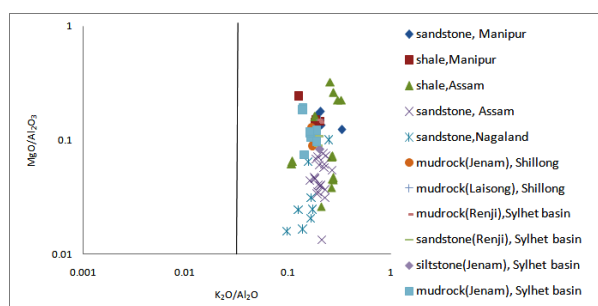
Barail Group of rocks from different areas indicates that these sediments were originally derived from different source rocks. Less weathered dominantly mafic composition of shale occurs towards the North Cachar Hills (Assam) of the Barail exposures. Samples plot on TiO_2 vs Al_2O_3 (Fig.4) after McLennan *et al.* (1980) and Schieber (1992) indicates that sediment were derived from a mixed source rocks from granitic to basaltic composition.

Tectonic Setting and Depositional Basin

The nature and proportion of their detrital components and the bulk composition reflects the tectonic setting of the basin (Sieve, 1979; Roser and Korsch, 1986). Active continental margin sediment are characterized by mixture of arc derived material and old upper crustal sources; whereas, passive margin sediments are generally dominated by old upper crustal sources (McLennan *et al.*, 1990). Tectonic setting of clastic sedimentary rock can be studied from major element oxides (Crook, 1974, Middleton, 1960). K_2O/Na_2O vs SiO_2 diagram is used to discriminate the

tectonic setting (Roser and Korsch (1986). Roser and Korsch (1986) plot seems to be somewhat better (~32–62% success) than Bhatia's (1983) plots (0–58% success) to determine tectonic setting (Armstrong-Altrin and Verma, 2005; Saha *et al.*, 2010).

In K_2O/Na_2O vs SiO_2 diagram (Fig. 5), the samples plot in the tectonic setting overlap between passive and active margin, which suggest a complex tectonic activities with mix of less weathered and recycled sediments. Certain major oxides have been used to distinguish depositional environments. The relationship between K_2O/Al_2O_3 vs MgO/Al_2O_3 was used by Roaldest (1970) to differentiate between the marine and non-marine vs sediments. In K_2O/Al_2O_3 vs MgO/Al_2O_3 diagram (Fig. 6) all the samples plotted in marine environment. Thus, from this study, it is can be inferred that the sediments of the Barail were deposited in marine depositional environment with different chemical composition and variable degree of chemical weathering in different parts of depositional basin, which, in turn, suggests the evolutionary history of complex tectonic activities.

Figure 4: Al_2O_3 vs. TiO_2 diagram (McLennan et al. 1980; Schieber 1992).Figure 5: Plot of SiO_2 vs. $\text{K}_2\text{O}/\text{Na}_2\text{O}$ of Barail (Roser and Korsch, 1986).Figure 6: $\text{Log K}_2\text{O}/\text{Al}_2\text{O}_3$ vs. $\text{Log MgO}/\text{Al}_2\text{O}_3$ plots for depicting depositional environment (Roaldest, 1978).

Conclusions

Geochemical studies of the Barail Group of sediments from different parts of the IMR show low to high degree of chemical weathering under arid to semi-arid/semi-humid climatic condition. The sediments were derived from multiple source rocks variables from granitic to basaltic composition but dominantly of basaltic composition. The sediments were deposited in a tectonic setting overlapping between passive and

active continental margins in a marine depositional basin. The sediment composition in different parts of the depositional basin of the Barail Group of rocks shows changes in tectonic activities which reflect the complex evolutionary history of the region.

Acknowledgements

Author would like to thank the Head, Department of Earth Sciences, Manipur University for providing necessary facilities and support. Author is also sincerely thankful the Department of Science and Technology, New Delhi for the Financial assistant under the WOS-A scheme SR/WOS-A/EA-31/2016 (G). Constructive criticism by two anonymous reviewers if highly appreciated which improved the MS substantially,

References

- Bhatia, M.R. (1983). Plate tectonics and geochemical composition of sandstones. *Journal Geology*, 91, p. 611-627.

- Armstrong-Altrin, J.S., Lee, Y.I., Kasper-Zubillaga, J.J., Trejo-Ramirez, E. (2017). Mineralogy and geochemistry of sands along the Manzanillo and El Carrizal beach area, southern Mexico: implications for Paleoweathering, provenance and tectonic setting. *Journal of Geology*, 52, p.559-582.
- Blatt, H., Middleton, G.V. and Murray R.C. (1980). *Origin of sedimentary Rocks*. Prentice Hall, 782 pp.
- Chaudhuri, A., Banerjee, S., and Chauhan, G. (2020). Compositional evolution of siliciclastic sediments recording the tectonic stability of a pericratonic rift: Mesozoic Kutch. *Marine and Petroleum Geology*, 111, p.476-495.
- Crook K.A.W. (1974). The significance of compositional variation in flysch arenites (greywackes) Society of Economical, Paleontological and Mineralogical Special Publication. v.19, p.304-310.
- Cullers, R.L., Chaudhuri S, Kilbane N and Koch, R. (1979). Rare earths in size fractions and sedimentary rocks of Pennsylvanian-Permian age from the mid-continent of the USA; *Geochimica Cosmochimica Acta* v.43, p.1285-1302.
- Devi, S. Ranjeeta, Mondal, M.E.A. and Armstrong-Altrin, John S. (2017). Geochemistry and the Factors Controlling on the Weathering and Erosion of the Barail Group of Rocks, NW Manipur, India. *Journal Indian Association of Sedimentologists*, v.34, p.9-16.
- Dickinson, W.R. and Suczek, C.A. (1979). Plate tectonics and sandstone compositions. *American Association of Petroleum Geology Bulletin*, v. 63, p.2164-2182.
- Fedo, C.M., Wayne Nesbitt, H., Young, G.M. (1995). Unravelling the effects of potassium metasomatism in sedimentary rocks and paleosols, with implications for Paleoweathering conditions and provenance. *Geology* 23, p. 921-924.
- Garver, J.I., Scot, T.J. (1995). Trace elements in shale as indicators of crustal provenance and terrane accretion in the southern Canadian Cordillera. *Geology Society of American Bulletin*, 107, p. 440-453.
- Mandal, S. (2009). *Sedimentation and Tectonics of Lower Cenozoic Sequences from Southeast of Shillong Plateau, India: Provenance history of the Assam-Vengal System, Eastern Himalayas*. Unpublished M.Sc Thesis, Auburn University, Alabama.
- McLennan, S.M., Nance, W.B. and Taylor, W.B. (1980). Rare earth element-thorium correlations in sedimentary rocks, and composition of the continental crust. *Geochimica Cosmochimica Acta*, v.44, p.1833-1839.
- McLennan, S.M., Nance, W.B., Taylor, W.B. (1980). Rare earth element-thorium correlations in sedimentary rocks, and composition of the continental crust. *Geochimica Cosmochimica Acta*, v. 44, p.1833-1839.
- Middleton, G.V. (1960). Chemical composition of sandstones. *Geology Society America Bulletin*, v.71, p.1011-1026.
- Nesbitt, H.W., Markovics, G. and Price, R.C. (1980). Chemical processes affecting alkalis and alkaline earths during continental weathering. *Geochimica Cosmochimica Acta*, v. 44, p.1659-1666.
- Paikaray, S., Banerjee, S. and Mukherjee, S. 2008. Geochemistry of shales from the Palaeoproterozoic to Neoproterozoic Vindhyan Supergroup: implications on provenance, tectonics and palaeoweathering. *Journal of Asian Earth Sciences*, 32, p. 34-48.
- Potter, P.E., Maynard, J.B. and Depetris, P.J. (2005). *Mud and mudstones: Introduction and overview*: Heidelberg, Springer-Verlag, 297p.
- Reimann, K.U. (1993). *Geology of Bangladesh*. Gebruder Borntraeger, Berlin, 160p.
- Rajkumar, H.S. and Klien, H. (2014). First perissodactyl footprints from flysch deposits of the Barail Group (Lower Oligocene) of Manipur, India. *Journal Earth System Science*, 123, p. 413-420.
- Rangarao, A. (1983). Geological and Hydrocarbon potential of a part Assam- Arakan Basin and adjacent regions. In: L.L.Bandari et al., (eds), *Petroliferous Basin of India*, Oil and Natural Gas Comm., India, Dehra Dun, p.127-158.
- Roser, B.P. and Korsch R.J. (1986). Determination of tectonic setting of sandstone- mudstone suites using SiO₂ content and K₂O/Na₂O ratio. *Journal Geology*, v.94, p.635-650.
- Sujata, Sen, P.K.Das, Bhagabaty, B, Borah, M. (2015). Geochemistry of Barail sandstones occurring in and around Dima Hasao District, Assam. *Journal of Applied Geochemistry*, v.17 (2), p.199-212.
- Saha, S., Stuart D. B, Banerjee, S. (2018). Mixing processes in modern estuarine sediments from the Gulf of Khambhat, western India. *Marine and Petroleum Geology*, 91 599-621
- Saha, S, Banerjee, S, Burley, S. D., Ghosh, A, Pratul, K. Saraswati, P.K. (2010). The influence of flood basaltic source terrains on the efficiency of tectonic setting discrimination diagrams: An example from the Gulf of Khambhat, western India. *Sedimentary Geology*, 228, p. 1-13.
- Schieber, J. (1992). A combined petrographical-geochemical provenance study of the Newland Formation. Mid-Proterozoic of Montana. *Geology Magazine*, v.129, p. 223-237.
- Singh, Y.R., Singh, B.P., A.K. Singh and Devi, S. Ranjeeta (2017). Palynology and Mineral composition of the Upper Disang flyschoid sediments from the southern Manipur, Northeast India. Age, Paleoenvironment and provenance reconstruction. *Himalayan Geology*, 38(1), p. 1-11.
- Siever, R. (1979). Plate tectonic control on diagenesis. *Journal Geology*, v.87, p. 127-155.
- Srivastava, S.K. (2013). Petrography and major element geochemistry of Oligocene Barail sediments in and around Jotsoma, Kohima, Nagaland. *Gondwana Geology Magazine*, v. 28 (2), p.159-164.
- Soibam I. (1998). On the Geology of Manipur. In *Souvenir, IX Manipur Science Congress (March, 25-27)* p.12-19.
- Suttner, L.J. and Dutta, P.K. (1986). Alluvial sandstone composition and paleoclimate Framework mineralogy. *Jour. Sedimentary Petrology*, v.56, p. 329-345.
- Wronkiewicz, D.J., Condie, K.C. (1987). Geochemistry of Archean shales from the Witwatersrand Supergroup, South Africa: source-area weathering and provenance. *Geochimica Cosmochimica Acta* 51, p. 2401-2416.
- Zakir Hossain, H.M and Barry Roser (2006). Major and trace element analyses of Tertiary sedimentary rocks from Sylhet basin, Bangladesh. *Geosciences Rept. Shimane Univ.* v. 25, p. 45-59.

(Received: 8 February 2020; Revised version accepted: 10 May 2021)

Appendix

Manipur, Devi et al., 2017 (sandstones and shale)

	Sandstone				Shale			
	BL-3	BH-5	BH-7	DL-25	TP-1	BL-2	KK-17	SPA-28
SiO ₂	75.85	79.88	76.78	84.29	63.75	63	68.75	76.19
TiO ₂	0.52	0.56	0.69	0.44	0.75	0.85	0.78	0.64
Al ₂ O ₃	11.46	8.86	11.84	6.92	14.84	16.67	14.28	11.24
Fe ₂ O ₃	3.81	3.18	2.47	2.14	6.48	5.93	5.34	3.32
MnO	0.048	0.061	0.047	0.039	0.095	0.09	0.073	0.067
MgO	1.41	1.57	1.61	1.15	3.61	2.39	2.13	1.63
CaO	0.34	0.35	0.28	0.3	1.11	0.55	0.57	0.35
Na ₂ O	1.94	1.25	0.53	0.8	2.12	1.36	1.45	1.24
K ₂ O	3.81	1.83	2.49	1.33	1.9	3.09	2.68	2.33
P ₂ O ₅	0.11	0.095	0.065	0.078	0.147	0.153	0.147	0.146

Assam, Sujata Sen et al., 2012, Devi et al. , 2017 (Shale)

	SS1	SS2	SS3	SS4	SS5	SS6	SS7	SS8	SS9	SS10	SS11	SS12	SS13	SS14	SS15	SS16
SiO ₂	45.59	57.58	57.31	54.48	64.48	57.43	45.39	42.79	44.78	56.54	45.52	62.86	44.3	57.33	44.79	56.52
TiO ₂	0.89	1.14	1.25	0.99	1.27	1.02	1.13	0.91	1.19	1.12	0.79	1.29	1.31	1.28	1.21	1.14
Al ₂ O ₃	12.63	14.77	15.12	13.43	13.44	13.68	11.64	11.85	13.32	14.7	11.69	13.25	11.69	15.1	13.33	14.75
Fe ₂ O ₃	4.43	6.07	6.43	6.17	5.92	5.58	6.01	5.13	6.37	6.01	4.41	5.95	5.59	6.44	6.36	6.03
MnO	0.05	0.13	0.13	0.28	0.16	0.11	0.13	0.12	0.15	0.12	0.05	0.19	0.15	0.12	0.14	0.13
MgO	0.78	0.69	3.98	4.36	2.15	0.52	2.62	0.31	0.94	0.66	0.76	2.14	2.63	3.96	0.96	0.67
CaO	0.64	7.35	7.79	8.08	0.15	7.44	8.26	5.76	7.68	7.3	0.63	6.14	8.22	7.75	7.71	7.29
Na ₂ O	2.17	2.27	2.32	2.25	2.2	2.25	2.29	2.2	2.19	2.21	2.15	2.24	2.27	2.34	2.21	2.23
K ₂ O	1.37	4.09	4.16	3.45	2.42	3.63	3.85	2.49	3.57	4.03	1.29	2.45	3.58	4.17	3.59	4.02
P ₂ O ₅	0.02	0.17	0.4	0.19	0.07	0.12	0.33	0.08	0.39	0.15	0.03	0.09	0.37	0.41	0.4	0.15

Appendix... cont.

Assam, Sujata Sen et al., 2015 (Sandstones)

	SS1	SS2	SS3	SS4	SS5	SS6	SS7	SS8	SS9	SS10	SS11	SS12	SS13	SS14	SS15	SS16	SS17	SS18	SS19	SS20
SiO ₂	60.53	59.68	65.8	62.17	65.98	64.3	67.86	64.98	65.78	66.25	61.73	59.67	62.77	64.92	66.22	65.72	64.25	76.82	66.22	60.48
TiO ₂	1.57	1.39	1.71	1.64	1.58	1.55	1.14	1.17	1.49	1.08	1.48	1.33	1.67	1.42	1.07	1.52	1.42	1.16	1.37	1.55
Al ₂ O ₃	16.98	15.09	17.67	15.89	14.01	17.65	14.51	14.21	15.68	14.18	15.25	15.09	17.54	14.38	14.27	15.66	16.92	14.49	15.82	17.03
Fe ₂ O ₃	7.41	8.45	7.33	6.98	7.99	6.55	5.8	7.98	6.91	6.77	7.83	8.37	6.52	7.78	5.89	6.89	6.44	5.83	6.89	7.39
MnO	0.12	0.29	0.2	0.22	0.18	0.68	0.13	0.27	0.06	0.57	0.26	0.26	0.67	0.2	0.65	0.06	0.21	0.24	0.06	0.13
MgO	0.53	1.02	0.71	0.21	1.06	0.62	0.53	0.81	0.71	0.62	0.61	1.08	0.59	0.88	1.04	0.72	1.02	0.78	0.74	0.67
CaO	0.51	0.36	0.48	0.48	0.36	0.46	0.58	0.51	0.61	0.67	0.47	0.44	0.49	0.52	0.59	0.65	0.45	0.51	0.66	0.39
Na ₂ O	2.1	1.92	2.12	2.44	2.17	2.17	2.1	2.11	2.15	1.13	2.41	1.98	2.13	2.09	2.1	2.13	2.42	2.18	2.11	2.36
K ₂ O	3.91	2.86	3.52	3.4	3.1	3.46	3.38	3.2	2.89	2.33	3.22	2.96	3.38	3.29	3.33	2.87	3.42	3.9	2.84	3.5
P ₂ O ₅	0.23	0.26	0.28	0.28	0.24	0.29	0.26	0.22	0.25	0.55	0.26	0.47	0.24	0.52	0.27	0.28	0.25	0.23	0.26	0.23

Nagaland, Srivastava, S.K., 2013

Sp. No.	R96/3	R96/10	R96/13	R96/27	R97/58	R97/99	R97/101	R97/113	R97/131	R97/133	R97/134	R97/137	R97/139	R97/110	R97/188	R97/189
SiO ₂	70.8	76.34	76.9	74.39	86.33	77.78	77.02	77.28	81.27	76.42	71.62	82.16	87.18	78.49	72.68	81.93
TiO ₂	1.21	1.03	1.09	1.23	0.55	0.87	0.9	0.89	0.69	1.01	1.16	0.71	0.5	0.76	1.03	0.59
Al ₂ O ₃	17.64	13.6	14.77	13.1	8.35	13.11	13.79	14.37	11.42	15.04	17.33	11.32	7.64	12.82	16.72	11.65
Fe ₂ O ₃	7.3	2.99	1.11	4	0	2.29	2.31	1.32	0.66	1.39	2.68	1.57	1.15	1.17	1.19	0.77
MnO	0.04	0.14	0.04	0.32	0.01	0.05	0.04	0.02	0.05	0.03	0.04	0.04	0.02	0.03	0.02	0.03
MgO	1.3	0.11	0.5	0	0.3	0.41	0.44	0.43	0.53	0.49	0.63	0.35	0.21	0.41	0.59	0.26
CaO	1.2	0.37	0.36	0.94	0.25	0.4	0.42	0.32	0.57	0.28	0.37	0.17	0.14	0.25	0.21	0.13
Na ₂ O	0.55	0.54	0.45	0.66	0.37	0.47	0.46	0.42	0.43	0.47	0.56	0.41	0.4	0.49	0.52	0.38
K ₂ O	2.07	1.62	1.59	2.11	0.55	1.37	1.37	1.27	1.12	1.56	2.24	1.1	0.6	1.46	2.37	1.1
P ₂ O ₅	0.13	0.15	0.13	0.2	0.2	0.14	0.13	0.13	0.12	0.14	0.14	0.13	0.11	0.15	0.12	0

Appendix... cont

Shillong Plateau, Mandal, S., 2009

	Jenam Fm		Laisong Fm	
	SM 15	SM19	SM22	SM24
SiO ₂	60.22	62.68	71.62	66.26
TiO ₂	1.01	1.05	0.87	1.04
Al ₂ O ₃	15.44	16.38	13.2	15.74
Fe ₂ O ₃	9.59	6.39	4.71	5.41
MnO	0.18	0.08	0.05	0.03
MgO	1.98	1.81	1.17	1.68
CaO	0.46	0.32	0.19	0.26
Na ₂ O	0.92	0.76	0.77	0.65
K ₂ O	2.63	2.9	2.29	2.97
P ₂ O ₅	0.14	0.13	0.11	0.09

Sylhet Basin, Zakir Hossain, H.M and Barry Roser, 2006

	Renji Formation								Jenam Formation		
	Mudstone			Fine sandstone					Siltstone	Mudstone	
	ZH-44	ZH-45	ZH-46	ZH-115	ZH-116	ZH-117	ZH-118	ZH-119	ZH-10	ZH-12	ZH-11
SiO ₂	76.2	76.1	76.14	64.67	71.18	70.82	72.42	69.98	66.74	63.98	68.83
TiO ₂	0.66	0.63	0.63	0.78	0.69	0.69	0.66	0.75	0.92	1.01	0.9
Al ₂ O ₃	10.64	10.67	10.6	15.09	12.04	12.64	11.59	10.07	15.22	17.18	14.48
Fe ₂ O ₃	4.09	4.02	3.97	6.24	4.84	5.25	4.76	3.75	6.5	6.17	5.63
MnO	0.05	0.05	0.05	0.08	0.06	0.06	0.06	0.24	0.09	0.06	0.04
MgO	1.28	1.29	1.26	2.27	1.71	1.89	1.67	1.09	1.36	1.44	1.21
CaO	0.9	0.94	0.95	1.34	0.99	0.88	0.94	4.7	0.3	0.23	0.22
Na ₂ O	1.88	1.9	1.89	1.46	1.6	1.71	1.58	1.83	0.84	0.84	0.89
K ₂ O	1.95	1.96	1.95	3.1	2.49	2.49	2.35	2.03	3.03	3.51	2.92
P ₂ O ₅	0.09	0.09	0.09	0.12	0.12	0.12	0.1	0.09	0.14	0.12	0.11

Petro-mineralogical and geochemical characteristics of Shahaba Limestone from Gogi-Kanchankayi sector, Bhima Basin, Karnataka with reference to Uranium mineralisation

Debasish Roy¹, Dheeraj Pande¹, Sikta Patnaik², S.K. Varughese¹, A.K. Pradhan¹,
B. Saravanan³, A.K. Bhatt^{3*}

Atomic Minerals Directorate for Exploration and Research,

¹Bengaluru, ²New Delhi, ³Hyderabad, *since retired

Corresponding author: debasishroy.amd@gov.in

Abstract

The Shahabad Limestone Formation of Bhima Basin from Gogi-Kanchankayi area occurs in heterogeneous forms like massive/blocky limestone, argillaceous/ siliceous limestone and laminated/ flaggy limestone. These limestones are primarily composed of micrite, which often alters into sparry calcite on diagenesis with associated impurities of quartz, feldspar, barite, chlorite, glauconite, sulphides and carbonaceous matter. Geochemically, these limestones comprises of variable CaO with low MgO and P₂O₅ content. Trace elements concentration shows elevated Ba, Rb and depleted Sr. The current study classified these limestones as non-dolomitic and non-phosphatic types deposited in shallow marine carbonate platform setting with low energy conditions. Post-sedimentation, basin tectonics has resulted in reactivation of the basin margin fault causing intense fracturing of limestone. Subsequent hydrothermal movement along those fractures has resulted in re-mobilisation and re-precipitation of sulphides and carbonaceous matter, and along with alteration has facilitated the precipitation of the uranium bearing minerals.

Keywords: *Gogi-Kanchankayi, Shahabad limestone, Bhima Basin and Uranium Mineralisation*

Introduction

The geochemistry of the carbonate rocks serves as potential tool for evaluating the depositional conditions, degree of diagenesis, tectonic settings, post sedimentation tectonics and provides insights to carbonate deposition (Nagarajan et al., 2011; Sen and Mishra, 2015). Although limestones primarily contain CaCO₃, it also comprises of various forms of major and trace elements that are attributed to terrigenous materials and scavenging from seawater (Elderfield and Greaves, 1982). The SiO₂, Al₂O₃, Fe₂O₃, P₂O₅ reflects the mineralogical nature of the carbonates while Mg, Sr, Ba are guiding tools in carbonate facies and diagenesis (Kamber and Webb, 2001; Madhavaraju et al., 2016). Holser (1997) has demonstrated that the elemental type and concentration depends on the plate tectonic environment of the basins. Limestones are liable to post-depositional recrystallization that obliterates primary texture; therefore the relationship between geochemistry of limestones and petromineralogical investigations provide criteria for recognizing ancient plate tectonic environments and secular changes in the chemistry of seawater (Webb and Kamber, 2000). From Gogi-Kanchankayi area the published literature describes the different modes of uranium minerals and pyrite within the deformed Shahabad limestones however; there is a gap in the detailed petrology and geochemistry of the undeformed and non-mineralised

limestones of this limestone sequence. The present study focuses on understanding the nature of the Shahabad limestone from Gogi-Kanchankayi traverse (~8 sq. km) and the post sedimentation basin tectonics impact in hosting uranium mineralisation.

Geological Setting

Bhima Basin occurs on the north-western fringe of the Eastern Dharwar Craton and is one of the youngest Meso-Neoproterozoic basins of Peninsular India (Kale and Phansalkar, 1991) (Fig. 1). It is an epicratonic sigmoidal basin where the northern and western extensions are covered by Deccan Trap basaltic flows and, the southern and eastern parts unconformably overlie the basement crystalline rocks comprising of TTG suite of rocks and Closepet Granite and its equivalents (Kale and Peshwa, 1995). Lithostratigraphic succession of the basin by Jayaprakash (1999), shows the Bhima sediments comprising of five formations (Table 1). The Bhima basin exhibits a sequence of an alternation of clastic and carbonate rocks (Akhtar, 1977; Nagarajan et al., 2007). Structurally, the basin is transacted by prominent E-W and NW-SE trending faults besides a number of N-S and NE-SW trending faults. The sediments of the basin are devoid of metamorphism (Kale and Peshwa, 1995).

The Gogi-Kanchankayi is located in the central part of the basin in the vicinity to Kurlagere-Gogi-

Gundanahalli fault (KG fault) (Fig. 2). The KG fault is an east-west trending, ~ 55 km long basin-margin fault that cuts across the sedimentary succession as well as the basement (Chaki et al., 2004). Lithologically, the southern part of the fault exposes basement granitoids while the northern part is occupied by sediments (Achar et al., 1997; Dhana Raju et al., 2002). The area between Gogi-Kanchankayi is largely covered by soil with

extensive cultivated lands and limited outcrops. Earlier structural studies on KG fault by the Geological Survey of India (GSI) identified it as a basin margin fault with discernible strike-slip component. Later surface and sub-surface investigations by Atomic Minerals Directorate (AMD) revealed the reverse nature of the fault near Gogi with presence of a cross-fault. Due to reverse faulting, basement granite from the south thrust

Table 1: Stratigraphy of the Bhima Basin

After Jayaprakash (1999)				
Group	Formation	Member	Lithology	
Deccan Trap			Basic flows with inter-trappean sediments	
Bhima Group	Harwal		Brown, pink to vermillion shale	
	Katama devarahalli		Deep grey, occasionally stylolitic flaggy limestone	
	Hulkal		Grey, blackish buff, dull and pale pink shale, occasionally with fine grained thin silty beds at the base	
	Shahabad	Mulkod Limestone		Deep grey to black flaggy limestone
		Gudur Limestone		Akin to Wadi limestone, yet slightly inferior in chemical composition
		Sedam Limestone		Variegated medium to thickly bedded siliceous limestone
		Wadi Limestone		Thickly bedded, stylolitic, relatively superior cement grade limestone
		Ravoor Limestone		Flaggy limestone with prominent fissility (Shahabad slabs)
	Rabanpalli	Korla shale		Fine silty base, grades into green shale, followed by chocolate brown shale with prominent parting
		Kundrapalle Sandstone		Fine grained quartz arenite, subfelspathic arenite, ferruginous cemented medium grained quartz arenite
Muddebihal Conglomerate			Pebbly orthoconglomerate, locally or at the top matrix supported and also granular	
-----Unconformity-----				
Basement Crystallines	Younger Granites, Eastern Block Greenstone Belt, Peninsular Gneisses.			

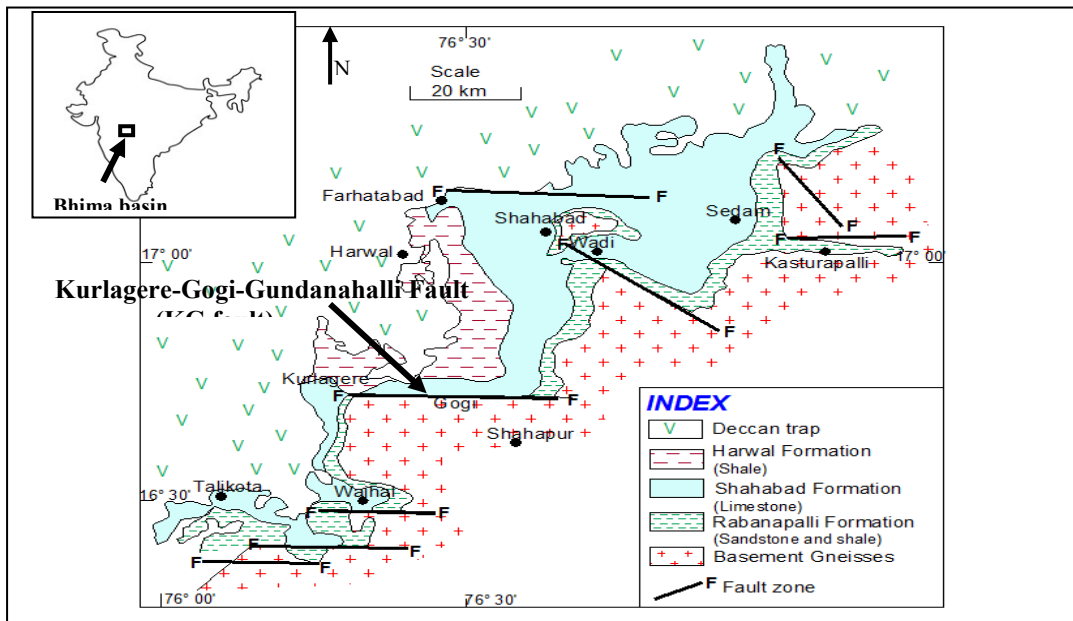


Fig. 1: Regional geological map of Bhima basin showing the location of Kurlagere-Gogi-Gundanahalli fault (modified after Kale and Peshwa, 1995)

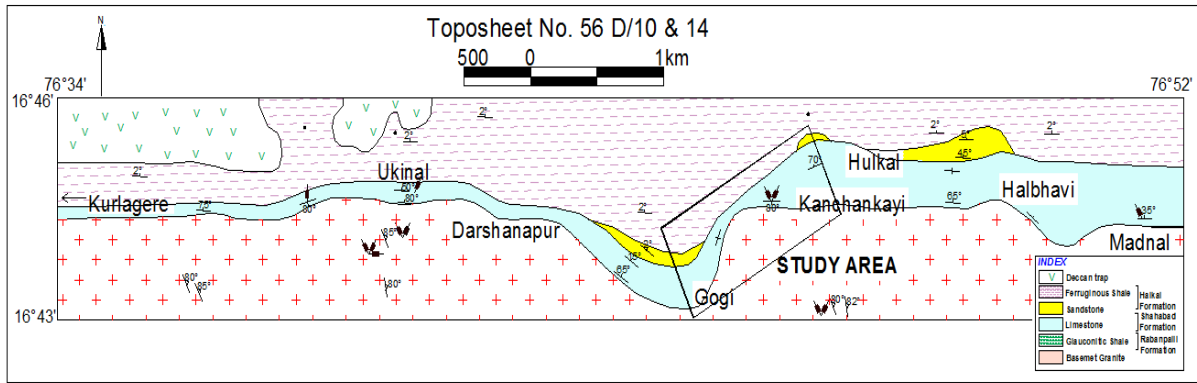


Fig. 2: Geological map around Kurlagere-Gogi-Gundanahalli fault showing the study area (modified after Achar et al., 1997)

over sediments in the north forming a southerly dipping fault (Fig. 3). Recent structural studies by Roy et al. (2016) describe the KG fault as a strike-slip fault with a transpressional zone at Gogi-Kanchankayi sector. In the Gogi-Kanchankayi area the imprints of faulting within the sediments are recorded in the limestones of Shahabad Formation (Fig. 4).

Sampling and Methodology

The study field transect has scanty outcrop and largely covered by soil, hence the research objectives were carried out from sub-surface core samples repository (n=21) of AMD. Petromineralogy study of

the polished thin section was carried out in the petrology laboratory of AMD, using a transmitted and reflected light microscope fitted with the image processing unit. Whole rock composition and trace elements were analysed by conventional wet chemical methods at the Chemistry laboratory of AMD. The SiO₂ and P₂O₅ were analysed by UV-visible spectrophotometry (Specord 210); Na₂O, K₂O by flame photometry and LOI by gravimetric methods. FeO is measured by volumetry, TiO₂, Al₂O₃, Fe₂O₃, MnO, CaO, and trace elements were analysed by AAS (Savant AA-GBC scientific Equipment) and ICP-AES (Jy-2000, GBC-Australia).

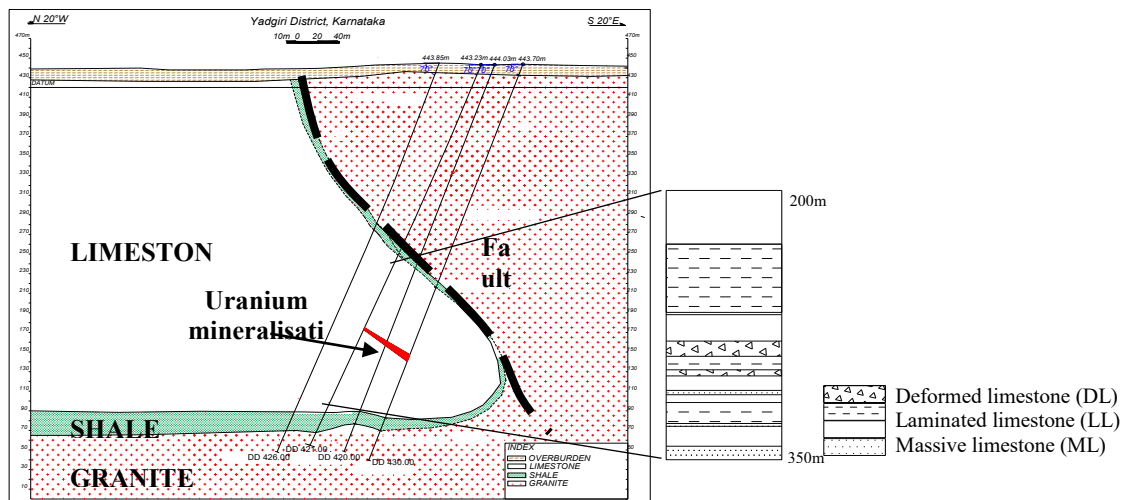


Fig 3: Representative transverse section through boreholes from Kanchankayi area (study area). The dotted line represents trace of the fault plane, inset shows the broad lithology of different types of limestones encountered in the boreholes and red zone shows the uranium mineralisation within the deformed limestones.

Petrography

The sedimentary core section shows three different types of facies of limestone i) laminated/flaggy limestone ii) massive/blocky limestone and iii) argillaceous/siliceous limestone. The post-sedimentation deformation, due to reactivation of the basin margin KG fault has resulted in intense fracturing and brecciation within all the three facies of limestone and it is classified as deformed limestone facies (Fig. 3). The laminated/flaggy limestone (LL) displays alternate light and dark grey laminations, micritic nature with

distinct conchoidal fracture (Fig. 5). Silica and calcite veins are parallel to the laminations. The laminations are straight to slightly curvilinear in nature, near parallel to each other with a thickness varying from 0.2-1.0 cm. At places, lenses of clay and packs of quartz grains are forming a load structure causing bending of lamination. Patches of small lumps of pyrite are dispersed throughout the facies. Besides, gypsum, specks of dolomite and barite are noticed. Stylolites are scanty. Microscopically, these samples exhibit cryptocrystalline texture with alternate light and dark lamination (Fig. 6). The recrystallized microspar and sparry calcite are

frequently seen in the facies. The passive filling of the pores and fractures and globular masses of organic matter are noticed at places. The presence of pyrite and

carbonaceous matter in the facies suggests existence of the patches of microbial colonies during the deposition of this facies.

Table 2: Major element concentration (wt%) of undeformed Shahabad limestone from Gogi-Kanchankayi area

Sample No	Rock Type	SiO ₂	TiO ₂	Al ₂ O ₃	Fe ₂ O ₃	FeO	MnO	MgO	CaO	Na ₂ O	K ₂ O	P ₂ O ₅	LOI
L-1.	Laminated Limestone (LL)	4.58	0.05	2.11	4.05	0.15	0.02	0.32	52.80	0.12	0.24	0.05	40.47
L-2.		5.33	0.08	2.35	0.70	0.39	0.05	0.57	52.30	1.61	0.63	0.13	35.10
L-3.		7.51	0.04	1.37	0.04	0.24	0.04	0.28	56.55	1.32	0.07	0.13	31.84
L-4.		8.82	0.04	1.47	0.11	0.30	0.03	0.75	46.07	2.66	0.34	0.06	38.69
L-5.		6.48	0.05	2.25	0.22	0.61	0.06	0.85	47.24	2.48	0.72	0.05	38.09
L-6.		5.54	0.04	1.62	0.23	0.49	0.05	0.81	47.50	2.66	0.38	0.08	39.32
L-7.		7.58	0.04	1.89	0.40	0.55	0.05	0.75	46.04	1.44	0.45	0.15	39.36
L-8.		6.56	0.05	2.10	0.62	0.42	0.03	0.82	47.10	1.36	0.66	0.13	40.12
L-9.		8.80	0.04	1.82	0.70	0.61	0.05	0.63	45.90	1.65	0.62	0.09	39.80
	Avg.	6.80	0.05	1.89	0.79	0.42	0.04	0.64	49.06	1.70	0.46	0.10	
M-1.	Massive Limestone (ML)	3.18	0.05	0.67	0.15	0.15	0.03	0.30	53.90	0.20	0.19	0.10	40.90
M-2.		4.69	0.05	1.14	0.05	0.39	0.02	0.50	53.06	0.32	0.33	0.05	40.42
M-3.		4.05	0.05	0.65	0.06	0.24	0.06	4.08	47.39	0.09	0.18	0.10	41.88
M-4.		4.89	0.04	1.57	0.28	0.30	0.05	0.49	51.20	1.06	0.23	0.06	39.62
M-5.		4.80	1.64	1.24	0.12	0.61	0.05	0.39	49.29	1.05	0.23	0.08	39.58
M-6.		3.20	0.02	0.72	0.11	0.49	0.03	3.11	53.65	0.32	0.22	0.05	38.09
M-7.		4.12	0.07	1.12	0.15	0.55	0.03	1.8	53.60	1.02	0.3	0.08	37.1
M-8.		3.85	0.05	0.76	0.2	0.2	0.03	2.62	51.85	0.09	0.2	0.06	39.65
	Avg.	4.10	0.25	0.98	0.13	0.35	0.04	1.66	51.74	0.52	0.23	0.07	
S-1	Siliceous limestone (SL)	30.05	0.06	1.27	0.09	0.30	0.03	0.23	38.80	0.18	0.36	0.30	29.25
S-2		32.51	0.05	1.18	0.10	0.38	0.07	0.37	36.90	0.12	0.29	0.19	28.24
S-3		29.05	0.06	1.37	0.09	0.30	0.06	0.35	36.80	0.18	0.36	0.30	30.25
S-4		30.51	0.05	1.21	0.11	0.30	0.07	0.27	37.90	0.13	0.29	0.20	28.24
S-5		31.25	0.05	1.36	0.08	0.30	0.07	0.31	38.90	0.13	0.29	0.20	26.24
S-6		30.85	0.06	1.25	0.09	0.36	0.06	0.23	37.80	0.14	0.36	0.30	29.25
	Avg.	30.70	0.05	1.27	0.09	0.32	0.06	0.29	37.85	0.15	0.33	0.25	
D-1.	Deformed /Mineralised Limestone (DL)	19.88	0.61	2.87	2.73	2.94	0.02	1.36	42.34	1.17	2.41	0.31	22.97
D-2.		17.41	0.51	4.84	3.26	2.11	0.02	0.57	42.66	0.92	1.56	0.15	23.08
D-3.		15.09	0.03	1.37	0.74	0.43	0.13	0.32	45.16	1.100	0.15	0.040	35.26
D-4.		16.65	0.11	3.47	14.65	2.16	0.29	0.53	33.01	0.940	0.46	0.170	25.93
D-5.		26.72	0.38	8.66	15.83	4.25	0.20	1.08	21.99	0.730	0.84	0.260	17.92
	Avg.	19.15	0.31	4.24	7.44	2.38	0.13	0.77	37.03	0.97	1.08	0.19	

The massive/blocky limestone (ML) is devoid of laminations and displaying light grey to yellowish grey colour (Fig. 7). Stylolites are distinct which are parallel, inclined and vertical with respect to the bedding plane (Fig. 8). Based on the geometry, the stylolites were classified as wavy and suture type which at places are filled with secondary calcite and pyrite. Secondary silica and twinned calcite veins are present. Minor deformation evidences like micro-faults, intraformational brecciation and shear bands are recorded at places.

The siliceous limestone (SL) is similar to ML but it varies in presence of grains of detrital quartz with less feldspars which is arranged in the form of layers resting over the micritic mass. In the core samples, silica banding is not visible but under microscope it shows parallel lamination (Figs. 9 and 10). This observation indicates the increase in the influx of the detrital material during its precipitation. The SL facies occurs intermediate between LL and ML facies indicating episodic supply of siliciclastic materials.



Fig 4: Steeply dipping limestones reflect surface expression of the Kurlagere-Gogi-Gundanahalli fault. Location: West of Gogi.

Deformed limestone (DL) is the result of post depositional deformation (faulting). This facies is moderate to highly brecciated, altered and having angular clasts of limestone of different sizes cemented by secondary calcite and chloritic cement (Fig. 11). Mineralogically, it is composed of micritic and sparry calcite along with varying amounts of quartz, chalcedony, chert, feldspar, barite, chlorite, clay, limonite, illite and sulphides. It is rich in sulphide veins, predominantly pyrite along with cross cutting calcite and silica veins (Fig. 12). Few core samples are dark grey in colour containing carbonaceous matter and clasts of basement granite and shale. Faulting and subsequent fault related fluid movement has resulted in its extensive hydrothermal alteration.

Geochemistry

Major Elements

Major element concentrations of the LL, ML, SL and DL are presented in Table 2. It is observed that the CaO in the LL and ML varies from 45.90% to 56.55% (avg. 49.06%, n = 9) and to 47.39% to 53.90% (avg. 51.74%, n = 8) respectively. Six samples analysed from (SL) horizon show lower CaO as compared to LL and ML i.e. 36.80% to 38.90% (avg. 37.85%, n = 6). SiO₂ content in LL and ML is 4.58% to 8.82% (avg. 6.80%) and 3.18% to 4.89% (avg. 4.10%) respectively, while in SL it is 29.05% to 32.51% (avg. 30.70%) indicating significant clastic input compared to LL and ML. SiO₂ vs CaO in LL and ML depicts a negative correlation, suggesting a relatively lower carbonate precipitation rate during clastic influx (Fig. 15a). The P₂O₅ and MgO content of LL, ML and SL vary from 0.05% to 0.30% and 0.30% to 4.08% respectively, indicating a low Mg and low P type. Al₂O₃ shows wide variations from 0.65% to 2.35%. A positive correlation exists between SiO₂ vs P₂O₅ in LL while SL is more phosphatic than the other two types of limestones (Fig.

15b). A scattered relationship between Sr and Al₂O₃ in all three types of limestones indicates the absence or insignificant proportion of the plagioclase as one of the phases (Fig. 15c). A relatively higher concentration of Fe₂O₃ in one sample (L-1) is probably the reflection of the clay minerals associated with it. MnO in all of the samples varies within a range of 0.02% to 0.07%. The low MnO content is subtle to the fact that it was deposited in the shallow marine environment in low energy conditions. The LL, ML and SL samples recorded low content of TiO₂, Na₂O and K₂O.

In DL it is observed that the CaO varies from 21.99% to 45.16% (avg. 37.03%) which is lower than that of the undeformed limestone indicating removal of carbonate minerals. In DL, there is an increase in SiO₂ content ranging from 15.09% to 26.72% (avg. 19.15%) as compared to LL and ML. The high SiO₂ content of SL is due to the presence of silica as detritus while elevated SiO₂ content of DL corresponds to the presence of silica veins formed during deformation and subsequent hydrothermal alterations. The P₂O₅ and MgO content of DL remains the same as in LL, ML and SL (Fig. 15d). The variation of CaO and SiO₂ between the deformed and undeformed limestones is shown in the binary plot (Fig. 15e). This also shows a negative correlation in deformed limestone. There is an increase of Al₂O₃ and Fe₂O₃ in DL possibly due to clay formation in the deformed and mineralised zone. K₂O/Al₂O₃ vs MgO/Al₂O₃ infers the clay is mostly illite (Fig. 15f).

Trace elements

Trace element concentration of LL, ML and SL (n = 23) displays the low concentration of Cu, Co, Ni, Zn, Mo with an enriched concentration of Sr, Rb and Ba (Table 3). The ML showed up to 1888ppm of Ba and Sr up to 202 ppm which is lower than the average Proterozoic carbonates (Sr = 610 ppm, Turekian and Wadepohl, 1961). The Ba content is higher as compared

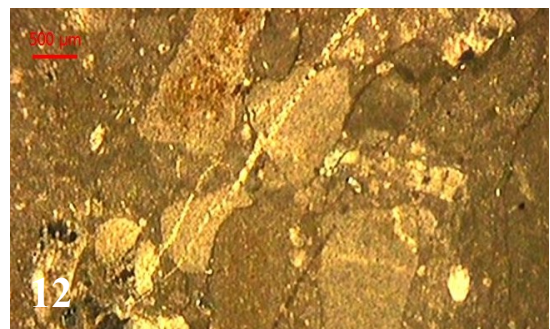
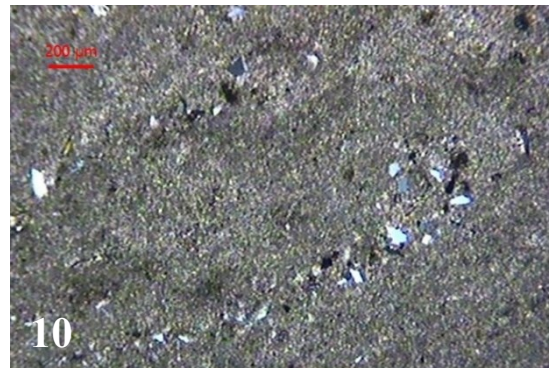
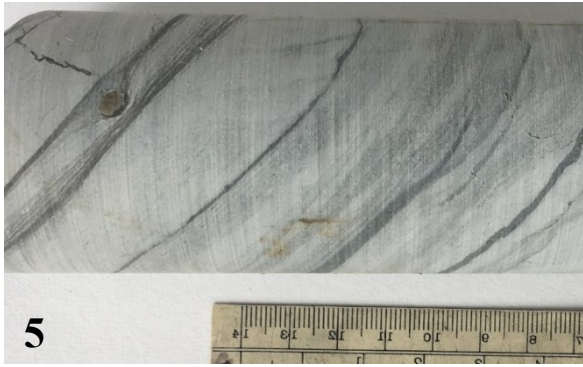


Fig. 5: Core of laminated limestone showing alternate dark and light colour laminations and a small lump of pyrite; location: Kanchankayi; Core size: NQ (Dia-47.6mm) Fig. 6: Photomicrograph of laminated limestone showing the persistent parallel lamination and clay lenses, 5X, TL, 1N. Fig. 7: Massive limestone with stylolites; Location: Kanchankayi; Core size: NQ (Dia-47.6mm) Fig. 8: Massive limestone with parallel stylolites, 5X, TL, 1N. Fig. 9: Siliceous limestone; Location: Kanchankayi; Core size: NQ (Dia-47.6mm) Fig. 10: Siliceous limestone with detrital fragments of quartz parallel to laminations; 5X, TL, 1N. Fig. 11: Deformed limestone showing brecciation and alterations; Location: Kanchankayi; Core size: NQ (Dia-47.6mm). Fig. 12: Brecciated limestone with brecciated fragments of micrite and sparry calcite are set in micritic limestone. 5X, TL, 1N.



Fig. 13: Core of brecciated pyritiferous uranium mineralised limestone; location: Kanchankayi; Core:NQ (Dia-47.6mm)

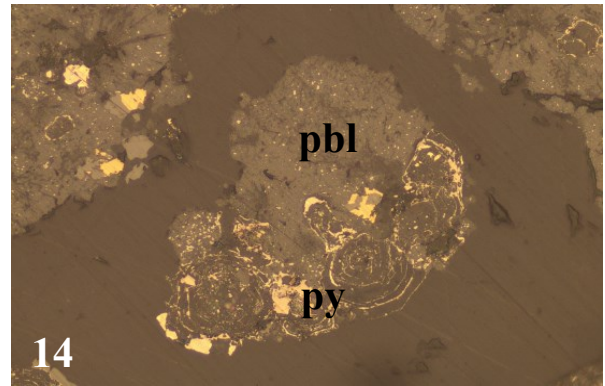


Fig. 14: Photomicrograph of mineralised limestone showing pitchblende (pbl) and pyrite (py) association, 20X, RL, XN

to the marine carbonate i.e. <60 ppm (Friedman, 1969). The abundance of Mn and Sr has been recognised as an interpretive tool to evaluate the diagenetic history of the carbonate (Viezer, 1983). Mn may be incorporated and Sr may be expelled from the carbonate system during diagenesis (Viezer, 1983). Mn/Sr ratio of 1-3 is accepted as an indicator of diagenetically unaltered limestone (Viezer, 1983; Jacobsen and Kaufman, 1999). The Mn/Sr ratio for the LL and ML is < 3 indicating these limestones were not subjected to severe diagenetic

alteration. Mn/Sr ratio for SL is >3 and this may be due to the presence of higher amount SiO₂. Trace element concentration of the DL (n = 5) shows contrast with respect to undeformed limestone (Table 4). It comprises of elevated concentration of Cu (18 - 490ppm), Co (65-770ppm), Ni (12 - 85ppm), Zn (10-165ppm), Mo (15-85ppm) and Cr (20 - 195ppm). The high concentration of the trace elements within the deformed limestone is attributed to the post sedimentation tectonics and followed by hydrothermal alterations.

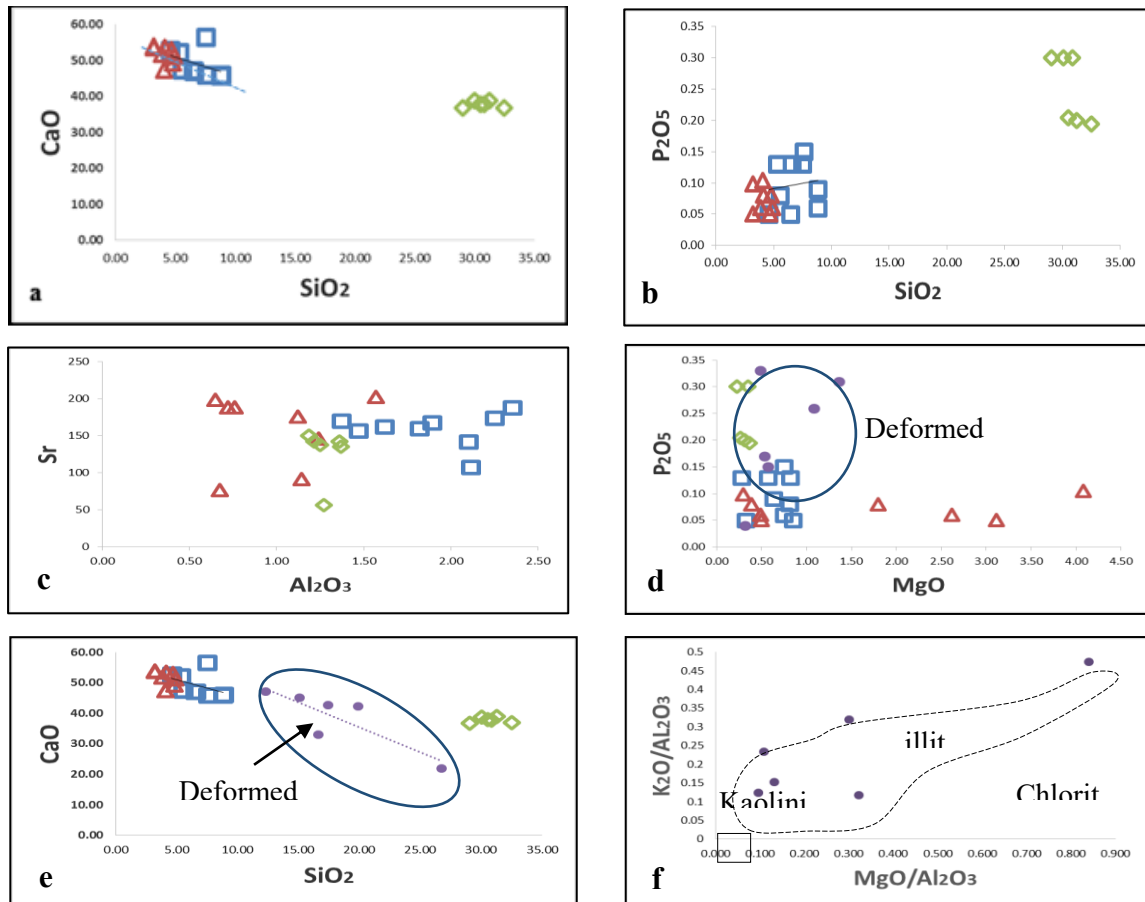


Fig 15 (a-f): Bivariate plots for the Shahabad limestones.

■ Laminated limestone
 ▲ Massive limestone
 ◆ Siliceous
 ● Deformed limestone

Uranium mineralisation

In Gogi-Kanchankayi sector, uranium mineralisation is associated with deformed limestone (DL). The deformation is due to the post-sedimentation tectonic movement along the KG fault which has resulted in the development of fracture and breccia zones, induced secondary porosity in the LL, ML and SL facies of Shahabad Limestone thus aiding in the generation and migration of the uranium rich hydrothermal fluids. The younger granitoids of Closepet equivalent, within the basement, are the likely source for uranium rich hydrothermal fluids. Pitchblende and

coffinite uranium minerals were identified (Fig. 13). The fracture/breccia zones within LL, ML and SL are rich in sulphides and carbonaceous matter that host the uranium mineralisation. Pyrite is the major constituent of sulphides and occurs in different morphological and textural varieties viz., lumpy, reticulate, botryoidal, oolitic, porous and zoned. Besides, other ore minerals identified are galena, chalcopyrite, pyrolusite, arsenopyrite, nicolite and cobaltite. The mineralised zones are invariably associated with sulphides and carbonaceous matter (Fig. 14). Patnaik et al. (2016) re-

Table 3: Trace element concentration (ppm) of undeformed Shahabad limestone from Gogi-Kanchankayi area

Sample No	Rock Type	Cu	Co	Ni	Rb	Zn	Pb	V	Sr	Zr	Mo	Ba	Ga	Mn	Mn/Sr
L-1.	Laminated Limestone (LL)	<10	<10	<10	11	<10	<25	<10	107	10	<10	56	<10	158	1.47
L-2.		12	<10	<10	11	<10	30	<10	188	<10	<10	60	<10	387	2.06
L-3.		<10	<10	<10	11	10	30	<10	170	<10	<10	82	<10	310	1.82
L-4.		10	<10	<10	9	<10	<25	<10	157	15	<10	145	<10	232	1.48
L-5.		<10	<10	<10	32	<10	<25	23	174	12	<10	80	<10	465	2.67
L-6.		<10	<10	<10	12	12	<25	<10	162	10	<10	175	<10	387	2.39
L-7.		<10	<10	<10	20	12	<25	<10	168	10	<10	150	<10	387	2.36
L-8.		<10	<10	<10	12	<10	30	<10	142	<10	<10	96	<10	232	1.62
L-9.		<10	<10	<10	18	10	<25	<10	160	12	<10	142	<10	387	2.42
M-1.	Massive Limestone (ML)	<10	<10	<10	10	10	<25	<10	77	10	<10	52	<10	226	2.94
M-2.		<10	<10	<10	18	10	<25	<10	92	10	<10	46	<10	168	1.82
M-3.		10	<10	<10	10	<10	<25	10	198	<10	<10	1888	<10	503	2.53
M-4.		10	<10	<10	10	<10	<25	10	202	<10	<10	560	<10	387	1.91
M-5.		14	<10	<10	15	<10	30	<10	116	<10	<10	48	<10	387	2.65
M-6.		<10	<10	<10	18	10	<25	<10	188	10	<10	72	<10	232	1.23
M-7.		<10	<10	<10	12	12	<25	<10	176	10	<10	72	<10	232	1.32
M-8.		10	<10	<10	10	10	<25	<10	188	<10	<10	250	<10	232	1.24
S-1	Siliceous limestone (SL)	<10	<10	<10	16	15	<25	<10	57	16	<10	107	<10	223	3.95
S-2		<10	<10	<10	10	10	<25	<10	150	11	<10	98	<10	536	3.56
S-3		<10	<10	<10	12	<10	<25	<10	135	11	<10	120	<10	456	3.37
S-4		<10	<10	<10	11	12	<25	10	142	12	<10	110	<10	536	3.77
S-5		<10	<10	<10	11	12	<25	10	142	12	<10	110	<10	542	3.81
S-6		<10	<10	<10	12	11	<25	10	138	12	<10	105	<10	464	3.36

Table 4: Trace element concentration (ppm) of deformed Shahabad limestone from Gogi-Kanchankayi area

Sample No	Rock Type	Cu	Co	Cr	Ni	Zn	Pb	V	Zr	Mo
D-1.	Deformed /Mineralised Limestone (DL)	490	65	195	25	165	1770	693	55	85
D-2.		155	770	175	65	150	7825	1545	50	25
D-3.		18	85	20	12	25	259	118	30	15
D-4.		75	152	65	30	10	375	50	60	15
D-5.		100	350	60	85	120	290	525	60	50

ported that the TOC content for mineralised deformed limestone varies from 34.3- 51.1 wt% (avg. 42.27wt %,

n = 4). The undeformed Shahabad limestone is the probable source for the carbonaceous matter and sulphi-

des which are re-mobilised and re-precipitated during deformation and act as a reductant for precipitation of uranium from the hydrothermal fluid within the fractures. The prominent hydrothermal alteration along the mineralised zone are chloritisation, silicification, calcification, hematitisation, illitisation and kaolinisation, which are distinct from the non-mineralised limestones. Hydrothermal alteration has resulted in depletion of CaO, with an increase in SiO₂, Al₂O₃, Fe₂O₃, Cu, Co, Ni, Zn, Mo and Cr. The depletion of CaO is an indication of the dissolution of limestone by hydrothermal fluid developing secondary porosity. The sulphides and carbonaceous matter along with alterations in the fracture zones have controlled the reduction of uranium from the hydrothermal fluids.

Conclusions

The study of sub-surface limestone core samples from Gogi-Kanchankayi sector revealed three different types of facies viz. massive/blocky, argillaceous/siliceous and laminated/flaggy limestones. The results of this study suggest that these limestones are micritic, non-dolomitic and non-phosphatic in nature with quartz (as detrital grains), sulphides (pyrite) and patches of carbonaceous matter as impurities. These limestone facies were deposited under shallow marine setting in low energy conditions with Mn/Sr ratio range of 1.4 to 3.5 indicating that these rocks are partially diagenetically altered.

Post sedimentation deformation associated with faulting resulted in the development of fractures and breccia zones, inducing secondary porosity and thus aiding the migration of hydrothermal fluids. Precipitation and deposition of remobilised sulphides and carbonaceous matter along with alteration in the fracture / breccia zones during pre-ore and syn-ore stages facilitated adsorption and reduction of uranium from the hydrothermal fluids.

Acknowledgement

The authors are thankful to the Director AMD, for granting permission to publish this work. Constructive suggestions and comments by anonymous reviewers which helped in improving the quality of the manuscript are thankfully acknowledged. Colleagues in the Chemistry laboratory, AMD, Bengaluru are gratefully acknowledged for providing the analytical facilities.

References

Achar, K.K., Pandit, S.A., Natarajan, V., Kumar, M. K. and Dwivedy, K.K. (1997). Uranium mineralisation in the Neoproterozoic Bhima Basin, Karnataka, India. In: Recent Developments in Uranium Resources, Production and Demand, IAEA, Vienna, 1-22.

Akhtar, K. (1977). Depositional environment, dispersal pattern and palaeogeography of the clastic sequence in the Bhima Basin. *Indian Mineralogist*, 18, 65-72.

Chaki, A., Pandit, S.A. and Achar, K.K. (2004). An appraisal of uranium exploration in the Kaladgi-Badami and

Bhima basins in Karnataka and identification of potential targets for uranium exploration by Geophysical Methods. *Exploration and Research for Atomic Minerals*, 15, 13-24.

Dhana Raju, R., Kumar, M.K., Babu, E.V.S.S.K. and Pandit, S.A. (2002). Uranium mineralisation in the Neo-Proterozoic Bhima Basin at Gogi and near Ukinal – Ore petrology and mineral chemistry. *Journal of the Geological Society of India*, 59, 299-321.

Elderfield, H. and Greaves, M.J. (1982). The rare earth elements in seawater. *Nature*, 296, 214-219.

Friedman, G.M. (1969). Trace elements as possible environmental indicators in carbonate sediments. In Friedman G.M. (Ed.), Dolomitisation and limestone diagenesis. *Society Econ. Paleon. Mineral Special Publication*, 13, 14-48.

Holser, W.T. (1997). Evaluation of the application of rare earth elements to paleoceanography. *Palaeogeography, Palaeoclimatology, Palaeoecology*, 132, 309-323.

Jacobsen, S.B. and Kaufman, A.J. (1999). The Sr, C and O isotopic evolution of Neoproterozoic seawater. *Chemical Geology*, 161, 37-57.

Jayaprakash A.V. (1999). Evolutionary history of Bhima basin. (V.S. Kale and R.H. Sawkar, Compilers), *Journal of the Geological Society of India*, 23-28.

Kamber, B.S. and Webb, G.E. (2001). The geochemistry of late Archaean microbial carbonate: Implications for ocean chemistry and continental erosion history. *Geochimica et Cosmochimica Acta*, 65, 2509-2525.

Kale, V.S. and Phansalkar, V. G. (1991). Purana basin of Peninsular India: a review. *Basin Research*, 3, 1-36.

Kale, V.S. and Peshwa, V.V. (1995). Bhima Basin. *Geological Society of India publication*, Bangalore, 10.

Madhavaraju, J., Löser, H., Lee, Y.I., Santacruz, R.L. and Pi-Puig, T. (2016). Geochemistry of Lower Cretaceous limestones of the Alisitos Formation, Baja California, Mexico: Implications for REE source and paleo-redox conditions. *Journal of South American Earth Sciences*, 66, 149-165.

Nagarajan, R., Madhavaraju, J., Nagendra, R., Altrin, J.S.A. and Moutte, J. (2007). Geochemistry of Neoproterozoic shales of the Rabanpalli Formation, Bhima Basin, Northern Karnataka, southern India: implications for provenance and paleoredox conditions. *Revista Mexicana de Ciencias Geológicas*, 24, 150-160.

Nagarajan, R., Madhavaraju, J., Armstrong-Altrin, J.S. and Nagendra, R. (2011). Geochemistry of neoproterozoic limestones of the Shahabad formation, Bhima basin, Karnataka, southern India. *Geosciences Journal*, 15, 9-25.

Patnaik, S., Chakrabarti, K., Pradhan, A. K. and Bhattacharya, D. (2016). Petrographic characteristics of carbonaceous matter associated with brecciated limestone at Kanchankayi area, Yadgir district, Karnataka: Genetic implications for uranium mineralization. *Journal of Applied Geochemistry*, 18 (3), 119-124.

Roy, D., Bhattacharya, D., Mohanty, R., Patnaik, S., Pradhan, A.K., Chakrabarti, K. and Syed Z. (2016). Study of Deformation pattern in Gogi-Kurlagere fault zone at Gogi-Kanchankayi sector of Proterozoic Bhima Basin of northern Karnataka: its implication in control of uranium mineralisation. *Journal of Exploration and Research for Atomic Minerals*, 26, 157-176.

Sen, S. and Mishra, M. (2015). Geochemistry of Rohtas limestone from Vindhyan Supergroup, Central India: evidences of detrital input from felsic source. *Geochemistry International*, 53, 1107-1122.

- Turekian K. K. and Wedepohl, H. K. (1961). Distributions of the elements in some major units of earth crust. *Geological society of America bulletin*, 72, 175-192.
- Veizer, J. (1983). Trace elements and isotopes in sedimentary carbonates, in Reeder, R.J. (ed.), *Carbonates: Mineralogy and Chemistry. U.S.A, Mineralogical Society of America, Reviews of Mineralogy*, 11, 265-299.
- Webb, G.E. and Kamber, B.S. (2000). Rare earth elements in Holocene reefal microbialites: a new shallow seawater proxy. *Geochimica et Cosmochimica Acta*, 64, 1557–1565.

(Received: 17 September 2020; Revised version accepted: 30 May 2021)

Facies Evaluation and Depositional Environments of Carbonates of the Bagh Group, Dhar District, Madhya Pradesh, India

Sreejita Chatterjee¹ and Dhiren Kumar Ruidas²

1. Atomic Minerals Directorate for Exploration and Research, DAE, Jaipur 302033

2. Department of Geology, Government General Degree College, Purulia, 723131.

schatterjee.amd@gov.in

Abstract:

A significant event of marine transgression took place in Central India during Late Turonian-Coniacian. Fossiliferous marine succession of Bagh Group is one of the few carbonate successions exposed in peninsular India which was in focus of the current study for understanding this event. The signatures of this event were identified in the carbonate succession. The carbonates of Bagh Group are composed of two formations: the lower part is represented by Nodular limestone Formation which is overlain by Bryozoan limestone Formation at the top. On the basis of grain size variation and sedimentary structures, the Nodular limestone is divisible into three facies: facies 'A', facies 'B' and facies 'C'. A hardground exists between facies B and facies C. Lack of sedimentary structures and high mud content indicates low energy depositional setting for the Nodular limestone Formation. Similarly, Bryozoan limestone Formation is divisible into five facies: facies 'D', facies 'E', facies 'F', facies 'G' and facies 'H' based on grain size variation and sedimentary structures. All of these five facies are fossiliferous. Glauconites are present within facies 'G' and have two modes of occurrence - as infilling within Bryozoan limestone and as altered feldspar. Presence of both small- and large-scale cross-stratification in Bryozoan limestone with lesser mud content are indicative of high energy shallow marine conditions. Large-scale cross-stratifications are possibly representing tidal bars while the small scale cross stratifications are formed in inter bar setting. Presence of reactivation surfaces within facies 'E' also supports their tidal origin. Increase in depositional energy condition is also evident from dominated by packstone facies.

Keywords- *facies, bryozoan limestone, nodular limestone, wackestone, packstone, marine transgression, tidal origin*

Introduction

The Bagh Group of rocks is generally exposed in isolated inliers within the Deccan Traps in the West Central India covering an area of 4000 sq. km. (approx). The exposures are mainly on the northern flank of the river Narmada. It is generally believed that the trend of the Narmada represents a tectonic lineament of mid continental rift (Biswas, 1999) which was associated with the Karoo rift system of Africa (Bosellini, 1989). It was later reactivated during separation of India and Madagascar. The rifting guided the present configuration of the western margin of India along relatively straight coastline representing the rifted passive margin (Gombos et al., 1995). Rock succession of the Bagh Group is highly fossiliferous (Contains fossils of bivalves, gastropod, bryozoan, etc). This is one of the few carbonate successions, exposed in peninsular India. Its fossil content always has drawn attention of the experts in fields of paleontology, palaeoecology, biostratigraphy, etc. The Bagh Group is well exposed in and around Dhar district, Madhya Pradesh (Survey of India toposheet no. 46N/3, 46J/15), especially along the river banks of River Man. Deccan volcanics occur on top of the Mesozoic outcrops in many places. Extensive mining activities have exposed workable sections of the Bagh Group. The deposition took place in this intra-cratonic basin as the eastern arm of the Tethys transgressed (Chiplonkar et al., 1976;

Jafar, 1982). Thus the carbonate succession is the product of Late Turonian-Coniacian transgression (Bardhan, 2002).

Numerous works on fossils in this group warranted a detailed study on its sedimentological aspects to supplement paleontological observations. Hence, a detailed microfacies analysis of the carbonates of the Bagh Group was attempted in Ratitulai, Rampura, Man river section, Zirabad and Mohi in Dhar district incorporating field observations as well as petrographic study.

Geological Setting

The carbonates of the Upper Cretaceous Bagh Group of Central India represent a fossiliferous shallow marine sequence. It consists of the lower Nodular limestone and upper Bryozoan limestone formations. However, Kennedy et al. (2003) showed alternations of Nodular limestone and Coralline limestone (Bryozoan Limestone of the present case) in the Hatni *nala* section. The Nodular limestone Formation is underlain by the fluvio-marine siliciclastic Nimar Formation which, in turn rests on the Precambrian crystalline rocks (Sarkar, 1973). However, at Karondia (lat. 22° 22' 30" N, long. 75° 4' 00" E) and Man River section, the Nodular limestone rests directly over the Precambrian granitic basement with a non-conformable contact. The beds in the Man River section are almost sub-horizontal

whereas, in the area around Bagh Cave, these beds dip at 12° - 15° due north. One of the noteworthy feature of the Bagh Group is the occurrence of several hardgrounds in the carbonate succession (Ruidas et al.,

2020). Bose, et al. (1982), proposed the name 'Bryozoan Limestone' instead of 'Coralline Limestone' because of paucity of corals and the dominance of Bryozoans.

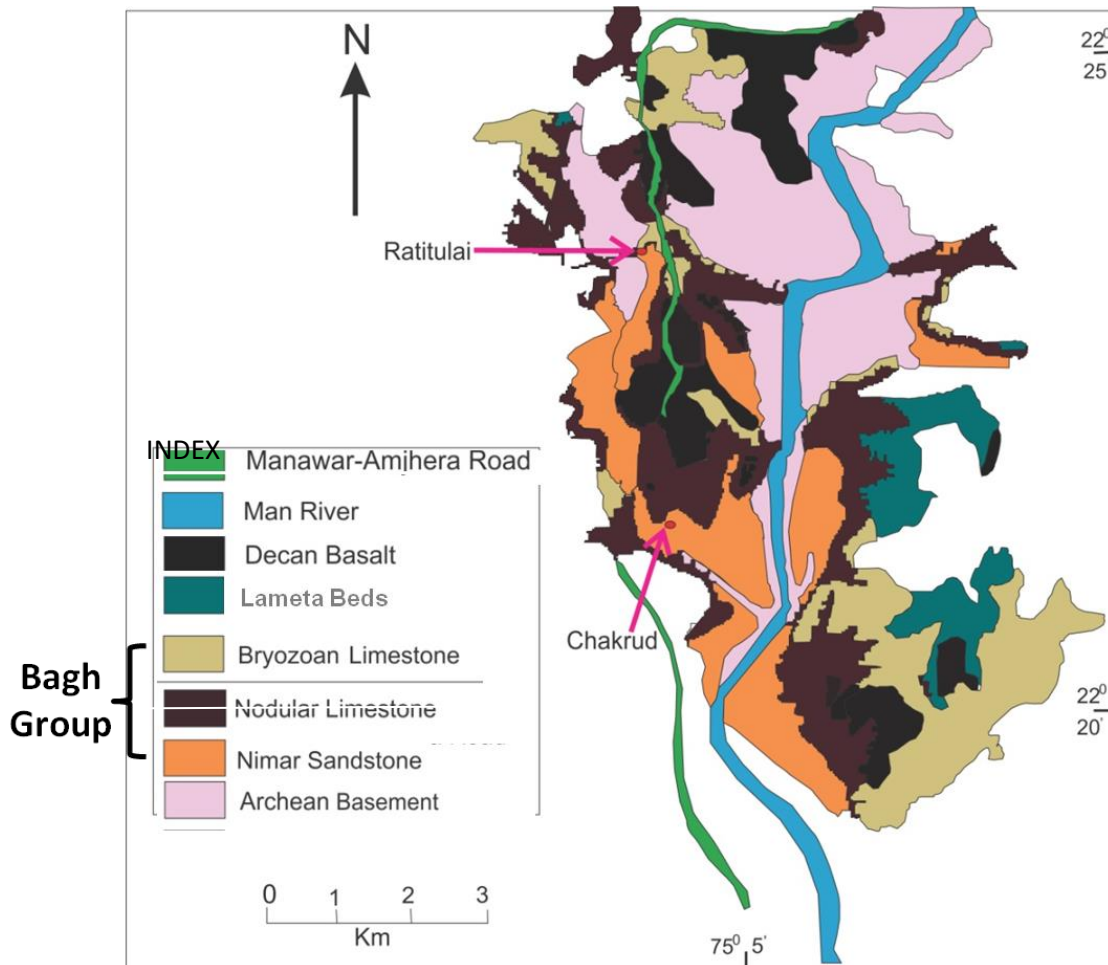


Fig. 1: Geological map of the study area (adapted from Khosla & Kapoor, 2003)

Materials and Methods

Detailed facies analysis through field observations and sampling of the Bryozoan Limestone of the Bagh Group at Ratitulai, Rampura, Chak road, Man River section, Zirabad, Mohi, Baria, Kosdana, Karondia, have been done. Litholog of the Bryozoan limestone from Baria (Fig-2) was prepared by taking traverse along the Man River (Fig-2). Grain size variation, different sedimentary structures, presence of burrows, etc. were minutely observed during the field work. As the beds dip very gently ($\sim 3^{\circ}$), care was taken to record the vertical sedimentary succession. Fresh samples were collected for petrography. Spot samples were collected for carrying out sedimentological and mineralogical analysis of glauconite. Thin sections were prepared using IsoMet Precision Saw (Buehler; 280-250; 0-300 rpm; 35cutting

capacity; gravity feed weight system with diamond cutting wheel). For Polishing EcoMet 3000 Slow Speed Precision GrinderPolisher (Buehler) was used. Petrographic observations were carried out using Leica DM 4500P polarizing microscope at the Department of Earth Sciences, IIT Bombay using both transmitted and reflected light with external stage micrometer (Scale: 1 mm/0.01 mm; Cole-Permar product).

XRD investigations were carried out using EMPYREAN diffractometer. Operating conditions were 40 mA, 45 kV with nickel filtered Copper Ka radiation and a 3-D Pixel detector. Samples were continuously scanned in a 2θ range of 60° with scan step size of 0.0260/ 100s. The samples were scanned in three modes, initially air dried mode, subsequently scanned in glycolation mode (after treating with ethylene glycol for 2 hours) and finally scanned in heating mode (after heating at 400°C for 30 minutes).

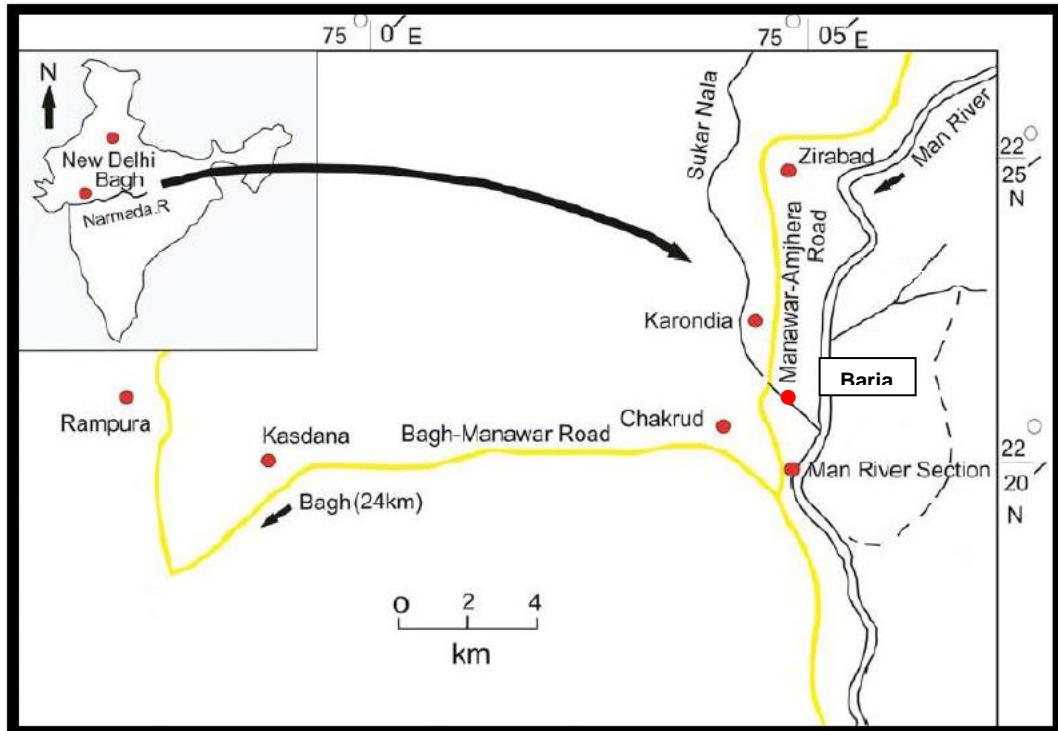


Fig. 2: Location map showing different study areas

Facies Description

Nodular Limestone

The Nodular limestones are exposed in Ratitulai, Rampura, Karondia, Chak road, Zirabad, Kosdana and Baria with maximum thickness of 7 m

at Karondia and overlain by Bryozoan limestone. The strata below this Nodular limestone is Nimar Sandstone, which is exposed in only one place (Near Bagh Cave). Nodular limestone is divisible into three facies- facies A, facies B and facies C (Fig-3,4)

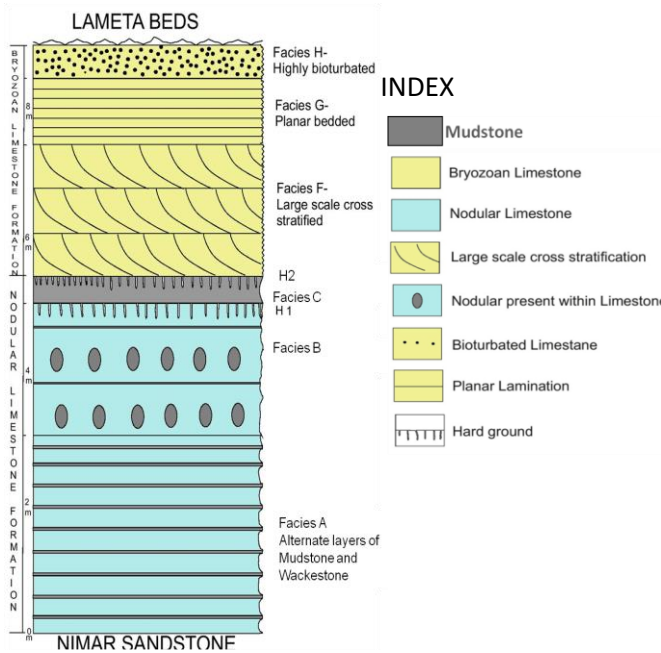


Fig. 3- Representative litholog (9m) of the Nodular limestone and the Bryozoan Limestone Formation of Bagh Group from Baria.

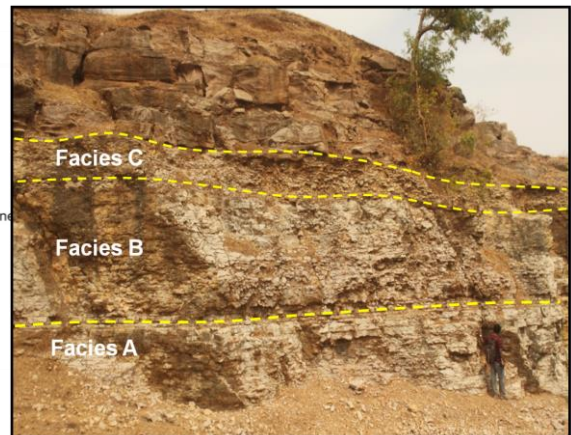


Fig. 4: Field photograph showing facies A, B & C

Description of Facies ‘A’: Mudstone-Wackestone Alternations. This facies is represented by alternate layers of mudstone and wackestone (Fig-5a). It attains a maximum thickness of 3m. The thickness remains more or less uniform laterally. Continuous beds are present at all the places. Bioturbation is rare. Ripple marks are present within thin mudstone layer. In the mudstone layer, micrite content is >95% (Fig-5b) and spar content <5%. In places, this mudstone is truncated by calcite veins (Fig-5b). In the wackestone layer, sorting is poor. Bioclasts (shells of gastropods, bivalves, foraminifers, etc. of varying sizes) are present as major allochems (Fig- 5c).

Description of Facies ‘B’: Highly Bioturbated Wackestone. In this facies bedded nature disappears and thickness of the mud layer decreases. This facies is nodular dominated (Fig-6a), formed due to chemical compaction, (Ruidas, et al., 2018). Size and shape of nodules are highly variable. The length: width ratio varies from 0.5 to 1.0 (Ruidas, et al., 2018). It is highly bioturbated and burrows are filled with silt sized particles (Fig-6b). Burrows are of both inclined as well as horizontal nature. Load casts are present at the base of this facies (Fig-6c). Pressure solution features are also found at many places. Within this facies, some patches, with high concentrations of *Turritella* shells are observed (Fig-6d). Shells of gastropods, bivalves and few foraminifers of varying sizes are present as bioclasts (Fig-6e). Sorting is poor. In some samples dissolution features are present. Bioclasts are mostly intact with few showing compaction features.

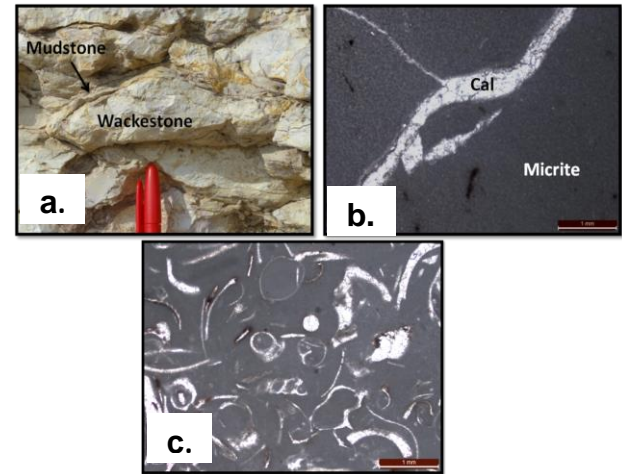


Fig- 5: a) Field photograph showing mudstone-wackestone alteration (scale = 3 cm),
 b) Photomicrograph of mudstone layer, PPL, 1N
 c) Photomicrograph of wackestone with bioclasts, PPL, 1N.
 Cal = Calcite

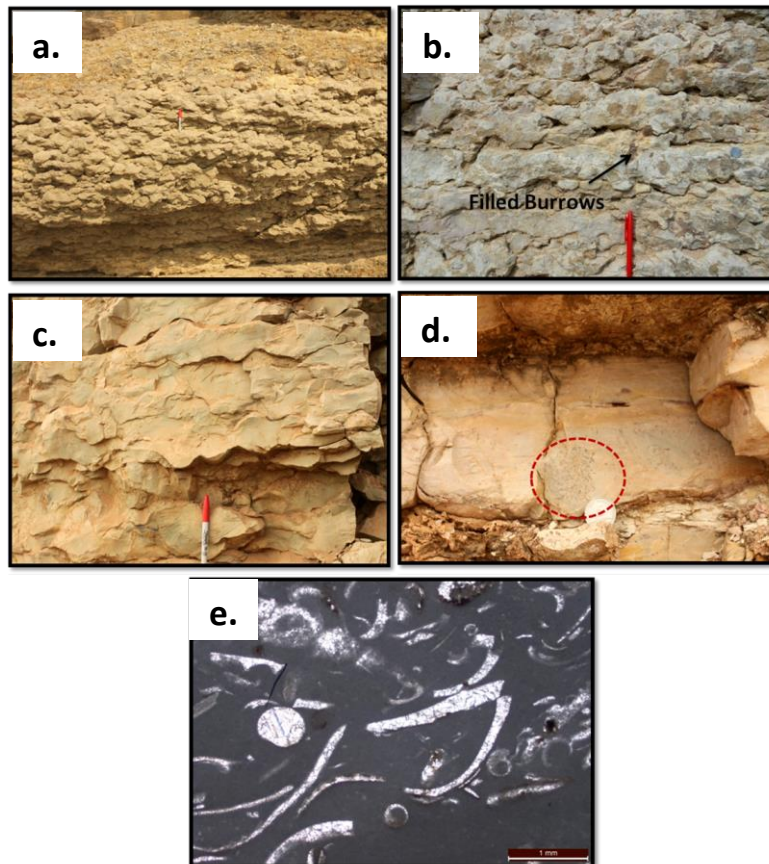


Fig-6: a) Field photograph showing nodular character of limestone, (scale= 14 cm) b) Bioturbated Nodular limestone; burrows filled with spar (scale= 14 cm), c) Load Casts in Nodular limestone (scale= 14 cm), d) Patches of *Turritella* shells, (scale= 2.5 cm), e) Photomicrograph of Wackestone, PPL, 1N.



Description of Facies ‘C’: Mudstone: This facies is locally developed and composed of mudstone (Fig-7a). This layer has a maximum thickness of 1.5m at Karondia. It is devoid of bioclasts (Fig-7b). A

hardground occurs between facies B and facies C (Fig-7c). Burrows are present within this hardground (Fig-7d).

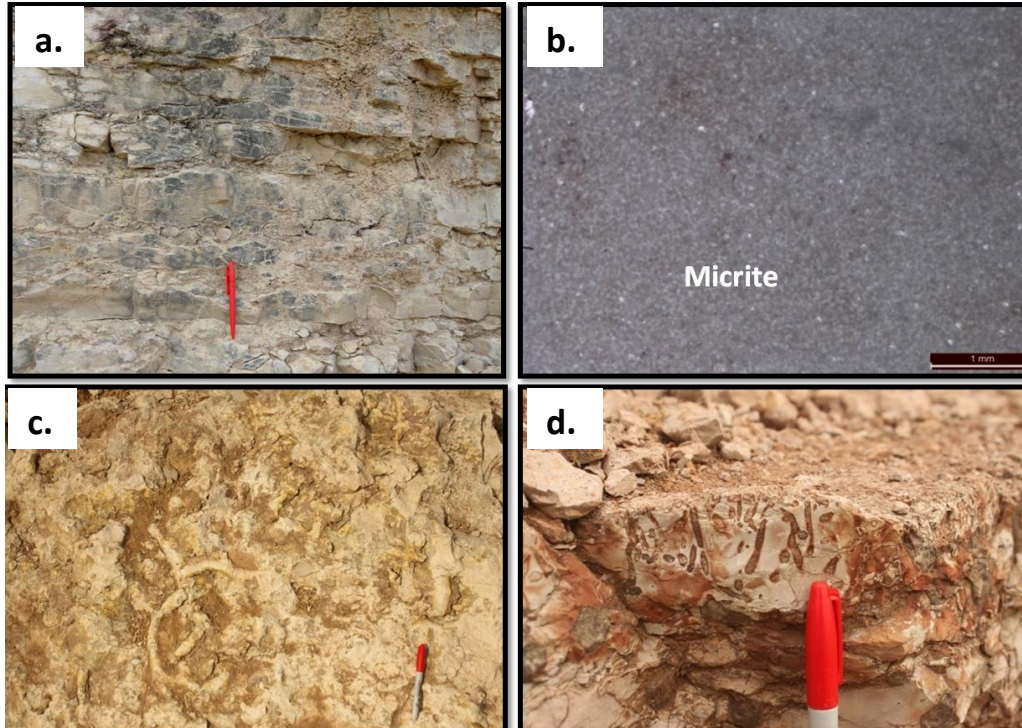


Fig-7: a) Field photograph of Mudstone, b) Photomicrograph of mudstone PPL, 1N, c) Field photograph of hardground, d) Burrows within hardground. (Scale= 14 cm).

Bryozoan Limestone

The Bryozoan Limestones (Fig-8a) are exposed in Ratitulai, Rampura, Karondia, Chak road, Zirabad, Kosdana, Baria. Maximum thickness of 4.5 meter was measured at Kosdana. At places, the Bryozoan Limestone is overlain by Deccan Trap, whereas at other places, like in Chak road, this is overlain by fluvial Lameta Formation. A highly bioturbated hardground

having a maximum thickness of 50cm exists between the Nodular limestone and the Bryozoan limestone formations (Fig-8b). Dominant bryozoa are *Cyclostome* sp. and *Cheilostome* sp. From bottom to top, micrite content decreases. Samples from different locations were collected at an interval of 30 cm and out of these 9 samples were studied under the microscope.

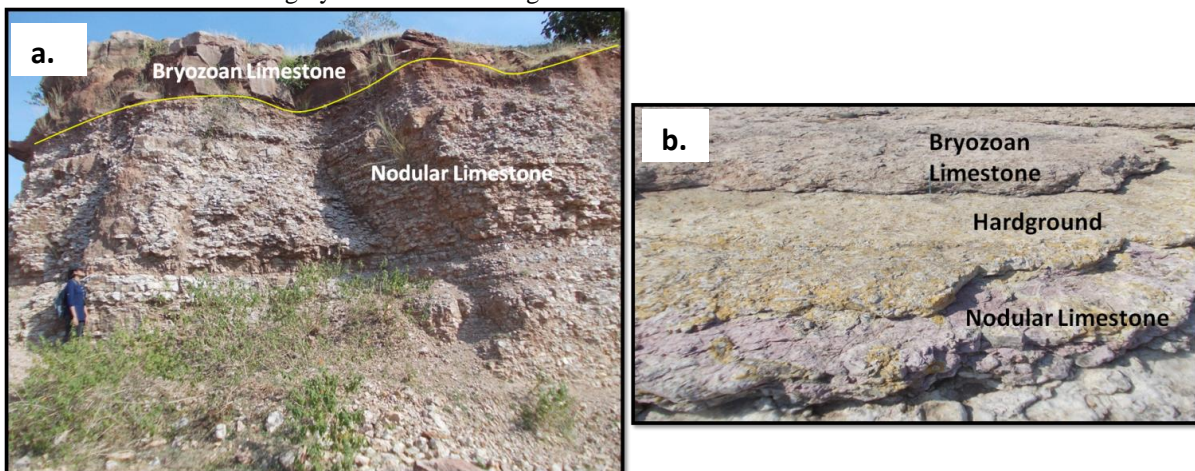


Fig-8: a) Field photograph of Bryozoan limestone overlying Nodular limestone, b) Field photograph of hard-ground between Nodular limestone and Bryozoan limestone. (Scale = 14.5 cm)

Description of Facies ‘D’: *In situ* wackestone. This is the lowermost facies, lying above Nodular limestone. This facies consists of bryozoan fossils of variable sizes (Fig-9a). Branching of bryozoa is preserved, thus indicates negligible reworking. Sorting is poor. This is a mud supported rock but contains >20% bioclasts (bryozoa). It gradationally passes upward to facies ‘E’.

Description of Facies ‘E’: Small-scale cross-stratified grainstone. This facies is exposed at Rampura and Mohi. Maximum thickness of this facies is 1 meter, exposed at Rampura. Bryozoans in this layer are

reworked. Small scale cross stratification have a dip of nearly 30° (Fig-9b). Cross-stratified beds are wavy, indicating dissolution. Reactivation surfaces are present at Zirabad. Ripples are asymmetric. Under the microscope, this is a grain supported rock with mud content <10% (Fig. 9). Skeletal particles include Bryozoa (~80%), and very few fragments of gastropods and echinoid spines are present (10-20%) and forming 90% of rock (Fig- 9c). Stylolites and sutured grain boundaries of bryozoan fossils are present at places. Sorting is poor.

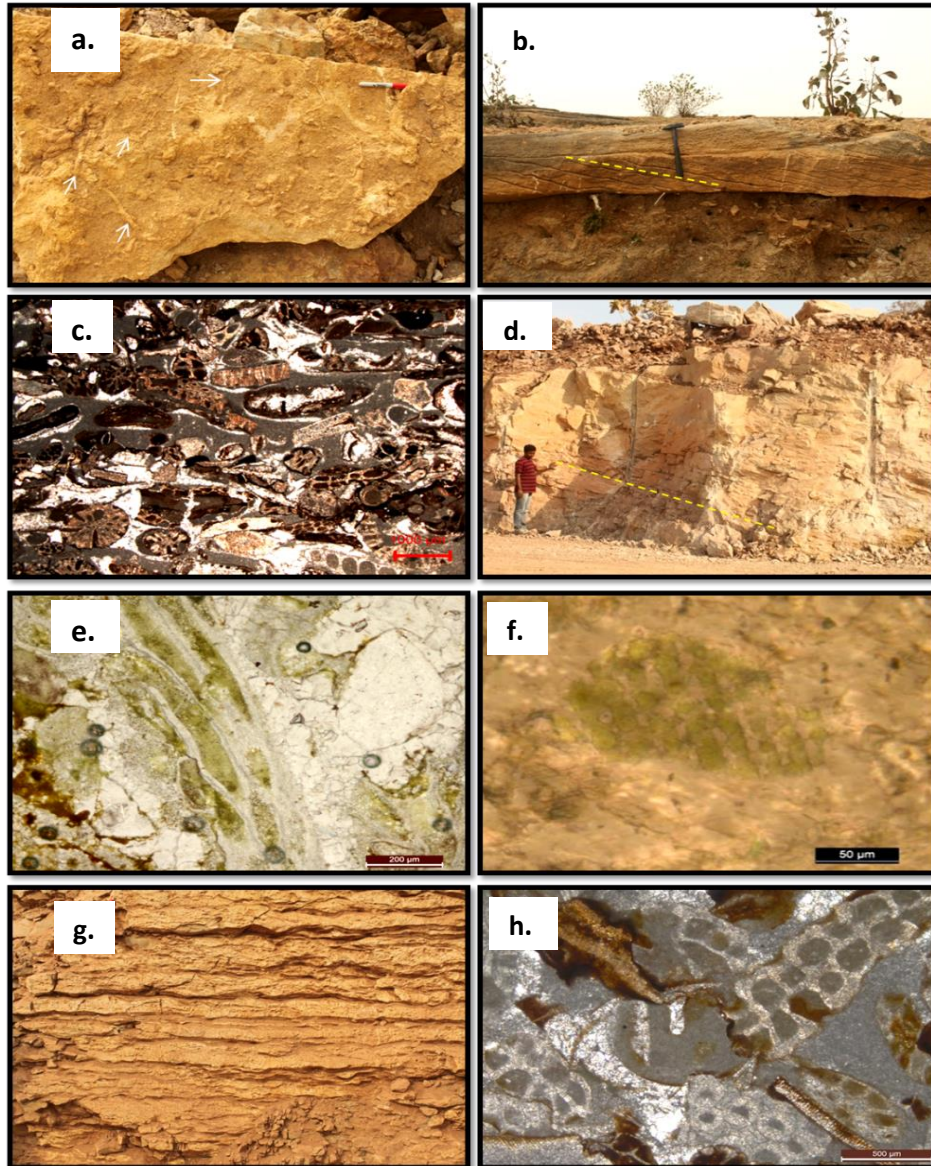


Fig- 9: a) *In situ* wackestone with bryozoa (scale = 14 cm), b) Field photograph of small scale cross stratification with reactivation surface (yellow trend line) (scale= 38 cm), c) Photomicrograph of grainstone PPL, 1N, d) Field photograph of large scale cross stratification (yellow trend line), e) Photomicrograph of Glauconite as infilling within bryozoa fossil, PPL, 1N, f) Photomicrograph of Glauconite as altered feldspar. PPL, 1N, g) Field photograph of planner laminated Wackestone, h) Photomicrograph showing boring in bryozoa fossil PPL, 1N.

Description of Facies ‘F’, Large-scale cross-stratified grainstone. This facies overlies on Facies E and is exposed at Karondia, Zirabad, Baria, Chak road,

Kosdana area with maximum thickness of 2.5 meter at Kosdana. This is a large-scale cross-stratified grainstone, composed of highly reworked bryozoan

fossils and large-scale (max. thickness of foreset 2.5m) cross-stratification (Fig-9d) Bryozoa, present in this layer are highly reworked. Sorting is moderate.

Description of Facies ‘G’, Planar laminated wackestone. This facies is well exposed in Karondia, Zirabad, Baria, Chak road, Kosdana, Ratitulai with a maximum thickness of 2 meter at Zirabad. This layer consists of planar laminations (Fig-9e). Glauconite is present in this layer at Ratitulai. Glauconite (Fig- 9 e & f) has two modes of occurrence - as infilling within bryozoa and as altered feldspar (Bansal et al., 2019). Sorting is moderate.

Description of Facies ‘H’, Highly bioturbated packstone. This facies is exposed at Kosdana, Baria,

Karondia with maximum thickness of 1 meter. This layer has profuse borings (Fig-9 g & h). It is a well sorted rock with lesser micrite content and >60% allochems. Allochems are bioclasts out of which 70% are of bryozoa, rest is bivalves and echinoids.

Chemical Analysis of Glauconite

According to Odin & Matter (1981) and Odom (1984) prominent peak between 10Å-14Å (001) basal reflections are characteristic of glauconite. The samples of Ratitulai exhibit characteristic peaks of glauconite at 9.8Å (001) (Fig-10) basal reflection, (020) reflection at 4.23 Å and (003) reflection at 3.05Å. Thus this confirms the existence of Glauconite in the analysed samples.

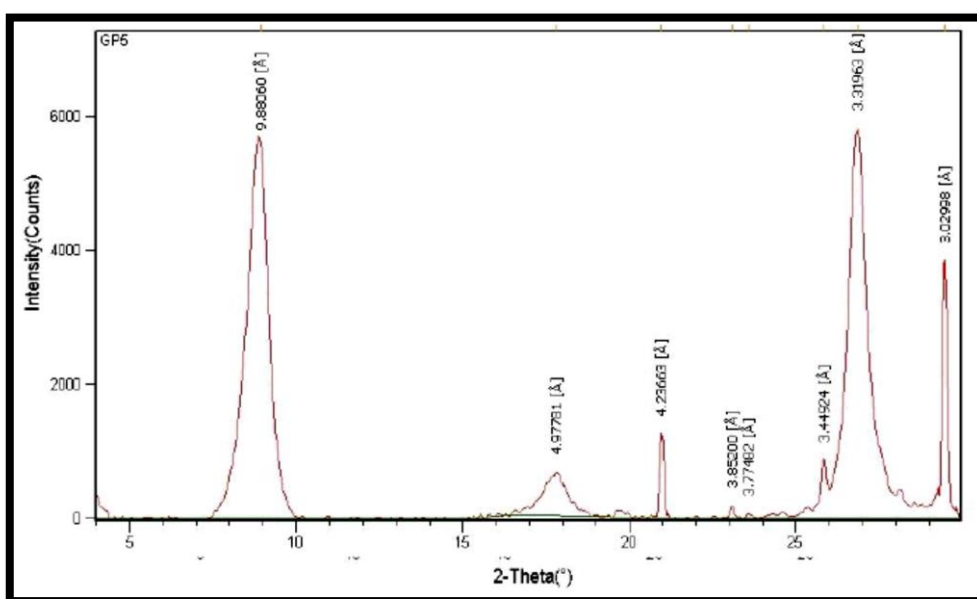


Fig.10 X-Ray diffractogram of sample collected from Ratitulai showing characteristic peak for glauconite

Discussion on Depositional Settings and Paleogeographic Shifts

The Nimar Formation at the base of the Bagh Group consists of shallow marine sandstone (Bhattacharya and Jha, 2014). The Nimar Formation is overall fining upward, exhibits transgressive trend at the upper part and gradationally passes over to the Nodular limestone in response to rise in relative sea level (Bhattacharya et al., 2014). The transgressive trend continued within the Nodular limestone and curtailment of clastic supply would have facilitated deposition of carbonate sediments. Carbonates are mostly mudstone, indicating low-energy depositional setting.

The facies A of the Nodular limestone is completely devoid of primary sedimentary structures indicating its deposition at a low energy depositional setting, possibly in the outer shelf. The deepening trend continued during the deposition of the facies B as carbonates are frequently dissolved forming nodules and dissolution seams. Primary sedimentary structures are

almost absent within it. Lack of sedimentary structures and dissolution of carbonates suggest increase in depositional depth during the deposition of facies B. The deepening of the sea continued till the deposition of facies C containing mudstone. Hardground at the top of this facies is the result of extremely low rate of sedimentation. The Bryozoa limestone exhibits both large and medium-scale cross-stratification. This is indicative of deposition of sediments in shallow marine conditions. Large scale cross stratification within Bryozoa limestone is possibly reflection of tidal bars while the medium-scale cross-bedding may have in inter bar setting. Presence of reactivation surfaces within the cross-stratified sets of the Bryozoa limestone indicates their tidal origin. Increase in depositional energy condition is also reflected in the microfacies, which is dominated by packstone. The highly bioturbated packstone indicates significantly low sedimentation rate. Formation of glauconite corroborates the low rate of sedimentation.

Conclusions

The major conclusions of this study are as follows: The Nodular limestone is divisible into three facies: facies A - planar laminated alternate layers of mudstone and wackestone, facies B - bioturbated wackestone and facies C - entirely consists of mudstone. Lack of sedimentary structures and high mud content of these facies suggests deepening of sea during its formation. A hard-ground exists between facies B and facies C. Formation of this hardground corresponds to a low rate of sedimentation.

Bryozoan limestone is divided into 5 facies. Lower most facies D consists of insitu bryozoa. Followed by facies E - small-scale cross-stratified limestone with reactivation surfaces, facies F- large-scale cross-stratified limestone, facies G - planar laminated and facies H- highly bioturbated limestone at the top. Moving from bottom to top of this Bryozoan limestone layer show decreasing micrite content indicating increase in depositional energy. Large-scale

cross-stratification and presence of reactivation surfaces indicate tidal origin. The presence of sedimentary structures and micro facies analysis indicate deposition of Bryozoan limestone in a shallow marine environment with high-energy condition.

Acknowledgements

Authors are indebted to their host institute IIT Bombay and the Department of Earth Sciences for providing the opportunity to carry out the study and for providing all the necessary facilities. Authors would like to express deepest gratitude towards their supervisor Prof. Santanu Banerjee for his guidance in every way possible. Authors are thankful to reviewers from Atomic Minerals Directorate for Exploration and Research (AMD) for their constructive suggestions and criticisms. We place on record sincere thanks to the anonymous reviewers for their critical comments on the MS.

References

- Bansal, U., Banerjee, S., Pande, K. and Ruidas, D.K. (2019), Unusual seawater composition of the Late Cretaceous Tethys imprinted in glauconite of Narmada basin, Central India. *Geological Magazine*, v. 157(2), p. 233-247.
- Bardhan, S., Gangopadhyay, T.K. and Mandal, U. (2002), How far did India drift during the Late Cretaceous?— *Platoniceras kaffrarium* Etheridge, 1904 (Ammonoidea) used as a measuring tape. *Sedimentary geology*, v. 147 (1-2), p. 193-217.
- Bhattacharya, B. and Jha, S. (2014), Late Cretaceous diurnal tidal system: a study from Nimar Sandstone, Bagh Group, Narmada Valley, Central India. *Current Science*, v. 107, p. 1032-1037.
- Biswas, S.K. (1999), A review on the evolution of rift basin in India during Gondwana with special reference to Western India Basin and their hydrocarbon prospects. *Proceedings Indian National Science Academy Part A*, v. 65(3). p. 261-283.
- Bosellini, A. (1989), The continental margins of Somalia: Their structural evolution and sequence stratigraphy. *Memorie Di Scienze Geologiche*, v. XLI. p. 373-458.
- Bose, P.K., Niyogi, S.C. and Charkraborty, A. (1982), Sedimentology of Bagh limestone and its palaeobathymetric implication. *Symposium Paleontology Stratigraphy Research*, v. 46, p. 14.
- Chiplonkar, G.W. and Ghare, M.A. (1976), Palaeontology of Bagh Beds- Part VII: Ammonoidea. *Bulletin Earth Science*, v. 4&5, p. 1-10.
- Gombos, A.M., Powell, W.G., and Norton, I.O. (1995), The tectonic evolution of western India and its impacts on hydrocarbon occurrences. *An Overview. Sedimentary Geology*, v. 96, p. 119-129.
- Jafar, S.A. (1982), Nannoplankton evidence of Turonian transgression along Narmada Valley, India and Turonian- Coniacian boundary problem. *Journal of the Palaeontological Society of India*, v. 27, p. 17-30.
- Kennedy, W.J., Phansalkar, V.G. and Walaszczyk, I. (2003), *Prionocyclus germari* a Late Turonian marker fossil from the Bagh Beds of Central India. *Cretaceous Research*, v. 24(4), p. 433-438.
- Khosla, A., Kapoor, V., Paul, C. (2003), First Dinosaur Remains from the Cenomanian-Turonian Nimar Sandstone, Bagh Beds, Dhar district, Madhya Pradesh, India. *Journal of the Palaeontological Society of India*, v. 48, p. 115-127.
- Odin, G.S. and Matter, A. (1981), *De glauconiarum origine*. *Sedimentology*, v. 28(5), p. 611-641.
- Odom, I.E. (1984), Glauconite and celadonite minerals. *Micas: Reviews in mineralogy 13*, Mineralogical Society of America, Washington DC, v. 13, p. 545-572.
- Ruidas, D.K., Pomoni-Papaioannou, F.A., Banerjee, S. and Gangopadhyay, T.K. (2020), Petrographical and geochemical constraints on carbonate diagenesis in an epeiric platform deposit: Late Cretaceous Bagh Group in central India. *Carbonates and Evaporites*, v. 35(3), p. 1-21.
- Ruidas, D.K., Paul, S. and Gangopadhyay, T.K. (2018), A reappraisal of stratigraphy of Bagh Group of rocks in Dhar District, Madhya Pradesh with an outline of origin of nodularity of Nodular Limestone Formation. *Journal of the Geological Society of India*, v. 92(1), p. 19-26.
- Sarkar, S.K. (1973), *Sedimentology of the Narmada Bagh Lameta complex around Awaldaman and Bagh areas, Dhar District, Madhya Pradesh*, Ph.D thesis, Jadavpur University, p. 190.

(Received on 29 October, 2020; Revised Accepted on 4 February, 2021)

Provenance and depositional characteristics of Lathi Formation in southern part of Jaisalmer Basin: Implications for exploration of sandstone type uranium mineralization

Shijo Mathew*, Pritam Karmakar, Rajeev Bidwai, S.K. Sharma, Navin Goyal and D.K. Sinha#

Atomic Minerals Directorate for Exploration and Research, Department of Atomic Energy, Jaipur, #Hyderabad
shijomathew.amd@gov.in

Abstract

The lower Jurassic Lathi Formation covers about 900 sq. km area and forms the lowermost unit of Jaisalmer Basin of western Rajasthan. Lithologically the Lathi Formation comprises of conglomerate, sandstone, siltstone, shale and mudstone. The sandstones are generally medium- to coarse-grained, moderately sorted and show variation in colour, grain-size and texture. Petrographic studies indicate a mixed provenance for the Lathi sandstone. On the basis of geochemical data, these sandstones are classified into sub-arkose, litharenite and sub-litharenite. Palaeo-weathering indices such as CIA (80.45), CIW (85.23) and PIA (84.23) suggest moderate to high degree of chemical weathering of the source area, intermediate and felsic igneous provenance, under humid to semi-humid climatic conditions. Further, the geochemical data indicate the sedimentation in a passive continental margin setting. The Bouguer gravity image clearly depicts the north westward slope of the basement. Modelling studies of the gravity data revealed average depth to the basement as 800m, 400m and 250m respectively in northwest, central and southeastern parts of the surveyed area. Exploration activities by Atomic Minerals Directorate for Exploration and Research have resulted in location of several uranium anomalies in the Lathi Formation. Lathi Formation is characterised by many favourable parameters such as fertile provenance, arkosic sandstones intercalated with shale/mudstone, reduced sedimentary facies with carbonaceous matter, lignite and pyrite deposited in continental to marginal marine environment. Malani Igneous Suit and metamorphic rocks constitute the basement for Jaisalmer Basin. Malani rhyolites and granites are fertile source of uranium, containing 6.7 ppm and 9.2 ppm average and intrinsic uranium respectively. Presence of carbonaceous matter and pyrite bearing sandstones, indicative of reducing environment at depth below water table (R.L. 150 m), was reported during subsurface exploration in Lathi sandstone which is a favourable condition for Lathi sediments to host uranium mineralization.

Keywords: *Lathi sediments, Provenance, Sandstone type, Jaisalmer Basin*

Introduction

The Jaisalmer Basin is a pericratonic basin, and is located on the western Rajasthan shelf dipping due northwest (Fig.1). It contains about 10,000 m thick sediments of alternating succession of terrigenous sediments and carbonates. The lower Jurassic sedimentary succession of the basin is characterized by gradual lateral and rapid temporal facies changes with rich and highly diverse faunal contents (Pandey et al., 2012). The Lathi Formation of Jurassic age shows unconformable relationship with the underlying basement rocks while it has conformable relationship with the overlying Jaisalmer Formation.

The study area is located in and around Rama-Koda villages, 40 km south of Jaisalmer town and exposes sandstone, siltstone and conglomerate strata.

This area is characterized by the presence of widespread oxidised sediments on the surface. The fresh and unaltered sediments and sections suitable for sedimentological studies and radiometric examination for uranium mineralisation are not exposed. Later, geological, geochemical and petro-mineralogical data obtained from the reconnaissance drilling carried out by AMD in southern part of the Jaisalmer Basin has further enhanced the understanding of the subsurface character of Lathi sediments. Though the oxidized sediments continue up to 150 m depth, the presence of reduced sandstone at depth below water table with carbonaceous matter and pyrite increases the favourable conditions of Lathi sediments to host uranium mineralization. Early stage of mechanical compaction and subsequent pervasive calcite and iron oxide cementation resulted in good amount of porosity with an average of 13.3% in the

Lathi Formation (Alam et al., 2000). The Lathi Formation drew attention of geologists and researchers over the past few decades due to its sedimentological attributes and fossil content. This formation has been studied by several workers especially for geology and basin configuration (Pareek, 1984), stratigraphy (Misra et al., 1993), diagenesis (Alam et al., 2000) and fossil content (Parihar et al., 2017). So far any substantial work has not been carried out on depositional characteristics of the Lathi Formation and its potential for uranium exploration. The present study focuses on sedimentological, petro-mineralogical and geochemical characterization to elucidate the facies pattern, provenance and depositional environment of the Lathi sediments in southern part of Jaisalmer Basin to assess favourability of the study area for hosting ‘sandstone type’ uranium mineralization.

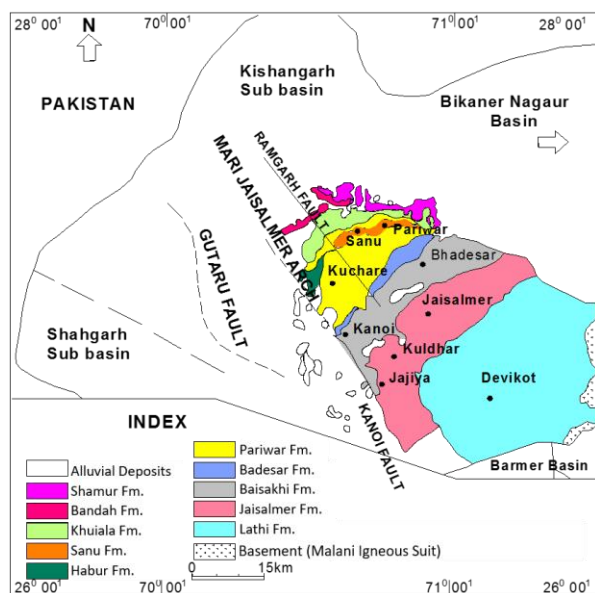


Fig. 1 Geological map of the Jaisalmer Basin (after Das Gupta, 1975)

Geological Setting

The Jaisalmer Basin with thick sedimentary succession has a long and well established sedimentation history from upper Palaeozoic to Quaternary with well-marked transgressive and regressive cycles (Singh, 2006, Table 1). The sedimentary strata have NE-SW strike and the basement configuration is characterized by westerly and north-westerly slope. The rhyolites and granites of Malani Igneous Suite and Proterozoic metamorphic rocks constitute the basement of the sedimentary successions in the Jaisalmer Basin. The sediments have been deposited in non-marine, shallow marine conditions, and range from terrestrial siliciclastic to marine carbonates. The Mesozoic succession of the Jaisalmer Basin start with fluvial, deltaic, or lacustrine sediments, followed by marginal marine sediments, which in turn are followed by several non-marine and

Table 1 Stratigraphy of the Jaisalmer Basin (Zadan et al., 2015)

Age	Formation	Rocktypes
Recent	Wind-blown sand/alluvium	Loose sand and alluvial material
Recent Pleistocene to	Shumar	Dune sand, gravel with ferruginous nodules
Middle Eocene	Bundah	Foraminiferal limestone, clays at base
Lower Eocene	Khuiala	Shales with limestone beds and calcareous silts
Paleocene	Sanu	Friable sandstone with minor clays
Upper Cretaceous	Parh	Marls and arenaceous limestone
Upper Cretaceous	Goru	Sandstone and Shale
Lower Cretaceous	Habur	Arenaceous limestone and calcareous sandstone
Neocomian	Pariwar	Sandstone and Shale
Upper Jurassic	Baisakhi/Bhadasar	Sandstone and Shale
Middle Jurassic	Jaisalmer	Sandstone and Limestone
Lower Jurassic	Lathi	Sandstone, Shale
Malani Igneous Suite (750-770 Ma)		

marine sediments (Das Gupta, 1975; Pareek, 1984; Mahendra and Banerji, 1989; Fursich et al., 1992; Pandey et al., 2005, 2006 a, 2012; Ahmad et al., 2017, 2020). The entire Mesozoic succession of the basin is divided into six formations viz. Lathi, Jaisalmer, Baisakhi, Bhadasar, Pariwar and Habur ranging in age from Lias to Albian. The Tertiary succession in the Jaisalmer Basin is divided into Sanu, Khuiala, Bandah and Shumar formations. Diverse micro and mega fossil assemblages comprising foraminifers, ostracods, corals and some plant fossils are dominantly present in these sediments and have attracted the attention of palaeontologists and sedimentologists (Ahmad et al., 2020). The Jurassic rocks of the Jaisalmer Basin begin with fluvial, deltaic or lacustrine sediments of the Lathi Formation, exposed in the south-eastern part of the basin (Srivastava, 1966; Lukose, 1972; Bonde, 2010). There have been several gradual changes in the depositional setting from fluvial/lagoonal, delta front, shoreface to offshore with fluctuating water energy and salinity (Pandey et al., 2006a, b; Bhat and Ahmad, 2013; Ahmad et al., 2017). The estimated thickness of the Lathi Formation is 330-360 m (Narayanan et al., 1961; Narayanan, 1964; Pareek, 1975). Based on the lithology and depositional environment, Lathi Formation is sub divided into Lower Odania and Upper Thaiat members (Das Gupta (1975).

Methodology

The methods of the study involved both field study and laboratory analyses. The study of sedimentological characteristics in terms of lithology, texture, sedimentary structures were carried out at both the outcrops and borehole samples. Petro-mineralogical studies have been carried out on 12 surface samples of the Lathi sandstone collected from Rama-Koda area. Thin section study was carried out using petrographic microscope (OLYMPUS BX50) at the petrology laboratory, AMD Jaipur. Geochemical characterization of the sediments was carried out on 133 surface and subsurface samples. Major oxides and trace element analysis of these samples was carried out using “ARL PERFORM’X (Thermo Fisher Scientific)” model of WD-XRF at XRF Laboratory, AMD Jaipur.

Lathi Sandstone

The Rama-Koda area (Fig.2) exposes sandstones as the dominant rock-type with minor siltstones and conglomerates. The beds are generally horizontal to gently dipping (2-5°) towards NW. Sandstones show variation in colour, grain-size and texture. They are medium- to coarse-grained, moderately sorted and the colour variations include red, reddish brown, brown, purple, grey, maroon and yellow. The conglomerates belong to the Odania Member of Lathi Formation and contain pebbles of quartz, jasper, chert, basic rocks, etc. of various sizes (<4 cm). The siltstones

are grey and occur as thin beds and lenticular bands within sandstones and are at places highly ferruginous. These sandstones are characterised by primary sedimentary structures such as cross-beddings, herringbone cross-stratifications and ripple marks, and secondary structures such as penecontemporaneous deformations, load casts and flame structures. Palaeocurrent directions were measured from cross-beddings, ripple marks, oriented pebbles and oriented petrified plant material which indicated a south-westerly palaeocurrent direction at Rama-Koda area (Fig.3).

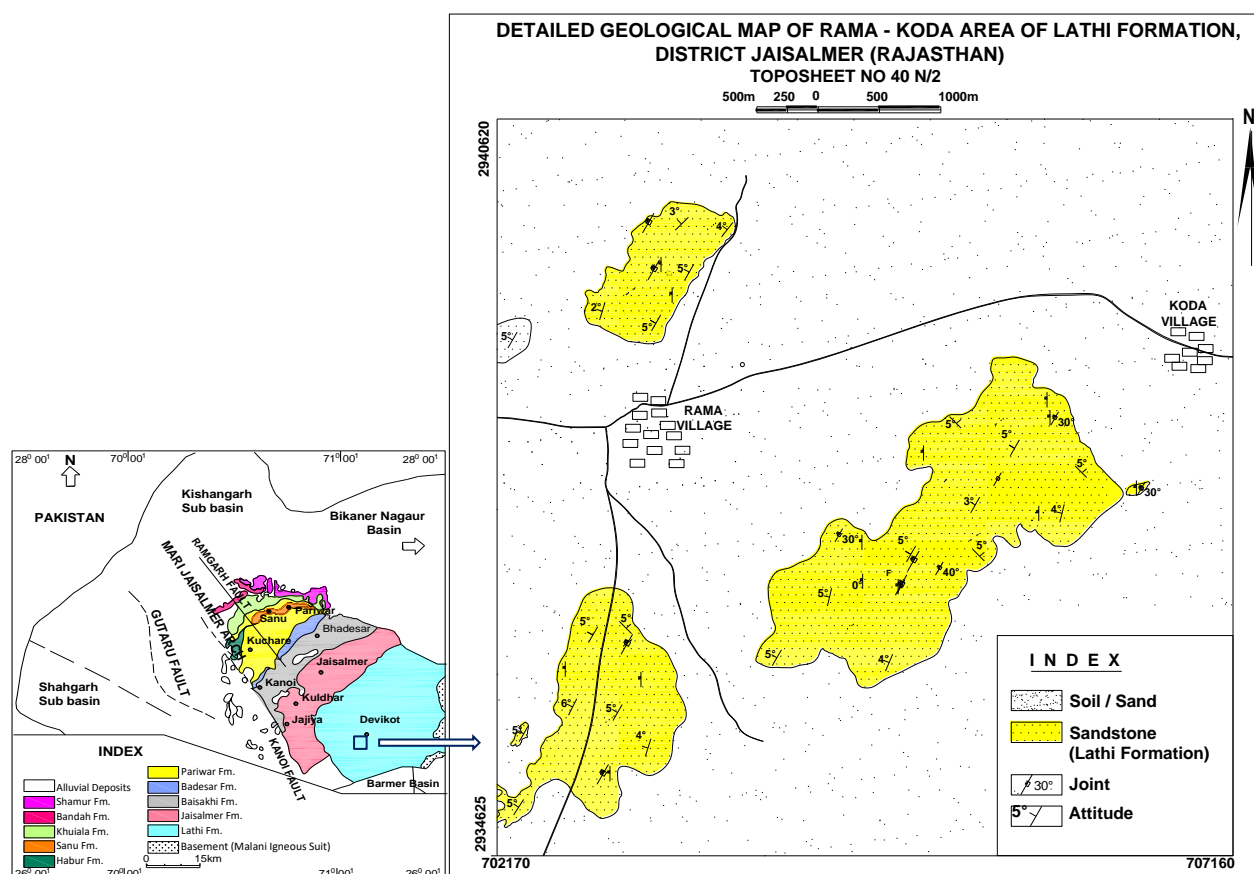


Fig. 2 Geological Map of Rama-Koda area, southern part of Jaisalmer District, Rajasthan

Based on lithological and sedimentological characters of the surface exposures as observed in road cutting and *nala* sections, four sedimentary facies were identified viz. a) Planar-laminated sandstone, b) Cross-bedded sandstone, c) Alternating siltstone and fine-grained sandstone and d) Conglomerate. Planar laminated sandstones are fine- to medium-grained, yellow to brown in colour with grain supported fabric and are moderately to well sorted. Cross-bedded sandstones are medium- to coarse-grained, moderately sorted, pale yellow to red and buff to brown in colour, often ferruginous and friable. They display sedimentary structures such as planar and trough cross bedding, ripple marks and

contains petrified plant material occasionally. Alternating siltstone and fine-grained sandstone unit is composed of dark-greyish and pale yellow coloured, well-sorted siltstone and very fine grained silty sandstone. Conglomerate facies unit is matrix-supported, and comprises of numerous silicified and ferruginised petrified plant matter.

The sub-surface exploration carried out by AMD in Rama-Koda area intercepted four major sedimentary units, i. e., fine- to medium-grained yellowish to reddish sandstone (SST-1), shale, medium- to coarse-grained, reddish to brownish sandstone (SST-2) and carbonaceous pebbly sandstone (Peb. SST).

Texturally the sandstone appears immature to moderately mature. The water table invariably occurs at 150-165m depth in boreholes. The pebbly sandstone occurring below water table is grey to off-white, coarse-grained to pebbly in nature and comprises of carbonaceous matter, lignite/coal with specks of pyrite. This pebbly sandstone unit is observed in the boreholes drilled between Rama in west to Dangri (Malani granite and rhyolite are in close proximity) in the east covering 40 km.

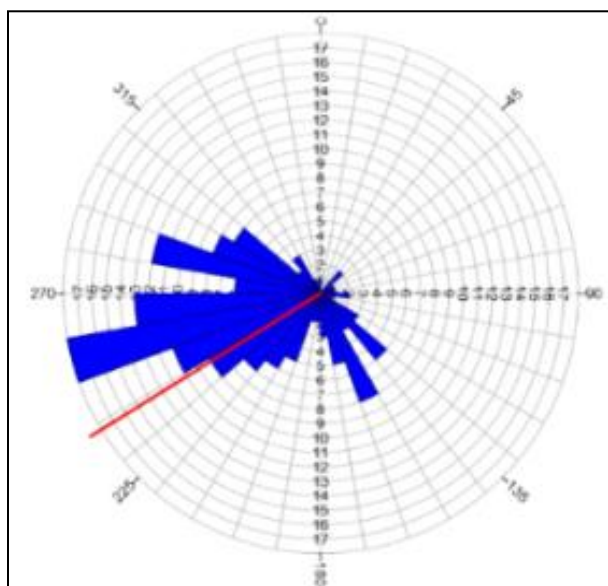


Fig. 3 Ross diagram showing the palaeocurrent direction of Lathi sediments at Rama-Koda area

Petro-mineralogical Studies

The Lathi sandstone is medium- to coarse-grained, moderately sorted and comprises of quartz, microcline, orthoclase, muscovite, lithic fragments including chert, quartzite (Fig.4a) and acidic volcanics and heavy minerals. The clasts are bound by hematite, hydrous iron oxide minerals and calcite cements (Fig.4b). Replacement of calcite by hematite indicates the late diagenetic activity. Rutile and zircon are the main heavy detritus, which together constitute 5% of the total clasts (Fig.4c). Quartz clasts are dominantly monocrystalline with undulose extinction indicating their derivation from deformed plutonic igneous provenance. In addition, the non-undulated quartz with straight extinctions in the Lathi sandstone might have derived from volcanic source. This is supported by bipyramidal six sided quartz crystals (Fig.4d). Thus, the clasts consisting of mildly deformed monocrystalline quartz, undeformed euhedral quartz and lithic fragments of rhyolite (Fig.4e) are inferred to have been derived from volcano-plutonic rocks of the Malani Igneous Suite (MIS) and older

granites. Presence of volcanic clasts indicates that a source for uranium existed in hydrologic continuity with the host sandstone (Adams and Cramer, 1985). Polycrystalline quartz includes strained, sutured grains indicating a metamorphic source. A minor fraction of the clasts is constituted by quartzite and sheared quartzite (Fig.4f), which indicates that metasedimentary rocks have also contributed and formed the provenance for the sandstones. Zircon is identified as the main radioactive mineral which is present as minor detritus. It constitutes approximately 1% of the total clasts in sandstones and in some cases occurs as thin lamellae. Minor amount of monazite is also identified.

Geochemistry

A total of 133 surface and subsurface samples of the Lathi sandstone from southern part of the Jaisalmer Basin were analysed for major oxides and trace elements (V, Cr, Co, Ni, Cu, Zn, Ga, Rb, Sr, Y) (Table 2). All the samples contain high SiO_2 (56.73% to 95.63%) with an average of 85.94% being higher than the post Archaean Australian Shale (PAAS) (62.80%) and Upper Continental Crust (UCC) (66.00%) (Taylor and McLennan, 1985). SiO_2 shows negative correlation with other major elements. This negative correlation might be because most of the silica being sequestered in quartz (Osman, 1996) and it suggests mineralogical maturity of the sandstones. The average $\text{K}_2\text{O}/\text{Al}_2\text{O}_3$ ratio of the Lathi sandstones is 0.025, which indicates the preponderance of alumina rich clay minerals over K- feldspars and micas (Cox et al., 1995). High concentration of Fe_2O_3 suggests that a part of the Fe_2O_3 was possibly precipitated as goethite/limonite during sedimentation and diagenesis. SiO_2 in the Lathi sediments does not show any relation with CaO, thus indicating the presence of secondary carbonates in the total CaO (Feng and Kerrich, 1990). Values of $\text{Al}_2\text{O}_3/\text{TiO}_2$ ratio of the sandstones are high (av. 22.98) and indicate derivation of the detrital material from a continental source (Fyffe and Pickerill, 1993).

In log ($\text{SiO}_2/\text{Al}_2\text{O}_3$) versus log ($\text{Na}_2\text{O}/\text{K}_2\text{O}$) plot after Pettijohn (1975), majority of the samples straddle in sub-arkosic field (Fig.5). The values of Chemical Index of Alteration (av. 80.45), Chemical Index of Weathering (av. 85.23) and Plagioclase Index of Alteration (av. 84.23) indicate a moderate to high degree of chemical weathering. In binary plot of SiO_2 vs ($\text{Al}_2\text{O}_3 + \text{K}_2\text{O} + \text{Na}_2\text{O}$) (Suttner and Dutta, 1986), majority of the sandstones plot in the field of humid to semi-humid climate with a notable proportion of samples indicating arid climate (Fig.6). $\text{Al}_2\text{O}_3/\text{TiO}_2$ ratios of the studied samples (6.2 to 48.8) suggest a geochemical signature of both intermediate and felsic igneous source rock. Location of the samples in the TiO_2 vs Zr scatter plot

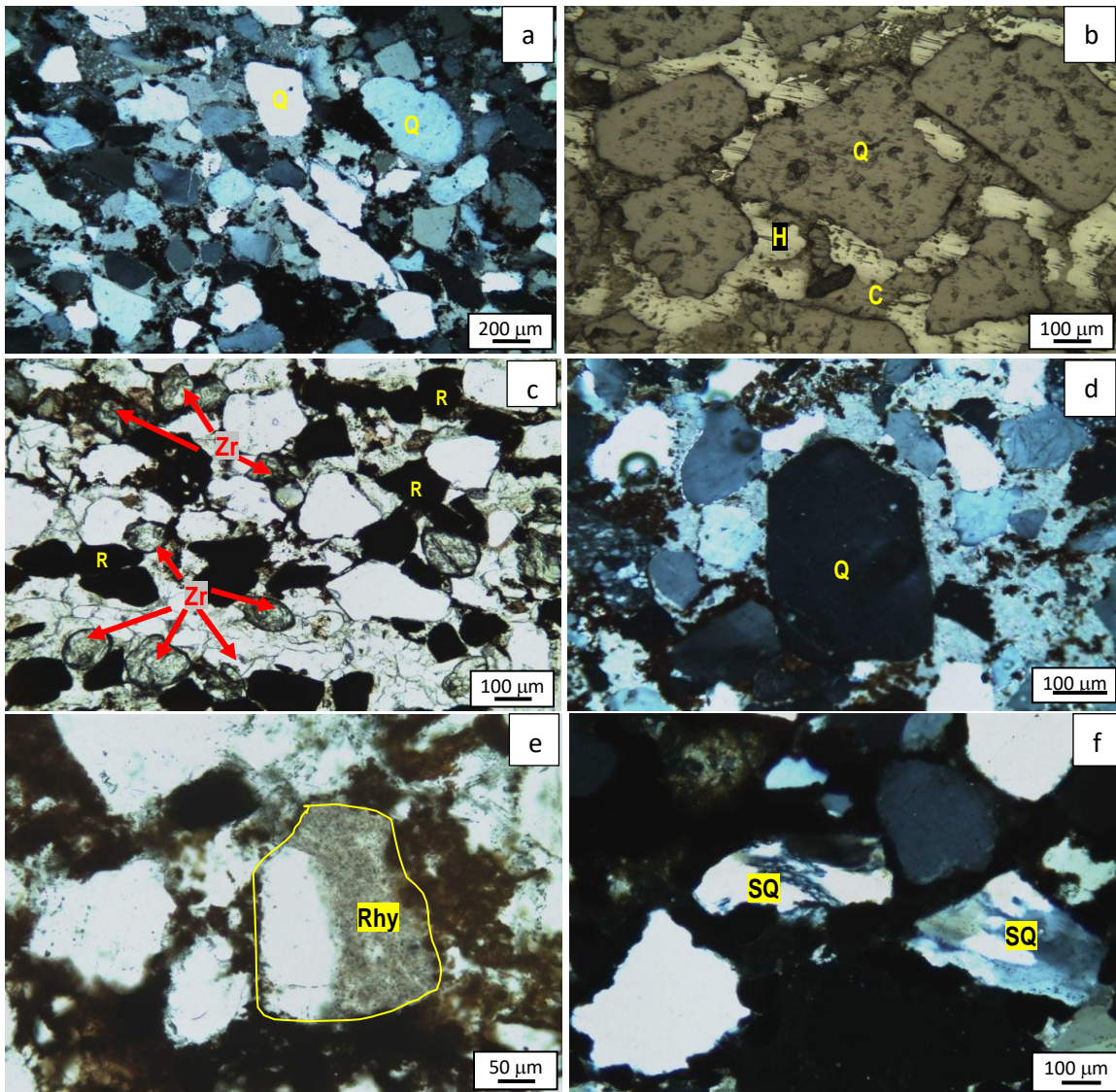


Fig 4 a. Fine grained closely packed clastic framework in calcareous sandstone; b. Coating of hematite (H) around quartz grains (Q) in sandstone; c. Rutile (R) having opaque grains and zircon (Zr) grains present as thin lamellae in sandstone; d. Bipyramidal quartz crystal of volcanic origin in sandstone; e. Fragment of rhyolite (Rhy) comprising quartz phenocryst and microcrystalline groundmass in sandstone; f. Rock fragments of sheared quartzite (SQ) in sandstone.

(Hayashi et., 1997) confirm geochemical signature of a provenance comprising of felsic igneous rock (Fig.7). In the $\text{SiO}_2\text{-K}_2\text{O}/\text{Na}_2\text{O}$ discrimination diagram (Roser and Korsch, 1986), most of the samples straddle in the passive margin field (Fig.8),

Gravity data and Bouguer anomalies

The Bouguer gravity image clearly depicts the basement topography (anomaly ranging from -4.8mGal to 1.7m Gal) in southern part of the Lathi Sub-basin around Rama-Koda- Bakhрани sector, Jaisalmer district. The negative gradient of regional anomaly from SE of Rama

to NW of Sethodi villages indicates that the general slope of the basement is towards NW. The high gravity signature near Rama village is attributed to basement upliftment and low gravity signatures represent the basement depressions, where thick pile of sediments have been deposited (Fig.9). Power spectrum analysis helped in estimating the average depth to the basement as 800m, 400m and 250m in North West, central and south eastern parts of the study area. Major structural features such as fractures and faults have been identified based on the gravity gradient patterns and anomaly variations.

Table 2: Geochemical data of Lathi sandstones from southern part of Jaisalmer Basin

	Subsurface Sandstone												Surface Sandstone (n=15)			
	SST-1 (n=42)				SST-2 (n=32)				Peb. SST (n=44)							
	Min	Max	Mean	Std. Dev	Min	Max	Mean	Std. Dev	Min	Max	Mean	Std. Dev	Min	Max	Mean	Std. Dev
SiO₂ (wt.%)	63.54	94.42	87.12	7.32	57.64	95.63	83.71	10.25	76.42	94.96	89.47	3.94	56.73	91.22	80.83	9.23
TiO₂ (wt.%)	0.10	1.04	0.36	0.26	0.09	1.04	0.53	0.27	0.05	0.97	0.28	0.16	0.14	1.52	0.61	2.29
Al₂O₃ (wt.%)	2.25	16.80	5.60	2.85	2.01	18.69	7.75	6.07	0.91	15.08	5.67	3.65	2.05	17.37	6.45	2.70
Fe₂O₃T (wt.%)	0.90	10.66	2.71	2.02	1.08	13.94	3.79	4.72	1.20	12.06	2.71	2.01	0.78	16.04	6.02	6.55
MgO (wt.%)	0.04	1.27	0.27	0.29	0.04	0.91	0.22	0.20	0.04	1.43	0.20	0.27	0.07	0.66	0.31	0.20
MnO (wt.%)	0.01	0.23	0.02	0.03	0.01	0.61	0.04	0.10	0.01	0.49	0.03	0.08	0.02	0.53	0.11	0.14
CaO (wt.%)	0.06	6.71	1.23	1.58	0.05	1.13	0.20	0.21	0.04	8.12	0.65	1.37	0.10	11.81	2.11	1.39
Na₂O (wt.%)	0.08	1.77	0.41	0.37	0.08	1.59	0.43	0.28	0.11	2.45	0.38	0.35	0.06	1.18	0.53	0.39
K₂O (wt.%)	0.05	1.89	0.45	0.38	0.03	1.80	0.49	0.50	0.08	3.23	0.57	0.64	0.01	0.53	0.15	0.07
P₂O₅ (wt.%)	0.02	0.11	0.06	0.02	0.03	0.47	0.08	0.07	0.02	0.10	0.05	0.02	0.01	0.09	0.06	0.02
V (ppm)	17	75	38	16	17	85	48	19	16	65	33	10	20	108	54	21
Cr (ppm)	31	254	67	40	21	552	76	84	27	317	57	40	40	197	74	32
Co (ppm)	5	34	9	6	5	71	13	12	5	31	8	5	5	63	21	17
Ni (ppm)	15	68	24	8	17	78	33	13	16	55	27	9	6	57	20	10
Cu (ppm)	6	24	12	4	5	37	15	7	5	22	12	3	8	16	10	1
Zn (ppm)	24	121	50	15	41	125	63	17	30	97	58	16	21	67	33	14
Ga (ppm)	10	22	16	2	8	24	17	3	11	21	16	1	7	20	13	3
Rb (ppm)	34	79	48	10	28	137	55	18	34	149	55	22	24	56	38	7
Sr (ppm)	24	129	52	29	22	116	49	24	18	243	41	36	11	102	44	26
Y (ppm)	5	35	10	6	5	28	11	6	5	27	9	4	8	41	22	12
Zr (ppm)	39	384	155	75	67	349	186	65	22	195	127	33	49	1816	465	731
Nb (ppm)	8	70	40	15	8	62	39	10	5	59	35	10	19	158	52	31
Ba (ppm)	28	197	77	41	25	359	122	71	31	238	80	41	25	362	141	93
La* (ppm)	25	150	75	45	25	343	86	75	26	132	51	39	45	305	143	64
Ce* (ppm)	27	241	92	66	37	396	110	85	32	225	77	70	30	1023	243	115
Pb (ppm)	22	63	47	8	32	65	52	7	22	66	48	6	5	54	33	14
CIA	52.20	94.78	78.80	9.80	65.55	92.62	85.39	5.60	63.20	94.32	80.90	6.00	60.31	95.87	85.86	5.40
PIA	52.93	97.96	83.20	9.00	66.82	96.22	88.67	5.60	66.30	94.20	85.50	5.00	59.50	95.80	85.85	6.20
CIW	56.44	98.08	78.82	9.00	68.22	96.38	89.23	5.40	69.42	94.45	86.60	5.00	60.31	95.87	85.86	5.60

SST-1: Fine to medium grained yellowish to reddish sandstones

SST-2: Medium to coarse grained, reddish to brownish sandstone; Peb. SST: Pebbly sandstone; *semi-quantitative data

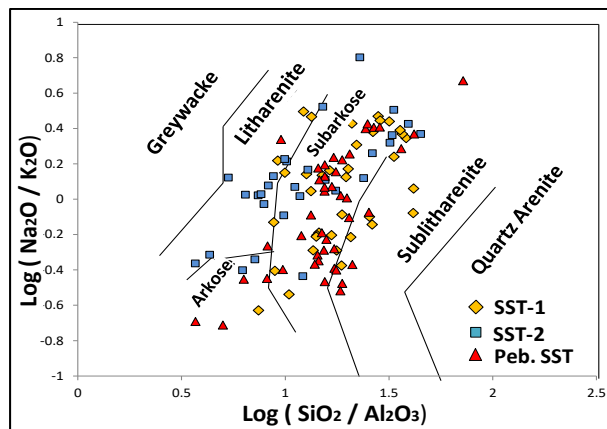


Fig. 5: Log (SiO₂/Al₂O₃) vs log (Na₂O/K₂O) plot (Pettijohn, 1975).

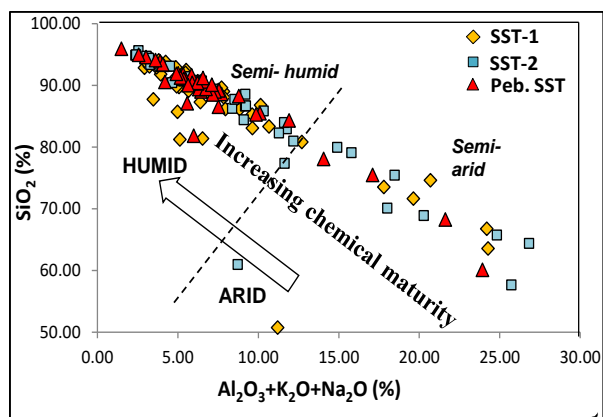


Fig. 6: SiO₂ vs (Al₂O₃ + K₂O + Na₂O) bivariate diagram (Suttner and Dutta, 1986). It indicates humid to semi-humid climatic condition at the time of deposition and increased chemical maturity of the sandstone.

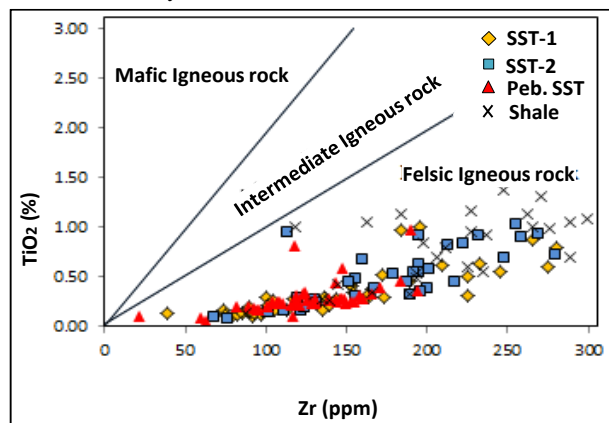


Fig. 7: TiO₂ versus Zr bivariate diagram (Hayashi et al., 1997), indicating geochemical signature of a provenance comprising felsic igneous rock.

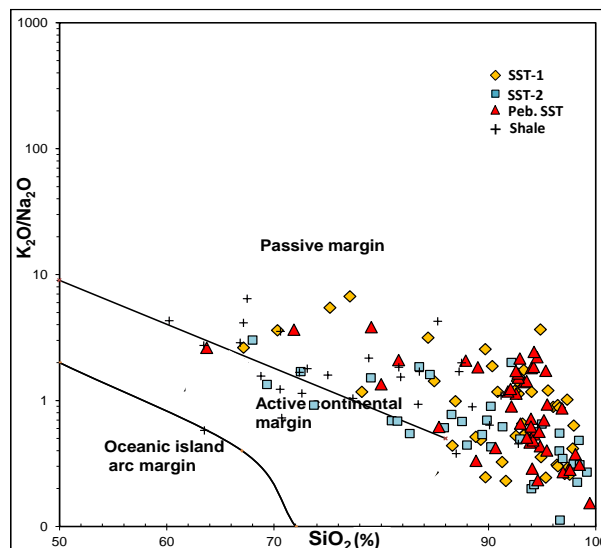


Fig. 8: SiO₂ versus K₂O/Na₂O discrimination diagram (Roser and Korsch 1986) indicating the deposition of Lathi sediments in passive margin tectonic setting.

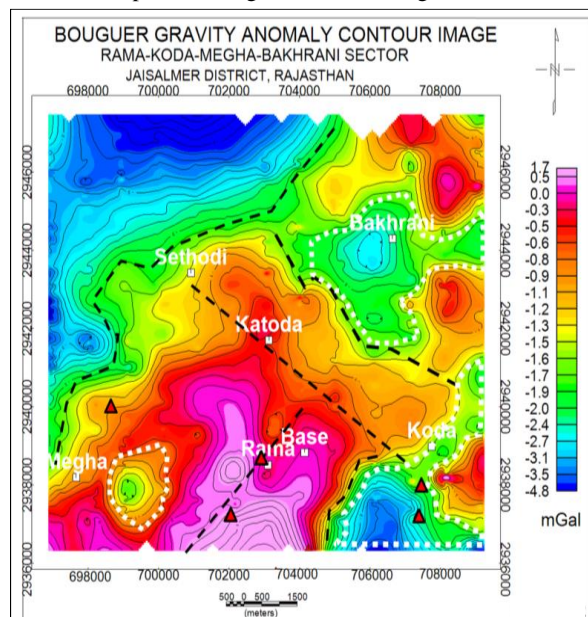


Fig. 9: Bouguer gravity anomaly contour image, Rama-Koda-Megha-Bakhrani sector, Jaisalmer District, Rajasthan

Discussion

In the present study, sedimentological, petro-mineralogical and geochemical studies have resulted in the interpretation of depositional environment, provenance, source area weathering, tectonic setting and rock classification. The Lathi sediments have been deposited in fluvial to marginal marine

conditions as evidenced from medium- to coarse-grained, moderately sorted sediments, occurrence of ripple laminations, cross- and herringbone cross stratifications. Geochemical characters of the Lathi sediments depict felsic igneous rocks as the provenance. The heavy mineral assemblage of zircon, monazite and xenotime indicate acid igneous rocks as provenance. Further, the metamorphic provenance is supported by the presence of garnet and rutile. Petrographic studies reveal the presence of clasts and lithic fragments of rhyolites and sheared quartzite in sandstones and suggest that Malani Igneous Suite of rocks and metasedimentary rocks of the Aravalli craton have acted as the provenance of the Lathi sediments in the study area. Malani rhyolites and granites are rich source for uranium, containing 6.7 ppm and 9.2 ppm average intrinsic uranium respectively (Jain et al., 1998).

The rocks of the Lathi Formation have a NE-SW strike with very low dip (2-5°) towards NW. A westerly palaeocurrent direction is interpreted for the Lathi sediments in the study area.

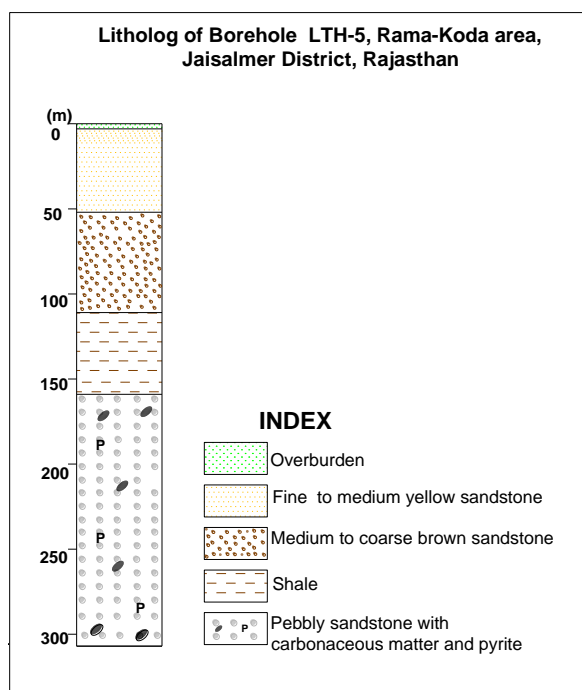


Fig.10: Litholog of borehole LTH-5 drilled at Rama-Koda area, Jaisalmer district, Rajasthan

The Bouguer gravity image and modelling studies has clearly depicted the north-westward slope of the basement topography. Weathering indices suggest a moderate to high degree of weathering of the source rocks and a passive margin as the tectonic

setting are interpreted for sandstones in the study area. The pebbly sandstone horizon occurs below the water table and contains carbonaceous matter and pyrite, suggests prevalence of reducing conditions during deposition (Fig.10). The Lathi sediments in the study area also contain huge amounts of petrified plant materials. The petrified wood samples (n=12) analysed showed 5- 39ppm eU₃O₈, <5-34 ppm eU₃O₈ (Ra) and <10-11 ppm ThO₂. Predominance of plant fossils in the Lathi sediments in Rama-Koda area suggest humid palaeoclimate conditions. Sandstone-type uranium deposits are commonly epigenetic concentrations of uranium occurring as uneven impregnations in sandstones and at places in conglomerates and finer grained inter-beds (Finch and Davis, 1985). The host-rocks are permeable, fairly well-sorted, unmetamorphosed clastic sediments ranging from mudstone to conglomerate, but fine- to medium-grained sandstones are the dominant hosts (Finch and Davis, 1985).

Exploration activities carried out by AMD over the last two decades, resulted in locating several surface radioactive anomalies associated with the Lathi sediments. The radioactive anomalies located at Dabla, Akal, Jodha, Rama, Koda, Megha, Narsingh Ki Dhani, Kita, Javandh, Jogidas Ka Gaon, Modha, Pithodai, Bombai hill and Bakhrani areas are associated with ferruginised sandstones and to some extent with conglomerates.

Conclusion

The Lathi Formation exhibits several favourable factors for hosting 'sandstone type' uranium mineralization such as its Jurassic age, arkosic composition of sediments, low dipping beds, fertile provenance, continental to marginal marine depositional environment, intercalation of sandstones with shale/mudstone, occurrence of reducing agents as carbonaceous matter, lignite and pyrite. Sandstone type uranium deposits dominantly occurs in Silurian and younger host rocks, which reflects the initial and continued development of vascular land plants. Thick sequences of sandstone interbedded with shale/mudstone and low dipping beds favours prolonged and focused ground water flow. Framework mineralogy and geochemical characterization reveals a mixed provenance of the Lathi sediments containing metamorphic rocks of Aravalli craton and felsic igneous rocks, which are fertile source for uranium. Arkoses and sub-arkoses contain stable clasts (quartz and feldspar) which help to retain sediment permeability and suggest its derivation from proximal

uplifted basement rocks which could facilitate high ground water flow (Adams and Cramer, 1985). The humid to semi-humid climatic condition prevailed during the sedimentation which afforded abundant plant material that was deposited in the potential uranium host rocks. Uranium occurrences located in the Lathi sediments so far, are associated with oxidized sandstones on the surface. The present study reveals reduced nature of the Lathi sediments below water table as depicted from subsurface exploration. Presence of lignite, pyrite and carbonaceous matter in the coarse grained pebbly sandstone below the water table favours the reduction of uranium from the oxidized ground waters. Though, present subsurface exploration could not record significant uraniferous occurrence, the Lathi Formation spreads over 900 sq.km area with extensive surface and subsurface persistence, provides ample scope for further subsurface exploration.

Acknowledgements

The authors are thankful to the scientists of the Atomic Minerals Directorate for Exploration and Research, Western Region who have extended their support during the field work and laboratory investigations. The authors are also thankful to the Director, AMD for the permission to publish this paper.

References

- Adams, S.S. and Cramer, R.T. (1985). Data processing criteria model for roll-front type uranium deposits. Geological environments of sandstone type uranium deposits. Report IAEA-TECDOC-328, 383-399.
- Alam, M.M., Ahmad, A.H.M. and Khan, M.H.A. (2000). Diagenetic features of Lower Jurassic Lathi sandstones, Jaisalmer Basin, Western Rajasthan. *Journal of the Geological Society of India*, 56, 415–424.
- Ahmad, F., Quasim, M. A. and Ahmad, A. H. M. (2020). Lithofacies characteristics and depositional environment interpretations of the Middle Jurassic Fort Member rocks, Jaisalmer Formation, Western Rajasthan, India. *Journal of Sedimentary Environments*, 5, 355-373.
- Ahmad, F., Quasim, M. A., Ghaznavi, A. A., Khan, Z., and Ahmad, A. H. M. (2017b). Depositional environment of the Fort Member of the Jurassic of Jaisalmer Formation (western Rajasthan, India), as revealed from lithofacies and grain-size analysis. *Geologica Acta*, 15(3), 153–167.
- Bhat, G. M., and Ahmad, A. H. M. (2013). Temporal facies and diagenetic evolution of the mixed siliciclastic-carbonate Jajiya Member (Callovian-Oxfordian), Jaisalmer Formation, West India. *Volumina Jurassica*, 11, 147–162.
- Bonde, S.D. (2010). A new genus of podocarpaceous wood from the Lathi Formation (Early Jurassic) of Rajasthan, India. *Geophytology*, 38, 19–24.
- Cox, R. and Lowe, D. R. (1995). Compositional evaluation of coarse clastic sediments in the south western United States from 1.8 to 0.2 G.A. and implications for relationships between the development of crustal blocks and their sedimentary cover; *J. Sedim. Res.*, 65A, 477–494.
- Das Gupta, S. K. (1975). Revision of the Mesozoic-Tertiary stratigraphy of the Jaisalmer Basin, Rajasthan: *Ind. J. Earth Sci.*, 2, 77–94.
- Feng, R. and Kerrich, R. (1990). Geochemistry of fine-grained clastic sediments in the Archaean Abitibi greenstones belt, Canada: Implications for provenance and tectonic setting; *Geochim. Cosmochim.Acta.*, 54, 1061–1081.
- Finch, W.I. and Davis, J.F. (1985). Sandstone-type uranium deposits-an introduction, in Geological environments of sandstone-type uranium deposits. TECDOC-328, IAEA, Vienna, 11-20.
- Fursich, F.T., Oschmann, W., Singh I.B. and Jaitly A.K. (1992). Hardgrounds, reworked concretion levels and condensed horizons in the Jurassic of western India: their significance for basin analysis. *Journal of the Geological Society*, 149, 313–331.
- Fyffe L.R. and Pickerill R.K. (1993). Geochemistry of Upper Cambrian-Lower Ordovician black shale along a northeastern Appalachian transects. *Bull. Geol. Soc. Am*, 105, 897- 910.
- Hayashi, K.I., Fujisawa, H., Holland, H.D. and Ohmoto, H. (1997). Geochemistry of ~1.9 Ga sedimentary rocks from northeastern Labrador, Canada. *Geochim Cosmochim Acta*, 61, 4115-4137.
- Jain, R.B., Hingoraney, S.P. and Jagmer Singh (1998). A note on radioactivity in the lower Jurassic sandstones of Lathi Basin, Western Rajasthan, India. *Journal of Atomic Mineral Sciences*, 1, 117-125.
- Khan, Z. and Khan, A.A. (2015). A review on lithostratigraphy and biostratigraphy of Jaisalmer Basin, Western Rajasthan, India. *International Research Journal of Earth Sciences*, 3(8), 37-45.
- Lukose, N.G. (1972). Palynological evidence on the age of Lathi Formation, Western Rajasthan, India. *Proceeding of Seminar on Palaeopalynology and Indian Stratigraphy (1971)*, Calcutta, 155–159.
- Mahendra, K. and Banerji R.K. (1989). Textural study and depositional environment of sand grains from rocks of Jaisalmer Formation, Jaisalmer District, Rajasthan, India. *Journal of the Geological Society of India*, 33, 228–242.
- Misra, P. C., Singh, N. P., Sharma, D. C., Kakroo, A. K., Upadhyay, A. and Saini, M. L. (1993). Lithostratigraphy of Indian petroliferous basins. West Rajasthan basins. Document-11, KDMIPE, ONGC, 1-6.
- Narayanan, K. (1964). Problems of Stratigraphy of the Rajasthan Shelf. In: *Proceedings of the Symposium*

- on Problems of the Indian Arid Zones, Government of India Publication, New Delhi, 92–100.
- Narayanan, K., Subrahmanyam M. and Srinivasan S. (1961). Geology of Jaisalmer. Unpublished report O.N.G.C. Dehradun, India.
- Osman, M. (1996). Recent to Quaternary River Nile Sediments: A Sedimentological Characterization on Samples from Aswan to Naga Hammadi, Egypt (Unpublished doctoral dissertation). University of Vienna, Vienna.
- Pandey, D.K., Choudhary S., Bahadur, T., Swami, N., Poonia, D. and Sha, J. (2012). A review of the Lower–lowermost Upper Jurassic facies and stratigraphy of the Jaisalmer Basin, western Rajasthan, India. *Volumina Jurassica*, 10, 61–82.
- Pandey, D.K., Sha, J. and Choudhary, S. (2006b). Depositional history of the early part of the Jurassic succession on the Rajasthan Shelf, western India: Progress in Natural Science (Special issue of IGCP 506 on the Jurassic Boundary Events), Beijing, 16, 176–185.
- Pandey, D.K., Sha J. and Choudhary, S. (2006a). Depositional environment of Bathonian sediments of the Jaisalmer Basin, Rajasthan, western India. Progress in Natural Science (Special issue of IGCP 506 on the Jurassic Boundary Events), Beijing, 16, 163–175.
- Pandey, D.K., Kashyap, D. and Choudhary, S. (2005). Microfacies and depositional environment of the Gharoi River section (upper Jaisalmer Formation), west of Baisakhi Village, Jaisalmer Basin, Rajasthan. Proceedings of the National Seminar on Oil, Gas and Lignite Scenario with special Reference to Rajasthan, Jaipur, 117–130.
- Pareek, H.S. (1975). Geological configuration of northwestern Rajasthan. Workshop on the Problems of the Desert in India, Sept. 16, Jaipur, 73.
- Pareek, H.S. (1984). Pre-Quaternary Geology and mineral resources of Northwestern Rajasthan: Memoir Geological Survey of India, 115, 1-95.
- Parihar, V.S., Nama, S.L. and Mathur, S.C (2017). Discovery of trace fossils from Lower Odonia Member of Lathi Formation of Jaisalmer Basin, Akal area, District-Jaisalmer, Western Rajasthan, India. *Advances in Ecological and Environmental Research*, 195-210.
- Pettijohn, F. J. (1975). Sedimentary rocks, third edition: New York, Harper & Row, 628.
- Roser, B.P. and Korsch, R.J. (1986). Determination of tectonic setting of sandstone mudstone suites using SiO₂ content and K₂O/Na₂O ratio. *Journal of Geology*, 94, 635–650.
- Singh, N.P. (2006). Mesozoic Lithostratigraphy of the Jaisalmer Basin, Rajasthan. *Jour. Palaeont. Soc. India*, 51(2), 1–25.
- Srivastava, S.K., 1966. Jurassic micro-flora from Rajasthan, India. *Micropalaeontology*, 12-1, .87–103.
- Suttner, L.J. and Dutta, P.K. (1986). Alluvial sandstone composition and paleoclimate. Framework mineralogy. *Journal of Sedimentary Petrology*, 56, 326–345.
- Taylor, S.R. and McLennan, S.M. (1985). The Continental Crust: its composition and evolution. Blackwell Scientific, Oxford, 311.

(Received on 28 November, 2020; Revised Accepted on 4 February 2021)

Legal Frame Work for Exploitation of Beach Sand Mineral Resources: Historical Perspective and Action by Government of India for conservation

Rohit Jaiswal, Iqbal Basha, Rajan Chopra and Eric D’Cruz

Atomic Minerals Directorate for Exploration and Research (AMD), Hyderabad, Department of Atomic Energy, Government of India

Abstract:

India is bestowed with several Beach Sand Mineral (BSM) occurrences along its 7200 km long coastline. The exploitation/recovery of BSM resources is governed by various provisions of the Acts and Rules issued by the Government of India. Till 1998, the mining of BSM was reserved (excluding garnet and sillimanite) for the public sector only. Department of Atomic Energy (DAE), intending to maximize the value addition of BSM within the country, brought out a policy resolution, which allowed the private entities in mining and processing of BSM resources except for the mineral monazite.

Mining and development of any mineral are governed by the Mines and Minerals (Development & Regulation) (MMDR) Act, 1957 and the rules made thereunder. MMDR Act, 1957 has undergone major amendments in 2015 and by virtue of the provisions under the Act, new rules were framed for the first time in the country, exclusively for grant of mineral concession in respect of atomic minerals. As per the provisions of a new rule, all BSM deposits (above threshold) come under the purview of the Government Company or Corporation owned or controlled by the Government. This paper deals with legal provisions for the exploitation of BSM resources and recent amendment by the Government of India for conserving these minerals of strategic importance, in the national interest.

Key words: *Beach sand, strategic minerals, mineral laws, conservation, amendments in laws, India*

Introduction

The BSM in the mining parlance means economic heavy minerals found in the teri or beach sands, which include ilmenite, rutile, leucoxene, garnet, monazite, zircon and sillimanite. Among these, monazite mineral contains thorium and rare earth elements (REE), which is of strategic importance. Further, thorium is notified as ‘Prescribed Substance’ under the Atomic Energy Act, 1962, as it has direct application in the atomic energy programme of the country. After DAE’s policy in 1998, private entrepreneurs were allowed to mine and process the BSM resources (except monazite). However, after the recent policy changes only the Government companies can exploit the BSM resources.

Historical Background

MMDR Act and Rules

The Government of India set out Industrial Policy Resolution on April 6, 1948 and as per the policy resolution, certain industries and minerals were reserved for the Government sector only. The Mines and Minerals Regulation and Development (MMRD) Act, 1948 was enacted with an objective to regulate mines and oilfields and for mineral development on the lines of Industrial Policy Resolution, 1948.

In 1957, Parliament decided that the regulation and development of Mines and Minerals should be under a separate Act and enacted, MMRD Act, 1957 on 28.12.1957. It extends to the whole of India. The

MMRD Act was later renamed as Mines and Minerals Development and Regulation (MMDR) Act, 1957 in 1999. Three types of mineral concessions are granted under this Act viz.,

Reconnaissance Permit
Prospecting License
Mining Lease

Beach Sand Minerals under MMDR Act, 1957

The mineral concession, conservation, development and mining of the BSM is sanctioned, governed and administered by the Central Government and the State Government under the provisions of MMDR Act, 1957, the Mineral Concession Rules (MCR), 1960 and the Mineral Conservation and Development Rules (MCDR), 1988. Initially, all the BSM except garnet and sillimanite were listed as ‘Specified Minerals’ under the first schedule of MMDR Act, 1957.

In 1986, a new thrust to the mineral development activity in the country was given with an amendment to MMRD Act, 1957; accordingly, a mining plan duly approved by the Central Government was made as a prerequisite for the grant of any mining lease. Director, AMD has been authorized to approve the mining plans in respect of certain ‘Specified Minerals’ listed under the first schedule of MMDR Act, 1957. The list includes some of the BSM viz., ilmenite, rutile, leucoxene, zircon and monazite for which mining

plans are to be approved by the Director, AMD. Mining Plans in respect of other BSM (garnet and sillimanite) are to be approved by the Indian Bureau of Mines (IBM). The mining leases were granted for a maximum period of thirty years and can be renewed for a period not exceeding twenty years.

In 1994, the first schedule minerals were divided into different categories as; Part-A: Hydrocarbons Energy Minerals, Part-B: Atomic Minerals and Part-C: Metallic and Non-Metallic Minerals. All the BSM (except for garnet and sillimanite) were listed under the category of Atomic Minerals.

Till 1998, the mining of BSM except for garnet and sillimanite was reserved for the Public Sector. Private firms entered the BSM industries towards the mid-eighties and were allowed to mine/recover only garnet and sillimanite. The mining leases were granted on a first-come-first-serve basis considering the financial and technical capabilities of the applicant.

The MMDR Act, 1957 has undergone major amendments in 2015 and as a result, the old practice of grant of mineral concessions from first come first serve basis was abolished and a method of competitive bidding including e-auction for grant of the lease was brought in. Several new rules in line with the amendments were promulgated, which include:

- 1) The Atomic Minerals Concession Rules (AMCR), 2016
- 2) The Minerals (Other than Atomic and Hydrocarbons 3) Energy Minerals) Concession Rules, 2016
- 3) The Mineral Conservation and Development Rules, 2017
- 4) The Mineral (Auction) Rules, 2015
- 5) Other allied rules

After the amendments, mineral concessions are to be granted through the auction for which separate rules i.e., the Mineral (Auction) Rules, 2015 were notified by the Central Government. However, the atomic minerals were kept out of the purview of auction mode for lease grants.

By virtue of the amendment in the Act, the Central Government has been vested with powers to make separate rules for grant of mineral concessions in respect of atomic minerals. In exercise of the powers conferred under the newly inserted section 11B of the MMDR Act, 1957, the Central Government promulgated the Atomic Minerals Concession Rules, 2016 on 11.07.2016 and the same day, all the BSM including garnet and sillimanite were brought under the list of Atomic Minerals.

AMCR, 2016 is promulgated for the regulation of mineral concessions in respect of Atomic Minerals. The concept of "Threshold Value" for Atomic Minerals was introduced in AMCR, 2016. In respect of the BSM, the threshold value of 0.75% monazite in total heavy minerals (THM) was notified. As per the provisions of the rules, Government Company or Corporation owned

or controlled by the Government were allowed to work in the BSM deposits containing monazite equal to or above the notified threshold value as defined in Schedule A of AMCR, 2016. The mineral concessions in respect of the BSM deposits containing monazite less than 0.75% in THM are governed by the provisions of Mineral (Other than Atomic and Hydrocarbons Energy Minerals) Concession Rules, 2016. The mining leases under AMCR, 2016 shall be granted for a period until the entire reserve of minerals in the mine is exhausted.

Atomic Energy Act and Rules

The Government of India enacted the Atomic Energy Act, 1948 (29 of 1948) for the development, control and use of atomic energy for the welfare of the people of India and other prescribed purposes. In 1962, the Atomic Energy Act, 1948 was superseded by the Atomic Energy Act, 1962 (33 of 1962). As per the Act, Prescribed Substance means any substance including any mineral which the Central Government may, by notification, prescribe, being a substance which in its opinion is or may be used for the production or use of atomic energy or research into matters connected therewith.

Under the BSM, monazite, ilmenite, rutile and leucoxene and zircon were under the list of 'Prescribed Substance'. As per the Industrial Policy Resolution, 1991, the mining and production of ilmenite, rutile, leucoxene and zircon were reserved for the Public Sector only. Considering the growing demand for ilmenite, rutile, zircon and/or their value-added products in the domestic as well as international markets and the BSM resources in the country, the BSM sector was opened for private entrepreneurs. DAE vide notification on "Policy on Exploitation of BSM" the entry of private entrepreneurs into beach sand operations for ilmenite, rutile, leucoxene and zircon. The entry of private entrepreneurs in the BSM operations has been placed in three categories:

- a) Mining and mineral separation.
- b) Value addition per se to the products of (a).
- c) Integrated activities (comprising both (a) and (b))

The main objective of the BSM policy (1998) was to maximize the value-addition to the raw-materials within the country, upgradation of the existing process technologies to international standards and attracting funds and new technology through private participation (domestic and foreign).

The handling/extraction of the 'Prescribed Substances' attracts the provisions of Atomic Energy (Working of the Mines, Minerals and Handling of Prescribed Substances) Rules, 1984, Atomic Energy (Radiation Protection) Rules, 2004 and other allied Rules/policy. The firm desirous to mine/extract the 'Prescribed Substances' are required to obtain a licence under Atomic Energy Rules, 1984 from DAE. The titanium minerals ilmenite, rutile and leucoxene, and

zircon were delisted from the 'Prescribed Substances' w.e.f. 01.01.2007.

As per the latest notification issued by DAE ((S.O. 1592(E) dated 28.04.2016)) on "Updation of the list of Prescribed Substances, Prescribed Equipment and Technology", the uranium and thorium ores that contain more than 300 ppm of uranium and/or thorium comes under the category of 'Prescribed Substance'. Hence, the extraction of the BSM having monazite containing more than 300 ppm of thorium and/or uranium attracts the provisions of AE Rules, 1984.

Step initiated by Government to Conserve BSM resources:

The BSM viz., ilmenite, rutile, leucoxene, monazite, zircon, sillimanite and garnet occur together as a group of associated minerals with varying concentrations in beach sands and other placers deposits. With the development of the latest technologies, monazite and zircon have found applications in strategic and hi-tech applications. Zircon, the main mineral of zirconium also contains the rare earth element, hafnium. Monazite is a mineral that contains rare earths and thorium. Zirconium, hafnium and thorium are very important and strategic elements for the 3rd Stage Nuclear Power Programme of the country. Monazite being the primary source of thorium and rare earths, occurring in association with the BSM, any loss or pilferage of monazite or zircon due to mineral processing or handling of the BSM will be a significant loss to the country, affecting the national security.

In view of National Security, to meet future strategic needs and to protect and conserve the critical elements viz., rare earths, thorium, zirconium and hafnium occurring in the BSM, Ministry of Mines (MoM) has amended the threshold value in respect of monazite in THM for BSM from 0.75 % to 0.00%. As a result, mineral concession in respect of the BSM deposits is now brought under the government control and firms other than government are not allowed to work in the BSM mining. Accordingly, MoM has issued an order dated 01.03.2019 to all the concerned State Governments for premature termination of all the mineral concessions of the BSM under the provisions of the MMDR Act, 1957 held by private companies.

Conclusion

The amendment of the threshold value of monazite in THM (0.00% monazite in THM) in

AMCR, 2016 implies that the mineral concessions in respect of the BSM deposits are to be granted to a government company or corporation owned or controlled by the government.

However, DAE's resolution dated 06.10.1998; "Policy on Exploitation of BSM" contemplates the private participation for mining, mineral separation and its value addition of the BSM resources. Further, the Consolidated FDI Policy Circular of 2017 issued by the Department of Industrial Policy and Promotion states that 100% Foreign Direct Investment (FDI) is permitted for mining and mineral separation of titanium-bearing minerals and ores, its value addition and integrated activities.

In order to overcome such ambiguity and to govern the BSM resources at par with MMDR Act, 1957, it is imperative for the government to revise the Consolidated FDI Policy Circular of 2017 for mining and mineral separation of titanium bearing minerals and ores issued by the Department of Industrial Policy & Promotion.

Acknowledgements

The authors are thankful to the Director, AMD for permission to publish this article. We are grateful to the anonymous reviewers for their constructive suggestion which improve the article substantially.

References

- The Mines and Minerals (Development and Regulation) Act, 1957; The Mineral Concession Rules, 1960; The Minerals (Other than Atomic and Hydro Carbons Energy Minerals) Concession Rules, 2016; MMDR (Amendment) Act, 2015 and the Atomic Minerals Concessions Rules of Ministry of Mines, Government of India <http://mines.gov.in>
- The Atomic Energy Act, 1962; The Atomic Energy (Working of Mines, Minerals and handling of Prescribed Substances) Rules, 1984, The Atomic Energy (Radiation Protection) Rules, 2004 of Department of Atomic Energy, Government of India <http://www.dae.gov.in/>
- Policy on Exploitation of Beach Sand Minerals, Notification dated 06.10.1998 of Department of Atomic Energy, Government of India
- Consolidated FDI Policy Government of India, Ministry of Commerce and Industry, Department of Industrial Policy and Promotion, <https://dipp.gov.in/>
- Rao, P. Seshagiri, Law of Mines and Minerals, v.1, 2 & 3, 20th Edition.

(Received: 29 November 2020; Revised version accepted: 17 March 2021)

Architecture and Source of Alluvial Fan deposits of the Gish and Lish Rivers, Sikkim-Darjeeling Himalaya, India

Ananda Badekar*, Uttaran Goswami and Sweta Samant

Department of Geology, Sikkim University, Gangtok-737102

*Ananda Badekar, Department of Geology, Sikkim University, Gangtok, Sikkim, India, 737102.

Email: rganapati@cus.ac.in

Abstract

The Gish and Lish rivers are flowing through Higher Himalaya, Lesser Himalaya, Sub Himalaya and Quaternary Alluvium of the Sikkim- Darjeeling region. These thrust bounded tectonostratigraphic zones are comprised of different lithologies. Comparative sedimentological studies of the sediments of these rivers were undertaken to understand landforms developed by these rivers and source to sink relationships of these sediments. The Gish River fans are broad and wider as compared to the narrow and linear shaped fans of the Lish River. Textural analysis of these fan sediments revealed high energy conditions of deposition within these rivers. The petrographic analysis of the Gish River sediments shows dominance of Quartz (Qt_{63%}F_{4%}L_{33%}) in the framework components, while the Lithic metamorphic fragments (Lm_{62%}LV_{0%}LS_{38%}) show dominance over Lithic sedimentary fragments. This is also supplemented by the dominance of Quartz Polycrystalline grains (Qp_{62%}LV_{0%}LS_{38%}) over Lithic sedimentary fractions. The Lish river sediments show dominance of Lithic fragments (Qt_{39%}F_{2%}L_{59%}) in the framework components, while the Lithic sedimentary fragments (Lm_{44%}LV_{0%}LS_{56%}) show dominance over lithic metamorphic fragments. This is also supplemented by Lithic sedimentary fractions (Qp_{41%}LV_{0%}LS_{59%}) dominance over the Quartz Polycrystalline grains. These results of Quartz dominance in the Gish River sediments indicate higher contribution is from gneissic and metamorphic sources. While, Lithic dominance in the Lish River sediments infers higher contribution from sedimentary and metamorphic sources.

Keywords- *Gish River; Lish River; Petrography; Fluvial, Provenance*

Introduction

The major rivers of Himalaya i. e., Indus, Ganges and Brahmaputra and their tributaries have developed their drainage system in the Himalayan terrain. These rivers provide best opportunity to study their landforms and their processes of formation. The landforms in the river courses are the result of fluvial processes influenced by different controlling factors such as climate and tectonics (Burbank and Anderson 2001; Srivastava et al., 2016; Mukul and Singh 2016). These rivers are characterized by their depositional landforms like alluvial fans, braided channels and deltas. The alluvial fans develop in the river system in response to the rapid changes in topographic gradient; therefore the majority of rivers flowing from Himalayan mountain ranges enter into planer terrains leading to formation of alluvial fans (Gupta, 1997; Chakraborty and Ghosh, 2010; Decelles and Cavazza 1999). The alluvial fan system is a very important depositional landform developed in the Himalayan foreland basin, which mark and preserve the record of fluvial processes which were active during the

deposition of the Siwalik Group of deposits. This is still continuing in the form of number of alluvial fans developed along the foothills of the Himalaya by major and minor river system (Valdiya 1999, Burbank et al., 1996; DeCelles and Giles, 1996; Najman et al., 2004; Bera et al., 2008; Kumar, 2003).

The structural framework of the Sikkim-Darjeeling Himalaya shows deformation of the region in the form of development of thrust system separating different lithounits in the area (Martin and Mukul, 2010, Mitra et al., 2010). The sedimentary record of the Himalayan foreland basin embedded within the Siwalik Group of sediments in the region has been studied from palaeontological, depositional environment, petrographic studies, palaeocurrent analysis and provenance point of view (Chakraborty et al., 2013; Mandal et al., 2014; Kundu et al., 2012, 2016; Taral et al., 2017). The Quaternary deposits in the region are represented by well developed alluvial fans along the Himalayan foothills which preserve the record of neotectonics and climate change (Bisaria, 2012; Goswami et al., 2013, 2019; Kar et al., 2014; Singh et al., 2016). These alluvial fan deposits have not been studied in depth for

understanding their development and, provenance and tectonic setting. The present study is focussed on sedimentary record preserved in the fans of the Gish and Lish rivers, the tributaries of Tista River (Fig.2) which discharges its sediment load into the mighty Brahmaputra River. These tributaries of Tista River carry large sediment load from different lithotectonic units of Himalaya and deposit them along the foothills zone. This provides an opportunity to analyse these deposits for facies architecture, textural analysis and petrography in order to understand the source to sink relationships and landform development by the Gish and Lish rivers in the region.

Regional Geology

The study area comprises a part of Sikkim-Darjeeling Himalaya. The stratigraphic succession in the area is ranging from Precambrian to Recent. The

succession comprises of tectonostratigraphic zones of Higher Himalaya, Lesser Himalaya, Sub Himalaya and Quaternary Alluvium. These different tectonostratigraphic zones are separated by number of major thrusts in the area i. e., Main Central Thrust (MCT), Ramgarh Thrust (RT), Main Boundary Thrust (MBT), and Main Frontal Thrust (MFT). The lithology of the region comprises of Darjeeling/ Kanchenjunga Gneiss, Paro Gneiss, Lingtse Gneiss composed of biotite schists and gneisses, the Daling Group comprising of phyllites, quartzites and slates, the Gondwana Group comprising of sandstones, shales, carbonates, diamictites and quartzites, the Siwalik Group comprising of conglomerates, sandstones and shales (Valdiya, 1980; Bhattacharya and Mitra, 2009; Mukul, 2010). The Tista River is a major river flowing through this region, while its tributaries Lethi, Lish, Gish, Ramathi, and Churanthi form drainage network in the area.

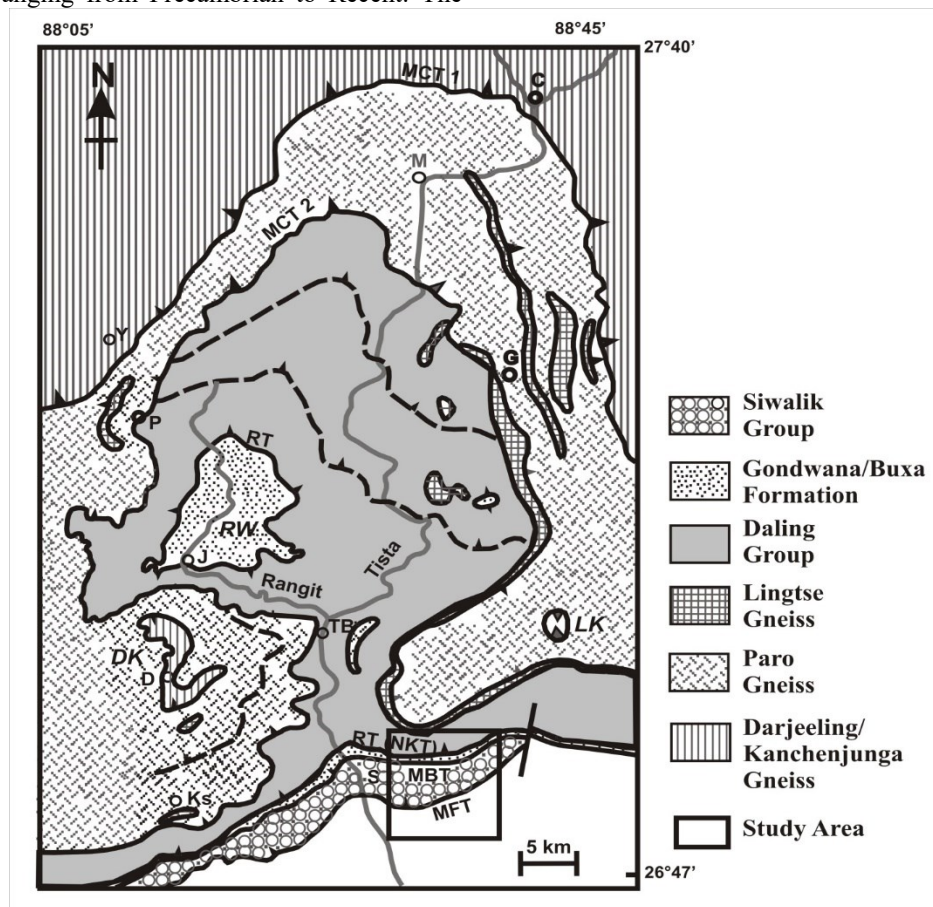


Fig.1 Regional geological map and the study area geology (Bhattacharya et al., 2010)

Materials and Methods

The methodology used for the present study consists of field sedimentology, grain size analysis and compositional analysis of sediments from the Gish and

Lish rivers, collected from near Odalabari town, Jalpaiguri district in the state of West Bengal. The Field sedimentology included detailed documentation of sedimentary deposits to delineate different sedimentary facies. Then the systematic sampling was carried out by

adopting standard procedures by collecting grab samples from surface as well as beds exposed in the outcrop sections of these river deposits (Fig. 2). Conning and quartering of the fine clastic samples was done to select representative samples for grain size analysis in the laboratory. They are collected from proximal, middle and distal parts of the alluvial fans. The facies terminology after Miall (1978) was adopted for the facies description. The grain size analysis was done by wet sieving using sieve shaker with sieves of 2000, 850, 425, 300, 180, 53 micron sizes and a base pan collector. The sieve data was used to calculate statistical parameters with the help of GRADISTAT V8 software (Blott and Pye, 2001). Then the sediments were used for petrographic analysis by preparation of polished thin sections and identification of minerals under the microscope.

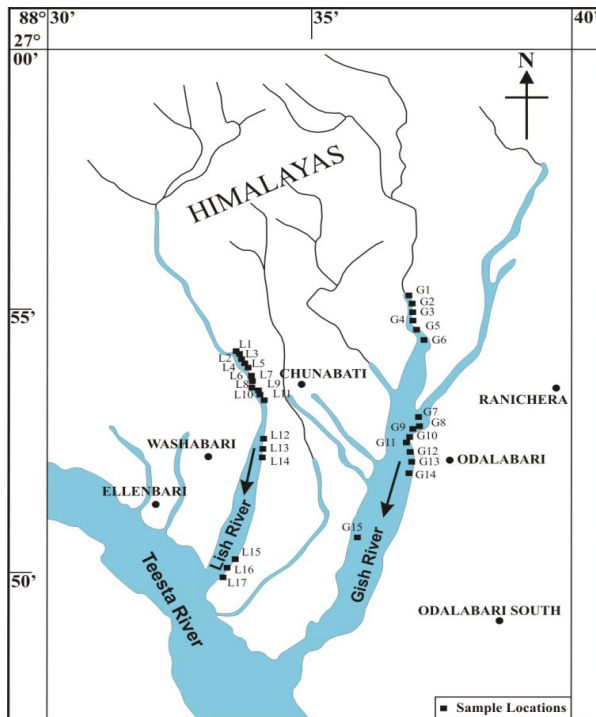


Fig.2: Sample location map (modified after Bisaria, 2012)

Field Sedimentological observations

The Gish and Lish rivers are major river systems developed in the study area (Fig.2). These rivers are flowing through major tectonostratigraphic zones of study area and contribute mixed lithological constituents to the basin. The sediment samples from both the rivers were collected from the recent representative fans situated along the river courses from south of MFT to their confluence with Tista River. These sediments were collected from the proximal-, mid- and distal parts of the alluvial fans.

The field sedimentological studies show, in

both the rivers, the proximal parts are characterized by debris flows and stream flow deposits. The mid fan parts show braided stream deposits while distal parts are dominated by flood plain deposits (Fig.3 & 4). In comparative approach, the Gish River form broad and wider alluvial fan development whilst the Lish River forms narrow and linear shaped fans. These alluvial fans are formed in the frontal parts of the mountains in the vicinity of thrusts. Apparently the mountain front is comparatively more active in the Lish River area restricting spread of the alluvial fans than the Gish river area. This reflects the tectonic control in the region on the shape of alluvial fans. The proximal part of the Gish river fan is dominated by active and abandoned channel deposits than the Lish River. The proximal part in the Lish River is more gravely in nature with abundant large size boulders than the Gish River. This is reflected in the facies encountered in the proximal part of both the rivers. The Gish River comprises of Gm, Gp and St facies association, while the Lish River comprises of Gms, Gm and Gt facies. This facies distribution pattern in the proximal part of the Gish River fan is characterized by stream deposits. On the other hand in the Lish River, facies of the fans are dominated by debris flow deposits. The Gish River mid fan deposit is more braided type and migratory in nature than the Lish River fan deposit. The facies recorded in the mid fans of the Gish River are Gt, Gp, St, and Sh, whereas in the mid fans of the Lish River, the facies observed include Gm, Gt, Gp, Sp, and St. The distal fan parts of both the rivers are characterized by Gp, Sh and Fl facies interfingering with flood plain deposits of gravely nature.

Grain Size analysis

The textural studies were carried out on sand size sediments and data are presented in Tables 1 & 2 for both the rivers and sample location is shown in Figure 2. The total 32 samples were used for this analysis, 15 samples from Gish River and 17 samples from Lish River. The statistical parameters of both the river samples show coarse size sand fractions are dominating, which is supported by finely skewed nature indicating coarser size fraction are contributing more to the sediments. The sorting is dominated by poorly sorted nature of sediments showing different size fractions are present in the sediments. This is also supported by dominance of bimodal nature in the samples. These sediments also show platykurtic dominance inferring coarser as well as finer size fractions are contributing to the sediment deposits. These observations suggest deposition of the sediments under high water flowing energy conditions of the stream with rapid sedimentation at the break of slope gradient leading to mixed size fractions.

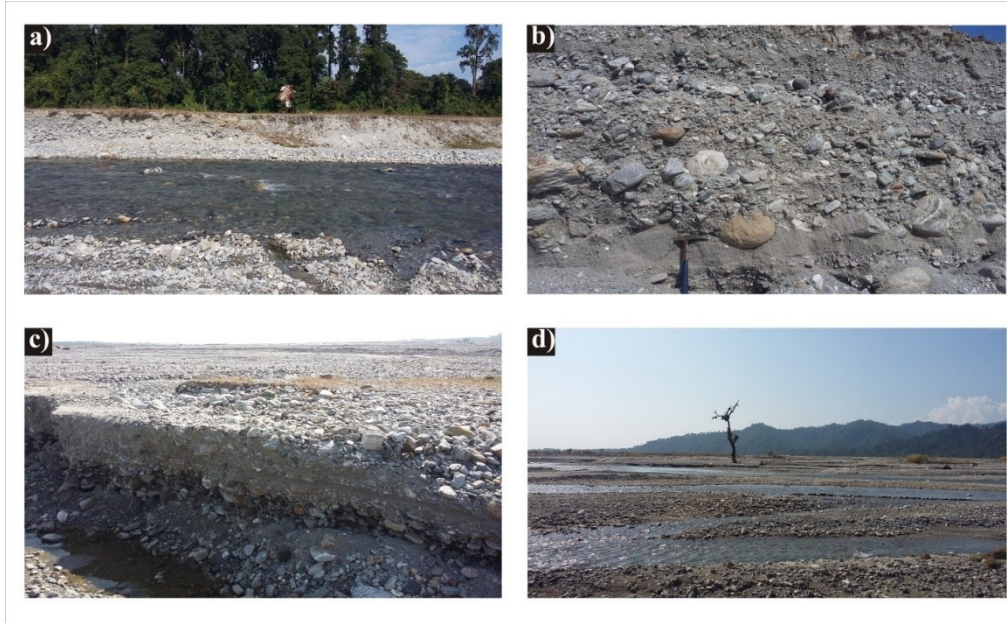


Fig.3: Field photographs showing sediment deposits of the Gish River a) Proximal part of alluvial fan, b) profile of proximal part the deposit, c) Profile of the mid fan bars, d) Mid fan bars.

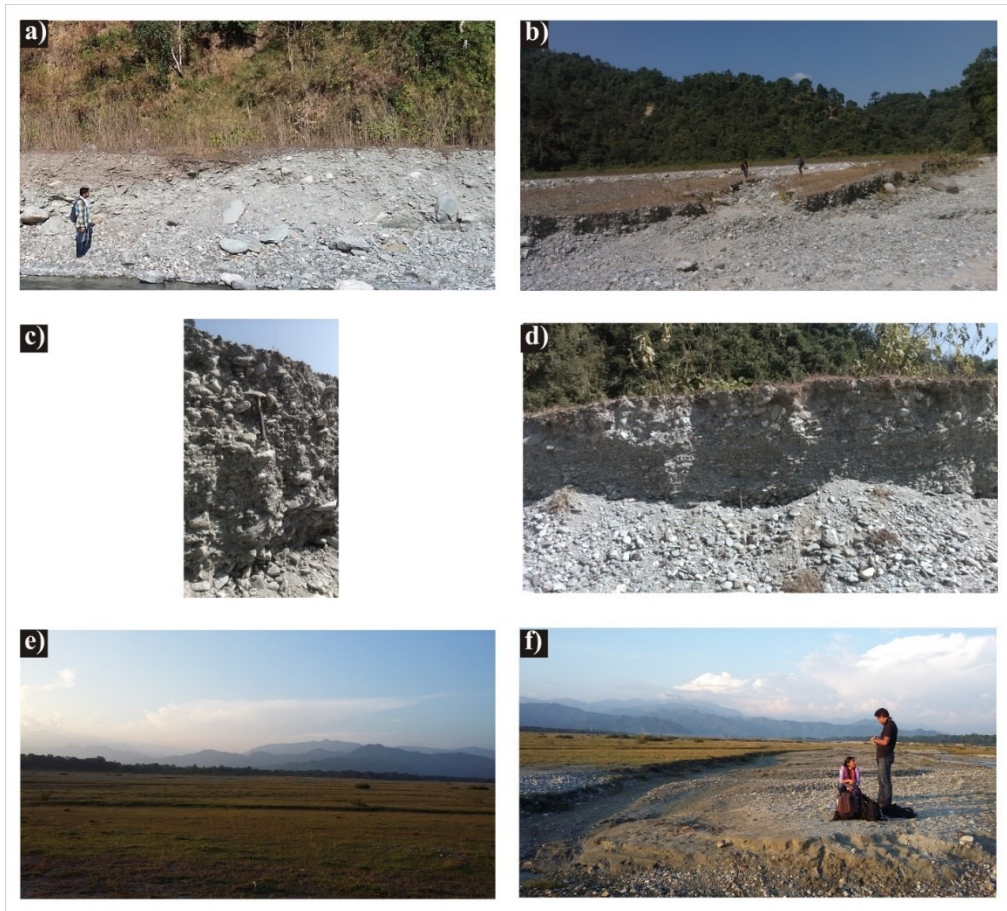


Fig.4: Field photographs showing sediment deposits of the Lish River fan deposits, a) Proximal debris flow deposit, b) Proximal stream flow deposit, c) Proximal deposit profile, d) Mid fan profiles, e) Distal fan characterized by flood plain deposit, f) Distal fan with channel deposit.

Table 1: The statistical parameters calculated from grain size analysis of the Gish River sediments.

Sample name	Folk and Ward method				Folk and Ward method (description)			
	Mean	Sorting	Skewness	Kurtosis	Mean	Sorting	Skewness	Kurtosis
GS1	0.720	1.537	1.377	0.494	Coarse Sand	Poorly Sorted	Very Fine Skewed	Very Platykurtic
GS2	0.237	1.010	1.375	0.639	Coarse Sand	Poorly Sorted	Very Fine Skewed	Very Platykurtic
GS3	1.419	1.715	-0.175	0.724	Medium Sand	Poorly Sorted	Coarse Skewed	Platykurtic
GS4	1.444	1.605	0.050	0.454	Medium Sand	Poorly Sorted	Symmetrical	Very Platykurtic
GS5	0.905	1.468	0.711	0.548	Coarse Sand	Poorly Sorted	Very Fine Skewed	Very Platykurtic
GS6	1.643	1.770	-0.274	0.591	Medium Sand	Poorly Sorted	Coarse Skewed	Very Platykurtic
GS7	0.403	1.034	0.530	0.476	Coarse Sand	Poorly Sorted	Very Fine Skewed	Very Platykurtic
GS8	0.705	1.418	1.012	0.585	Coarse Sand	Poorly Sorted	Very Fine Skewed	Very Platykurtic
GS9	0.637	1.389	0.216	0.704	Coarse Sand	Poorly Sorted	Fine Skewed	Platykurtic
GS10	-0.070	0.617	1.877	1.888	Very Coarse Sand	Moderately Well Sorted	Very Fine Skewed	Very Leptokurtic
GS11	-0.446	0.125	-0.025	-0.850	Very Coarse Sand	Very Well Sorted	Symmetrical	Very Platykurtic
GS12	-0.371	0.312	-3.879	-1.431	Very Coarse Sand	Very Well Sorted	Very Coarse Skewed	Very Platykurtic
GS13	-0.185	0.517	2.071	-2.343	Very Coarse Sand	Moderately Well Sorted	Very Fine Skewed	Very Platykurtic
GS14	-0.558	-0.117	1.551	-0.351	Very Coarse Sand	Very Well Sorted	Very Fine Skewed	Very Platykurtic
GS15	0.553	0.948	0.437	0.583	Coarse Sand	Moderately Sorted	Very Fine Skewed	Very Platykurtic

Petrographic analysis

The total 32 thin sections of the Gish and Lish river sediments were studied for petrographic analysis. The sediment fractions of 180 micron size of all the samples were used for thin section preparations. The detailed petrographic analysis was carried out using Gazzi-Dickinson point counting method (Gazzi, 1966; Dickinson, 1970). The counting of more than 300 grains per thin section was carried out and normalized to 100% and the results are presented in Tables 3 & 4. The Framework constituents were classified into quartz monocrystalline (Qm), polycrystalline quartz (Qp), feldspar (F), lithic sedimentary fragments (Rs/Ls), metamorphic lithic fragments (Rm/Lm), and lithic igne-

ous fragment (Ri/Ls). The petrographic framework components of the sediments are presented in Figures 5 and 6 along with ternary plots representing their contribution from different sources.

Gish River sediments petrographic results

The total 15 thin section slides were analyzed from sediment samples of Gish River (Table 3). The compositional study of the framework components of each sample reveals average contribution of different framework constituents i. e., Qm₄₁ Qp₂₂ F₄ Ls₁₃ Lm₂₀ Li₀. This shows dominance of quartz as compared to feldspar and lithic fragments. In quartz the Q_m are more

abundant than Qp indicating crystalline as well as metamorphic contributions. The Lm fragments are more abundant than Ls fragment inferring that metamorphic sources sedimentary provenance is also

contributing to the sediments. The presence of abundant lithic fragments indicates compositionally immature sediments.

Table 2: The statistical parameters calculated from the grain size analysis of the Lish River sediments.

Sample name	Folk and Ward method				Folk and Ward method (description)			
	Mean	Sorting	Skewness	kurtosis	Mean	Sorting	Skewness	Kurtosis
LS1	0.062	0.802	1.696	1.417	Coarse Sand	Moderately Sorted	Very Fine Skewed	Leptokurtic
LS2	0.150	0.912	1.590	0.676	Coarse Sand	Moderately Sorted	Very Fine Skewed	Platykurtic
LS3	0.195	1.008	1.507	1.132	Coarse Sand	Poorly Sorted	Very Fine Skewed	Leptokurtic
LS4	0.288	1.102	1.304	0.742	Coarse Sand	Poorly Sorted	Very Fine Skewed	Platykurtic
LS5	-0.581	-0.175	4.047	-0.104	Very Coarse Sand	Very Well Sorted	Very Fine Skewed	Very Platykurtic
LS6	0.078	0.849	1.580	4.589	Coarse Sand	Moderately Sorted	Very Fine Skewed	Extremely Leptokurtic
LS7	0.101	0.807	1.569	11.970	Coarse Sand	Moderately Sorted	Very Fine Skewed	Extremely Leptokurtic
LS8	1.368	1.738	-0.094	0.677	Medium Sand	Poorly Sorted	Symmetrical	Platykurtic
LS9	0.634	1.303	0.910	0.656	Coarse Sand	Poorly Sorted	Very Fine Skewed	Very Platykurtic
LS10	0.089	0.838	1.693	0.620	Coarse Sand	Moderately Sorted	Very Fine Skewed	Very Platykurtic
LS11	-0.067	0.645	1.734	-3.894	Very Coarse Sand	Moderately Well Sorted	Very Fine Skewed	Very Platykurtic
LS12	0.489	1.191	1.078	0.672	Coarse Sand	Poorly Sorted	Very Fine Skewed	Platykurtic
LS13	1.469	1.682	-0.133	0.545	Medium Sand	Poorly Sorted	Coarse Skewed	Very Platykurtic
LS14	0.417	1.135	1.065	0.681	Coarse Sand	Poorly Sorted	Very Fine Skewed	Platykurtic
LS15	0.481	1.305	1.418	0.766	Coarse Sand	Poorly Sorted	Very Fine Skewed	Platykurtic
LS16	1.667	1.643	-0.078	0.436	Medium Sand	Poorly Sorted	Symmetrical	Very Platykurtic
LS17	0.540	1.240	0.952	0.685	Coarse Sand	Poorly Sorted	Very Fine Skewed	Platykurtic

The recalculated values of Qp%, Lv%, Ls% show decreasing percentage of Qp% (avg. 69%) in the proximal samples and (avg. 58%) in distal part samples. This may be due to addition of sediment load from tributary in the distal part, while lithic sedimentary contribution indicates provenance from the Siwalik Group of rocks. The recalculated Lm%, Lv%, Ls % values show higher (avg. 62%) contribution of Lm% than lower (38%) contribution of Ls %, inferring

metamorphic dominant source in the Daling Group than the Siwalik Group. The ternary diagrams of the framework constituents (after Folk, 1974) show the distribution of samples clustering in Lithic-Arenites range. The Q%, F%, L% diagram shows sand samples clustering in the areas of recycled orogen, while Qp, Lv, Ls triangular plots depicts their source in the collision suture and fold belt. The Lm, Lv, Ls ternary plot shows the clustering of samples in the suture zone.

Table 3: Framework composition and components of triangular plots of the Gish River sediments

Sample Name	Framework components recalculated to 100%						QFL recalculated to 100%			Qt FL recalculated to 100%			Qp Lv Ls recalculated to 100%			Lm Lv Ls recalculated to 100%		
	Q _m	Q _p	F	L _s	L _m	L _i	Q	F	L	Q _t	F	L	Q _p	L _v	R _s	L _m	L _i	L _s
GS1	38	31	6	8	16	0	38	6	56	69	6	25	79	0	21	66	0	34
GS2	45	22	5	10	19	0	45	5	50	66	5	28	69	0	31	66	0	34
GS3	54	22	3	7	14	0	54	3	43	76	3	21	76	0	24	68	0	32
GS4	18	37	2	16	27	0	18	2	80	55	2	43	70	0	30	64	0	36
GS5	38	23	2	16	22	0	38	2	60	61	2	37	60	0	40	58	0	42
GS6	32	30	2	19	17	0	32	2	66	62	2	36	62	0	38	48	0	52
GS7	43	4	10	14	30	0	43	10	47	47	10	43	23	0	77	68	0	32
GS8	55	20	5	4	16	0	55	5	40	75	5	20	82	0	18	79	0	21
GS9	39	16	2	22	21	0	39	2	59	55	2	43	42	0	58	49	0	51
GS10	38	17	1	27	18	0	38	1	61	54	1	45	38	0	62	41	0	59
GS11	37	28	6	14	14	0	37	6	57	66	6	28	66	0	34	50	0	50
GS12	50	16	2	14	19	0	50	2	49	65	2	33	54	0	46	59	0	41
GS13	59	20	7	4	11	0	59	7	34	79	7	14	85	0	15	74	0	26
GS14	18	40	1	12	29	0	18	1	81	58	1	41	77	0	23	72	0	28
GS15	50	11	3	10	27	0	50	3	47	61	3	36	53	0	47	73	0	27

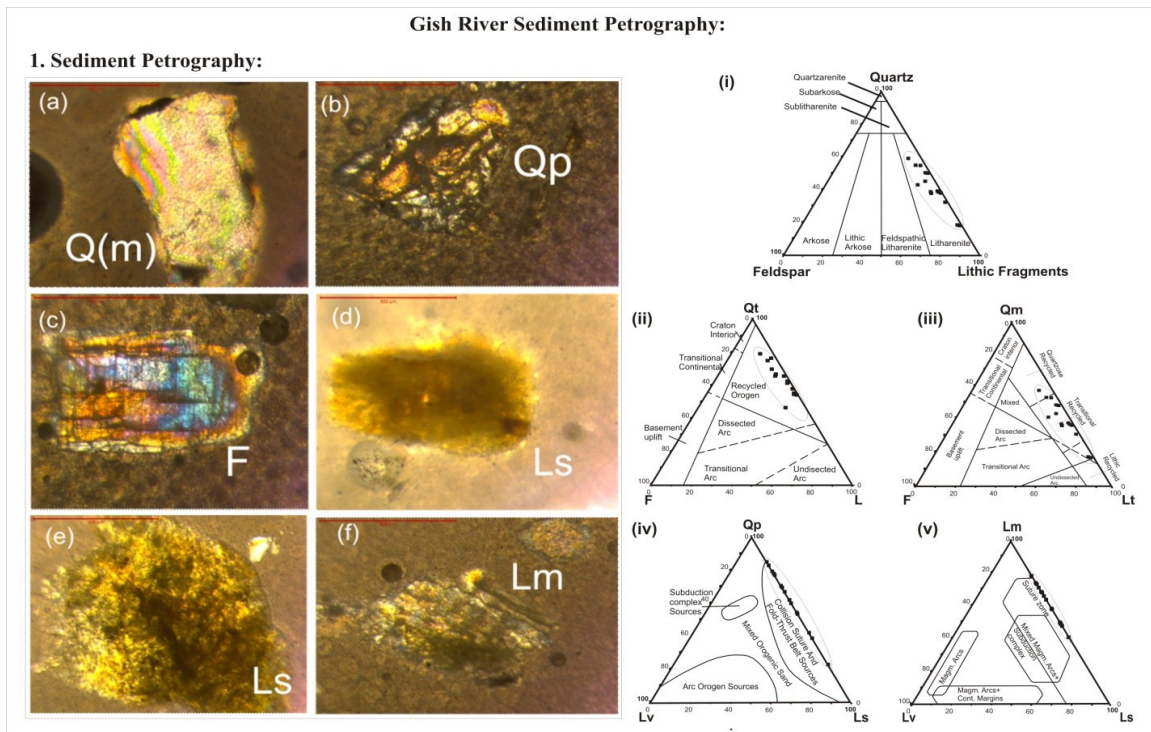


Fig. 5: Microphotograph of sediment samples from Gish River shows (a) Quartz, (b) Quartz Polycrystalline, (c) Feldspar, (d) Lithic sedimentary, (e) Lithic sedimentary and (f) Lithic metamorphic. Ternary diagram of framework components are presented in Figs 5: (i) QFL%, (ii) Qt FL%, (iii) QmFL%, (iv) Qp Lv Ls% and (v) LmLvLs%.

Lish River sediments petrographic results

The 17 thin sections of the samples were used for petrographic analysis of the Lish River and the results are presented in Table 4. The framework components of these sediments contribute average percentage of Qm₁₇ Qp₂₂ F₂ Ls₃₃ Lm₂₆ Li₀. This shows that lithic fragments are present in abundance than quartz and feldspar. This indicates sediments are compositionally immature in nature. Qp is dominating over the Qm, inferring metamorphic sources are contributing more than the crystalline sources. In the Lithic fragments Ls are contributing more than the Lm, indicating sedimentary provenance of Siwalik Group along with metamorphic provenance from Daling Group. The recalculated QmFL% (avg. Qm₁₇ F₂ L₈₁) shows lithic grains are dominating throughout the samples. The recalculated QtFL% also show Quartz and Feldspar contribute less than Lithic fragments in the

proximal part (avg. Qt₃₅ F₂ L₆₃), mid fan part (avg. Qt₄₃ F₂ L₅₅) and distal fan part (avg. Qt₄₈ F₁ L₅₁). The recalculated QpLvLs% (avg. Qp₃₉ Lv₀ Ls₆₁) shows lithic sedimentary fragments are more abundant than the Quartz polycrystalline indicating metamorphic provenance. This is also supported by recalculated LmLvLs% (avg. Lm₄₄ Lv₀ Ls₅₆) which also shows sedimentary lithic fragments are dominating over the metamorphic sedimentary fragments.

The ternary diagram for the framework grains shows (after Folk, 1974) clustering in the Lithic-Arenites Zone. The Ternary diagram of QtFL shows recycled orogen source of these sediments. The QmFLt ternary diagram shows lithic recycled source of these sediments. The dominance of lithic fragments is also reflected in QpLvLs triangular diagram which depicts their origin in collision suture and fold thrust belts. The triangular plot for LmLvLs shows the clustering of samples in the suture zone.

Table 4: Framework composition and components of triangular plots of the Lish River sediments

Sample Name	Framework components recalculated to 100%						QFL recalculated to 100%			Qt FL recalculated to 100%			Qp Lv Ls recalculated to 100%			Lm Lv Ls recalculated to 100%		
	Qm	Qp	F	Ls	Lm	Li	Q	F	L	Qt	F	L	Qp	Lv	Rs	Lm	Li	Ls
LS1	12	20	2	34	32	0	12	2	86	33	2	66	38	0	62	49	0	51
LS2	13	17	1	37	32	0	13	1	87	30	1	69	32	0	68	46	0	54
LS3	20	21	3	40	17	0	20	3	78	41	3	57	34	0	66	30	0	70
LS4	15	28	3	31	24	0	15	3	83	43	3	55	47	0	53	44	0	56
LS5	17	13	2	47	21	0	17	2	81	30	2	68	22	0	78	30	0	70
LS6	18	15	2	45	20	0	18	2	80	33	2	65	25	0	75	31	0	69
LS7	27	16	3	32	22	0	27	3	71	43	3	54	33	0	67	41	0	59
LS8	17	18	1	33	32	0	17	1	83	34	1	65	35	0	65	49	0	51
LS9	9	15	3	38	34	0	9	3	87	25	3	72	29	0	71	47	0	53
LS10	12	34	3	34	17	0	12	3	85	46	3	51	51	0	49	34	0	66
LS11	22	9	3	31	36	0	22	3	76	31	3	67	22	0	78	54	0	46
LS12	13	28	2	34	22	0	13	2	84	41	2	56	45	0	55	39	0	61
LS13	16	32	3	21	29	0	16	3	82	47	3	50	60	0	40	58	0	42
LS14	18	24	0	29	30	0	18	0	82	41	0	59	45	0	55	51	0	49
LS15	23	19	2	33	24	0	23	2	76	41	2	57	36	0	64	42	0	58
LS16	24	26	0	23	26	0	24	0	76	51	0	49	53	0	47	53	0	47
LS17	16	36	1	28	19	0	16	1	83	53	1	46	57	0	43	41	0	59

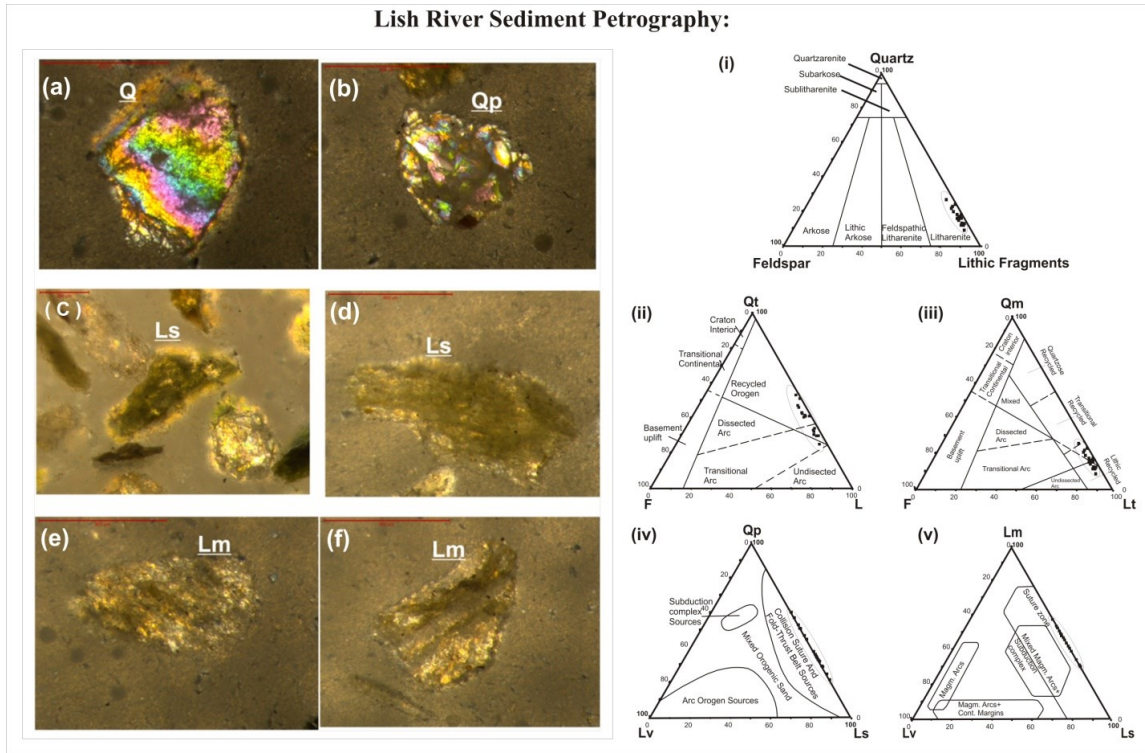


Fig. 6: Microphotograph of sediment sample from Lish river shows (a) Quartz, (b) Quartz Polycrystalline, (c) and (d) Lithic sedimentary, (e) and (f) Lithic metamorphic. Ternary diagram of framework components are presented in Figs 5: (i) QFL%, (ii) Qt FL%, (iii) QmFL%, (iv) Q_p L_v L_s% and (v) L_mL_vL_s%.

Conclusions

The alluvial fan deposits developed by the Gish and Lish rivers are characterized by differential landform geomorphology. The Gish River deposits have formed in response to higher sediment load and wider accommodation space while that of the Lish River deposits have formed in response to higher sediment load and comparatively narrow accommodation space. This infers the tectonic processes operating along the thrusts influence the shape of the basin. The textural immaturity of both the river deposits represents higher sediment load carried by the rivers and depositing in the foothills zone of the Himalaya. This is also reflected in the compositional immaturity of the sediments inferring proximity to the sources. The source rock lithology is contributing differentially in sediments. i. e., higher contribution of Lithic metamorphic fragments in the Gish river is from the Lesser Himalayan provenance, while the higher contribution of Lithic sedimentary fragments in the Lish river is from Sub-Himalayan provenance. Furthermore, metamorphic fragments are higher in the Gish River which infers maximum contribution from the Daling Group of rocks, while that of sedimentary rock fragments are dominant in the Lish River sediments indicating higher contribution from the Siwalik Group of rocks.

Acknowledgements

Ananda Badekar and Uttran Goswami and Sweta Samant acknowledge the Head, Department of Geology, Sikkim University, Gangtok, for support and laboratory facility. The authors are highly grateful to the two anonymous reviewers whose critical assessment and comments on the article improved its quality.

References

- Bera. M.K., Sarkar. A, Chakraborty, Loyal R.S., and Sanyal, P., (2008). Marine to Continental transition in Himalayan Foreland. Geological Society of America Bulletin, 120, 1214-1232.
- Bhattacharyya, K., and Mitra, G. (2009), A new kinematic evolutionary model for the growth of a duplex-an example from the Rangeet duplex, Sikkim Himalaya, India, Gondwana Research, volume 16, pp no 697-715.
- Bisaria, B.K. (2012). Evidences of Neotectonic activity along the foothills of Sikkim and Darjeeling Himalayas in Teesta Basin. Geology, mineral and water resources of Sikkim. GSI special publication, 93, 38-42.
- Blott, S.J., and Pye, K. (2001). GRADISTAT: A grain size distribution and statistics package for the analysis of unconsolidated sediments. Journal of Earth Surface Processes and Landforms, 26, 1237-1248.
- Burbank, D.W., and Anderson, R.S. (2001). Tectonic Geomorphology, John Wiley and sons. 287

- Burbank, D.W., Beck, R.A., and Mulder, T. (1996). In: Yin, A., Harrison, T.M., (Eds.). *The Himalayan Foreland Basin: the Tectonic Evolution of Asia*. Cambridge University Press. 149-188.
- Chakraborty, A., Stephen, H., Ghosh, B., and Bhattacharya, N., (2013). Fluvial trace fossils in the middle Siwalik (Sarmatian-Pontian) of Darjeeling Himalayas, India. *Journal of Earth System Science*, Volume 122 (4), pp.1023-1033.
- Chakraborty, T., and Ghosh, P. (2010). The geomorphology and sedimentology of the Tista megafan, Darjeeling Himalaya: Implication for megafan building processes. *Journal of Geomorphology*, 115, 252-266.
- Decelles, P.G., and Cavazza, W., (1999). A comparison of fluvial megafans in the Cordillarians (Upper Cretaceous) and modern Himalayan foreland basin systems. *Bulletin of the Geological Society of America*, 111, 1315-1334.
- DeCelles, P.G., and Giles, K. A., (1996). Foreland basin systems. *Basin Research*, 8, 103-123.
- Dickinson, W.R. (1970). Interpreting detrital modes of graywacke and arkose. *Journal of Sedimentary Petrology*, 40, 695-707.
- Gazzi, P. (1966). Le arenarie delflysch sopracretaceo dell' Appennino modense; correlazioni con il flysch di Minghidorio, *Mineral. Pet. Acta*, 12, 69-97
- Goswami C, Jana P, and Weber J. C. (2019). Evolution of landscape in a piedmont section of Eastern Himalayan foothills along India-Bhutan border: A tectono-geomorphic perspective. *Journal of Mountain Science*, 16 (12), 2828- 2843.
- Goswami, C., Mukhopadhyay, D., and Poddar, B.C., (2013). Geomorphology in relation to tectonics: A case study from the eastern Himalayan foothills of West Bengal, India. *Quaternary International*, 298, 80-92.
- Gupta, S. (1997). Himalayan drainage patterns and the origin of fluvial megafans in the Ganges foreland basin. *Geology*, 25 (1), 11-14
- Kar, R., Chakraborty, T., and Chakraborty, C. (2014). Morpho-sedimentary characteristics of the Quaternary Matiali fan and associated river terraces, Jalpaiguri, India: Implications for climatic controls. *Geomorphology*, 227, 137-152.
- Kumar, R., Ghosh, S.K., Sangode, S.J., (2003). Mio-Pliocene sedimentation history in the northwestern part of the Himalayan foreland basin, India. *Current Science*, 84 (8), 1006-1113.
- Kundu, A., Matin, A., and Mukul, M. (2012). Depositional environment and provenance of Middle Siwalik sediments in Teesta valley, Darjeeling District, Eastern Himalayas, India; *J.Earth science*. 121, No 1, pp73-89.
- Kundu, A., Matin, A., and Eriksson, P., (2016). Petrography and geochemistry of the Middle Siwalik sandstones (tertiary) in understanding the provenance of Sub-Himalayan sediments in the Lish River Valley, West Bengal, India. *Arabian Journal of Geosciences*, 9, 162.
- Mandal, S., Sarkar, S., Chakraborty, N., and Bose, P. (2014). Palaeogeography, Palaeohydrology and Palaeoclimate of Mio-Pliocene Siwalik group, Eastern India, *Journal of Palaeogeography*, 3(3), 270-296.
- Matin, A., and Mukul M., (2010) Phases of deformation from crosscutting structural relationship in external thrust sheets; insights from small-scale structures in the Ramgarh thrustsheet, Darjeeling Himalaya, West Bengal. *Current Science*, 99(10), 1369-1377.
- Miall, A. (1978). Lithofacies types and vertical profile models in braided rivers: a summary in A.D. Miall, ed., *Fluvial Sedimentology*, Can. Soc. Petrol. Geol. 5, 597-604.
- Mitra, G., Bhattacharyya, K., and Mukul, M. (2010). The Lesser Himalayan Duplex in Sikkim: Implications for Variations in Himalayan Shortening, *Journal of Geological Society of India*, volume 75 (1), 289-301.
- Mukul, M. (2010). First-order kinematics of wedge-scale active Himalayan deformation: Insights from Darjiling-Sikkim-Tibet (DaSiT) wedge. *Journal of Asian Earth Sciences* 39 645-657
- Mukul, M., and Singh, V., (2016). Active Tectonics and Geomorphological Studies in India During 2012-2016. *Proceeding of Indian National Science Academy*, 82 (3), 727-735.
- Najman, Y., Johnson, C., White, N.M., and Oliver, G. (2004). Evolution of the Himalayan foreland basin, NW India. *Basin Research*, 16, 1-24.
- Singh, A., Jaiswal, M., Pattanaik, J., and Maha Dev. (2016). Luminescence chronology of alluvial fan in North Bengal, India: Implications to tectonics and climate. *Geochronometria*, 43, 102-112.
- Srivastava, P., Ray, Y., Phartiyal, B., and Sundriyal, Y.P. (2016). Rivers in the Himalaya: Responses to Neotectonics and Past Climate. *Proceeding of Indian National Science Academy*. 82 (3), 763-772.
- Taral, S., Kar, N., and Chakraborty, T. (2017). Wave-generated structures in the Siwalik rocks of Tista valley, eastern Himalaya: Implication for regional palaeogeography. *Current Science*, 113, 1-13.
- Valdiya, K.S. (1980). The two intracrustal boundary thrusts of the Himalaya. *Tectonophysics*, 66, 323-348.
- Valdiya, K.S. (1999). Rising Himalaya: advent and intensification of monsoon. *Current Science*, 76 (4), 514-524.

Received on 3 Dec 2020 Revised Accepted on 10 May 2021

Sediment Budget and Sediment Trap efficiency of Baglihar Hydroelectric project Reservoir – a calibrated model for prediction of longevity of the Dam

Romesh Kumar¹, Ahsan Ul Haq^{2*}, G M Bhat², Yudhbir Singh², Javid Ahmed Dar¹

1: Jammu and Kashmir State Power Development Corporation

2: Department of Geology, University of Jammu, Jammu-180006

Corresponding Author: ahsanmalik4uly@gmail.com

Abstract

The field investigation of the reservoir area of Baglihar Hydropower project shows that the sediment budget to the reservoir is controlled by fragile rock type like shales, sandstones, phyllites and slates, soil characteristics, steep hill slopes, rainfall and landslides. The rocks are highly weathered, fissile and micaceous in nature and very sensitive to water absorption. The analysed sediments are characterised by dominance of sands, silts and clays with lower values of plasticity (14.3PL), liquidity (23.5 LL), cohesion (118) and shear strength (202 Kpa). The slope wash deposits are highly susceptible to landslides and slope failures and directly contribute to the sediment budget in the reservoir. In addition tributaries of Chenab River also bring sediments in the reservoir from the catchment area.

The empirical relationship for estimating the long-term reservoir trap efficiency for large storage based on correlation between the relative reservoir size and trap efficiency was simulated in 3D model which shows that the annual sediment trap efficiency of the Baglihar reservoir is of 0.39%. The extrapolation of the calculated values shows that the total sediment load shall increase by 11% in the next 30 years and 20% in the next 50 years and correspondingly 40% in the next 100 years that shall induce corresponding decrease in the reservoir volume over the time. By applying flushing schemes, life span of the reservoir can be extended. It is estimated that after 100 years the reservoir shall lose ~35.6% storage volume. On further extrapolation, the trap efficiency will decrease from 25.5% after 30 years to 23% after 100 years. The estimated trap efficiency of Baglihar reservoir is 60%, which is greater than that based on numerical results, showing a significant overestimation.

Keywords: *Baglihar Reservoir, Chenab Basin, Sediment budget, Sediment Trap Efficiency*

Introduction

Reservoirs are key tools for the management of water resources. They provide a means for reducing the effects of inter-seasonal and inter-annual stream flow fluctuations and hence facilitate water supply, flood control, hydroelectric power generation, recreation, and other water uses. Nilsson et al. (2005) found that over half of the world's large river systems are currently impacted by dams. Monitoring of catchment area, reservoir characteristics and dam itself is one of the main aspects for the civil engineering project. The efficient and effective management of hydropower reservoirs is vital for hydroelectric power plant operation. The continuous and extreme rainfall events in the catchment area and subsequent sedimentation into the reservoir are important to monitor at regular intervals to avoid the underestimation of safety measures (Khaba and Griffiths, 2017; Verstraeten and Poesen, 2000). One of

the critical factors that contribute to successful hydropower reservoir management is through reliable monitoring infrastructure, equipment and technology. Therefore, the continuous monitoring of inflow is an essential tool for hydropower dam operators by providing real-time data for decision making in power generation and planning (Basri et al., 2019). This is the main reason of why most of the governments and water supply companies today continue to face the problems when it comes to the control management of dams. A potential failure mode is a physically plausible process for dam failure resulting from an existing inadequacy or defect related to a natural foundation condition, the dam or appurtenant structures design, the construction, the materials incorporated, the operations and maintenance, or aging process, which can lead to an uncontrolled release of the reservoir. Furthermore, it is necessary to execute the investigation carefully from the early stage

so as not to generate stagnation or retreat because the dam project is large-scale and needs huge amount of money for construction. Because the appearance of the dam reservoir exerts adverse influence on the geo-environment, the mitigation or conservation should be considered to decrease the influence as much as possible.

The Baglihar Hydroelectric Project lies on the Chenab River in Ramban District of Jammu and Kashmir. The project is a major hydel scheme comprising of two stages i.e, Stage-I and Stage-II each producing 450 Mw of electricity. The catchment area of this project covers about 1500 km² comprising of glaciers bound mountains in the Pir Panjal and Dauladhar ranges in the Higher Himalaya - a perennial source of water to the Chenab River. The dam site lies at Baglihar village situated between Batote and Ramban falling in the Lesser Himalaya. The dam site is connected with Jammu by NH44 whereas the reservoir lies along the Batote-Doda Highway and is covered in the Survey of India toposheets 43 O/8, O/15 and O/16. Several active landslides and sinking zones are present within the reservoir area which contribute large amount of sediments to the reservoir (Singh et al., 2012). In addition a number of large and small upstream perennial tributaries of the Chenab River bring sediments into the reservoir.

The reservoir capacity is defined as the ratio of deposited sediment to the total sediment inflow for a given period within the reservoir's economic life time. The reservoir storage capacity, drainage area, river discharge flow and time factor have been helpful to calculate the sediment trap efficiency. The monitoring of sediment trap efficiency of the dams is of paramount importance that leads to understand the series of complex processes occurring at the interface between hill slopes and valley-floor systems (Walder and Connor, 1997). The trap efficiency depends primarily upon the fall velocity of the various sediment particles; flow rate and velocity through the reservoir; as well as the reservoir size, depth, and shape; and operation rules of the reservoir (Strand and Pemberton, 1982). The particle fall velocity is a function of sediment particle size, shape, and density; water viscosity; and the chemical composition of the water and sediment. The reservoir sediment trap efficiency tends to decrease over time as sediment fills the reservoir. However, the trap efficiency also decreases temporarily during floods as flow velocity increases through the reservoir. The relative size of the reservoir is a useful index to initially estimate the sediment trap efficiency. The reservoir sediment trap efficiency increases with the relative size of the reservoir. Churchill (1948) and Brune (1953) developed empirical relationships for reservoir sediment trap efficiency from Tennessee Valley Authority reservoirs in the southeast

United States. Churchill (1948) developed a trap efficiency curve for settling basins, small reservoirs, flood retarding structures, semi-dry reservoirs, and reservoirs that are frequently sluiced. He correlated the percentage of the incoming sediment load passing through a reservoir with the ratio of the reservoir retention time to the mean velocity (sedimentation index). The sedimentation index can be made dimensionless by multiplying it by the acceleration due to gravity (g). Brune (1953) developed an empirical relationship for estimating the long-term reservoir trap efficiency for large storage based on the correlation between the relative reservoir size and the trap efficiency. Using this relationship, reservoirs with the capacity to store more than 10 percent of the average annual inflow would be expected to trap between 75 and 100 percent of the inflowing fine sediment. Reservoirs with the capacity to store 1 percent of the average annual inflow would be expected to trap between 30 and 55 percent of the inflowing fine sediment. Significant progress has been made during the recent years in estimation of the sediment trapping in the reservoirs (e. g., Garg & Jothiprakas, 2008; Revel et al., 2015; Tan et al., 2019). Heidarnejad et al. (2006) suggested monthly sediment rating curve to estimate the suspended and bed loads in the reservoir whereas, Lewis et al. (2013) suggested daily sediment trapping estimation based on the daily flow volumes. Earlier the Baglihar reservoir was studied with the objective to appraise the geotechnical and structural setup of the region and impact of reservoir on the geo-environment (Singh et al., 2012; Kumar et al., 2020). However, reservoir monitoring and the factors affecting its longevity were not taken up. According to Singh et al. (2012), the reservoir has induced landslides within the reservoir area and adjoining areas of Baglihar due to soil response to pore water pressure. The interpolation of the previous hydrological data using geometric parameters suggests significant contribution of sediments into the reservoir. The objective of this study is to monitor catchment area of Baglihar reservoir and understand various geological, geotechnical and slope aspect related problems which increase sediment budget and sediment trapping which in turn affect the reservoir competency and longevity of the project.

Geological and Structural Setup of the Area

The study area comprises of the Lesser Himalayan rocks, bounded between two prominent thrusts i.e, Panjal Thrust (PT) in the north and Murree Thrust (MT) in the south (Fig.1). The rocks in this region are folded and faulted normally dipping towards the regional north dipping thrusts. Stratigraphically, significant part of the study area comprises of oldest Salkhalas and youngest Murree Formation (Fig.1). The

Salkhalas are the Pre-Cambrian rocks composed of metamorphosed, less varied, easily identifiable assemblage of phyllites and slates with characteristic rock type of deep black graphitic slates, black crystalline limestone, snow white marble and flaggy quartzite (Jangpangi et al., 1986). The other rock types sandwiched between PT and MT include Gamir-, Baila-, Ramban-, Bhimdasa- and Sincha formations. These are the group of metamorphic rocks with rarely occurring limestones and cherty shales (Jangpangi et al., 1986). The Murree Formation Comprises of the sandstones, mudstones and shales with ripple marks and

pseudo-conglomeratic structure (Bagati, 1991). The chief rock types of the Murree strata are sandstones, shales and claystones marked by graded-bedding; ripple marks, micro cross-lamination and crude cross-stratification. The river terraces along the Chenab River constitute the youngest Quaternary-Recent units in this area (Haq et al., 2019). All the rock types exposed within the reservoir and surrounding areas are highly jointed, weathered and fragile. The phyllites of Salkhalas are highly micaceous, fissile and extremely weathered to micaceous clays.

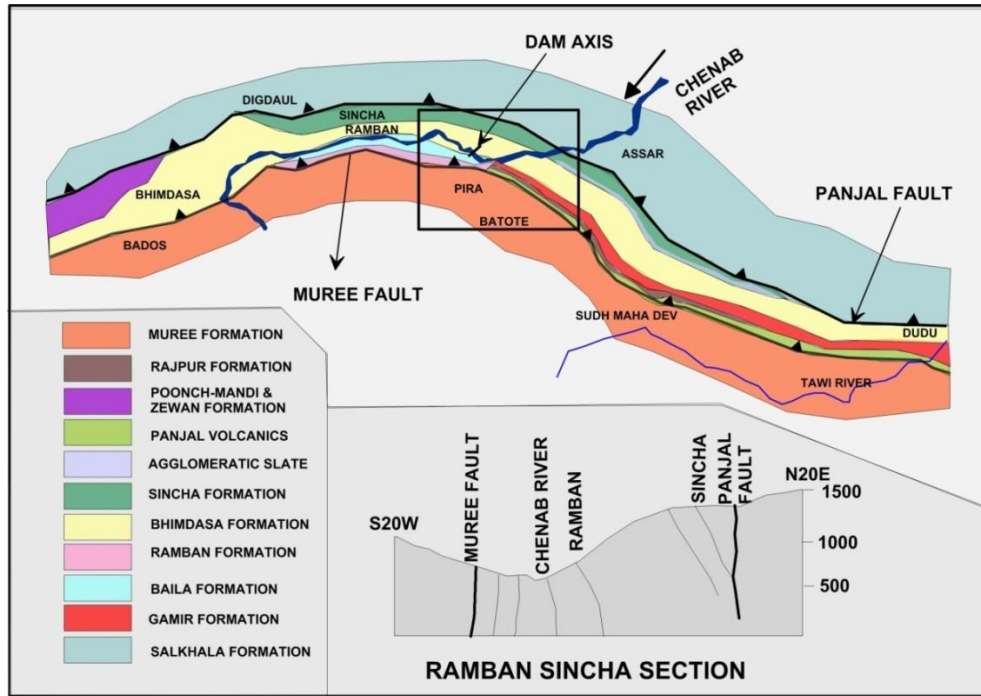


Fig.1: Geological and structural map of the study area (after Jangpangi et al., 1986).

Materials and Methods

Detailed field investigation was conducted to establish the factors responsible for contributing the sediment budget to the reservoir of the project. Field data on lithology, current landslides and structure was collected from the reservoir area. Soil samples from different locations including landslide sites within the reservoir area were collected for analysis of the engineering parameters of the soils following standard procedures in vogue. The grain size analysis was done with the help of sieving and for determination of plastic limit, liquid limit, plastic index, cohesion and shear strength, standard procedures after Lambe (1977) were applied. The rainfall data and the daily water discharge data for

the period from 1976 to 2009 was taken from the detailed project report of Baglihar hydroelectric power project. The discharge flow data was collected from three standard gauge and discharge (G&D) stations installed at Dharamkund, Baglihar dam and Premnagar (Fig.2). The trap efficiency model was prepared with the help of elevation data and other geometrical parameters i.e, area of the reservoir and water storage. The data was taken from the Digital Elevation Model (DEM) with 30 m resolution available on the bhuvan website (https://bhuvan.nrsc.gov.in/bhuvan_links.php). The slope map and modelling of the sediment trap efficiency was made in the Arc GIS software. The data generated was equated by trap efficiency equation of Brown (1944):

$$Ca,t = t-1 / [1 + 0.00021 * (Ka,t-1/Wa)]$$

where $C_{a,t}$ is trap efficiency (expressed as a decimal percent) of reservoir ‘a’ at time step ‘t’; $K_{a,t-1}$ is reservoir storage capacity (m^3) ‘a’ at time step ‘t-1’, and W_a is drainage area (km^2) of reservoir ‘a’.

Laboratory Observations

Grain Size Analysis

A total 10 samples were analysed to determine different soil parameters i.e. grain size by Wet Sieving Method and Atterburg’s Limits on Casagrande Liquid Limit Apparatus. During grain size analysis the soil samples were subjected to wet sieve analysis. To obtain the grain size the soaked soil after treating with distilled water and sodium oxalate were passed through a series of different sieves of sizes, 4.75 mm, 2.0 mm, 1.18 mm, 1.0 mm, 150 μ , 300 μ , 600 μ and 700 μ . The fractions of materials collected from different sieves were converted into percentage by using the formulae:

$$P = (W_1/W) \times 100$$

Where, W_1 = mass retained in the sieve and W = total mass of soil sample taken for soil analysis. For absorption value, the samples were dried in oven followed by complete saturation in distilled water for 36 hours and then weighed again. The absorption value of the soil sample was calculated in percentage using the formulae:

$$A = [(S-W)/W] \times 100$$

Where, S = the saturated weight of the sample and W = total mass of soil sample taken for analysis. The soil samples were classified as per code (IS 2720).

Atterberg’s Limits

The Atterberg’s Limits which include liquid limit, plastic limit, plasticity index and absorption value were estimated by using standard liquid apparatus. The liquid limit test involves use of groove of standard width of 1.1 cm at the top surface under the impact of 25 blows to mark the boundary between liquid and plastic state of soil. In plastic limit, the soil samples were passed through 425-micron sieve to determine minimum moisture content at which the soil can be rolled into 3 mm threads without showing any sign of cracks to mark boundary between liquid and plastic and semi-solid state of soil. The numerical difference between liquid limit and plastic limit was calculated to estimate the plasticity index values.

The field moisture values of the samples were taken from slides. All the samples were taken at a depth of 50 cm. The airtight samples were carried to the laboratory and weight W_1 was noted carefully. The samples were then oven dried at the temperature of 105°-110° C for 24 hours and the weight W_2 was taken to calculate water content by using the formula:

$$W = [(W_1-W_2)/W_2] \times 100$$

Where, W_1 = weight of moist soil sample and W_2 = weight of oven-dry soil sample.

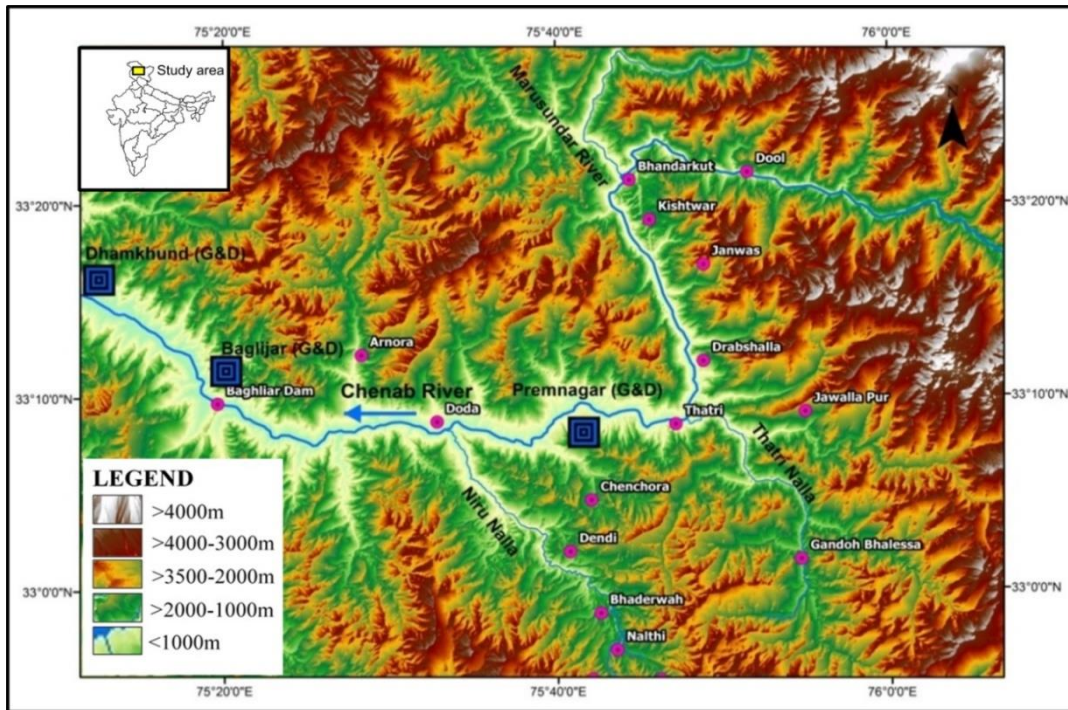


Fig.2. The topographic map of the study area showing dam site and reservoir area, the blue boxes show gauge and discharge stations installed to collect the hydrological data

Observations and Discussion

Soil Characteristics

The balance between soil forming processes and soil erosion is depicted by the depth of soil which controls the tolerance of a slope to all destabilizing factors. The inclination and orientation of structural surface have the greatest effect on the stability of the slopes (Crozier, 1986). Soil texture determines its ability to absorb and store water, generally this is referred to as liquefaction, a condition when the soil momentarily liquefies and tends to behave as dense fluid which is required for landslides to occur. Sand and silts or a combination of both are the most important textures that control liquefaction (Bryant, 1991; Msilimba, 2002; Msilimba and Holmes, 2005). Soils such as silt and clay are weaker and they have complex (colloids) or multiple planes of weakness (clay-humus complex) in common which increases the occurrence of landslides. Soils with high clay content are known to swell when it is wet and shrink in dry condition (Krhoda, 2013).

The grain size analysis of soils of the Baglihar reservoir shows the highest fraction of sand followed by silt and clay in order of dominance with average natural moisture content of 6.54% whereas the critical water absorption value of these samples ranges from 16.05-22.12% beyond these values, these soils plastically flow (Table.1). In addition, low to moderate values of liquid limit (23.5), plastic limit (14.3) and plasticity index (9.2) of these soils indicate that the soils are less consistent (Table. 2). The soils failed at these threshold values with the critical water absorption value of 22.12% (Table. 2). At this critical value of water absorption, the cohesion and shear strength values were at 118 and 202 Kpa respectively. In case of samples with higher proportion of sand content cohesion and shear strength values were relatively low at 126 and 140 kPa respectively. The reduced soil shear strength was overcome by gravity force resulting into landslides (Singh et al., 2012). The phyllites are highly crushed and weathered, and major joints run sub-parallel to the general slope of the area and percolation of rain water into these joints reduces shear strength in the soils.

Table. 1: Grain size analysis of the sediments in the study area.

S.No	Sample No.	Grain Size				Soil Type
		Gravel	Sand	Silt	Clay	
1	RS1	8.252	22.031	42.751	27.021	Silty Clay
2	RS2	26.012	11.051	34.252	28.713	Silty Clay
3	RS3	26.023	34.252	28.753	11.013	Sandy Silt
4	RS4	8.533	30.032	38.52	23.012	Silty Sand
5	RS5	23.014	9.902	27.02	40.113	Clayey Silt
6	RS6	11.531	12.613	45.31	30.614	Silty Clay
7	RS7	16.512	21.013	25.142	37.431	Clayey Silt
8	RS8	23.013	16.611	30.121	30.312	Clayey Silt
9	RS9	21.213	15.313	29.013	33.512	Clayey Silt
10	RS10	14.414	33.531	31.231	20.911	Sandy Silt

Table. 2: Atterberg’s limit and Absorption values of the soil samples

S.No	Sample No	Atterberg’s Limit			Absorption Value (in %)
		Liquid Limit (LL)	Plastic Limit (PL)	Plasticity Index (IP)	
1	RS1	28.012	23.012	5	7.21
2	RS2	18.532	15.512	3.02	17.43
3	RS3	24.013	17.513	6.5	12.23
4	RS4	22.714	14.613	8.101	11.13
5	RS5	31.541	17.814	13.727	7.12
6	RS6	23.513	15.131	8.382	9.23
7	RS7	25.412	14.731	10.681	21.43
8	RS8	17.012	15.821	1.191	17.53
9	RS9	24.513	17.131	7.382	9.13
10	RS10	26.012	15.641	10.371	11.12

Rainfall

Rainfall is also one of the factors that trigger landslides in the hilly areas and wash away the sediments (Van Schalkwyk and Thomas, 1991). The Baglihar catchment area receives a good amount of precipitation and due consideration has been given to its variability between the Baglihar and Dhamkund catchments. The annual isohyets maps of Chenab basin up to Baglihar and Dhamkund based on the rainfall/snowfall data in the catchment for the period of investigation was worked out at 950 mm and up to Baglihar at 937 mm. The rainfall variability between the two catchments was found only of the order of 2%. The catchments also show the peak discharge in the months of June, July and August whilst the flow recedes in the months of November, December

and January. The Baglihar H.E. Project is located on Chenab downstream of the Premnagar site and upstream of the Dhamkund site where daily discharge observations were carried out by Central Water Commission (Fig.3). During the summer periods, the prolonged rainfall changes the moisture content of the regolith or weathered rock materials on the hill slopes that adversely affect slope stability. An increase in pore water pressure increases the weight and gravitational force activates the slides. Further, saturation of soil also reduces cohesion and friction between the grains, and increased moisture also reduces frictional resistance along the zones of weakness in the bedrock and soil interfaces, causing materials above to slide along the lubricated bedding plane.

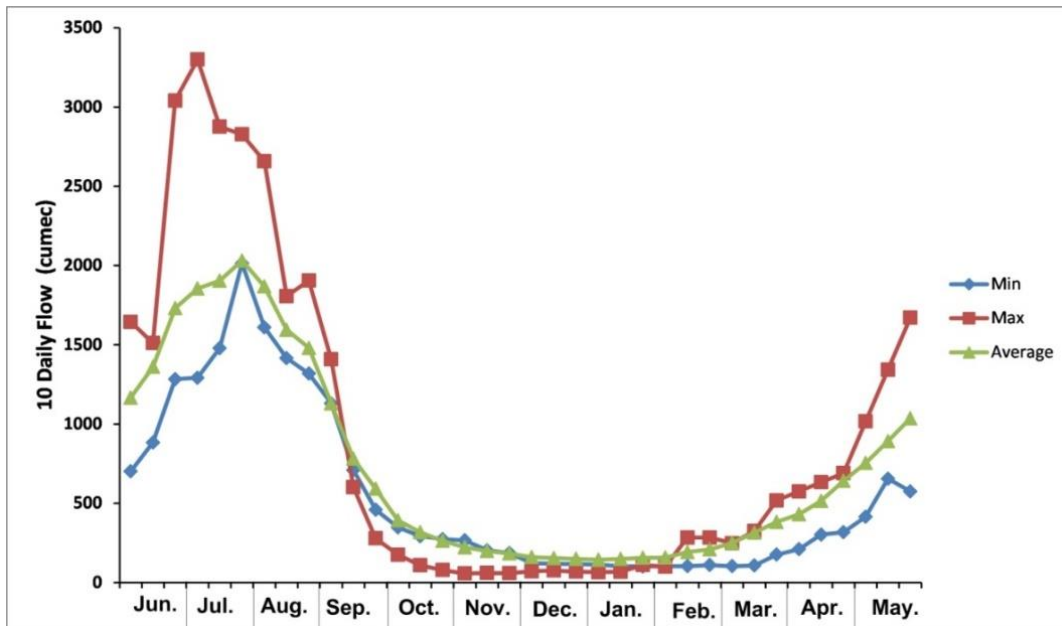


Fig.3. Maximum, Minimum and Average computed flow at Baglihar HEP, (source: DPR of the project; modified).

Landslides

The anthropogenic activities are still the major factors that cause slope failures (Sharpe, 1938; UNESCO/UNEP, 1988). Human activities in the study area increase the frequency of landslides and rockslides due to undercutting for roads and removal of lateral support to the existing building structures. Landslides are easily triggered by removal of lateral support that causes slope failure especially along the roads cuts, construction of houses and foot paths on the slopes. The catchment area of Baglihar show steep slopes and had

witnessed some of the prominent landslides during the recent years and resulted in the blockade of roads, destroying the existing infrastructure and more importantly damming the reservoir at number of places (Fig.4; Fig.5a-f). The Assar landslide is a prominent shallow rotational slide in this area induced by capillary rise in the reservoir area (Singh et al., 2012). The slope materials within the reservoir area include weak and weathered rocks mostly of slates and phyllites, slope wash debris which directly contribute sediments to the reservoir and cause silting problem to the reservoir (Fig. 5g).

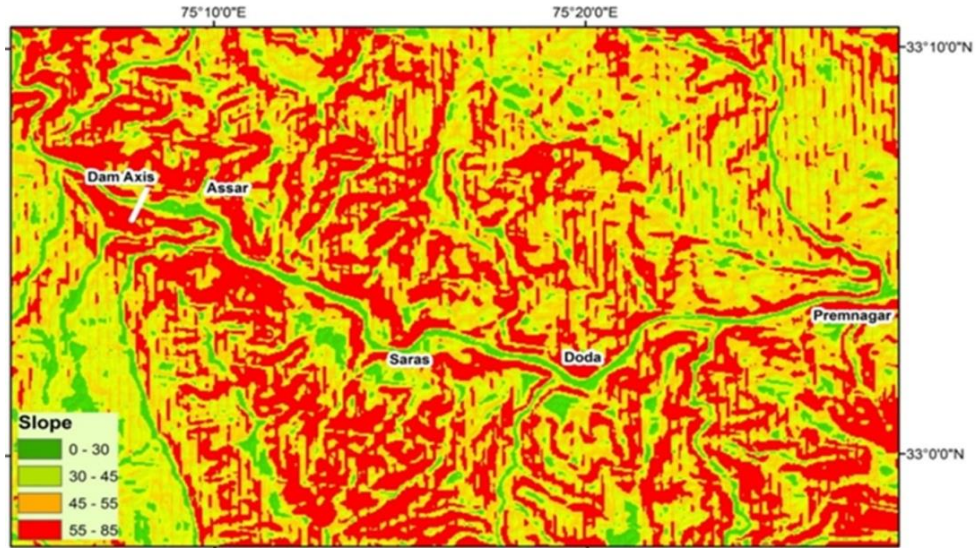


Fig.4. Slope map of Baglihar catchment showing steep slopes (slope > 80°)



Fig.5. Field photographs showing the prominent landslides within the reservoir area of the dam

Sediment trap efficiency Model

Reservoir trap efficiency is defined as the ratio of deposited sediment to the total sediment inflow for a given period within the reservoir's economic life. Trap efficiency is influenced by many factors, of which primary factors are: the sediment fall velocity, the flow rate through the reservoir and the reservoir operation rules. The relative influence of each of these factors on the trap efficiency has not been evaluated to the extent that quantitative values can be assigned to individual factors. The retention-storage time with respect to character of sediment appears to be the most significant governing factor in most reservoirs (Gottschalk, 1964). Trap efficiency estimates are empirically based upon measurements of deposited sediment in a large number of reservoirs mainly in USA. Among others, Brune's curves are the most widely used (Fig.6). Brune presented a set of envelope curves applicable to normal ponded reservoirs using the capacity-inflow relationship. Based on the empirical relationship it is inferred that the high flux of sediments to Baglihar reservoir is primarily due to the fragile lithology, steep slopes, distinguished physical soil characteristics and excess of rainfall. The calibrated model was applied for the prediction of long-term simulations of the water and bed level changes in the river reach and the effect of flushing activities on the trap efficiency of the reservoir. The results of reservoir capacity changes due to sedimentation for a long time period show that after 100 years the reservoir will lose 40% of its initial volume. By applying flushing schemes, life of the reservoir can be reasonably increased; after 100 years the reservoir will lose only 35.6% storage volume. The predicted trap efficiencies will decrease due to the reduction of reservoir storage capacity. Applying flushing schemes, the trap efficiency will decrease from 25.5% after 30 years to 23% after 100 years. According

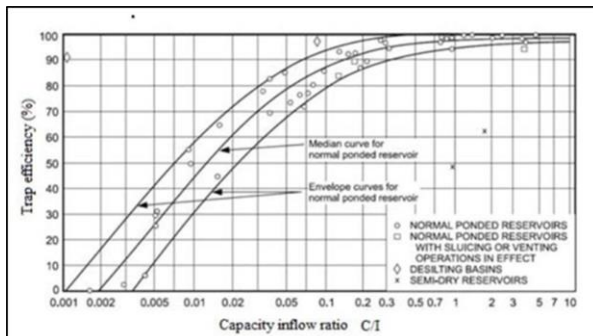


Fig.6. Reservoir trap efficiency as a function of capacity inflow ratio (Brune, 1953).

to Brune's curves, the estimated trap efficiency of Baglihar reservoir is 60%, which is greater than the estimates based on numerical results, showing a significant overestimation (Fig.7).

Conclusions

The field investigation of the reservoir area shows a number of causative factors are responsible for contributing sediments to the reservoir. The major among them include fragile rock type, slope wash deposits on steep hill slopes, rainfall and landslides. The landslide hazard in the reservoir area is due to lithology, structure, soil depth and texture, geomorphology, slope angle, etc. The steep slopes (slope > 80°) and convexity of the slope increases the landslide hazard in the catchment area. The presence of highly weathered phyllites, shales and slates in the catchment area shows more susceptibility to landslides than hard and massive rock types in the area. The soil parameters also reveal the dominance of sands and silts in the slide zones with lower values of plasticity (14.3PL), liquidity (23.5 LL), cohesion (118) and shear strength (202) Kpa.

Furthermore, the saturation of soils during rainfall also reduces cohesion and friction between grains, and increase in the moisture content reduces the friction along the zones of weakness in the bedrock and soil interfaces, causing material above to slide along the lubricated bedding planes resulting in slope failures. The human activities in the study area increase the frequency of landslides and rockslides due to undercutting for roads and removal of lateral supports to the existing built structures which results into the damming of reservoir.

Estimation of changes in reservoir storage capacity, and thus sedimentation volume showed that the estimated trap efficiency of Baglihar reservoir is 60% with annual efficiency of 0.39%. The predicted trap efficiencies will decrease due to the reduction of reservoir storage capacity. The sediment trap efficiency of the reservoir reveals the annual sediment trap efficiency of the Baglihar reservoir is of 0.39% with increase in the load of 11% in the next 30 years and 20% in the next 50 years and subsequent 40% in the next 100 years that reflects the corresponding decrease in the reservoir volume as well. Applying flushing schemes, the trap efficiency will decrease from 25.5% after 30 years to 23% after 100 years.

The countermeasures for the reduction in sedimentation rate in the reservoir are needed for the longevity of dam reservoir. The most important ones

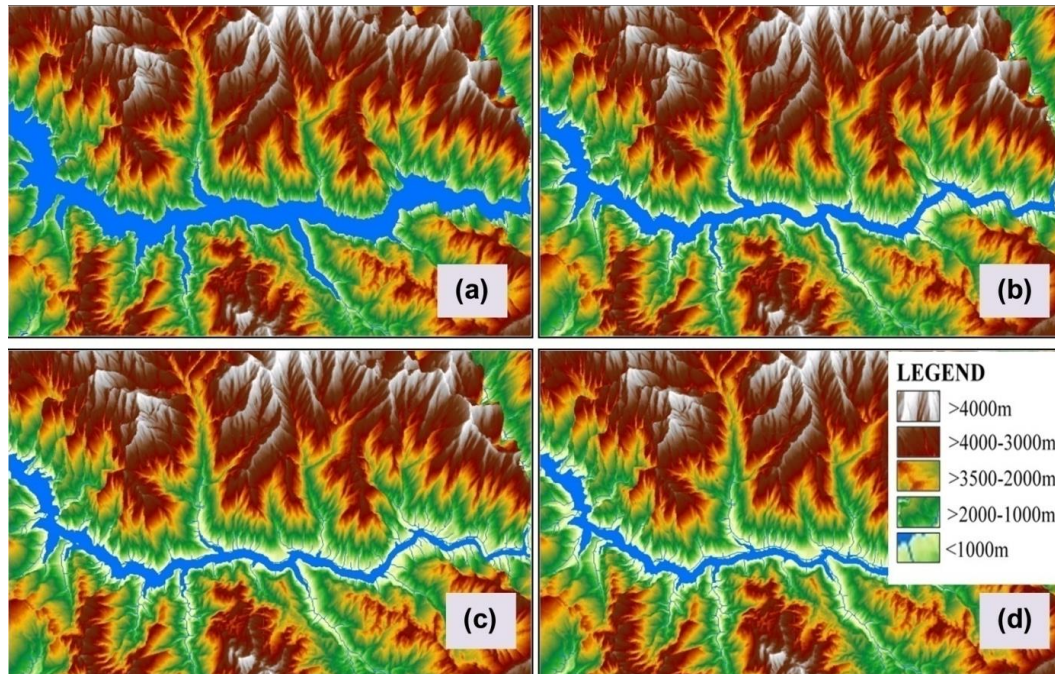


Fig.7. Calibrated model for the prediction of long-term simulations of the water and bed level changes in the river reach and the effect of flushing activities on the trap efficiency of Baglihar reservoir (a) Present condition (b) trap efficiency of 11% in next 30 yr. (c) trap efficiency of 20% in next 50 yr. (d) trap efficiency of 40% in next 100 yr. (values calculated from trap efficiency equation after Brown, 1944).

for the area are: (1) landslides on both the right and left banks of the reservoir can be stabilize at places where feasible by stepping and terracing to reduce the slope gradient (2) In the reservoir area, landslides and slope failures can be prevented by using reservoir rim treatment to stop capillary action that destabilise the slope soil cover on either side of the reservoir.

Acknowledgment

Dr. Romesh Kumar is thankful to JKSPDC and Department of Geology University of Jammu for allowing him to carry out this research as a part of Doctorial thesis. We are thankful to two anonymous reviewers for their critical comments on the manuscript.

References

Bagati, T. N., Kumar, R., and Ghosh, S. K. (1991). Regressive-transgressive sedimentation in the Ordovician sequence of the Spiti (Tethys) basin, Himachal Pradesh, India. *Sedimentary Geology*, vol.73 (1-2), pp.171-184.

Basri, H, Sidek, L.M., Chua, L.H.C., Razad, A.Z.A., and Kamarulzaman, M. S. (2019).Hydro-meteorological monitoring for hydropower reservoirs in remote areas. *Earth and Environmental Science*, vol.257, pp.1-11.

Brown, C. B.(1944). Discussion of Sedimentation in Reservoirs. (Ed.) J. Witzig., Proceedings of the American Society of Civil Engineers, vol.69, pp. 1493–1500.

Brune, G.M. (1953). Trap efficiency of reservoirs. *Transactions of the American Geophysical Union*, vol.34, pp.407–18.

Bryant, E.A. (1991). *Natural Hazards*. Cambridge. Cambridge University Press.

Churchill, M.A. (1948). Discussion of Analyses and use of reservoir sedimentation data by L.C. Gottschalk. In *Proceedings of the federal interagency sedimentation conference*, Denver, Colorado, Washington, DC: US Geological Survey, pp.139–40.

Crozier, M.J. (1986). “Landslides - Causes, Consequences And Environment.” Croom Helm, London.

Garg, V., & Jothiprakash, V. (2008). Estimation of useful life of a reservoir using sediment trap efficiency. *Journal of Spatial Hydrology*, 8(2).

Gottschalk L.C. (1964). Reservoir sedimentation. *Handbook of Applied Hydrology*, V.T. Chow Editor, MacGrawHill, New York.

Heidarnejad, M., Golmaee, S. H., Mosaedi, A., & Ahmadi, M. Z. (2006). Estimation of sediment volume in Karaj Dam Reservoir (Iran) by hydrometry method and a comparison with hydrography method. *Lake and Reservoir Management*, 22(3), 233-239.

IS:2720 part 5 (1985). Method of test for soils—Determination of Liquid and Plastic Limits.

Jangpangi, B. S., Kumar, G., Rathore, D. R., & Dutta, S. A. B. I. R. (1986). Geology of the ‘Autochthonous Folded Belt’, Jammu & Kashmir Himalaya with special reference to the Panjal Thrust. *Journal Palaeontological Society of India*, 31, 39-51.

Khaba, L., & Griffiths, J. A. (2017). Calculation of reservoir capacity loss due to sediment deposition in theMuela

- reservoir, Northern Lesotho. *International Soil and Water Conservation Research*, 5(2), 130-140.
- Krhoda. (2013). Landslides in densely populated county at the foot slopes of Mount Elgon (Uganda): Characteristics and causal factors. *Journal of Geomorphology*, vol.73, pp.149–165.
- Kumar Romesh., Bhat, G. M., Singh, Y., Singh, A, and Haq, A. U. (2020). Kinematic Analysis of the Dam and Powerhouse Sites of the Baglihar Hydropower Project, *International Journal of Innovative Technology and Exploring Engineering*, 9(3) pp.3687-3695.
- Lambe, T.W. (1977). *Soil Testing for Engineering*. The Massachusetts Institute of Technology. Published by Vinod Kumar for Wiley Eastern Limited. New Delhi.
- Lewis, S. E., Bainbridge, Z. T., Kuhnert, P. M., Sherman, B. S., Henderson, B., Dougall, C. & Brodie, J. E. (2013). Calculating sediment trapping efficiencies for reservoirs in tropical settings: a case study from the Burdekin Falls Dam, NE Australia. *Water Resources Research*, 49(2), 1017-1029.
- Msilimba, G.G. (2002). Landslides Geohazard Assessment of the Vunguvungu/Banga Catchment Area in Rumph District. MSc. Environmental Science Thesis, Unpublished, Zomba, University of Malawi.
- Msilimba, G.G. and Holmes, P.J. (2005). A Landslide Hazard Assessment and Vulnerability Appraisal Procedure; Vunguvungu/Banga Catchment, Northern Malawi. *Natural Hazards*, vol.34, pp.199 - 216.
- Nilsson, C., Reidy, C., Dynesius, M and Revenga, C. (2005). Fragmentation and flow regulation of the world's large river systems. *Science*, vol.308, pp.405-408.
- Pushkarenko, V. P., & Nikitin, A. M. (1988). Experience in the regional investigation of the state of mountain lake dams in central Asia and the character of breach mudflow formation. *Landslides and Mudflows*. UNEP/UNESCO, Moscow, pp. 359-362.
- Revel, N. M. T. K., Ranasiri, L. P. G. R., Rathnayake, R. M. C. R. K., & Pathirana, K. P. P. (2015). Estimation of Sediment Trap Efficiency in Reservoirs-An Experimental Study. *Engineer: Journal of the Institution of Engineers, Sri Lanka*, 48(2).
- Sharpe, C. F. (1938). Landslides and related phenomena.
- Singh, Y., Bhat, G.M., Sharma, V., Pandita, S.K and Thakur, K.K. (2012). Reservoir Induced Landslide at Assar, Jammu and Kashmir: A Case Study. *Geological Society of India*, vol.80, pp.435-439.
- Singh, Y., Haq, A. U., Bhat, G. M., Pandita, S. K., Singh, A., Sangra, R., & Kotwal, S. S. (2018). Rainfall-induced landslide in the active frontal fold–thrust belt of Northwestern Himalaya, Jammu: dynamics inferred by geological evidences and Ground Penetrating Radar. *Environmental Earth Sciences*, 77(16), 1-17.
- Strand, R.I., and Pemberton, E.L. (1982). Reservoir Sedimentation Technical Guidelines for Bureau of Reclamation, U.S. Bureau of Reclamation, Denver, Colorado, 48 pp.
- Tan, G., Chen, P., Deng, J., Xu, Q., Tang, R., Feng, Z., & Yi, R. (2019). Review and improvement of conventional models for reservoir sediment trapping efficiency. *Heliyon*, 5(9), e02458.
- Ul Haq, A., Pandita, S. K., Singh, Y., Bhat, G. M., Pandey, S. J., Singh, A., & Bansal, B. K. (2019). Evidence of Active Tectonic Deformation in Kishtwar Area, Jammu and Kashmir, Northwest Himalaya, India. *Journal of the Geological Society of India*, 93(3), 331-342.
- Van Schalkwyk, A and Thomas, M.A. (1991). Slope failures associated with the floods of September 1987 and February 1988 in Natal and Kwa-Zulu, Republic of South Africa. *Geotechnics in the African Environment*, Blight et al. (Eds), pp.57-63.
- Verstraeten, G., & Poesen, J. (2000). Estimating trap efficiency of small reservoirs and ponds: methods and implications for the assessment of sediment yield. *Progress in Physical Geography*, 24(2), 219-251.
- Walder, J.S. and Connor, J.E. (1997). Methods for predicting peak discharge of floods caused by failure of natural and constructed earthen dams. *Water Resources Research*, vol.33, pp.2337-2348.

(Received: 13 January 2021; Revised version accepted: 3 May 2021)

Provenance Characterization and Palaeoenvironmental Analysis of the Meta-Sedimentary Rocks of Sonaghati Formation, Betul District, Madhya Pradesh Using Geochemical Approach

Shradha Shukla^{1*}, Biswajeet Lenka², Hemraj Suryavanshi³, Subhrasuchi Sarkar¹

¹Geological Survey of India, SU: Madhya Pradesh, Bhopal.

² Geological Survey of India, SU: Orrisa, Bhubaneshwar.

³ Geological Survey of India, NMH-II, Nagpur

* Corresponding author email: shradha.sukla@gsi.gov.in.

Abstract

Betul belt, ENE-WSW trending, 135 km long, prominent litho-tectonic unit exposed in the central part of Central Indian Tectonic Zone (CITZ) is composed of meta-sedimentary & meta-volcanic rocks intruded by mafic-ultramafic and granitic suite of rocks, belonging to Palaeoproterozoic to Neoproterozoic age. This belt is traversed by several ENE-WSW trending, sub-vertical ductile shear zones.

The meta-sedimentary rocks of Sonaghati Formation were geochemically characterized and their geochemical composition was interpreted for provenance characterization and paleo-environmental assessment. The weathering indices including Chemical index of Alteration, Chemical index of Weathering, Plagioclase Index of Alteration and Weathering Index of Parker indicate that these meta-sedimentary rocks have witnessed the substantial amount of weathering at the source without any evidence of potash metasomatism. The Bivariate plots using the major and trace element composition show co-linear trends, which reflect that all these samples belong to co-genetic population and the visible compositional variation could be attributed to chemical, mineralogical and textural maturity.

The Sonaghati metasedimentary rocks are enriched in REE with negative Eu anomaly. The LREE enrichment varies from 122 to 174 times and that of the HREE enrichment ranges from 12 to 31 times of Chondrite indicating highly varied protoliths. The provenance characterization was attempted using the large ion lithophile elements and high field strength elements. The results show that the precursor for these meta-sedimentary litho-units are mixed source with the major contributor being felsic to intermediate and minor contribution has come from the mafic end members. These meta-sedimentary rocks were deposited in the overall semi arid climate with a sequential transition, suggesting the variable climatic conditions ranging from semi-arid to arid. The Cu/Zn, V/Cr ratios, and presence of pyrites dissemination and stringers eventually indicate the prevalence of reducing environmental conditions during the deposition of these meta-sediments.

Key words: *Betul Belt, Meta-Sedimentary, Geochemistry, Graphite, Central Indian Tectonic Zone*

Introduction

The paleo-environmental reconstruction and characterization for understanding the ancient geological architecture is always enigmatic. The geochemistry is one of the classical tools having wide acceptability and ubiquitous applicability in deciphering the past geological processes. Nearly 70% of the global sedimentary mass is made up of the fine grained terrigenous sediments (Garrels and Mackenzie, 1971; Taylor and McLennan, 1985), therefore the geochemical characterization of these sediments can eventually provide the synoptic understanding about the overall crustal composition and subsequently after eliminating the effects of weathering and

metamorphism the provenance characterization can also be attempted. (Nesbitt and Young, 1982, 1984, 1989; Hayashi et al., 1997)

The Betul belt, is ENE-WSW trending, 135 km long, prominent litho-tectonic unit exposed in the central part of Central Indian Tectonic Zone (CITZ). Its northern limit is defined by Son- Narmada South Fault (SNSF) and southern limit by Gavilgarh Tan Shear zone (GTS). Predominantly, Betul belt is composed of meta-sedimentary and meta-volcanic rocks intruded by mafic-ultramafic and granitic suite of rocks, belonging to Palaeoproterozoic to Neoproterozoic age (Srivastava and Chellani, 1995). The latest detailed tectono-stratigraphy of the Betul belt after Chakraborty et al. (2009) is given in the Table 1.1. The base-metal

mineralization is hosted within the meta-volcanic rocks whereas, the graphite mineralization is mainly concentrated within the meta-sedimentary rocks (GSI Bulletin series A-69, 2018).

Table 1.1: The tectonostratigraphic succession of Betul belt (after Chakraborty et al., 2009)

DECCAN TRAPS	Basaltic lava flows and dolerite dykes	
<i>Intrusive contact / Disconformity</i>		
GONDWANA SUPERGROUP	Conglomerate, sandstones, and shales	
<i>Unconformable / Tectonic Contact</i>		
BETUL GROUP	INTRUSIVES	Basic dykes, pegmatites, quartz veins, homophanous amphibole-mica granite, porphyritic granite
	<i>Intrusive / Tectonic contact</i>	
	PADHAR MAFIC – ULTRAMAFIC SUITE	Diorite, epidiorite, gabbro, norite, pyroxenite, hornblendite, websterite, harzburgite, anorthosite, diorite, talc – serpentinite rock, quartz – epidote rock
	<i>Intrusive / Tectonic contact</i>	
	SONAGHATI FORMATION	Intercalated sequence of quartzite, quartz-mica schist and graphite schist
	<i>Conformable / Tectonic contact</i>	
	BARGAON FORMATION	Meta-sediments (mica schists), meta-rhyolite and felsic metatuff, metabasalt and amphibole – chlorite schist
	<i>Conformable / Tectonic contact</i>	
RANIPUR FORMATION	Phyllite, banded hematite / magnetite quartzite, BIF, granulite, meta-basalt, amphibolites, carbonaceous phyllites, calcareous quartzite, calc-silicates, marble	
<i>Un-conformable / Tectonic contact</i>		
AMLA GNEISS	BASEMENT ROCK	Banded migmatite gneiss, Quartzo-feldspathic mica schist /gneiss

The geochemical characterization of different litho-units of Betul Supracrustal rocks has been earlier attempted (Alam et al., 2009; Mishra et al., 2011; Praveen et al., 2016; Yousuf et al., 2019) but till date the metasedimentary rocks including the quartz mica schist and graphite schist of the Sonaghati Formation have neither been geochemically characterized nor interpreted in detail for provenance and depositional environment delineation. In the present study the geochemical characterization of meta-sediments of the Sonaghati Formation exposed in the Tikari-Gauthana-Chiklar area, Betul district, was attempted for provenance delineation. The samples of Graphite schist and Quartz Mica Schist were geochemically analyzed and interpreted. Considering the limited extent of disposition and the mono-mineralic nature of the quartzite band inter-bedded with the quartz mica schist; the quartzites were not utilized in the synoptic interpretation of plaeoarchitecture.

Geology

The Tikari-Gauthana-Chiklar area is located in the western part of Betul belt, which extends from Chhindwara in the east to Chicholi in the west in the ENE-WSW direction (Fig.1). The Betul belt is traversed by several ENE-WSW trending, sub-vertical ductile shear zones and the NE-SW trending Sonaghati Shear Zone is one of the prominent one running across the present study area. The Sonaghati Shear Zone

separates the metasedimentary rocks exposed in the western and northwestern part from the bimodal volcano-sedimentary rocks exposed in the eastern and central parts of Betul belt (Chakraborty et al., 2009). The Tikari-Gauthana-Chiklar area exposes the basement Granite Gneisses with amphibolites and the meta-sedimentary package including Quartz Mica Schist (QMS), Graphite Schist (GS) and Quartzite belonging to Sonaghati Formation. These are intruded by multiple generations of pegmatite, and quartz veins.

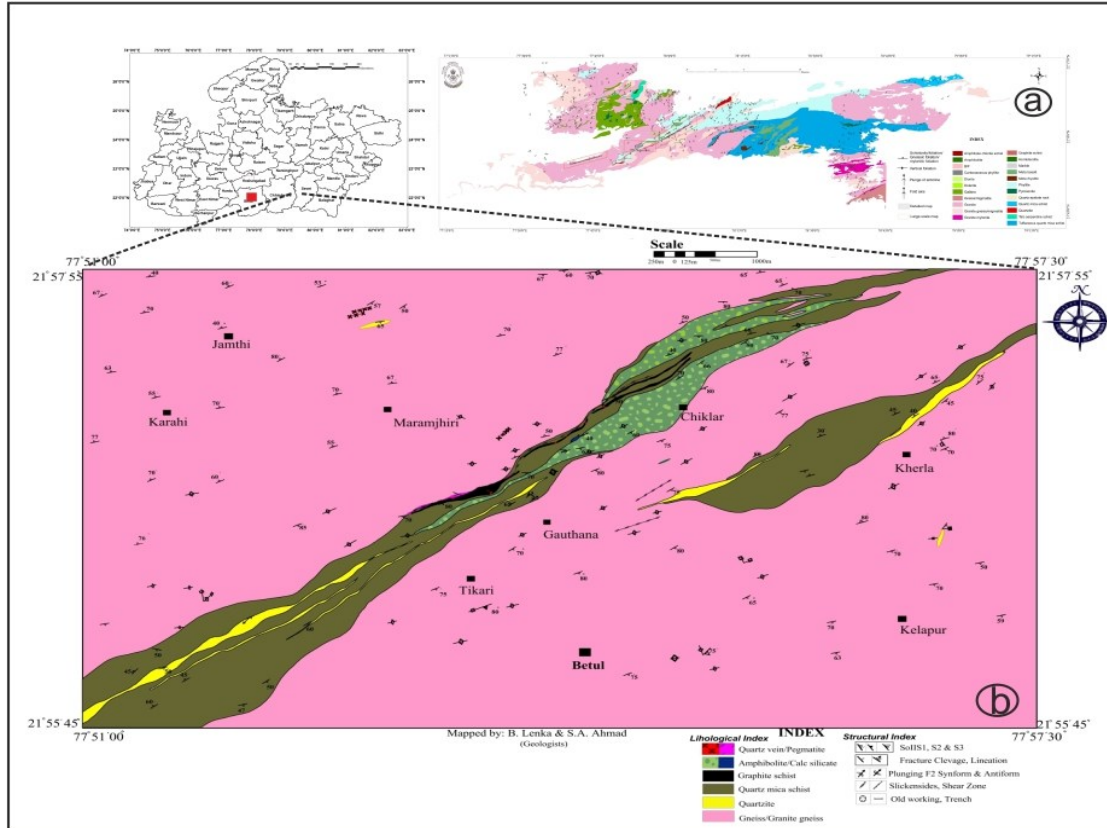


Fig.1: Regional Geological Map of Betul belt showing the location of Tikari-Gauthana-Chiklar area, Betul district (Inset: District Map of Madhya Pradesh showing the location of Betul district). b) Large Scale Map on 1:12,500 scale of Tikari, Gauthana and Chiklar and surrounding areas Betul district (after Lenka & Ahmad, 2013)

Although these intrusive rocks from the present study area were not studied for systematic geochronological studies, till date but one of the post-tectonic granitic phases in the vicinity has yielded a Rb–Sr age of ca. 850 ± 50 Ma (Sarkar, 1986; Raut and Mahakud, 2002; Roy and Prasad, 2003), which constrains the upper age of Betul supracrustal sequence. The secondary calcite veins are also recorded (Lenka and Ahmad, 2013).

Megascopically, the QMS is fine to medium grained, thinly foliated, with S_0 parallel S_1 and exposed as continuous band having the strike of ENE-WSW and vertical to sub vertical dip with variable direction. The dominant mineral phases are quartz, sericite, muscovite, biotite and chlorite with some epidote and \pm garnet (Lenka and Shukla, 2016). The discontinuous lensoidal quartzite bands, inter-bedded with micaceous quartzite and QMS having the gradational contact with each other are also recorded at some places. This lithological variation within the meta-sedimentary package in limited areal extent is attributed to the mineralogical disparity within the precursor lithology of each litho-unit. The lensoidal inter-banding of quartzite within the QMS showing pinching and swelling (Fig. 2a) nature is developed during two phases of deformation (Lenka, 2014), due to different rheological properties of these

litho-units. The evidences of two generations of folding were also observed within this QMS (Lenka, 2014). The GS is exposed in lenticular discontinuous bodies disposed in an en-echelon pattern over a strike length of 3.5 km within the QMS. In the present study area three bands of GS (5 m to 135 m wide) have been identified by Lenka and Ahmad (2013) (Fig.1b).

Megascopically, the GS is black to steel grey in color, fine to medium grained, soft, greasy and schistose with closely spaced foliation defined by parallel alignment of mica and graphite flakes (Fig. 2b). The dominant minerals include flaky and amorphous graphite, quartz, muscovite and feldspars in varying proportions. The lensoidal and pinching - swelling behavior of the graphite bearing bands and intermittent quartzo-feldspathic siliceous partings has been recorded within GS by Lenka and Shukla (2016). The evidences of shearing and three generations of folding are also well preserved (Fig. 2 c, d). The F_1 folds are tight isoclinal and rootless in nature whereas the F_2 and F_3 are tight to open, inclined with moderate to steep plunge (Lenka and Ahmad, 2013). The later intrusive calcite and quartz veins with mm to cm thickness were recorded in the outcrop and thin sections.

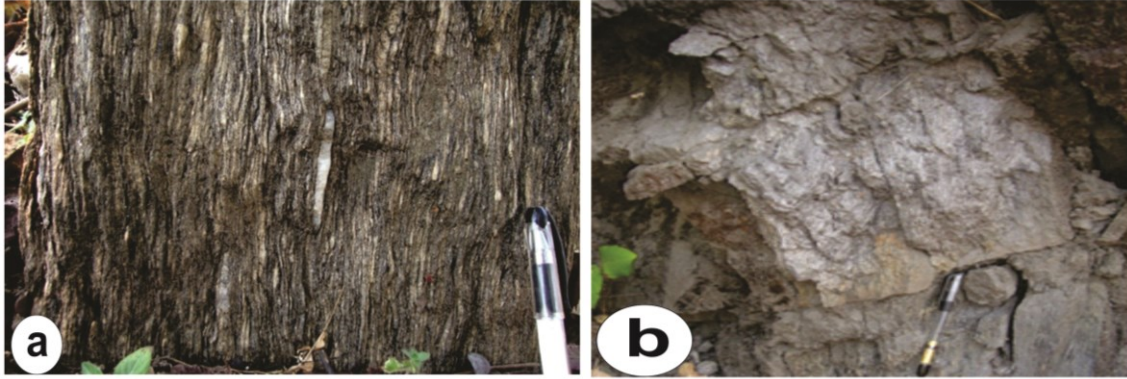


Fig. 2 (a) The field photograph of QMS, north of Sonaghati ridge, Sonaghati area ($21^{\circ}55'57''\text{N}$ $77^{\circ}53'13''\text{E}$) showing well developed schistosity and stretched and flattened quartz grains along the schistosity plain. (b) The field photograph of Graphite Schist exposed in an old working north of Tikari village ($21^{\circ}55'42''\text{N}$ $77^{\circ}53'17''\text{E}$).



Fig. 2 (c) The field photograph of F₂ folds enveloped by F₃ warps in GS exposed in NW of Chiklar village ($21^{\circ}56'46''\text{N}$; $77^{\circ}54'38''\text{E}$). (d) The field photograph of F₂ folding in quartzite plunging SW exposed in north of Gauthana village ($21^{\circ}56'12''\text{N}$; $77^{\circ}53'53''\text{E}$).

Material & Methodology

The current study forms a part of the annual field season program of Geological Survey of India (GSI), G2 Stage exploration for graphite in Tikari-Gauthana-Chiklar block, Betul district for establishing the strike and depth continuity and resources augmentation. The petrochemical characterization of the host and the associated lithounits was also carried out for better understanding of the geological setup and the mineralization. In the present study sixteen randomly selected core samples of different meta-sedimentary rock units including GS and QMS from varying depths were selected for geochemical characterization from Sonaghati Formation of the Betul belt. The due care was taken for homogeneous and true representation of the rock formations. The samples were collected from 06 boreholes, with the sample depth ranging from 100.50 m to 209.70 m below the surface (Table 2). Another factor considered during samples selection was the fixed carbon content. These samples were selected in such a way that the overall

chemical variation of the major and trace elements with reference to the fixed carbon content (ranging from 0 to 18.50 %) could be determined and interpreted.

The collected samples were pulverized up to 120-mesh size following the standard procedure of sample processing for petrochemical analysis of the GSI (SOP GSI, 2010) and all the adequate precautions were adapted to avoid anthropogenic contamination. These samples were analyzed using the M/S Analytical, X-Ray Fluorescence Spectrometer at Chemical Laboratory, GSI, SR, Hyderabad for major and trace elements. The precision of XRF for major oxide data is $\pm 5\%$ and that of trace element data is $\pm 10\%$. The standards GSR-1M were used for routine calibration and quantification. The analysis for fixed carbon content and the volatile matter was carried out at Chemical Lab, Bhopal using Atomic Absorption Spectrophotometer - Graphite Furnace of Varian make model no. AA-220, instrument. The precision of AAS for fixed carbon analysis is $\pm 2\%$. Out of the 16 samples, 05 samples were analyzed for rare earth

Table: 2: The Analytical results of Major and Trace Elements for the samples of meta-sedimentary from, Sonaghati Formation

Sample No.	PCS-3	PCS-7	PCS-11	PCS-12	PCS-13	PCS-14	PCS-15	PCS-16	PCS-17	PCS-18	PCS-19	PCS-20	PCS-21	PCS-22	PCS-23	PCS-24
Rock Type	Quartz Mica schist	Quartz Biotite schist	Graphitic schist	Graphiti c schist	Graphiti c schist	Graphitic schist	Graphiti c schist	Graphiti c schist								
Borehole No.	BBT-11	BBT-12	BBT-08	BBT-08	BBT-08	BBT-09	BBT-09	BBT-09	BBT-11	BBT-11	BBT-12	BBT-12	BBT-13	BBT-13	BBT-14	BBT-14
Sample depth	100.50m	209.70m	122.90m	132.10m	187.30m	135.7	154.00m	164.70m	123.80m	133.55m	158.00m	188.25m	150.50m	157.90m	156.00m	163.10
FC (%)	0	0	0.45	7.82	13.73	0.78	13.51	8.17	0.53	8.03	10.92	18.5	1.6	9.41	3.35	16.08
SiO ₂ (%)	64.07	59.50	69.62	63.86	75.26	68.77	68.74	68.53	67.28	68.82	68.57	64.98	62.38	72.25	64.07	69.20
Al ₂ O ₃ (%)	8.37	13.96	11.75	16.71	12.25	10.00	13.59	14.44	12.47	14.17	12.37	17.55	16.04	13.89	18.84	15.72
Fe ₂ O ₃ (%)	14.81	7.91	8.38	7.86	4.59	8.25	4.40	6.70	11.57	8.16	6.40	5.00	9.48	3.56	5.57	5.44
MnO (%)	0.83	0.52	0.76	0.21	0.06	0.63	0.12	0.20	0.52	0.24	0.16	0.13	0.43	0.12	0.21	0.16
MgO (%)	6.35	9.14	3.63	4.19	2.47	3.65	5.14	3.69	3.23	3.96	3.25	3.10	4.97	4.37	3.49	3.24
CaO (%)	1.31	2.64	1.42	1.33	0.87	5.79	2.16	1.63	1.08	0.38	5.67	2.85	2.35	1.66	1.63	1.38
Na ₂ O (%)	0.97	1.60	0.94	1.00	0.83	0.51	1.47	0.78	0.73	0.80	0.21	0.73	0.42	0.22	0.89	0.76
K ₂ O (%)	2.17	3.66	2.75	4.08	3.13	1.80	3.75	3.47	2.20	2.88	2.74	4.63	2.75	3.23	4.63	3.08
TiO ₂ (%)	0.54	0.91	0.62	0.61	0.43	0.50	0.47	0.47	0.72	0.51	0.45	0.63	0.59	0.52	0.53	0.53
P ₂ O ₅ (%)	0.58	0.16	0.14	0.15	0.11	0.10	0.17	0.08	0.19	0.09	0.18	0.41	0.59	0.18	0.15	0.49
Ba (ppm)	1102	715	1304	693	661	705	608	1185	1022	945	323	961	850	653	575	530
Ga (ppm)	5.9	18	8.7	<5	19	<5	15	17	7.9	9.0	15	14	<5	18	19	14
Sc (ppm)	53	26	24	44	29	<3.5	13	28	36	36	6.9	34	20	26	28	24
V (ppm)	157	81	269	758	1108	254	1309	636	261	746	1586	1848	281	1610	317	1411
Th (ppm)	<4	<4	<4	<4	<4	<4	<4	<4	<4	<4	<4	<4	8.3	<4	<4	<4
Pb (ppm)	33	<2	<2	<2	<2	15	<2	<2	44	19	74	<2	51	<2	<2	20
Ni (ppm)	46	66	60	171	145	51	177	119	49	132	299	155	98	234	88	171
Co (ppm)	22	15	16	7.0	14	8.4	8.1	22	21	6.4	23	7.7	14	9.8	9.7	7.1
Rb (ppm)	78	233	117	128	96	81	196	127	112	106	98	154	106	116	185	120
Sr (ppm)	57	121	65	81	96	75	131	74	68	73	65	113	62	62	77	77
Y (ppm)	6.3	21	18	30	31	19	45	28	16	27	45	49	36	49	28	34
Zr (ppm)	86	196	109	156	145	84	139	138	105	116	91	137	121	133	124	131
Nb (ppm)	20	30	22	19	7.5	22	17	19	22	23	23	19	25	20	52	22
Cr (ppm)	98	163	139	259	298	123	367	241	122	272	455	629	140	526	161	438
Cu (ppm)	98	12	94	258	444	79	577	423	149	363	916	322	249	604	173	423
Zn (ppm)	98	66	117	312	625	79	334	227	98	285	767	155	293	694	179	364
CIA	65.28	63.87	69.71	72.27	71.72	55.23	64.84	71.06	75.67	77.76	58.93	68.14	74.40	73.11	72.51	75.05
ICV	3.22	1.89	1.57	1.15	1.01	2.11	1.29	1.17	1.61	1.19	1.53	0.97	1.31	0.98	0.90	0.93
CIW	78.60	76.71	83.28	87.74	87.79	61.32	78.94	85.69	87.32	92.36	67.76	83.08	85.29	88.10	88.22	87.99
WIP	3184.17	5234.48	3340.10	4489.93	3377.08	2963.50	4713.73	3868.45	2691.35	3252.32	3481.66	4869.13	3330.09	3435.21	4831.04	3458.54

elements (REE) using the ICP-MS, Perkin Elmer Sciex, model no. ELAN -6100, instrument at Chemical Lab, GSI, Nagpur following the standard procedure of analysis with the accuracy and precision of $\pm 5\%$. The four samples were analyzed at Mineral Physics Laboratory, GSI, CR, Nagpur using the XRD instrument for identification of minerals. The sampling and analytical details are given in Lenka and Shukla (2016).

Results

Petrography

The GS and QMS are fine grained rocks with equigranular hypidiomorphic texture. The dominant mineral phases in QMS are muscovite, quartz and

opaques (graphite/ Fe-Ti oxides) whereas chlorite, k-feldspar, plagioclase, biotite, hornblende and diopside occur in minor proportions with variations in samples. The kyanite and andalusite are also present in traces. The above-mentioned minerals also occur in GS. In addition these rocks also contain flaky and amorphous type of graphite. Muscovite/ biotite occur as tabular elongated grains and define the schistosity (Fig.3a-b), whereas quartz occurs as anhedral grains with equigranular interlocking granoblastic texture. Quartz shows undulose extinction and stretched quartz grains define the schistosity. Graphite occurs along the foliation planes as isolated, flat, plate-like minerals. It also occurs as irregular or angular crystalline flakes and, as opaque anhedral to cryptocrystalline globular porphyroblasts (Fig. 3e-f).

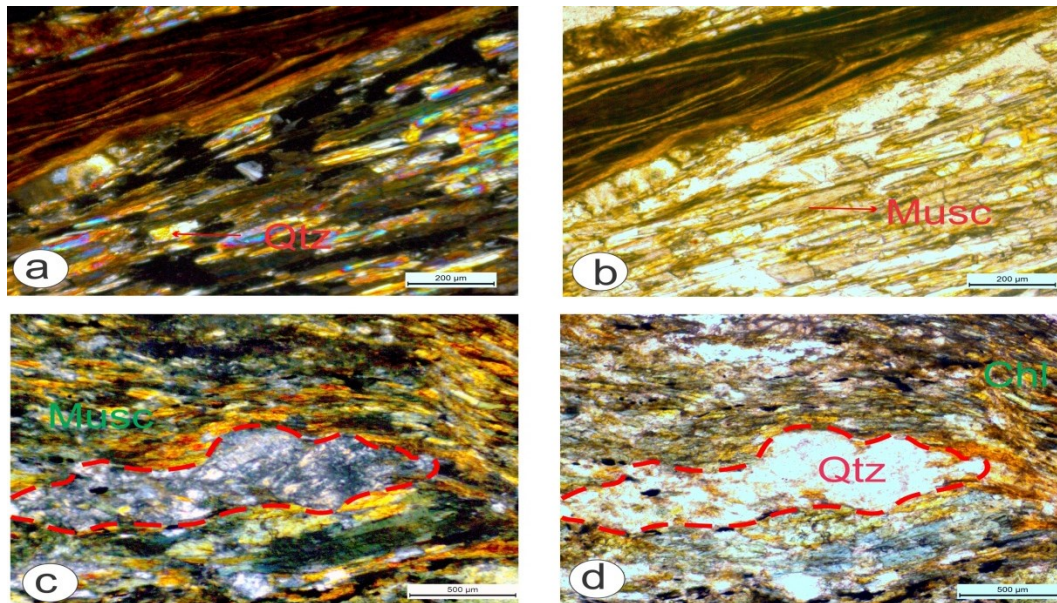


Fig.3 (a & b): Photomicrograph of Quartz Mica Schist with porphyroblasts having flow banding typical aligned along the dominant schistosity defined by quartz and muscovite (c & d): Photomicrograph of Quartz Mica Schist with pinching and swelling of Q domain along the dominant schistosity.

The schistosity is well developed and defined by parallel alignment of graphite flakes (Fig. 3e-f & Fig. 4a), biotite and muscovite. Both Q-domain and M-domain can be identified (Fig. 3g-h) in the thin sections. The M-domain is dominantly composed of tabular micaceous grains and graphite with occasional presence of quartz whereas; Q-domain is defined mainly by quartz with small amount of mica in the inter-granular spaces. In some cases, typical granoblastic texture is observed along with the development of triple junctions. Evidence of shearing is depicted by pinch and swell structure (Fig. 3c-d) and presence of mica fish. The lithic fragment (rhyolite?) is observed in thin section of QMS (Fig. 3a-b).

XRD Studies

The four surface samples of GS from Tikari-Gauthana-Chiklar area, were analyzed using the XRD for mineral identification. The major minerals identified were quartz (45% to 57%), muscovite (25% to 40%), montmorillonite (0 to ~16%), clinochore (0 to ~15%), graphite (3% to 4%), calcite (0 to ~15%), nontronite (0 to ~10%), and kanemite (0 to ~2%) (Fig.4b; Table 3).

Major Oxides

The detailed geochemical analytical results of the samples of Graphite Schist and Quartz Mica Schist of Sonaghathi Formation are presented in Table 2. The SiO_2 content in the analyzed samples varies from 59.50% to 75.26% and the Al_2O_3 varies from 8.37% to

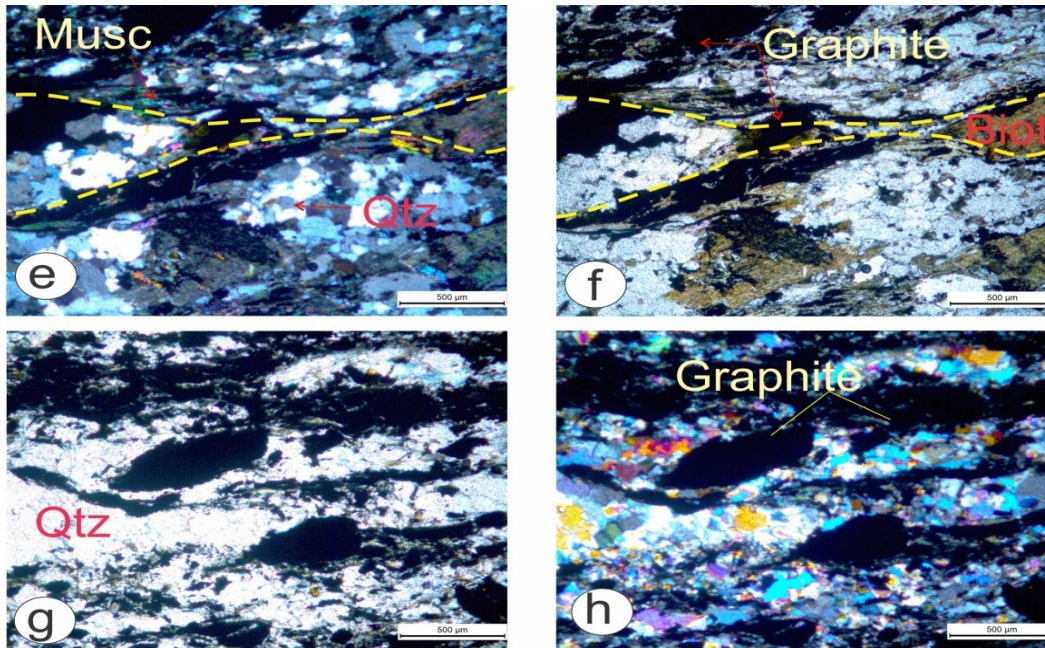


Fig.3: (e & f): Photomicrograph of Graphitic Schist with alternate Q and M domains, pinching and swelling is also observed. (g & h): Photomicrograph of Graphitic Schist with alternate domains of quartz rich layer and graphite rich layers. The graphite flaks is distinctly observed. (PPL and cross nicol view- right and left half respectively).

Table 1.3. The results of XRD analysis for the samples of meta-sedimentary from, Sonaghati Formation.

Sample No	Rock Type	Location	
GR-01	Graphite Schist	21° 58' 40.3166" 77° 54' 30.9045"	Quartz ≈ 45.00%; Muscovite ≈ 35.00%; Montmorelonite ≈ 16.00%; Graphite ≈ 04.00 %
GR-02	Graphite Schist	21° 56' 23.1230" 77° 54' 7.2839"	Quartz ≈ 57.00%; Muscovite ≈ 40.00%; Graphite ≈ 03.00 %
GR-03	Graphite Schist	21° 56' 14.5125" 77° 53' 50.4474"	Quartz ≈ 55.00%; Muscovite ≈ 27.00%; Clinochore ≈ 15.00%; Graphite ≈ 03.00 %
GR-04	Graphite Schist with Calcite veins	21° 56' 3.7390" 77° 53' 22.5696"	Quartz ≈ 45.00%; Muscovite ≈ 25.00%; Calcite ≈ 15.00%; Nontronite ≈ 10.00%; Graphite ≈ 03.00 %; Kanimite ≈ 02.00 %

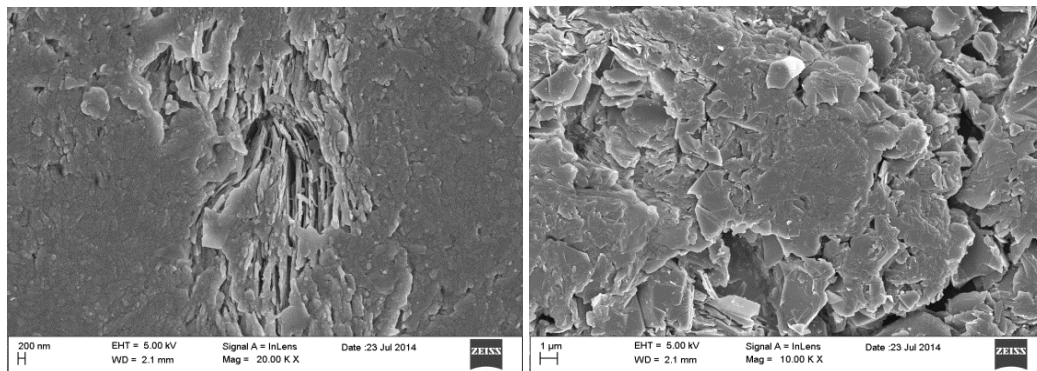


Fig. 4: (a). SEM microphotograph of GS of Tikari-Gauthana-Chiklar area, Betul district showing crystalline elongated graphite with intrinsic flaky morphology along with the shattered grains along the foliation planes.

Table 4: The Correlation Matrix for the samples of meta-sedimentary rocks from, Sonaghati Formation, showing the elemental inter relationship.

	FC (%)	SiO ₂ (%)	Al ₂ O ₃ (%)	Fe as Fe ₂ O ₃	MnO (%)	MgO (%)	CaO (%)	Na ₂ O (%)	K ₂ O (%)	TiO ₂ (%)	P ₂ O ₅ (%)	Ba (ppm)	Ga (ppm)	Sc (ppm)	V (ppm)	Pb (ppm)	Ni (ppm)	Co (ppm)	Rb (ppm)	Sr (ppm)	Y (ppm)	Zr (ppm)	Nb (ppm)	Cr (ppm)	Cu (ppm)	Zn (ppm)	
FC (%)	1.00																										
SiO ₂ (%)	0.44	1.00																									
Al ₂ O ₃ (%)	0.39	-0.31	1.00																								
Total Fe as	-0.72	-0.44	-0.62	1.00																							
MnO (%)	-0.83	-0.36	-0.62	0.82	1.00																						
MgO (%)	-0.45	-0.66	-0.16	0.33	0.41	1.00																					
CaO (%)	-0.04	-0.09	-0.22	-0.09	0.09	0.00	1.00																				
Na ₂ O (%)	-0.11	-0.38	0.04	0.09	0.16	0.58	-0.34	1.00																			
K ₂ O (%)	0.47	-0.26	0.83	-0.59	-0.61	0.01	-0.22	0.34	1.00																		
TiO ₂ (%)	-0.45	-0.67	0.12	0.33	0.42	0.63	-0.10	0.47	0.11	1.00																	
P ₂ O ₅ (%)	0.04	-0.38	0.05	0.37	0.32	0.18	-0.07	-0.13	-0.10	0.09	1.00																
Ba (ppm)	-0.39	-0.09	-0.24	0.52	0.56	0.05	-0.43	0.15	-0.20	0.24	0.08	1.00															
Ga (ppm)	0.38	0.09	0.57	-0.80	-0.70	0.01	0.28	0.00	0.69	-0.12	-0.39	-0.59	1.00														
Sc (ppm)	-0.28	-0.24	-0.15	0.59	0.40	0.12	-0.61	0.19	-0.06	0.22	0.21	0.50	-0.52	1.00													
V (ppm)	0.92	0.47	0.28	-0.71	-0.77	-0.42	0.13	-0.32	0.36	-0.44	0.04	-0.45	0.35	-0.38	1.00												
Pb (ppm)	0.01	-0.30	0.09	-0.01	-0.22	-0.05	0.33	-0.66	0.17	0.01	0.10	-0.35	0.42	-0.62	0.30	1.00											
Ni (ppm)	0.71	0.37	0.25	-0.63	-0.75	-0.30	0.23	-0.40	0.28	-0.47	-0.10	-0.63	0.42	-0.53	0.86	0.56	1.00										
Co (ppm)	-0.39	-0.04	-0.51	0.50	0.40	0.12	0.12	-0.13	-0.42	0.06	0.06	0.31	-0.26	-0.02	-0.29	0.77	-0.12	1.00									
Rb (ppm)	0.07	-0.47	0.51	-0.37	-0.23	0.51	-0.08	0.70	0.71	0.52	-0.19	-0.19	0.51	-0.25	-0.01	0.07	-0.04	-0.25	1.00								
Sr (ppm)	0.41	-0.15	0.26	-0.45	-0.35	0.31	0.04	-0.70	0.56	0.27	-0.18	-0.22	0.43	-0.21	0.26	-0.59	0.06	-0.37	0.76	1.00							
Y (ppm)	0.77	0.25	0.52	-0.80	-0.81	-0.28	0.21	-0.32	0.51	-0.34	0.01	-0.52	0.58	-0.61	0.87	0.51	0.83	-0.36	0.21	0.32	1.00						
Zr (ppm)	0.24	-0.27	0.51	-0.43	-0.40	0.44	-0.32	0.58	0.66	0.48	-0.17	-0.15	0.65	0.10	-0.16	0.08	-0.30	0.74	0.67	0.25	1.00						
Nb (ppm)	-0.40	-0.54	0.46	0.04	0.11	0.19	0.06	0.09	0.33	0.26	-0.02	-0.17	0.20	-0.05	-0.38	0.29	-0.25	-0.10	0.45	-0.10	-0.15	0.01	1.00				
Cr (ppm)	0.88	0.34	0.36	-0.70	-0.73	-0.32	0.13	-0.29	0.44	-0.28	0.07	-0.40	0.38	-0.33	0.98	0.24	0.81	-0.33	0.09	0.29	0.87	0.19	-0.30	1.00			
Cu (ppm)	0.68	0.51	0.09	-0.57	-0.71	-0.38	0.22	-0.43	0.11	-0.62	-0.12	-0.54	0.34	-0.62	0.80	0.63	0.94	0.06	-0.14	0.00	0.77	-0.08	-0.31	0.71	1.00		
Zn (ppm)	0.55	0.58	0.04	-0.55	-0.65	-0.34	0.12	-0.51	0.04	-0.56	-0.13	-0.61	0.43	-0.50	0.69	0.66	0.88	0.02	-0.25	-0.13	0.67	0.00	-0.33	0.59	0.88	1.00	

18.84%. The proportion of other oxides ranges from 3.56% to 14.81% (Fe₂O₃), 0.43% to 0.91% (TiO₂), 0.06% to 0.83% (MnO), 2.47% to 9.14% (MgO), 0.38% to 5.79% (CaO), 0.21% to 1.60% (Na₂O), 1.80% to 4.63% (K₂O) to 0.08% and 0.59% (P₂O₅).

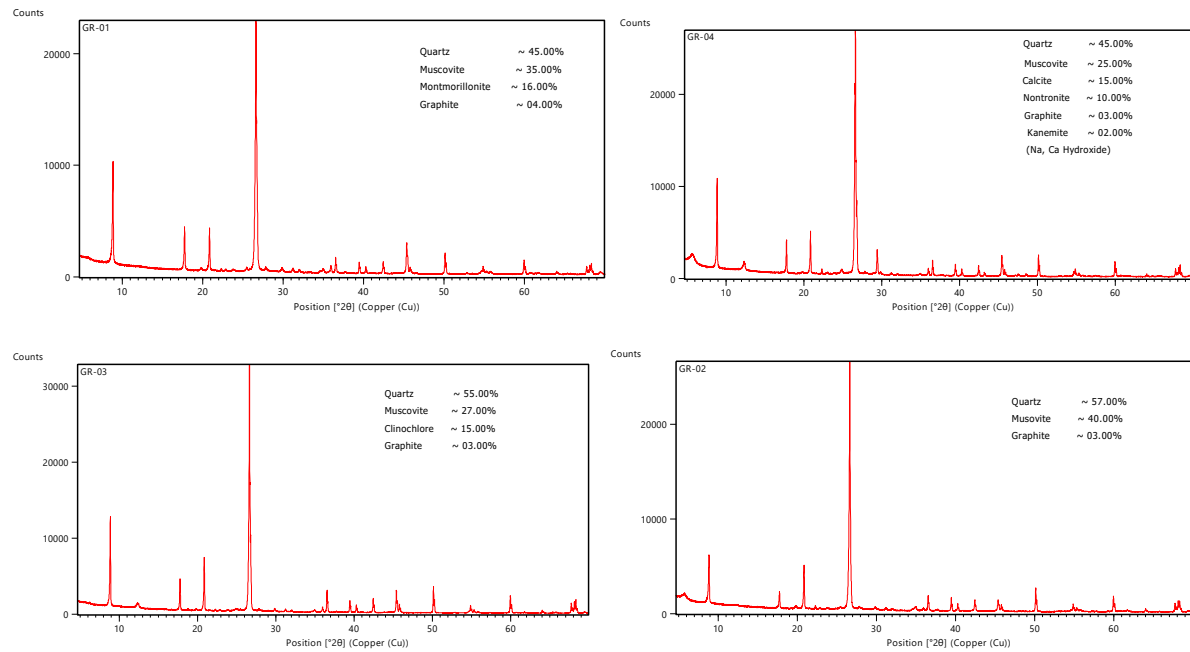


Fig. 4 (b): The XRD results of the samples of Graphite schist of Tikari-Gauthana-Chiklar area, Betul District showing the proportion of major mineral phases.

The bivariate XY plots of major oxides versus SiO₂ wt. % (Fig. 5a) displays a moderate to strong negative correlation between silica and all the other major oxides for all the samples of Sonaghati metasediments except the outlier samples for CaO. The co-linear trends in the XY plots indicate that the elemental characters of GS and QMS are attributed to mineral fractionation and textural maturity. The possible minerals influencing the geochemical signatures are quartz, clay minerals, opaques (Ti-Fe-Mg oxides) and some mafic minerals. The strong positive correlation between Al₂O₃ and K₂O, K₂O and Na₂O

suggests the dominance of clay minerals and muscovite (Fig. 5b). The higher concentration of calcium oxide within the outlier sample (PCS-14) is due to the presence of calcite vein, and the same is also validated by petrographic analysis. The sample with calcite vein was selected to understand the variation in bulk rock geochemistry of the meta-sediments after secondary enrichment of calcite and to identify the relation (if any) between REE's, fixed carbon and secondary calcite enrichment in meta-sediments.

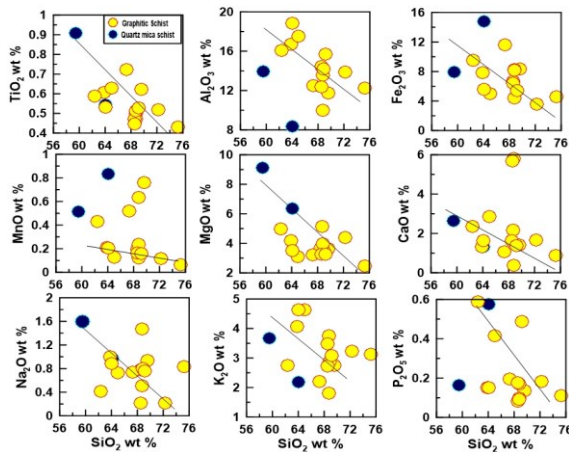


Fig 5 (a) X-Y Variation plots of major oxides with SiO₂ as differentiating index, after Harker.

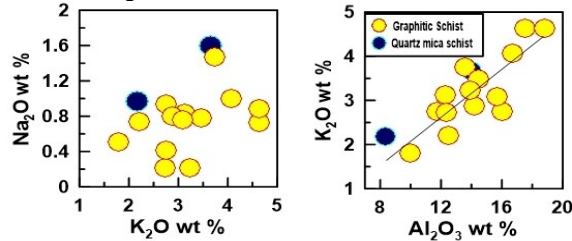


Fig 5 (b). X-Y Variation plots of Na₂O versus K₂O and Al₂O₃ versus K₂O.

The overall assessment of geochemical signatures of outlier sample (PCS-14) suggests that it is having the high concentration for CaO but other elemental association of all the other major oxides and trace elements and REE's are similar with the other samples of meta-sediments. No visible correlation between CaO, REE's, fixed carbon, and other trace elements is recorded (Table 4). The scattered elemental correlation between aluminum and sodium is attributed to the high mobility and low partitioning coefficient of sodium.

The K₂O/Al₂O₃ ratio for the samples of metasediments of Sonaghati Formation ranges from 0.17 to 0.28 with an average of 0.23. This ratio also eventually supplements our inference on the presence of clay minerals (K₂O/Al₂O₃ ratio range = 0.00 to 0.40) (e. g., Cox et al., 1995; Dar et al., 2020).

Trace Elements

A set of trace elements data of the samples of meta-sedimentary units including GS and QMS of Sonaghati Formation is presented in Table 2. The compatible trace elements (Cr, Co, Ni, and V) have a wide range of variations. The concentration ranges (in ppm) are 98 to 629 for Cr, 46 to 299 for Ni, 81 to 1848 for V, 6 to 23 for Co and 12 to 916 for Cu, and 66 to 767 for Zn. In-comparison to the Compatible elements the large ion lithophile elements (LILE's) have

restricted abundance range except for barium. The concentration ranges (in ppm) are 78 to 233 for Rb, 57 to 131 for Sr, 323 to 1304 for Ba and <2 to 74 for Pb. The variation of high field strength elements: Y, Sc, Th, U, Zr, Nb and REE's of the GS and QMS of Sonaghati Formation varies from (in ppm) 06 to 49 for Y, 84 to 196 for Zr, 8 to 52 for Nb, for 116.71 to 191.65 for Σ REE and <3.5 to 53 for Sc. The thorium content within all the samples is below detection limit except one sample with 8.3 ppm. The High field strength elements have low mobility and high partitioning coefficient (Taylor and McLennan, 1985), therefore are insoluble and least mobile in the surface conditions.

The multi elemental correlation of the elements elucidates very significant to significant correlation between the fixed carbon, vanadium, chromium, nickel, yttrium, copper and zinc. Another set of elements having the moderately significant correlation among them are sodium, potassium, rubidium, strontium and gallium Table 4.

The binary plots of trace elements (Zr, Cu, Y, V, Ba, Zn and Co) versus nickel are plotted for understanding the effect of mafic and opaque minerals in these elemental abundances. The binary trace element plots of Ni shows a strong positive correlation of Zr, Cu, Y, V and Zn and a moderate negative correlation with Ba and Co (Fig.6a) Along with these, a strong positive relationship between rubidium and strontium is also recorded. These trace element correlations further attenuate the inference derived from the correlation of major oxides that the mineral and textural maturity had impacted the geochemical signatures of these metasediments. Interestingly a strong positive correlation between fixed carbon and vanadium is also noticed. This intricate relationship suggests the possibility for co-genetic organic origin and metamorphic enrichment, of graphite and vanadium mineralization within these meta-sedimentary rocks of Betul belt. The co-linear trends among the compatible elements and high field strength elements suggest that the data set belongs to co-genetic population, eventually uninfluenced by the secondary process of chemical alterations and preserving the primordial elemental signatures.

Rare Earth Elements

The meta-sediments of the Sonaghati Formation are enriched in REE elements with negative Eu anomaly. The LREE enrichment varies from 122 to 174 times and that of the HREE enrichment ranges from 12 to 31 times of Chondrite (Fig.6b, Table 5), indicating highly varied protoliths. For the same group of samples, their (La/Lu)_N varies from ~5.76 to ~14.29 with an average of 9.03, (La/Sm)_N varies from 3.65 to 5.34 with an average of 4.20 and (Gd/Lu)_N varies from 1.00 to 1.70 with an average of 1.44. Thus, the Chond-

Table 5: The Analytical results of Rare Earth Elements for the samples of meta-sedimentary rocks from, Sonaghathi Formation

Sample NO	PCS-14	PCS-15	PCS-16	PCS-17	PCS-18
La (pg/g)	41.33	42.49	30.53	28.96	31.66
Ce (pg/g)	75.36	68.57	60.74	59.99	62.78
Pr (pg/g)	8.12	9.63	7.22	6.78	7.41
Nd (pg/g)	30.19	35.37	26.97	25.95	27.02
Sm (pg/g)	5.00	6.67	5.08	5.12	5.11
Eu (pg/g)	1.18	1.40	1.16	1.04	1.23
Gd (pg/g)	4.26	6.41	4.50	4.86	4.75
Tb (pg/g)	0.68	1.08	0.74	0.79	0.76
Dy (pg/g)	3.96	7.15	4.38	5.10	4.86
Ho (pg/g)	0.79	1.59	0.86	0.98	0.90
Er (pg/g)	2.19	4.87	2.41	2.76	2.65
Tm (pg/g)	0.34	0.81	0.38	0.41	0.39
Yb (pg/g)	1.98	4.82	2.21	2.52	2.38
Lu (pg/g)	0.31	0.79	0.37	0.41	0.39
(La/Lu) _N	14.29	5.76	8.84	7.57	8.70
(La/Sm) _N	5.34	4.11	3.88	3.65	4.00
(Gd/Lu) _N	1.70	1.00	1.50	1.47	1.51

rite normalized REE patterns suggests that Sonaghathi meta-sediments have much more fractionated LREE's dispersal with nearly flat and enriched HREE's. The presence of strong negative Eu anomaly indicates the

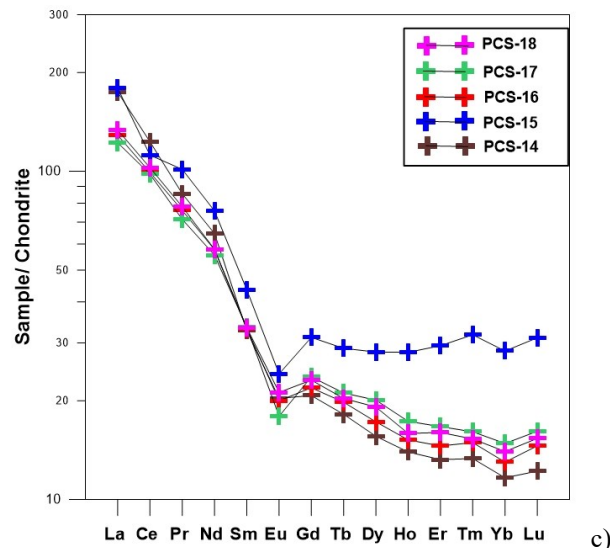


Fig. 6 b) chondrite normalized REE plots for the samples of Tikari-Gauthana-Chiklar area. The chondrite values are after Taylor & MacLennan, 1985. c) The NASC normalized REE plots for the samples of Tikari-Gauthana-Chiklar area.

Proterozoic age for the precursor of the metasediments. The overall abundance of REE in these meta-sediments is comparable with the North American Shale Composite (NASC) with slight depletion in HREE's except the sample no PCS15. The NASC values are after Gourmet et al. (1984). The sample 'PCS 15' is comparatively more fractionated and displays an enrichment of HREE's in comparison to both Chondrite and NASC (Fig. 6c).

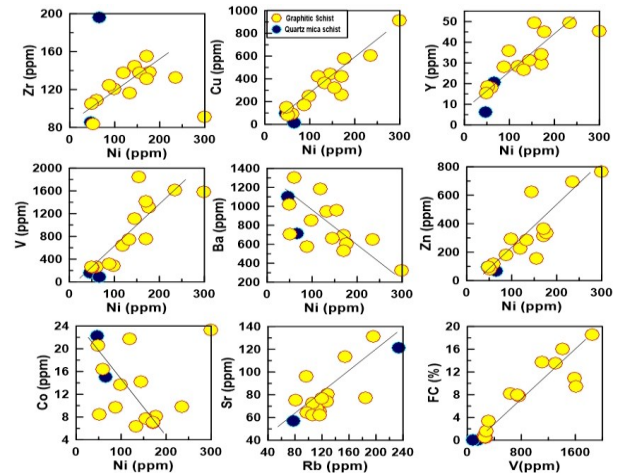
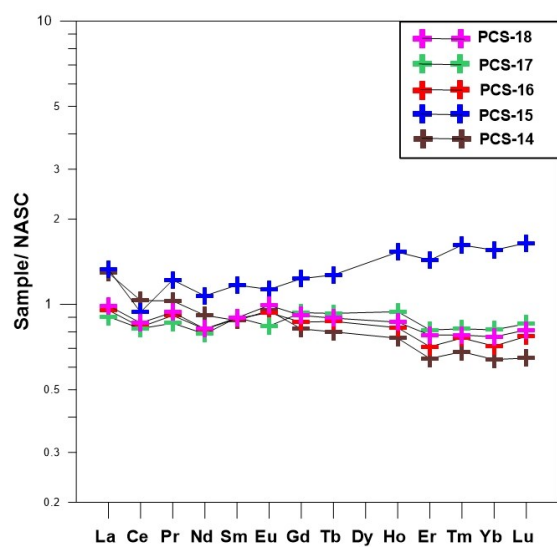


Fig. 6.(a) Variation plots of trace elements { Zircon (Zr), Copper (Cu), Yttrium (Y), Vanadium (V), Barium (Ba), Zinc (Zn), Cobalt (Co)} versus Nickel (Ni); Rubidium (Rb) versus Strontium; Vanadium (V) versus fixed Carbon.



Indices of Chemical Weathering

The geochemical data processing for understanding the provenance of the meta-sedimentary rocks was carried out. Thus, the chemical weathering

indices such as chemical index of alteration (CIA), chemical index of weathering (CIW), plagioclase index of alteration (PIA) and weathering index of parker (WIP) were calculated for the assessment of degree of metamorphism and weathering of the source terrain.

The CIA was calculated using the equation $[\text{Al}_2\text{O}_3 / (\text{Al}_2\text{O}_3 + \text{CaO} + \text{Na}_2\text{O} + \text{K}_2\text{O})] \times 100$ where all the oxides are in molar proportion and CaO represents Ca in silicate fraction (Nesbitt and Young, 1982, 1984; Fedo et al., 1995; Maynard et al., 1995). The CIA value of all the samples varies from 55.2 to 77.8 with an average of 69.3, is comparable with the average CIA values for global shale (~ 70 to ~ 75) by (Nesbitt and Young, 1982). This range of CIA value indicates the presence of muscovite, illite and smectite within the metasediments of Sonaghati Formation. These samples when plotted on the $\text{Al}_2\text{O}_3 - \text{CaO} + \text{Na}_2\text{O} - \text{K}_2\text{O}$ (A-CN-K) ternary diagram (Nesbitt and Young, 1984) shows trend sub parallel to A-CN axis, within the limits of weathering and follow the pattern of substantial weathering trend of the source terrain without displaying any evidence of potash metasomatism (Fig.7a).

The Chemical index of Weathering (CIW) (Harnois, 1988) was calculated using the equation $[\text{Al}_2\text{O}_3 / (\text{Al}_2\text{O}_3 + \text{CaO} + \text{Na}_2\text{O})] \times 100$ and the CIW values of all the samples vary from 61.32 to 92.36 with an average of 82.51. The Prince and Velbel (2003) had defined that the CIW values for the unaltered/ fresh samples should be ≤ 50 and that for the optimum weathered samples should be 100. The CIW values for the samples of the present study ranges in between the limits of fresh and optimum weathered samples, with an average value of 82.51. Therefore, considering intermediate CIW values for the meta-sedimentary rocks of Betul belt, it can be inferred that this belt had witnessed the substantial amount of weathering and the elemental data set generated can be effectively utilized for provenance characterization and plaeo-climatic reconstruction.

Prince and Velbel (2003) had also validated the WIP as the most robust indicator with its value 0 for optimum weathered sample and >100 for fresh/unaltered samples. Parker (1970) introduced the term WIP for silicate rocks. Eswaran et al., (1973) and Hamdam and Bumham (1996) were the pioneer workers involved in assessment and validation of the equation for other litho-units. The WIP values for the samples of the present study was calculated using the equation $[(2 \text{Na}_2\text{O}/0.35) + (\text{MgO}/0.9) + (2\text{K}_2\text{O}/0.25) + (\text{CaO}/0.7)] \times 100$ (Hamdam and Bumham, 1996). The WIP value for the GS and QMS of Sonaghati Formation ranges from 2691.35 to 5234.48 with an average of 3782.55. This high value of WIP are supportive with our initial inferences that the metasediments of Sonaghati Formation had undergone substantial weathering and are very much suitable for the source area characterization. This index is based on the proportion of the most mobile alkali and alkaline earth metals (sodium, potassium, magnesium and

calcium), therefore is most appropriate for evaluation of weathering profile of heterogeneous meta-sedimentary parent rocks (Prince and Velbel, 2003).

The values of all these weathering indices when compared with the sample depth, indicates that CIA and CIW shows an inverse relation and the WIP is having a positive relation with the sample depth. Hence, the degree of alteration in the metasediments of Sonaghati Formation is inversely proportional to the depth (Fig. 7b).

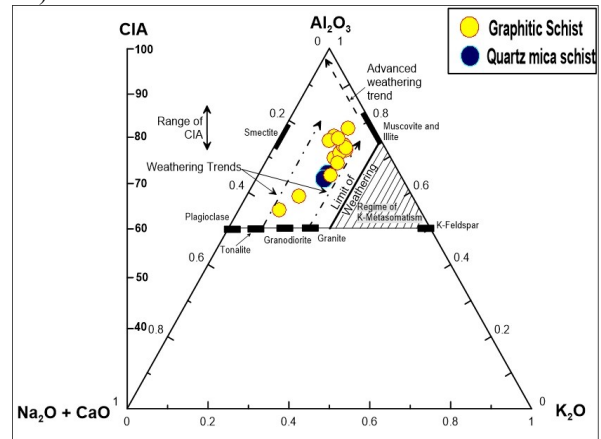


Fig. 7 a) A-CN-K ternary diagram (after Nesbitt and Young, 1984) showing weathering trends for the meta-sediments of Tikari-Gauthana-Chiklar area, Betul District.

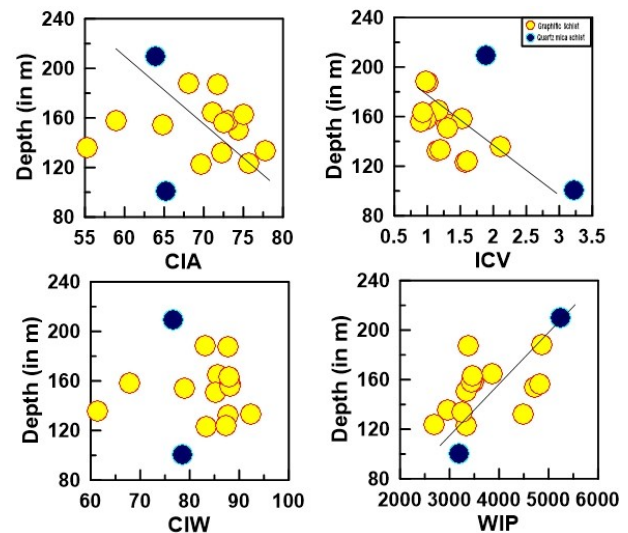


Fig. 7 b) The Bivariate plot of Chemical Weathering Indices (CIA, ICV, CIW and WIP) versus sample depth (in meters) for the meta-sediments of Tikari-Gauthana-Chiklar area, Betul District

Hydraulic Sorting

The index of compositional variability (ICV) after Cox et al. (1995) is useful to ascertain the effect of hydraulic sorting on the geochemical signatures. The

formula used for calculation of ICV is: $Fe_2O_3 + K_2O + Na_2O + CaO + MgO + MnO + TiO_2 / Al_2O_3$. The ICV values for samples from the present study area ranges from 0.90 to 3.22 with an average of 1.43. The figure 6a shows that the ICV had an inverse relationship with the sample depth. The progressive decreasing values of ICV indicate the progressive increase in the degree of hydraulic sorting (Cullers, 2000).

Classification

The Classification of fine clastic meta-sediments using the geo-chemical data has severe limitations but some of the ratio and ternary plots are widely acceptable. The most convenient graphical representation for sedimentary and meta-sedimentary rocks is log weighted ratios of SiO_2 / Al_2O_3 versus $(Na_2O+CaO) / K_2O$ after Garrels and Mackenzie, (1971) and Gilboy (1982). The ratio SiO_2 / Al_2O_3

distinguishes the siliceous sediments from argillaceous sediments whereas $(Na_2O+CaO) / K_2O$ separates the argillaceous from the calcareous. The samples of the present study area fall in the domain of argillaceous pelagic sediments to siliceous ooze (Fig. 8a). These elemental ratios also elucidated that the metasediments of Sonaghati Formation have composition very similar to that of Proterozoic shales. In figure 8b all the samples from the present study are clustered around the average concentration of Proterozoic shale's given by Garrels and Mackenzie (1971). In the diagram showing the relationship between the composition of igneous rocks and those of sedimentary rocks after Garrels and Mackenzie (1971) the samples from the present study shows the scattered dispersion varying between granite- to granodiorite thus suggests that they may have the felsic dominant precursor ranging in composition from granite- to granodiorite (Fig. 8a,b).

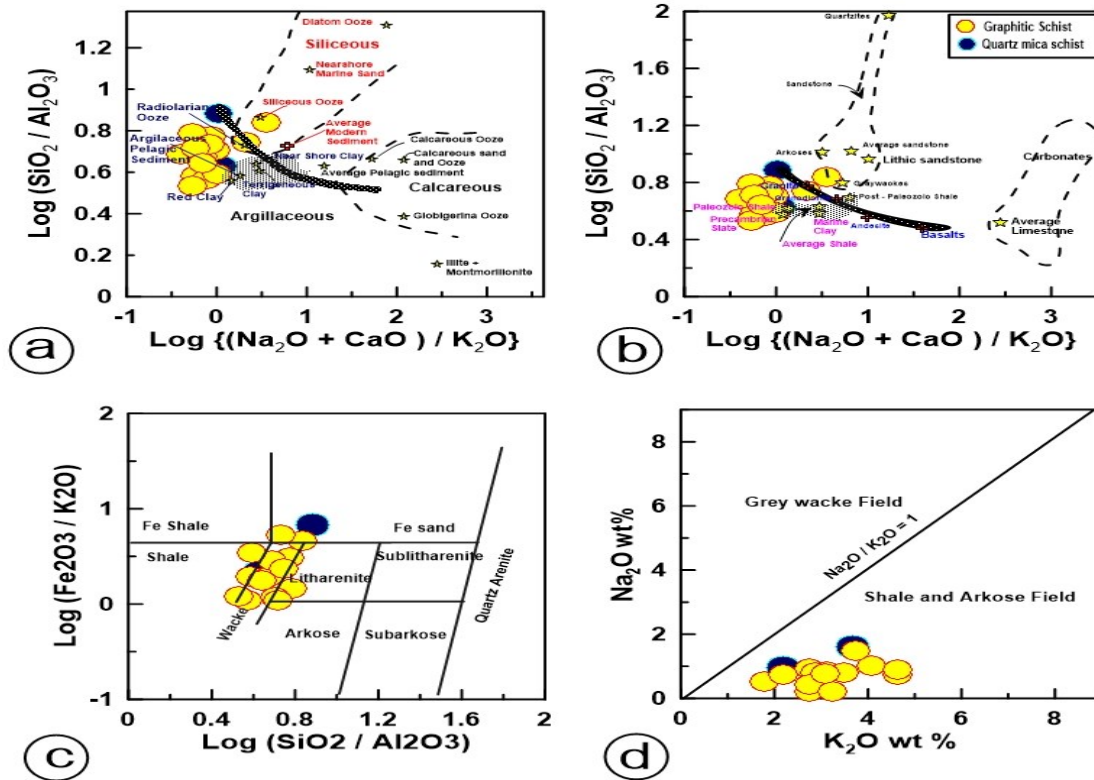


Fig. 8. a) $\text{Log } SiO_2 / Al_2O_3$ vs. $(Na_2O+CaO) / K_2O$ plot (after Garrels and Mackenzie, 1971). (b) Relationship between the composition of igneous rocks and those of sedimentary rocks after Garrels and Mackenzie (1971), The shaded banana shaped area denotes the range of composition of igneous rocks with more silica, sodium, potassium rich rocks to the left grading into magnesium rich rocks to the right. (c) Classification of fine clastics from MSB after Herron (1988). (d) Classification scheme given after Pettijohn, 1963

Herron (1988) classification is a scatter diagram of $\text{log}(Fe_2O_3/K_2O)$ vs. $\text{log}(SiO_2/Al_2O_3)$. This classification system is designed to distinguish subtle composition classes such as sub-arkoses from arkoses and sub-litharenites from litharenites, as well as to

distinguish the major sandstone and shale classes. Although the samples of the present study had witnessed the low to medium grade of metamorphism and had lost most sedimentological attributes, but the calculation of weathering indices indicates the

substantial weathering of these rocks. Secondly the chemical signatures of provenance and precursor lithology are still preserved within the detrital grains and other petrographic properties related to sediment maturity within the metamorphic rocks (Culler, 2000; Heinrichs, 2012). Therefore the chemographic scheme given by Herron (1988), Pettijohn (1963) and Gilboy (1982) are utilized for classification of metasediments. In $\log(\text{Fe}_2\text{O}_3/\text{K}_2\text{O})$ vs. $\log(\text{SiO}_2/\text{Al}_2\text{O}_3)$ (Fig. 8c) bivariate plot the samples of GS and QMS fall in the fields of wacke with some of the samples falling in the border areas of litharenites and shales. These sample have wide variable range of $\text{Fe}_2\text{O}_3/\text{K}_2\text{O}$ and the restricted abundance of $\text{SiO}_2/\text{Al}_2\text{O}_3$. The classification scheme dependent on the total abundance of alkalis (Na_2O and K_2O) given after Pettijohn (1963) and Gilboy (1982) also all the samples fall in the arkosic fields (Fig. 8d).

The sedimentary fractionation tends to concentrate clay minerals and the titanium oxides within the fine clastics and zircon within the coarser components of the same sedimentary suites. Therefore, apparently the concentration of Al_2O_3 tends to increase with increasing TiO_2/Zr within the respective sedimentary system (Gracia et al., 1994). The metasediments pertaining to the present study when projected on the ternary diagram of Al-Ti-Zr after

Gracia et al. (1994) gives a clustered appearance. They range in composition from Common shale to Alumina rich shale displaying the progressive chemical transition from the bulk source composition (Fig. 9).

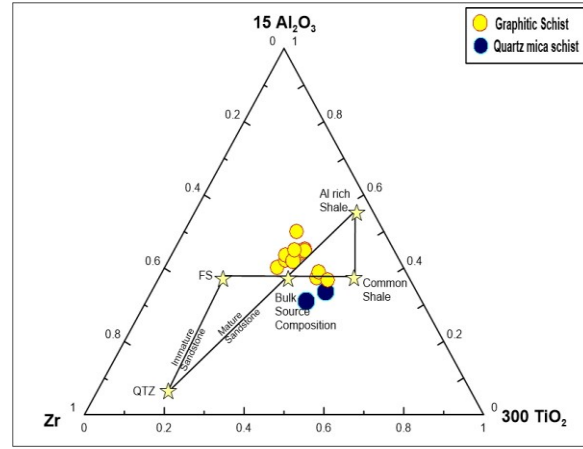


Fig. 9. Classification scheme after Gracia et al. (1994). Model compositions and mixing lines between sandstones and complementary shales are based on an arbitrary bulk source composition. Acronyms: QTZ: quartzite and FS: feldspar rich sandstone.

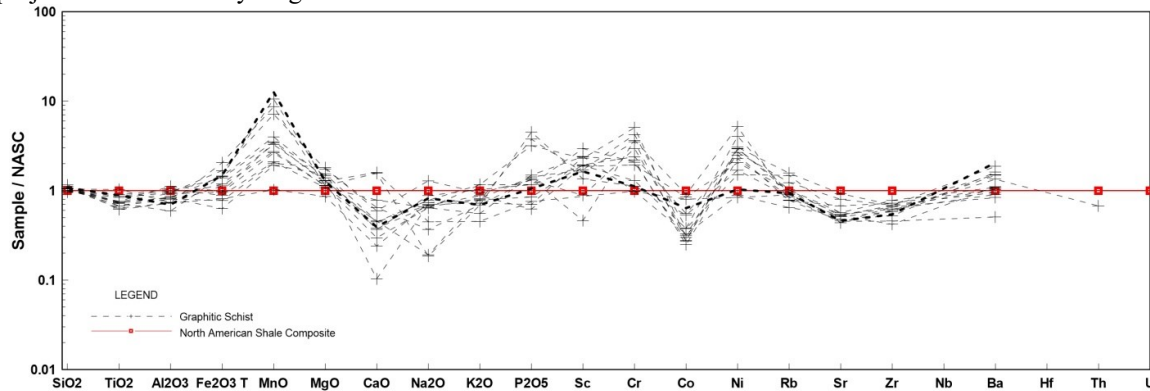


Fig. 10: NASC (North American shale composite)–normalized average major- and trace-element composition of all the samples of graphitic schist. NASC values are from Groumet et al. (1984).

Discussion

The elemental signatures are the keys for understanding the depositional environment and the source composition of the sedimentary rocks. Owing to the fine grained nature of the meta-sediments the major and trace elemental signatures were precisely analyzed and the systematic provenance characterization was attempted using the elements with low partition coefficient between natural water and upper crust and short oceanic residence time. The North American Shale Composite (NASC) normalized multi element diagram indicates that all these samples are comparable

with NASC (Fig. 10) but slightly enriched in MnO, P_2O_5 , Cr, Sc, Ni and Ba and depleted in CaO, Na_2O , Co, Sr & Zr. The NASC values are after Gourmet et al. (1984).

Provenance

The geochemical characters of a meta-sedimentary litho-assemblage vary as a function of primary and secondary process. The primary processes indicate towards the source characters and the secondary process includes intensity and duration of weathering, sedimentary recycling, digenesis/low grade

metamorphism and sorting. (Swyer, 1986; Wronkiewicz and Condie et al., 1987; McLennan et al., 1993). Various authors have given several elemental relationships for provenance identification and characterization although each has some limitations, but meaningful inferences could be drawn from combined evaluation. In the present study the provenance delineation of the meta-sediments, from Sonaghati Formation, was attempted using the elements having low partition coefficient between natural water, upper

crust and short oceanic residence time. One such promising tool is zirconium concentration, when unaffected by sedimentary recycling of quartzose precursor. The average zircon abundance within the samples of our study ranges from 84 to 196 ppm, which actually gives the hunch for felsic-dominated precursor. This assumption was subsequently validated with the TiO_2 (wt. %) vs. Zr (ppm) bivariate plot (Hayashi et al., 1997) and K_2O (wt. %) and Rb (ppm) bivariate plot (Floyd and Leveridge, 1987 and Floyd et al., 1989).

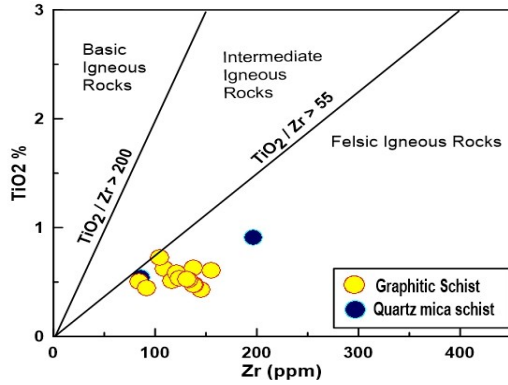


Fig. 11 a) TiO_2 (wt %) versus Zr (ppm) bivariate diagram (after Hayashi et al., 1997).

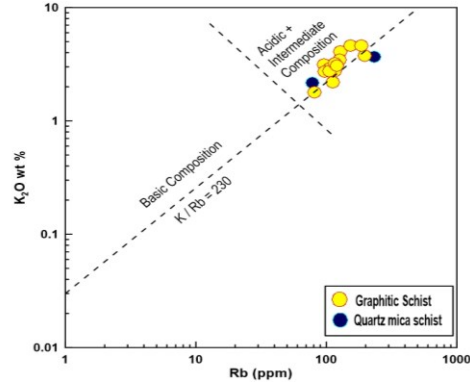


Fig. 11 b) K_2O (wt. %) versus Rb (ppm) bivariate diagram (after Floyd and Leveridge, 1987, Floyd et al., 1989). (The magmatic line or 'main trend' with the ratio of $K/Rb = 230$ is after Shaw, 1968)

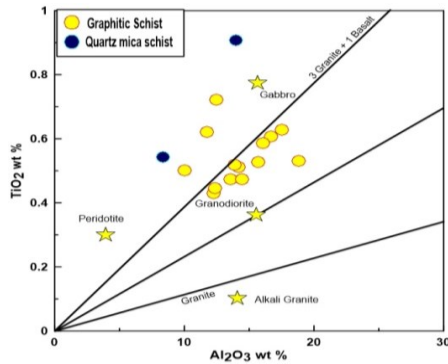


Fig. 11 c) TiO_2 (wt %) versus Al_2O_3 (wt. %) bivariate diagram (after McLennan, Fryer and Young, 1979).

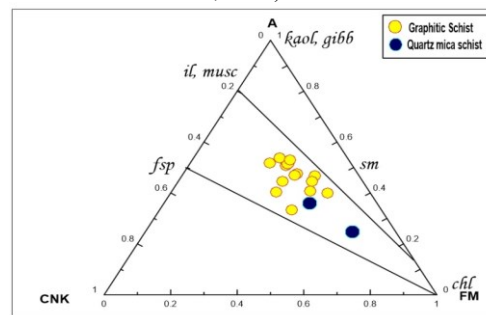


Fig. 11 d). A-CNK-FM diagram after Nesbitt and Young (1989) (Mineral abbreviations: kaol, kaolinite; gibb, gibbsite; chl, chlorite; sm, smectite; il, illite; kfsp, potash feldspar; pl, plagioclase. musc, muscovite and fsp, feldspars.)

The different magmatic sources i.e., felsic, intermediate and mafic can be appreciably differentiated using the TiO_2/Zr weight ratio. Hayashi et al. (1997) defined that TiO_2/Zr weight ratio generally has a negative correlation with SiO_2 , whose value is > 200 for mafic igneous rocks, 195-55 for intermediate igneous rocks and < 55 for felsic rocks. The samples from the present study plotted well within the field of felsic igneous rocks (Fig. 11a). The similar inference of acidic to intermediate precursor of magmatic lineage for the meta-sediments of the present study was derived

from the widely accepted LILEs (Fig. 11b) based on K_2O (wt. %) and Rb (ppm) bivariate plot (Floyd and Leveridge, 1987; Floyd et al., 1989). The Hayashi et al. (1997) suggested that Al_2O_3 / TiO_2 ratios within fluviially transported detrital siliciclastic sedimentary rocks are concurrent with its magmatic precursor. The felsic source has the value for $Al_2O_3 / TiO_2 > 21$ whereas the mafic is defined by a range of 3 to 8 and the intermediate source lies in between. The sample values for Al_2O_3 / TiO_2 vary from 15.39 to 35.47 with an average of 25.32 and are actually concomitant with

our earlier inference of felsic to intermediate precursor with a mixed source composition. This inference is further amplified by quantification of calculated SiO₂ contents within the theoretically inferred magmatic source of the metasediments. Hayashi et al. (1997) suggested an empirical equation considering relative immobility of aluminum and titanium within the fluvial system and residual weathering of silica content assessment of the probable source rock for siliciclastic sediments. The equation is defined as,

$$\text{SiO}_2 \text{ (wt. \%)} = 39.34 + 1.2578 (\text{Al}_2\text{O}_3/\text{TiO}_2) - 0.0109 (\text{Al}_2\text{O}_3/\text{TiO}_2)^2$$

The calculated silica content of the samples of the Sonaghati Formation ranges from 56.11 to 70.24 with an average of 63.84, which substantiate the mixed source precursor with acidic and mafic components. Later on, owing to low solubility of Al and Ti oxides and hydroxides in low temperature aqueous solutions, McLennan et al. (1979) proposed a binary plot which can be used as an index of provenance and estimator of the average bulk chemical composition of the source area. These plots also suggest that all the samples of the present study follow the trend falling in between the granodiorite and 3 granite + 1basalt (Fig. 11c)

The source composition of meta-sediments can also be back traced using the CIA values of these samples, which indicate that the speculated precursor varies from granite to granodiorite in composition. The index of ICV can also be utilized for provenance determination since the ICV values for the different magmatic suites are unaffected by the degree of weathering (Cox et al., 1995). The dominance of rock forming minerals i.e., K-feldspars, plagioclase, pyroxenes and amphiboles is indicated by ICV value > 0.84, whereas the dominance of alteration products such as kaolinite, illite, and muscovite is denoted by the ICV values < 0.84 (Cox et al., 1995; Cullers, 2000). The average ICV value for the metasediments of Sonaghati Formation is 1.43, hence the dominance of rock forming minerals is further confirmed.

Cox et al., (1995) had also established the existence of an inverse relationship between ICV and CIA, and had also validated that the clastic sedimentary rocks derived from the variable precursor have different ICV values even after witnessing the same degree of weathering (as reflected by same CIA). The unaltered basalt and granite yield strongly contrasting ICV values of 2.20 and 0.95 (Cox et al., 1995). The ICV values for samples from the present study area ranges from 0.90 to 3.22 with an average of 1.43 a mixed source precursor of metasediments of the present study area. The plot of all the samples on A-CN-K-FM diagram i.e.,

$$\text{Al}_2\text{O}_3 - (\text{CaO} + \text{Na}_2\text{O} + \text{K}_2\text{O}) - (\text{Fe}_2\text{O}_3(\text{T}) + \text{MgO})$$

after Nesbitt and Young (1989) (Fig. 11a) show most of the samples plot along a mixing line between illite-muscovite and chlorite compositions in contrast to the trend of recent weathering profiles (Fig. 11d). The mixing trend between chlorite and muscovite-illite indicates the presence of mafic rocks in the provenance and also the metasomatic introduction of K₂O during alteration. The LREE enriched and fractionated pattern of these of metasediments also corroborates with the inference of mixed source protolith (McLennan et al., 1984). The contemporary probable source rocks from the vicinity may include Amgaon, Tirodi and Betul basement gneisses, granites, amphibolites and basic dykes and Betul rhyolites.

The provenance characterization can also be carried out using the ratio of transitional elements i.e., Cr and Ni. The dominance of felsic rocks within the provenance is indicated by low Cr and Ni contents and vice versa is for mafic to ultramafic rocks (Condie, 1991; Armstrong-Altrin et al., 2004). The average Cr/Ni ratio ranges from 1.42 to 4.05 with an average of 2.20 thus eventually confirms the mixed source with both the basic and intermediate to felsic precursors.

The results indicate that all these meta-sediments are immature, arkosic sediments having the composition very similar of NASC and the average shale derived from the mixing of felsic, intermediate and mafic magmatic end members. But the dominant contributor for this formation is acidic and intermediate precursor, with small fraction of mafic component.

Paleoclimate

The palaeo-redox conditions during sedimentation of siliciclastic rocks can also be evaluated from their chemistry. The oxygen fugacity, humidity, CO₂ concentration, biological productivity, etc. are the key factors which influence the whole rock chemistry of any sedimentary succession either of present or past. Therefore, detailed study of weathering index of ancient sediments provides useful inferences on past climate. The binary plot of SiO₂ wt. % versus (Al₂O₃ + K₂O + Na₂O) wt. % proposed by Suttner and Dutta (1986) indicates that analysed samples plot in the field of semi arid climate (Fig. 12) but shows a sequential variation, suggesting that they were deposited under variable climatic conditions ranging from semi-arid to arid. According to Hallberg (1976); the values of Cu/Zn ratio are considered as an indicator of palaeo-redox conditions, the high values of Cu/Zn ratio indicate reducing conditions, while their lower values suggest oxidizing conditions. The Cu/ Zn ratio of all the samples is high (greater than 0.75) except the QMS (0.18), and the V/Cr ratio of GS samples varies from 1.97 to 3.71 with an average of 2.8 and for QMS samples it varies from 1.6 to 1.7. Similarly V/Cr ratio could also be used as a Paleoclimate proxy. The

reducing environment is suggested by value greater than 2 whereas the reverse is true for value lower than 2 (Jones and Manning, 1994).

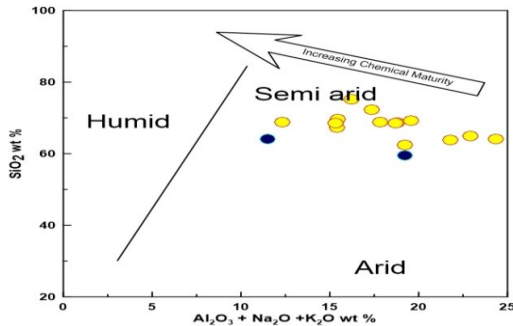


Fig. 12 Bivariate SiO₂ (wt. %) versus Al₂O₃ + K₂O + Na₂O (wt. %) Paleoclimate discrimination diagram. Fields after Suttner and Dutta (1986).

The high values of Cu/Zn and V/Cr ratio suggest that these fine clastics were deposited under reducing conditions. The presence of pyrite in the form of disseminations, specks and stringers along and across the foliation planes (Fig. 13) also supports the reducing environment of crystallization.

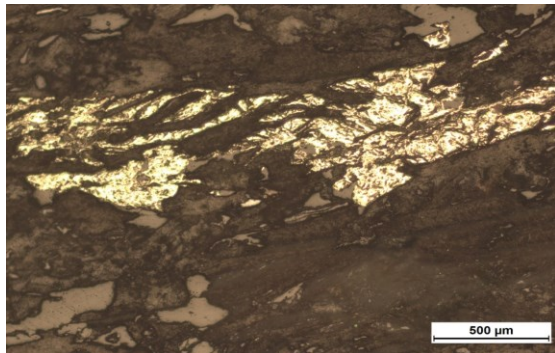


Fig.13: Photomicrograph of Quartz Mica Schist from borehole no. BBT-1, showing Pyrite occupying the interstitial spaces of the ground mass and also present as specks.

Summary & Conclusions

The schematic geochemical characterization of metasediments of Sonaghati Formation, Betul belt, from Tikari-Gauthana-Chiklar area Betul District, Madhya Pradesh was attempted with the aptitude for utilizing the geochemical analogy for provenance delineation and plaeo-climatic reconstruction.

From the meta-sedimentary rocks including Quartz Mica Schist and Graphite Schist sixteen core samples were randomly selected from varying depth for geochemical characterization of these metasediments. These metasediments are fine grained with equigranular hypidiomorphic texture. The dominant minerals are muscovite, quartz and opaques (\pm graphite/Fe-Ti oxides) whereas chlorite, k feldspar, plagioclase, biotite,

hornblend and diopside (\pm Kyanite & \pm andalusite) occur in minor amounts with varying proportion within the samples. The schistosity is well developed and defined by parallel alignment of flaky graphite, biotite and muscovite. The shearing is evidenced by pinch & swell structure, mica fish and sigmoidal prophyroblasts. The Bivariate XY plots of Major Oxides versus Silica displays a moderate to strong negative correlation between silica and all the other major oxides except the outlier samples for CaO. The collinear trends in the XY plots indicate that the sediments belong to single / related population and the visible compositional variation could be attributed to chemical, mineralogical and textural maturity. The geochemical signatures were probable governed by the following minerals {quartz, clay minerals, opaques (Ti-Fe-Mg Oxides) and some mafic minerals}. The strong positive correlation between Al₂O₃ and K₂O, K₂O and Na₂O also suggests the dominance of clay minerals. The CIA value varies between 55.2 and 77.8 with an average of 69.3 and is comparable with the average CIA values for global shale (\sim 70 to \sim 75) given. This also implies the presence of muscovite, illites and smectite within the samples of metasediments of Sonaghati Formation. The co-linear trends among the Compatible and High Field Strength Elements further suggests that the data set belongs to a single/ related population, eventually uninfluenced by the secondary process of chemical alterations and preserving the primordial elemental signatures.

The samples of metasediments from Songhati Formation have an enriched REE pattern with negative Eu anomaly. This fractionated LREE's dispersal with nearly flat and enriched HREE's on Chondrite normalized REE plot implies that Sonaghati meta-sediment have a mixed source protolith. The presence of strong negative Eu anomaly further affirms with the Proterozoic age for the precursor of the metasediments. The overall abundance of Rare Earth Elements in these meta-sediments is comparable with the North American Shale Composite (NASC) with very slight depletion in HREE's.

The Geochemical signatures of the metasediments indicates that these meta-sediments are immature, arkosic sediments having the composition very similar of NASC and the average shale and had witnessed substantial weathering of the source terrain without any evidence of potash metasomatism. It can be further concluded that these were derived from the mixing of felsic, intermediate and mafic magmatic end members but the dominant contributor being the acidic and intermediate precursor, with small fraction of mafic component. The Major Oxide relations also suggest that these sediments were deposited under variable climatic conditions ranging from semi-arid to arid. Cu/Zn , V/Cr ratios and presence of pyrites, graphites suggest that

these fine clastics were deposited under reducing conditions.

Acknowledgement

The assignment was executed as a part of G2 Stage General Exploration for graphite in Tikari-Gauthana- Chiklar and surrounding areas, Betul District, M.P under item No. 068/ME/CR/MP/2015/048, Field Season 2015-16 of Geological Survey of India, Ministry of Mines. The authors gratefully acknowledge Director General, Geological Survey of India, Additional Director General and HOD, Geological Survey of India, Central Region, for providing

References

- Alam, M., Naushad, M., Wanjari, N., Ahmad, T. (2009). Geochemical characterizations of mafic magmatic rocks of the Central Indian Shield: Implication for Precambrian crustal evolution, in Talat Ahmad, Francis Hirsch, and Punya Charusiri (eds.), *Journal of the Virtual Explorer*, 32, paper 8, doi: 10.3809/jvirtex.2009.00246.
- Armstrong-Altrin, J. S., Lee, Y. I., Verma, S. P., & Ramasamy, S. (2004). Geochemistry of sandstones from the upper Miocene Kudankulam Formation, southern India: Implications for provenance, weathering, and tectonic setting. *Journal of Sedimentary Research*, 74(2), 285–297.
- Chakraborty, S.K., Chore, S.A., Vishwakarma, L.L. (2009). Report on the geological studies of the volcano-sedimentary lithoassemblage of Betul belt, Central Indian Tectonic Zone, M.P GSI, Unpublished final report for FS 2000-01 & 2001-02 of Geological Survey of India.
- Condie, K.C., Wilks, M., Rosen, D.M., and Zlobin, V.L. (1991). Geochemistry of metasediments from the Precambrian Hapschan Series, eastern Anabar Shield, Siberia. *Precambrian Research*, 50, 37-47.
- Cox, R., Low, D. R., & Cullers, R. L. (1995). The influence of sediment recycling and basement composition on evolution of mud rock chemistry in the south-western United States. *Geochimica et Cosmochimica Acta*, 59, 2919 – 2940.
- Cullers, R. L. (2000). The geochemistry of shales, siltstones, and sandstones of Pennsylvanian-Permian age Colorado, U.S.A.: Implications for provenance and metamorphic studies. *Lithos*, 51, 181–203.
- Dar S. A., Khan K. F., & Mir A. R. (2020). Provenance and paleo-weathering of Paleoproterozoic siliciclastic sedimentary rocks of Bijawar Group, Sonrai Basin, Uttar Pradesh, India: using a geochemical approach. *Journal of Sedimentary Environments*, <https://doi.org/10.1007/s43217-020-00024-5>.
- Eswaran, H., Stoops, G., D Paepe, R. (1973). A Contribution to the study of soil formation of Isla Santa Cruz Galapagos. *Pedologie*, 23, 100-122.
- Fedo, C.M. Eriksson, K.A., Krogstad, E.J. (1996). Geochemistry of shales from the Archean (~ 3.0ga) Buhwa Greenstone Belt, Zimbabwe: Implications for provenance and source-area weathering. *Geochimica et Cosmochimica Acta* , 60, 1751-1763.
- Fedo, C.M., Nesbitt, H.W., & Young, G.M. (1995). Unravelling the effects of Potassium metasomatism in the sedimentary rocks and paleosols with implications for paleoweathering conditions and provenance. *Geology*, 23, 921-924.
- necessary facilities, technical, administrative and financial for successful completion of the research. The authors are also thankful to Mineral Physics Lab, Nagpur and Chemical Lab, Nagpur, Hyderabad and Bhopal for sample analysis and all the administrative and support system staff for their direct & indirect efforts in bringing up of this manuscript. The authors also express kind acknowledgement towards the expert reviewer for their keen scrutiny and valuable comments for betterment of the manuscript. The competent authorities of GSI are also dully acknowledged for giving necessary approval for publication of this manuscript.
- Floyd, P.A. and Leveridge, B.E. (1987). Tectonic environment of the Devonian Gramscatho basin, south Cornwall: framework mode and geochemical evidence from turbidite sandstones. *Journal of the Geological Society of London*, 144, 531–542.
- Floyd, P.A., Winchester, J.A., and Park R.G. (1989). Geochemistry and Tectonic Setting of Lewisian Clastic Metasediments from the Early Proterozoic Loch Maree Group of Gairloch, NW Scotland. *Precambrian Research*, 45, 203-214.
- Garrels, R.M., Mackenzie, F.T. (1971). *The Evolution of Sedimentary Rocks*. W.W. Norton, New York.
- Gibbs, A. K., Montgomery, C. W., O'day, P. A. and Erslev E. A. (1986). The Archean-Proterozoic transition: Evidence from the geochemistry of metasedimentary rocks of Guyana and Montana. *Geochimica et Cosmochimica Acta*, 50, 2125-2141.
- Gilbo, C.F. (1982). Classification of Clastic metasediments. Saskatchewan Mineral resources, Open File report 82-3, 33 p.
- Gracia, D., Fonteilles, M., and Moutte, J. (1994). Sedimentary Fractionations between Al, Ti, and Zr and the Genesis of Strongly Peraluminous Granites. *The Journal of Geology*, 102 (4), 411-422.
- Gromet, L.P., Dymek, R.F., Haskin, L.A., and Korotev, R.L. (1984). "The North American shale composite": its compilation, major and trace element characteristics. *Geochimica et Cosmochimica Acta*, 48, 2469–3482.
- GSI, Bulletin series A-69, (2018). Zinc- Copper Mineralization of Betul Belt, Betul and Chhindwara districts Madhya Pradesh (2018). Bulletin series A, No.69, Geological Survey of India, Nagpur, ISSN 0536-8782.
- Hallberg, R.O. (1976). A geochemical method for investigation of palaeoredox conditions in sediments. *Ambio*, 4, 139–147, Special Report.
- Hamdam, J., and Bumham, C.P. (1996). The contribution of nutrients from the parent material in three deeply weathered soils of Peninsular Malaysia. *Geoderma*, 74, 219-233.
- Harnois, L. (1988). The CIW index: a new chemical Index of weathering. *Sedimentary Geology*, 55, 319-322.
- Hayashi, K.I., Fujisawa, H., Holland, H.D., and Ohomoto, H. (1997). Geochemistry of ~ 1.9 Ga sedimentary rocks from northern Labrador, Canada. *Geochim Cosmochim Acta*, 61 (19), 4115–4137.
- Heinrichs, T., Siegesmund, S., Frei, D., Drobe, M., and Schulz, B. (2012). Provenance signatures from whole-rock geochemistry and detrital zircon ages of metasediments from the Austroalpine basement south of the Tauern Window (Eastern Tyrol, Austria). *Geo. Alp*, 9, 156–185.
- Herron, M. M. (1988). Geochemical classification of terrigenous sands and shales from core or log data: *Journal of Sedimentary Petrology*, 58(5), 820- 829.

- Jones, B. and Manning, D.C. (1994). Comparison of geochemical indices used for the interpretation of paleo-redox conditions in Ancient mudstones. *Chemical Geology*, 111(1-4), 111-129.
- Lenka, B. (2014). Investigation for graphite in Tikari-Gauthana-Chiklar and surrounding area, Betul district, M.P (G3 stage). Unpublished final report of Geological Survey on India for FS-2013-14. Accession No CR-023185.
- Lenka, B. and Ahmad, A. (2013): Investigation for graphite in Tikari, Chiklar, Gauthana area, Betul district, M.P. Unpublished final report of Geological Survey on India for FS-2012-13. Accession No 22887, pp. 92.
- Lenka, B. and Shukla, S. (2016). General Exploration For Graphite in Tikari- Gauthana- Chiklar and surrounding areas, Betul district, M.P (G2 Stage). Unpublished final report of Geological Survey on India for FS-2015-16. Accession No CR-023185.
- Maynard, J.B., Sutton, S.J., Robb, L.J., Ferraz, M.F., and Meyer, F.M. (1995). A paleosol developed on hydrothermally altered granite from the hinterland of the Witwatersrand basin: characteristics of a source of basin fill. *Journal of Geology*, 103, 357-377.
- McLennan, S.M., Fryer, B.J., Young, G.M. (1979). The geochemistry of the carbonate-rich Espanola Formation (Huronian) with emphasis on the rare earth elements. *Canadian Journal of Earth Sciences*, 16, 230-239.
- McLennan, S.M., Hemming, S., McDaniel, D.K., and Hanson, G.N. (1993). Geochemical approaches to sedimentation, provenance and tectonics, in Johnsson, M.J., Basu, A. (Eds.), *Processes Controlling the Composition of Clastic Sediments*. Geological Society of America Special Paper 284., Boulder, Colorado, p. 21-40.
- McLennan, S.M., Taylor S. R. and Mcgregor, V. R. (1984). Geochemistry of Archean metasedimentary rocks from West Greenland. *Geochimica et Cosmochimica Acta*, 48, 1-13.
- Mishra, M.K., Devi, S.J., Kaulina, T., Dass, K.C., Kumar, S. and Ahmad, T. (2011). Petrogenesis and tectonic setting of the Proterozoic mafic magmatic rocks of the Central Indian Tectonic Zone, Betul Area: Geochemical Constraints. in Srivastava, R.K. (Ed.), *Dyke Swarms: Keys for Geodynamic Interpretation*, Berlin Heidelberg: Springer-Verlag, p. 189-201.
- Nesbitt, H.W. and Young, G.M. (1989). Formation and diagenesis of weathering profiles. *Journal of Geology*, 97, 129-147.
- Nesbitt, H.W., & Young, G.M. (1982). Early Proterozoic climates and plate motions inferred from major element chemistry of lutites. *Nature*, 299, 715-717.
- Nesbitt, H.W., & Young, G.M. (1984). Prediction of some weathering trends of plutonic and volcanic rocks based on thermodynamic and kinetic considerations. *Geochim Cosmochim Acta*, 48, 1523-1534.
- Parker, A. (1970). An index of weathering for Silicate rocks. *Geological Magazine*, 107, 501-504.
- Pettijohn, F. J. (1963). Chemical composition of sandstones—excluding carbonate and volcanic sands, in Fleischer, M., ed., *Data of Geochemistry*, sixth edition, U. S. Geological Survey Professional Paper 440-S, 21 p.
- Praveen M.N. (2016). Geochemistry and petrogenesis of rhyolites hosting VMS mineralization in the eastern Betul belt, Central India. PhD thesis submitted to the Cochin University of Science and Technology, Cochin.
- Prince J. R. & Velbel M. A. (2003) Chemical weathering indices applied to weathering profiles developed on heterogeneous felsic metamorphic parent rocks. *Chemical Geology*, 202, 397-416.
- Raut, P.K., Mahakud, S.P. (2002). Geology, geochemistry and tectonic setting of volcano-sedimentary sequence of Betul belt, Madhya Pradesh and ore genesis of related Zinc and Copper sulphide mineralization. Proceedings of the National Seminar on Mineral Exploration and Resource Surveys, by Geological Survey of India, held at Jaipur.
- Roy, A., and Prasad, H.M. (2003). Tectonothermal events in Central Indian Tectonic Zone (CITZ) and its implications in Rodinian crustal assembly. *Journal of Asian Earth Sciences*, 22, 115-129.
- Sarkar, S.N., Trivedi, J.R., Gopalan, K., (1986). Rb-Sr whole rock and mineral isochron age of the Tirodi gneiss, Sausar Group, Bhandara district, Maharashtra. *Journal of Geological Society of India*, 27, 30 – 37.
- Sawyer, E.W. (1986). The influence of source rock type, chemical weathering and sorting on the geochemistry of clastic sediments from the Quetico Meta-sedimentary belt, Superior Province, Canada. *Chemical Geology* 55, 77-95.
- Shaw, D. M. (1968). A review of K-Rb fractionation trends by covariance analysis. *Geochimica et Cosmochimica Acta*, 32, 573-602.
- Srivastava, S.K and Chellani, S.K. (1995). Report on Special thematic mapping of Archean Proterozoic rocks in area north of Bordehi & around Khari Betul dist., M.P, Unpublished final report of Geological Survey on India for FS-1994-1995. Accession No CR-021502.
- SOP (2010). Standard procedure of sample processing for petrochemical analysis of Geological Survey of India. www.gsi.gov.in.
- Suttner, L.J. and Dutta, P.K. (1986). Alluvial sandstone composition and palaeoclimate Framework mineralogy. *Journal of Sedimentary Petrology*, 56(3), 329-345.
- Taylor, S.R. and McLennan, S.M. (1985). *The Continental Crust: Its Composition and Evolution*. Oxford, Blackwell, p. 311.
- Wronkiewicz, D.J. and Condie, K.C. (1987). Geochemistry of Archean shales from the Witwatersrand Supergroup, South Africa: Source-area weathering and provenance. *Geochimica et Cosmochimica Acta*, 51, 2401-2416.
- Yousuf, I., Subba Rao, D.V., Balakrishnan, S., and Ahmad, T. (2019). Geochemistry and petrogenesis of acidic volcanics from Betul-Chhindwara Belt, Central Indian Tectonic Zone (CITZ), Central India. *Journal of Earth System Sciences*, 128, 227.

(Received on 16 February, 2021; Revised Accepted on 3 May 2021)

Provenance of the Sawa Formation Sandstones, Vindhyan Super Group, Southeast Rajasthan, India

Jyoti Mathur*, Mujeebul Hasan and Abdullah Khan

Department of Geology, Aligarh Muslim University, Aligarh- 202002

*E-mail: mathurjyoti52@gmail.com

Abstract

Integrated petrographical and geochemical analysis of Sawa Formation sandstones was analyzed to reconstruct their source area weathering, paleoclimate, tectonic setting and provenance conditions. Petrographically, quartz is dominant detrital mineral followed by feldspar, mica, rock fragments and heavy minerals. Sawa Formation sandstones have been classified as quartzarenite with subordinate sub-arkose and sub-litharenite type. Major oxide element abundances revealed the sandstones have high SiO₂ concentration, high K₂O/ Na₂O ratio, which is consistent with the petrographic data. These sandstones were derived mainly from stable cratonic with minor collision suture and fold thrust belt source and deposited in rifted continental margin basin setting, reflecting high maturity of sediments and high stability of the source area. The CIA, CIW and PIA values of these sandstones indicate high intensity of weathering condition in the source area under warm and humid climate.

Keywords: *Petrography, Geochemistry, Source area weathering, Paleoclimate, Tectonic setting*

Introduction

Siliciclastic sediment composition has been investigated to infer the provenance, weathering conditions, sediment transport, climate and tectonic environment (Taylor and McLennan 1985; Bhatia and Crook 1986; Johnsson and Basu, 1993; Cox et al. 1995; Nesbitt et al. 1996; Armstrong-Altrin, 2015). Variables including the nature of source rock, degree of weathering, transportation and diagenesis influences composition of clastic sediments (McLennan et al., 1993). However, the tectonic setting of the sedimentary basin may play a predominant role over other variables, because different tectonic settings can provide different type of source materials with variable chemical signatures (Bhatia and Crook 1986). The largest of Intracratonic Proterozoic sedimentary basins (Purana basins) is the Vindhyan Basin in the Indian subcontinent (Soni et al., 1987; Kale and Phansalkar, 1991). This sedimentary basin occurs as a large sickle shaped basin, covering an area of about 100,000 km² in Uttar Pradesh, Bihar, Madhya Pradesh and Rajasthan. The Vindhyan basin overlies the stable Bundelkhand craton of Archean-Palaeoproterozoic age (Roy, 1988; Chakraborty and Bhattacharya, 1996; Bose et al., 2001;

Acharyya, 2003). An unmetamorphosed and undeformed sequence of Meso-Neoproterozoic sedimentary rocks about 4,500 m thick occupies mainly the northern fringe of peninsular India (Fig. 1). Thick Vindhyan Basin sediments show variably marine, aerially extensive, well exposed, lithologically variable, and largely unmetamorphosed successions (Chanda and Bhattacharya, 1982; Bose et al., 2001, 2015).

Geological Setting

The Meso-Neoproterozoic Vindhyan Super Group covers an area of about ~100,000 km² and a significant part of this Super Group is concealed below Deccan continental flood basalt traps and Indo-Gangetic alluvium (Venkatachala et al., 1996; Gopalan et al., 2013). The Vindhyan succession overlies the ~2.5Ga old Bundelkhand granite massif which is bounded to the northwest by the Great Boundary Fault and to the southeast by the Narmada-Son lineament (Fig. 1). The thick strata of Vindhyan Basin are subdivided into Lower Vindhyan sequence (the Semri Group) and the Upper Vindhyan sequence (the Kaimur, Rewa, and Bhandar groups), separated by a major hiatus of unknown duration (Bose et al., 2001).

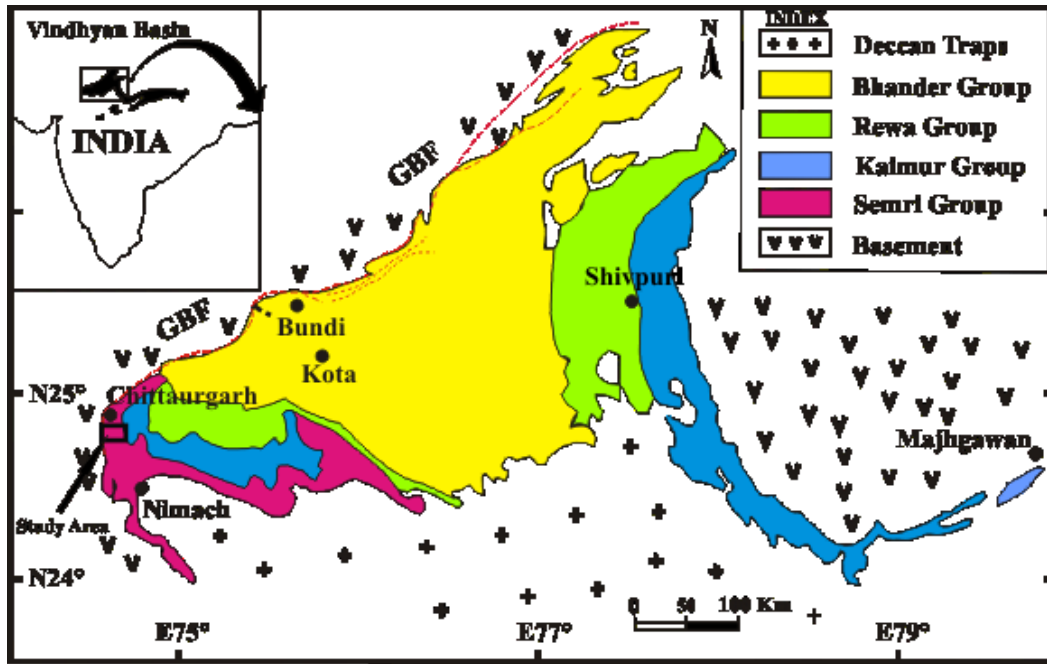


Fig. 1: Generalized regional geological map of Vindhyan Basin showing study area and lithological units (various groups) of Vindhyan Super Group (modified after Soni et al., 1987). GBT= Great Boundary Fault.

Table 1: Lithostratigraphic Succession of the Vindhyan Sequence, Southeastern, Rajasthan (after Prasad, 1984; Casshyap et al., 2001).

Group	Formation	Lithology	Thickness (m)	Age (Ma)
Upper Vindhyan	Kaimur	Sandstone, Conglomerate	20-70	
-----Unconformity-----				
Lower Vindhyan	Suket	Shale	120	} 1616±50 U-Pb (Zircon) (Shukla, 2011)
	Nimabhara	Limestone	100-150	
	Bari	Shale	45	
	Jiran	Sandstone	30-60	
	Binota	Shale	250	
	Palri	Shale	30-60	
	Sawa	Sandstone	30-60	
	Bhagwanpura	Limestone	30-50	
	Khardeola	Sandstone	70-200	
Khairmala	Volcanic flows and tuffs	40-100		
-----Unconformity-----				
Basement comprises BGC, Quartzite, Phyllite, etc.				

The detailed geology of the area has been worked out by Prasad (1984). The stratigraphic succession of the Lower Vindhyan Group of southeastern Rajasthan is summarized in Table 1. The Sawa Formation comprises mainly of sandstones with conglomerate. The sandstone assemblage overlies Bhagwanpura Limestone Formation and crops out in narrow ridges of sandstone (Fig. 2).

Methodology

A total of thirty five sandstone samples were collected from Sawa Formation and thirty samples were selected for detailed petrographic investigations. In each thin section, 250–300 grains were counted using standard Gazzi–Dickinson method (Ingersoll et al., 1984). For petrofacies analysis, the detrital modes

were recalculated to 100 percent by summing up of Qt, Qm, F, L and Lt following Dickinson's (1985) method. After useful thin section screening, ten representative samples were selected for geochemical analysis. Major element oxides were determined using standard X-ray Fluorescence (XRF) spectrometer (Philips PW-2440 Magix-PRO) at National Geophysical Research Institute (NGRI), Hyderabad. Moreover, the total iron is expressed as Fe₂O₃. Major oxide data were recalculated to an anhydrous (LOI-free) basis and adjusted to 100% before using them in various diagrams.

Results

Petrography

The modal composition and detrital petrofacies (based on Dickinson, 1985) of the Sawa Formation sandstones are given in Table 2. The average petrographic composition of the studied sandstones is quartz (97.23%) followed by feldspars (average 1.34%), micas (0.70%), rock fragments (0.54%) and heavy

minerals (0.20%). Most of the quartz grains are monocrystalline (common quartz) and some polycrystalline grains (recrystallized and stretched quartz) (Plate 1a, b). Some monocrystalline quartz with undulation or non-undulation is characterized by inclusion of heavy minerals. Feldspar is present in the form of K- feldspar (microcline) (Plate 1a) and plagioclase feldspar (Plate 1c). K-feldspar is dominant variety than the plagioclase feldspar. Mica usually occurs as elongated muscovite due to mechanical compaction (Plate 1c) and inclusion of biotite in the monocrystalline quartz grain (Plate 1 d). The rock fragments comprise of chert (Plate 1e), granite, phyllite, schist and siltstone. Heavy minerals constitute minor component of the samples and include rounded zircon (indication of recycling) (Plate 1f), tourmaline, rutile, staurolite, epidote and opaque minerals. According to Folk's (1980) classification scheme, the studied sandstones are classified as quartzarenite with subordinate sub-litharenite and sub-arkose (Fig. 3).

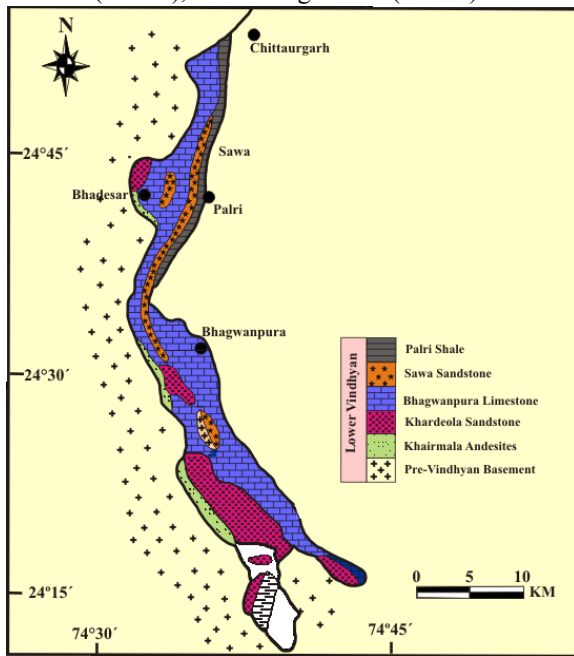


Fig. 2: Geological map of Sawa Formation and other sequences

Major element concentrations

The major oxides in wt % for the Sawa Formation sandstones are listed in Table 3. The sandstones have higher SiO₂ content (>90 wt %) because of the presence of greater amount of quartz. The lower TiO₂ indicate smaller content of Ti-bearing minerals like ilmenite, titanite, etc. The low values of MgO and CaO also suggest the lesser presence of the

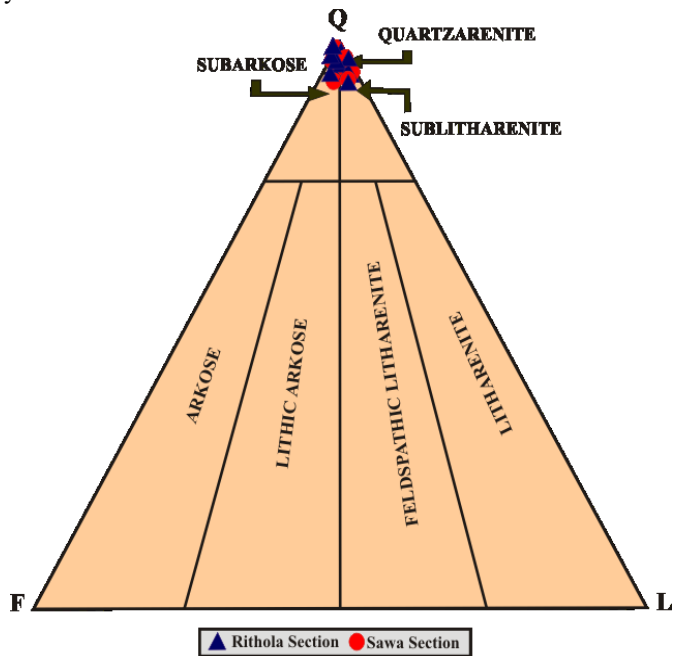


Fig. 3: Q-F-L diagram for the Sawa Formation sandstones (after Folk, 1980).

calcitic components. K₂O shows more enrichment than Na₂O, (K₂O/Na₂O ranges from 6.00-6.50, average 6.23) (Table 3) suggesting dominance of K-feldspar over plagioclase feldspar which is also confirmed by the petrographic data. The extremely low concentration of P₂O₅ may be explained by the very low concentration of phosphates in the source rocks or their dissolution and mobilization during transport.

Table 2: Modal composition of the Sawa Formation sandstones, Vindhyan Super Group, Southeastern Rajasthan (after Suttner et al., 1981; Dickinson et al. 1985)

Sample No.	Q	F	R	Qt	F	L	Qm	F	Lt	Qp	Lv	Ls	Qm	P	K
RS-1	94.34	2.07	3.58	96.48	2.07	1.45	90.35	2.06	7.59	73.70	0.00	26.30	97.53	0.43	2.03
RS-2	93.86	4.60	1.54	95.04	4.60	0.36	92.86	4.61	2.53	71.22	0.00	28.78	95.08	1.36	3.57
RS-3	99.16	0.84	0.00	99.16	0.84	0.00	96.03	0.84	3.13	100.00	0.00	0.00	99.10	0.26	0.64
RS-4	97.71	2.29	0.00	97.71	2.29	0.00	96.95	2.29	0.76	100.00	0.00	0.00	97.67	1.01	1.32
RS-5	99.09	0.91	0.00	99.09	0.91	0.00	95.74	0.91	3.35	100.00	0.00	0.00	99.03	0.13	0.84
RS-6	98.50	1.50	0.00	98.50	1.50	0.00	97.40	1.50	1.10	100.00	0.00	0.00	98.46	1.28	0.25
RS-7	96.14	1.11	2.75	97.62	1.11	1.27	92.21	1.11	6.68	78.20	0.00	21.80	98.71	0.40	0.89
RS-8	98.66	1.34	0.00	98.66	1.34	0.00	95.15	1.34	3.51	100.00	0.00	0.00	98.56	0.49	0.95
RS-9	99.88	0.12	0.00	99.88	0.12	0.00	98.76	0.12	1.12	100.00	0.00	0.00	99.88	0.00	0.12
RS-10	98.79	0.25	0.97	99.75	0.25	0.00	97.83	0.25	1.92	70.52	0.00	29.48	99.74	0.12	0.13
RS-11	98.96	0.31	0.73	99.32	0.31	0.37	97.81	0.31	1.88	80.65	0.00	19.35	99.68	0.15	0.16
RS-12	98.98	1.02	0.00	98.98	1.02	0.00	97.86	1.02	1.12	100.00	0.00	0.00	98.97	0.85	0.18
RS-13	98.40	1.60	0.00	98.40	1.60	0.00	97.11	1.60	1.29	100.00	0.00	0.00	98.36	0.37	1.27
RS-14	98.77	1.11	0.12	98.61	1.11	0.28	97.83	1.11	1.06	89.83	0.00	10.17	98.87	0.22	0.91
RS-15	99.48	0.52	0.00	99.48	0.52	0.00	98.31	0.52	1.17	100.00	0.00	0.00	99.47	0.16	0.36
RS-16	99.56	0.44	0.00	99.26	0.44	0.30	97.52	0.44	2.04	90.27	0.00	9.73	99.54	0.17	0.29
SS-1	98.15	1.26	0.59	98.15	1.26	0.59	97.56	1.26	1.18	100.00	0.00	0.00	98.71	0.38	0.90
SS-2	98.25	1.75	0.00	98.25	1.75	0.00	97.66	1.75	0.59	100.00	0.00	0.00	98.22	0.49	1.29
SS-3	99.63	0.37	0.00	99.63	0.37	0.00	99.63	0.37	0.00	100.00	0.00	0.00	99.63	0.13	0.24
SS-4	97.79	2.21	0.00	97.79	2.21	0.00	95.00	2.21	2.79	100.00	0.00	0.00	97.67	0.24	2.10
SS-5	98.72	0.30	0.98	98.72	0.30	0.98	97.85	0.30	1.85	100.00	0.00	0.00	99.69	0.19	0.11
SS-6	99.70	0.30	0.00	99.34	0.30	0.36	98.76	0.30	0.94	87.04	0.00	12.96	99.70	0.13	0.17
SS-7	99.58	0.42	0.00	99.58	0.42	0.00	99.21	0.42	0.37	100.00	0.00	0.00	99.59	0.17	0.24
SS-8	95.43	4.57	0.00	95.10	4.57	0.34	92.95	4.57	2.48	86.71	0.00	13.29	95.20	1.33	3.47
SS-9	97.45	2.55	0.00	97.45	2.55	0.00	95.61	2.55	1.84	100.00	0.00	0.00	97.35	1.32	1.32
SS-10	98.50	1.50	0.00	98.50	1.50	0.00	96.10	1.50	2.40	100.00	0.00	0.00	98.42	0.26	1.32
SS-11	98.38	1.15	0.47	98.50	1.15	0.35	95.84	1.15	3.01	95.68	0.00	4.32	98.77	0.19	1.04
SS-12	94.03	5.16	0.81	94.18	5.16	0.66	91.34	5.16	3.50	92.79	0.00	7.21	94.46	2.02	3.52
SS-13	95.98	4.02	0.00	95.98	4.02	0.00	95.16	4.02	0.82	100.00	0.00	0.00	95.92	1.18	2.90
SS-14	98.98	1.02	0.00	98.98	1.02	0.00	94.41	1.02	4.57	100.00	0.00	0.00	98.87	0.18	0.95

Q = Total quartz grain (Qm+Qp), where Qm = Monocrystalline quartz & Qp = Polycrystalline quartz.

F = Total feldspar (P+K), where P = Plagioclase & K = K-feldspar. R = Total rock fragments including chert.

L = total unstable lithic fragments (Lv+Ls), where Lv = volcanic/metavolcanic lithic fragments, Ls = sedimentary/metasedimentary lithic fragments

Discussion

Source area weathering

The chemical composition of the clastic rocks can provide useful information about weathering condition in the source area. The weathering indices like chemical index of weathering (CIW), chemical index of alteration (CIA) and plagioclase index of weathering (PIA) were widely used to infer paleo-weathering conditions in the source areas. CIA can be calculated following the equation using molecular proportion as proposed by Nesbitt and Young (1982): $CIA = [Al_2O_3 / (Al_2O_3 + CaO^* + Na_2O + K_2O)] \times 100$, where CaO^*

represents the amount of CaO incorporated in the silicate fraction of the studied sandstone samples. CIA values in sandstones range from 80.15 to 83.48 (average 81.04) (Table 3), which suggests that the source rocks were subjected to high degree of weathering under a warm and humid tropical climate conditions with abundant rainfall in the source area. CIW can be calculated following the equation using molecular proportion as proposed by Harnois (1988). $CIW = [Al_2O_3 / (Al_2O_3 + CaO^* + Na_2O)] \times 100$, which ranges from 88.37 to 93.63 (average 91.65) (Table 3), suggests higher degree of weathering in the source area. PIA can be calculated following the equation using molecular proportion as proposed by Fedo et al. (1995): $PIA = [(Al_2O_3 - K_2O) /$

$(Al_2O_3+CaO^*+Na_2O-K_2O)] \times 100$. PIA values of the sandstones range from 87.07 to 92.35 (average 90.41)

(Table 3) and suggests intense plagioclase weathering in the source area.

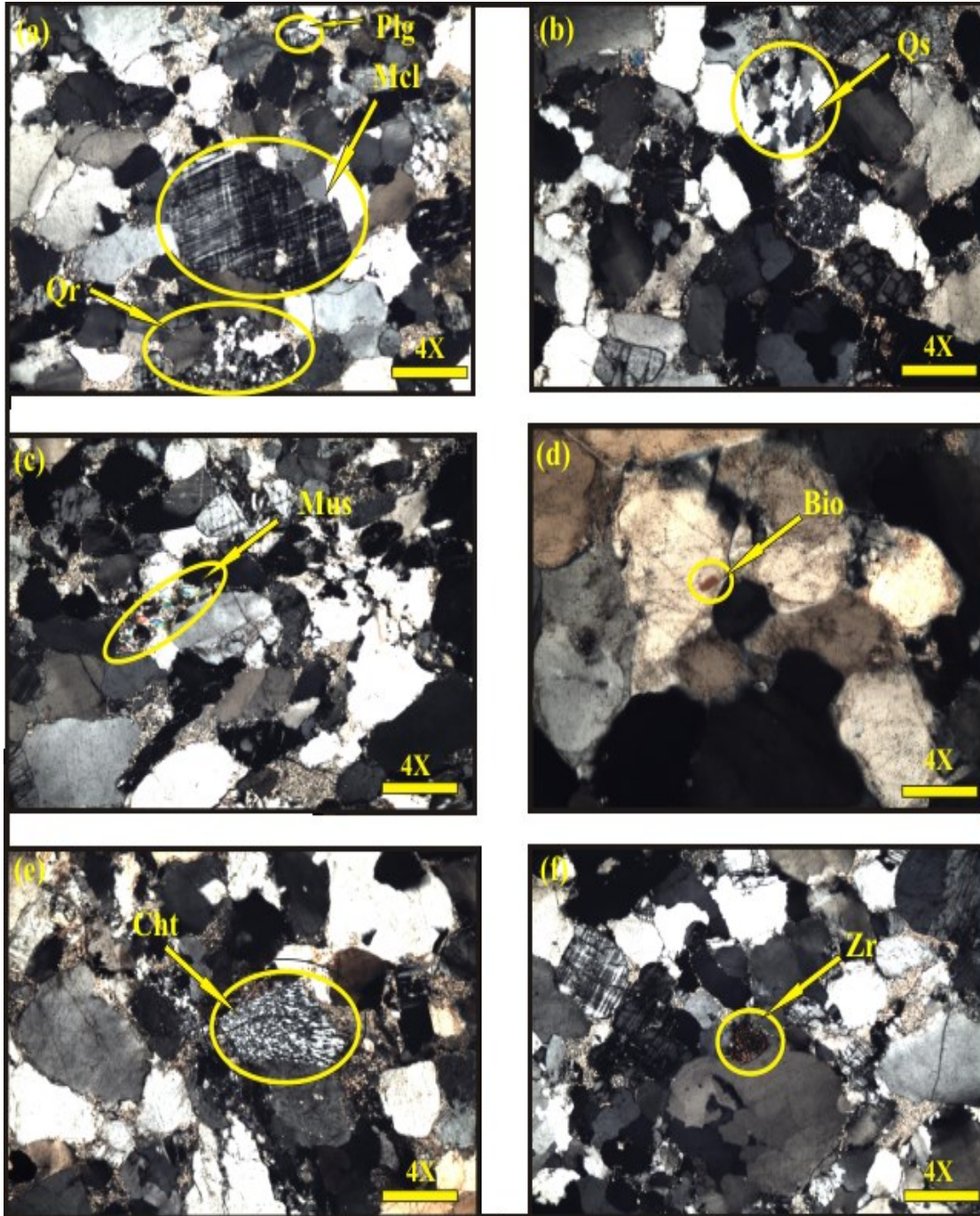


Plate 1: Photomicrograph showing (a) Recrystallized quartz (Qr), microcline (mcl) and plagioclase (plg), (b) Stretched quartz (Qs), (c) Muscovite, (d) Inclusion of biotite (bio) in quartz, (e) Chert (cht), (f) Rounded zircon (Zr).

Table 3: Major element concentrations (wt. %) for the Sawa Formation sandstones, Vindhyan Super Group, Southeastern Rajasthan

	RS-3	RS-8	RS-9	RS-13	RS-15	SS-2	SS-3	SS-7	SS-11	SS-12	Range	Average
SiO ₂	94.89	95.92	95.98	96.02	93.47	94.12	95.12	96.16	96.13	93.98	93.47-96.16	95.18
Al ₂ O ₃	1.68	1.79	1.36	1.91	1.75	1.75	1.87	1.14	1.78	2.14	1.14-2.14	1.72
Fe ₂ O ₃	0.31	0.03	0.01	0.01	0.03	0.01	0.36	0.02	0.06	0.01	0.01-0.36	0.09
MnO	0.00	0.01	0.00	0.01	0.01	0.00	0.00	0.00	0.00	0.00	0.00-0.01	0.00
MgO	0.53	0.38	0.41	0.42	0.43	0.35	0.47	0.26	0.64	0.42	0.26-0.64	0.43
CaO	0.11	0.12	0.11	0.11	0.12	0.10	0.11	0.13	0.11	0.11	0.10-0.13	0.11
Na ₂ O	0.03	0.05	0.04	0.02	0.03	0.04	0.05	0.02	0.06	0.06	0.02-0.06	0.04
K ₂ O	0.23	0.27	0.16	0.34	0.24	0.28	0.21	0.13	0.27	0.36	0.13-0.36	0.25
TiO ₂	0.09	0.11	0.02	0.02	0.09	0.18	0.22	0.07	0.15	0.18	0.02-0.22	0.11
P ₂ O ₅	0.01	0.01	0.01	0.01	0.01	0.01	0.01	0.01	0.01	0.03	0.01-0.03	0.01
Total	97.88	98.69	98.10	98.87	96.18	96.84	98.42	97.94	99.21	97.29	96.18-99.21	97.94
LOI	2.12	1.31	1.90	1.13	3.82	3.16	1.58	2.06	0.79	2.71	0.79-3.82	2.06
CIA	81.95	80.27	81.44	80.25	81.78	80.65	83.48	80.28	80.18	80.15	80.15-83.48	81.04
CIW	92.31	91.33	90.07	93.63	92.11	92.59	92.12	88.37	91.28	92.64	88.37-93.63	91.65
PIA	91.19	89.94	88.89	92.35	90.96	91.30	91.21	87.07	89.88	91.28	87.07-92.35	90.41
K ₂ O/ Na ₂ O	7.67	5.40	4.00	17.00	8.00	7.00	4.20	6.50	4.50	6.00	6.00-6.50	6.23

Palaeoclimate conditions

Climate might have been an important factor in the production of compositionally mature quartz-rich sandstones. The QFR ternary diagram of Suttner et al. (1981) indicates a metamorphic source rock in a humid climate (Fig. 4). The Palaeoproterozoic Pre-Aravalli metamorphic rocks are the basement of Vindhyan Supergroup so most of the sediments may have derived from this basement. However, this particular diagram can discriminate only sources of metamorphic and plutonic rocks (humid or arid conditions), and it does not discriminate between different tectonic settings. Humid climatic condition was also confirmed by bivariate plot of SiO₂ against total Al₂O₃+K₂O+Na₂O proposed by Suttner and Dutta in 1986 (Fig. 5).

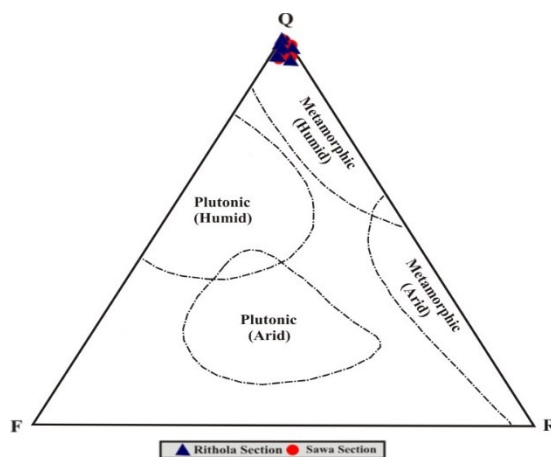


Fig. 4: Q-F-R ternary diagram for the Sawa Formation sandstones (after Suttner et al., 1981).

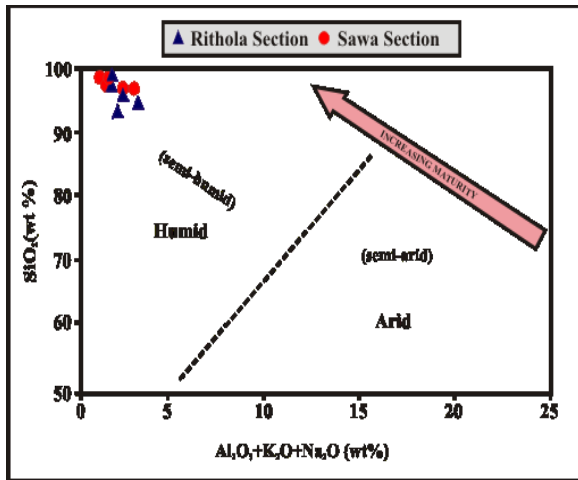


Fig. 5: SiO₂ versus Al₂O₃+K₂O+Na₂O bivariate plot for the Sawa Formation sandstones (field after Suttner and Dutta, 1986).

Provenance

Petrography gives the primary idea about the provenance of clastic rocks. The relative abundance of monocrystalline to that of polycrystalline quartz reflects the maturity of the sediments indicating a long distance transport and a distal provenance or recycling. Dominant medium to strong undulose monocrystalline quartz grains suggest metamorphic origin with slightly undulose to non undulose quartz grains suggest plutonic source (Basu, 1975; Potter, 1978a). Original polycrystalline quartz grains are disintegrated during high energy or long distance transport from the metamorphic source (Dabbagh and Rogers, 1983). The low percentage of feldspars and rock fragments indicates that the rock is chemically weathered and recycled. Euhedral zircon grains and flakes of muscovite indicate a plutonic source rock (Banerjee and Banerjee, 2010). The most probable source of Sawa Formation sandstone is the Palaeoproterozoic Pre-Aravalli metamorphic rocks and Berach granite.

Major element based discriminant function diagram (Roser and Korsch, 1988) is generally employed to distinguish between four fields of sedimentary provenance, namely: mafic igneous (P1), intermediate igneous (P2), felsic igneous (P3) and quartzose sedimentary or recycled (P4). In this diagram, the studied samples of the Sawa Formation sandstones plot in the quartzose sedimentary or recycled (P4) field (Fig. 6) indicating their derivation from granitic-gneissic terrain or mature polycyclic continental sedimentary source rocks.

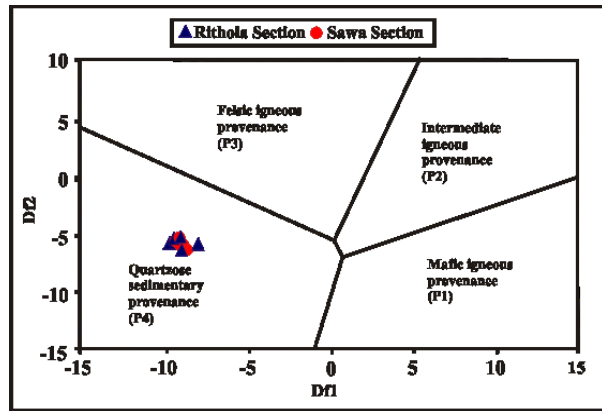


Fig. 6: Discriminant function diagram (after Roser and Korsch, 1988) for provenance of Sawa Formation sandstones. Df1 and Df2 refer to $-1.773\text{TiO}_2 + 0.607 \text{Al}_2\text{O}_3 + 0.76 \text{Fe}_2\text{O}_3 - 1.500 \text{MgO} + 0.616 \text{CaO} + 0.509\text{Na}_2\text{O} - 1.224 \text{K}_2\text{O} - 9.09$ and $0.445 \text{TiO}_2 + 0.070 \text{Al}_2\text{O}_3 - 0.250 \text{Fe}_2\text{O}_3 - 1.142 \text{MgO} + 0.438 \text{CaO} + 1.475 \text{Na}_2\text{O} - 1.426 \text{K}_2\text{O} - 6.861$.

Tectonic Setting

Tectonic setting of the Sawa Formation sandstone was determined by using detrital framework components plotted on standard ternary diagrams i.e., Qt-F-L, Qm-F-Lt, Qp-Lv-Ls and Qm-P-K (Dickinson, 1985). In Qt-F-L diagram, most of the samples plot in the stable, mature continental block provenance (Fig. 7a) suggesting their derivation from metasedimentary and sedimentary rocks which were originally deposited along former passive continental margins (Dickinson and Suczek, 1979; Dickinson, 1985). In Qm-F-Lt diagram, most of the samples fall in continental block provenance followed by recycled orogen provenance (Fig. 7b). In Qp-Lv-Ls diagram, most of the samples fall in rifted continental margin basin setting with minor contribution of collision suture and fold thrust belt setting (Fig. 7c) reflecting no contribution from the volcanic source. In Qm-P-K diagram, all the samples plot in the continental block basement uplift provenance (Fig. 7d) which reflects high mineralogical maturity of the sediments and high stability of the source area.

Using K₂O/Na₂O ratio and SiO₂, Roser and Korsch (1986) devised a binary tectonic discrimination diagram for the tectonic setting of terrigenous sedimentary rocks. The samples of Sawa Formation sandstones plot in the passive margin (PM) tectonic setting (Fig. 8) indicating that they are largely quartz-rich sediments derived from plate interiors or stable continental areas and deposited in stable intra-cratonic basin or on passive continental margins (Roser and Korsch, 1986).

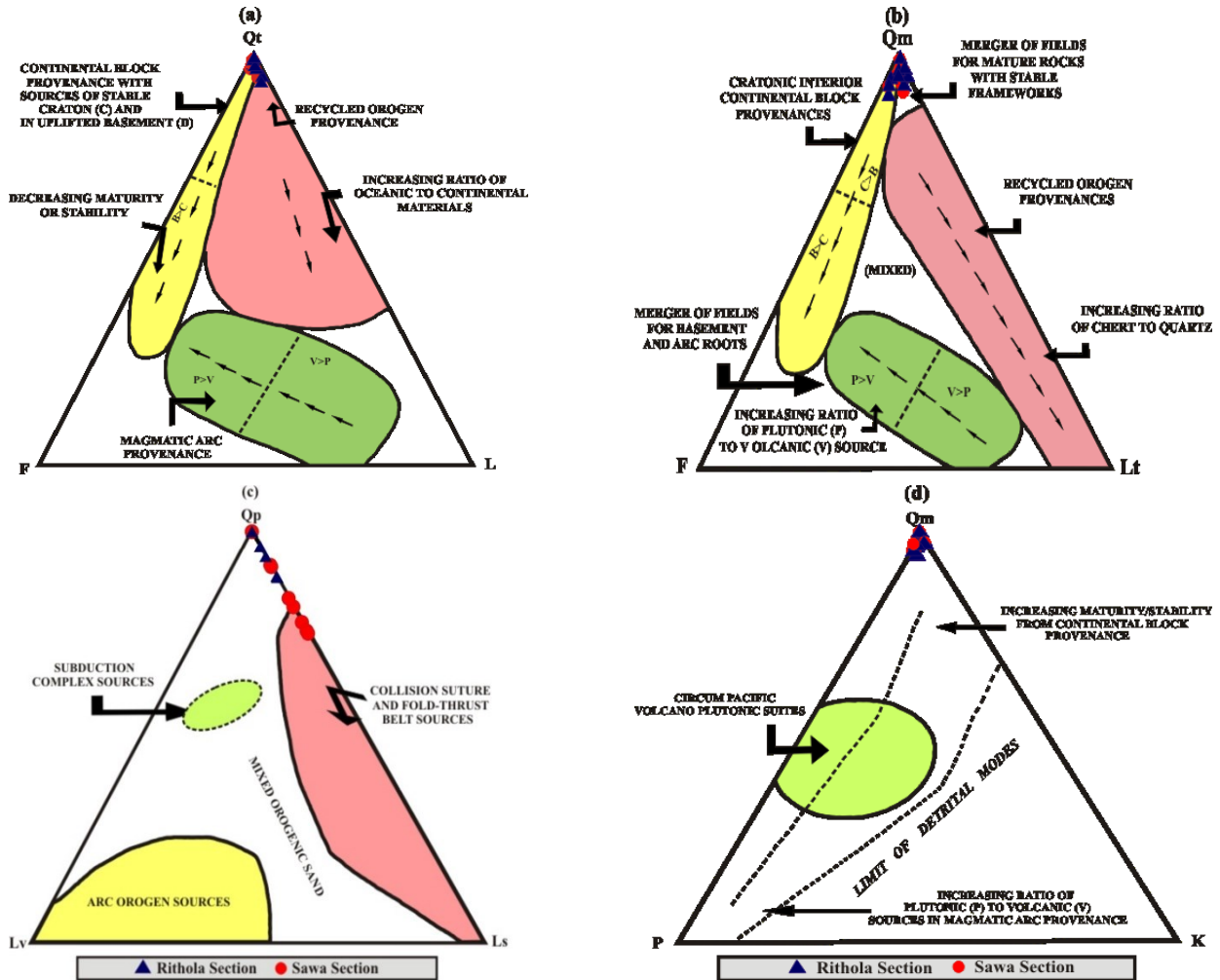


Fig. 7: (a) Qt-F-L (b) Qm-F-Lt (c) Qp-Lv-Ls (d) Qm-P-K ternary diagrams for the Sawa Formation sandstones (after Dickinson, 1985).

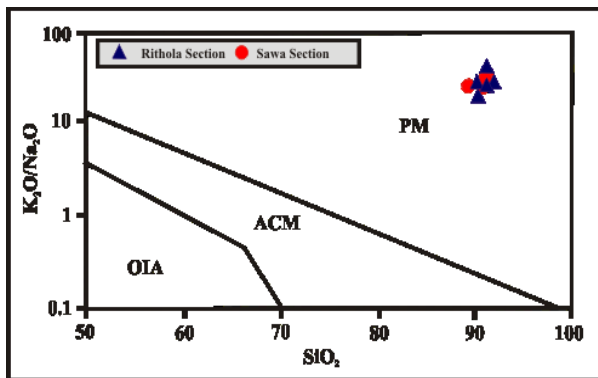


Fig. 8: SiO₂ versus K₂O/Na₂O tectonic discrimination diagram for the Sawa Formation sandstones (Roser and Korsch, 1986).

Conclusions

1. The detrital mineral composition of Sawa Formation sandstones is characterized by mainly quartz followed by feldspar, mica, rock fragments and heavy minerals. These sandstones are classified as quartzarenite with subordinate subarkose and sublitharenite.
2. The petrofacies analysis of these sandstone suggest that sediments were derived mainly from stable craton source and deposited mainly in rifted continental margin basin reflecting high maturity of sediments and high stability of source area.
3. Major oxide analysis revealed that these sandstones having high SiO₂ concentration, high K₂O/Na₂O ratio, were derived from granitic-gneissic terrain deposited in passive margin setting under warm humid tropical climate.
4. CIA, CIW, and PIA values indicate high degree of weathering condition in the source area.

Acknowledgements

The authors gratefully thank the Chairperson, Department of Geology, AMU, Aligarh for providing the necessary research facilities. The authors are also thankful to NGRI, Hyderabad for providing laboratory facilities.

References

- Acharyya, S.K. (2003), A plate tectonic model for Proterozoic crustal evolution of Central Indian tectonic zone: *Gondwana Geological Magazine*, v. 7, p. 9-31.
- Armstrong-Altrin, J.S. (2015), Evaluation of two multi-dimensional discrimination diagrams from beach and deep sea sediments from the Gulf of Mexico and their application to Precambrian clastic sedimentary rocks. *International Geology Review*, v. 57(11-12), p. 1446-1461.
- Banerjee, A., and Banerjee, D. M. (2010), Modal analysis and geochemistry of two sandstones of the Bhandar Group (Late Neoproterozoic) in parts of the Central Indian Vindhyan basin and their bearing on the provenance and tectonics. *Journal of earth system science*, v. 119(6), p. 825.
- Basu, A., Young, S. W., Suttner, L. J., James, W. C., Mack, G. H. (1975), Re-evaluation of the use of undulatory extinction and polycrystallinity in detrital quartz for provenance interpretation. *Journal of Sedimentary Research*, v. 45(4), p. 873-882.
- Bhatia, M.R., and Crook, K.A. (1986), Trace element characteristics of graywackes and tectonic setting discrimination of sedimentary basins. *Contributions to mineralogy and petrology*, v. 92(2), p. 181-193.
- Bose, P.K., Sarkar, S., Chakrabarty, S. and Banerjee, S. (2001), Overview of the Meso- to Neoproterozoic evolution of the Vindhyan basin, Central India. *Sedimentary Geology*, v. 141, p. 395-419.
- Bose, P.K., Sarkar, S., Das, N.G., Banerjee, S., Mandal, A. and Chakraborty, N. (2015), Proterozoic Vindhyan Basin: configuration and evolution. *Geological Society London Memoirs*. v. 43, p. 85–102.
- Casshyap, S.M., Bhardwaj, B.D., Raza M., Singh A. and Khan A. (2001), Barrier inlet and associated facies of shore zone. An example from Khardeola Formation of Lower Vindhyan sequence in Chittaurgarh, Rajasthan. *Journal of Geological Society of India*, v. 58, p. 97-111.
- Chakraborty, C. and Bhattacharyya, A. (1996), Fan-delta sedimentation in a foreland moat: Deoland Formation, Vindhyan Supergroup, Son valley. In: Bhattacharyya, A. (eds) *Recent Advances in Vindhyan Geology*. *Memoirs Geological Society of India*, v. 36, p. 27–48.
- Chanda, S.K. and Bhattacharyya, A. (1982), Vindhyan sedimentation and Paleogeography: Post-Auden developments. In: Valdiya, K.S., Bhatia, S.B., Gaur, V.K. (Eds.), *Geology of Vindhyaal: Prof. R. C. Misra Volume*. Hindustan Publishing Corporation Delhi, p. 88–101.
- Cox, R., Lowe, D.R., and Cullers, R.L. (1995), The influence of sediment recycling and basement composition on evolution of mudrock chemistry in the southwestern United States. *Geochimica et Cosmochimica Acta*, v. 59(14), p. 2919-2940.
- Dabbagh, M. E. and Rogers, J. J. (1983), Depositional environments and tectonic significance of the Wajid Sandstone of southern Saudi Arabia. *Journal of African Earth Sciences*, v. 1(1), p. 47-57.
- Dickinson, W.R. (1985), Interpreting provenance relations from detrital modes of sandstones. In: Zuffa, G.G. (ed.), *Provenance of Arenites*. Reidel Publishing Company, Reidel, p. 333–361.
- Dickinson, W.R. and Suczek C.A. (1979), Plate tectonics and sandstone compositions. *AAPG Bulletin*, 63(12), 2164-2182.
- Fedo, C.M., Nesbitt, H.W. and Young, G.M. (1995), Unraveling the effects of potassium metasomatism in sedimentary rocks and paleosols, with implications for weathering conditions and provenance. *Geology*, v. 23, p. 921–924.
- Folk, R.L. (1980), *Petrology of Sedimentary Rocks*. *Hampbill Publishing Company, Texas*, p. 182.
- Gopalan, K., Kumar, A., Kumar, S. and Vijayagopal, B. (2013), Depositional history of the Upper Vindhyan succession, central India: time constraints from Pb–Pb isochron ages of its carbonate components. *Precambrian Research*, v. 233, p. 103–117.
- Harnois, L. (1988), The CIW index: A new chemical index of weathering. *Sedimentary Geology*, v. 55, p. 319–322.
- Ingersoll, R.V., Bullard, T.F., Ford, R.L., Grimm, J.P., Pickle, J.D., Sares, S.W. (1984), The effect of grain size on detrital modes: a test of the Gazzi-Dickinson point-counting method. *Journal of Sedimentary Petrology*, v. 54, p. 103-116.
- Johnsson, M.J. and Basu, A. (1993), Processes controlling the composition of clastic sediments. *Geological Society of America*, v. 284.
- Kale, V.S. and Phansalkar, V.G. (1991), Purana basins of peninsular India: a review. *Basin Research*, v. 3, p. 1–36.
- McLennan, S.M., Hemming, S., McDaniel, D.K., and Hanson, G.N. (1993), Geochemical approaches to sedimentation, provenance, and tectonics. *Special Papers-Geological Society of America*, v. 284, p. 21-40.
- Nesbitt, H.W. and Young, G.M. (1982), Early Proterozoic climates and plate motions inferred from major element chemistry of lutites. *Nature*, v. 299, p. 715–717.
- Nesbitt, H.W., Young, G.M., McLennan, S.M., & Keays, R.R. (1996), Effects of chemical weathering and sorting on the petrogenesis of siliciclastic sediments, with implications for provenance studies. *The Journal of Geology*, v. 104(5), p. 525-542.
- Potter, P. E. (1978a), Petrology and chemistry of modern big river sands. *Journal of Geology*, v. 86, p. 423-449.
- Prasad B. (1984), *Geology, sedimentation and paleogeography of the Vindhyan Supergroup, SE Rajasthan*, Geological Survey of India, v. 116, p. 1-102.
- Roser, B.P. and Korsch, R.J. (1986), Determination of tectonic setting of sandstone-mudstone suites using SiO₂ content and K₂O/Na₂O ratio. *The Journal of Geology*, v. 94, p. 635–650.
- Roser, B.P. and Korsch, R.J. (1988), Provenance signatures of sandstone mudstone suites determined using discrimination function analysis of major element data. *Chemical Geology*, v. 67, p. 119–139.
- Roy, A.B. (1988), Stratigraphic and tectonic framework of the Aravalli mountain range. In: Roy, A.B. (ed.). *Precambrian*

- of the Aravalli Mountain. Rajasthan (India), Memoir of Geological Society of India, v. 7, p. 3-31.
- Soni, M.K., Chakraborty, S. and Jain, V.K. (1987), Vindhyan Super Group—a review. Memoir Geological Society of India, v. 6, p. 87-138.
- Suttner, L.J., Basu, A. and Mack, G.H. (1981), Climate and the origin of quartzarenites. Journal of Sedimentary Research, v. 51, p. 1235–1246.
- Suttner, L.J. and Dutta, P.K. (1986), Alluvial sandstone composition and paleoclimate, I. Framework mineralogy. Journal of Sedimentary Petrology, v. 56, p. 329-345.
- Taylor, S.R. and McLennan, S.M. (1985), The continental crust: its composition and evolution. Blackwell, Oxford, p. 311.
- Venkatachala, B.S., Sharma, M., & Shukla, M. (1996), Age and life of the Vindhyan - Facts and conjectures. Memoir Geological Society of India, v. 36, p. 137–165

Received on 17 February 2020 Revised Accepted on 11 January 2021

On the occurrence of ichnogenera *Planolites* and *Psilonichnus* from the Jogira Formation (Early-Middle Eocene), Bikaner Basin, Western India: implications on depositional environment

Shyam N. Mude, Ravindrasing G. Pardeshi, Manoj Memane

Department of Geology, Fergusson College (Autonomous), Pune- 411004, India

Email*: shyam.mude@fergusson.edu

Abstract

The Cenozoic sediments of the Bikaner basin are lithostratigraphically classified into Palana Formation, Marh Formation, Jogira Formation and Kolayat Formation in ascending order of superposition. The present paper records ichnofossils namely, *Planolites montanus*, *P. beverleyensis* and *Psilonichnus* isp from the Jogira Formation (Lower Middle Eocene) of Bikaner basin, Western India. The presence of these ichnofossils in a succession exposed in a quarry southeast of Jogira Lake plays a significant role in deciphering the depositional environment of the Jogira Formation. In the present section, two ichnofossil horizons are marked. The lower horizon is dominated by *Psilonichnus* isp whereas upper horizon is marked by *Planolites montanus*, and *P. beverleyensis*. From the sedimentological characteristic features and associated ichnofossils from the studied succession, we infer that the deposition of the sediments of the Jogira Formation began in a lagoonal to backshore environment with the formation of mudstone and sandy shale. Later, with the change in the bathymetry shallow marine fossiliferous limestone was deposited.

Key words: Bikaner basin, Jogira Formation, mudstone, shale, Ichnofossils, Depositional environment

Introduction

Most of the areas of Bikaner district are covered by the desert sands and sandy alluvium of Quaternary Period. The Bikaner basin lies between 26°10"-30°00' N latitudes and 71°31'-74°26' E longitudes. The Bikaner-Nagaur basin is a sedimentary basin trending NNE-SSW, covering an area of over 35,000 sq. km. The Cenozoic sedimentation in the Bikaner- Nagaur basin (Table 1, Fig. 1) began with Palana Formation that was

deposited during the Paleocene, followed by Marh Formation, Jogira Formation and Kolayat Formation (Ghosh, 1983; Ghosh, 1983 and Pareek, 1984). During the close of Mesozoic, encroachment of sea was seen through an embayment between the two fault ridges trending ESE-WNW. The Tertiary sediments of Bikaner basin occur in distinctly separated areas which witnessed marine transgression. Exposures of the Tertiary rocks can be found as detached outcrops well exposed about 50 to 60 km WSW of Bikaner

Table No 1- Cenozoic sequence of the Kolayat area (after Ghosh, 1983)

Age	Formation	Lithology
Pleistocene to Recent	Kolayat	Sand and sandy alluvium; Ironstone nodules, sandy calcareous grit kankar, gypsite Ferruginous bands, semi-consolidated conglomerate; Erratic boulders of quartzite
~~~~~Unconformity~~~~~		
Early to Middle Eocene	Jogira	Shaly and marly limestones with foraminifers ( <i>Alveolina</i> , <i>Discocyclina</i> , <i>Nummilites</i> ); Unfossiliferous, white clayey marl Dirty brown impure limestone with broken shells of ostrea and foraminifers ( <i>Assilina</i> ); Fuller's earth with shale partings having casts of lamellibranchs and gastropods; Yellow shales, marl with smaller foraminifers ( <i>Nummilites</i> , <i>Assilina</i> )
~~~~~Unconformity~~~~~		
Late Paleocene	Marh	Upper clay horizon with one clay bed Ferruginous sandstone, gritty sandstone and sugary sandstone with white glass sand (local) Middle clay horizon with five clay beds and sandstone partings Ferruginous sandstone, gritty sandstone, grit, various siltstone with leaf impressions
~~~~~Gradational Contact~~~~~		
Early Paleocene	Palana	Fine grained sandstone, carbonaceous shale and lignite

Various researchers including Ghosh (1983), Khosla (1973) and Pareek (1984) made valuable contributions in the systematic study of the geology and stratigraphy of the area. In the present paper, an attempt is made to

understand the depositional environment of the Jogira Formation on the basis of ichnofossils and sedimentological characteristic features.

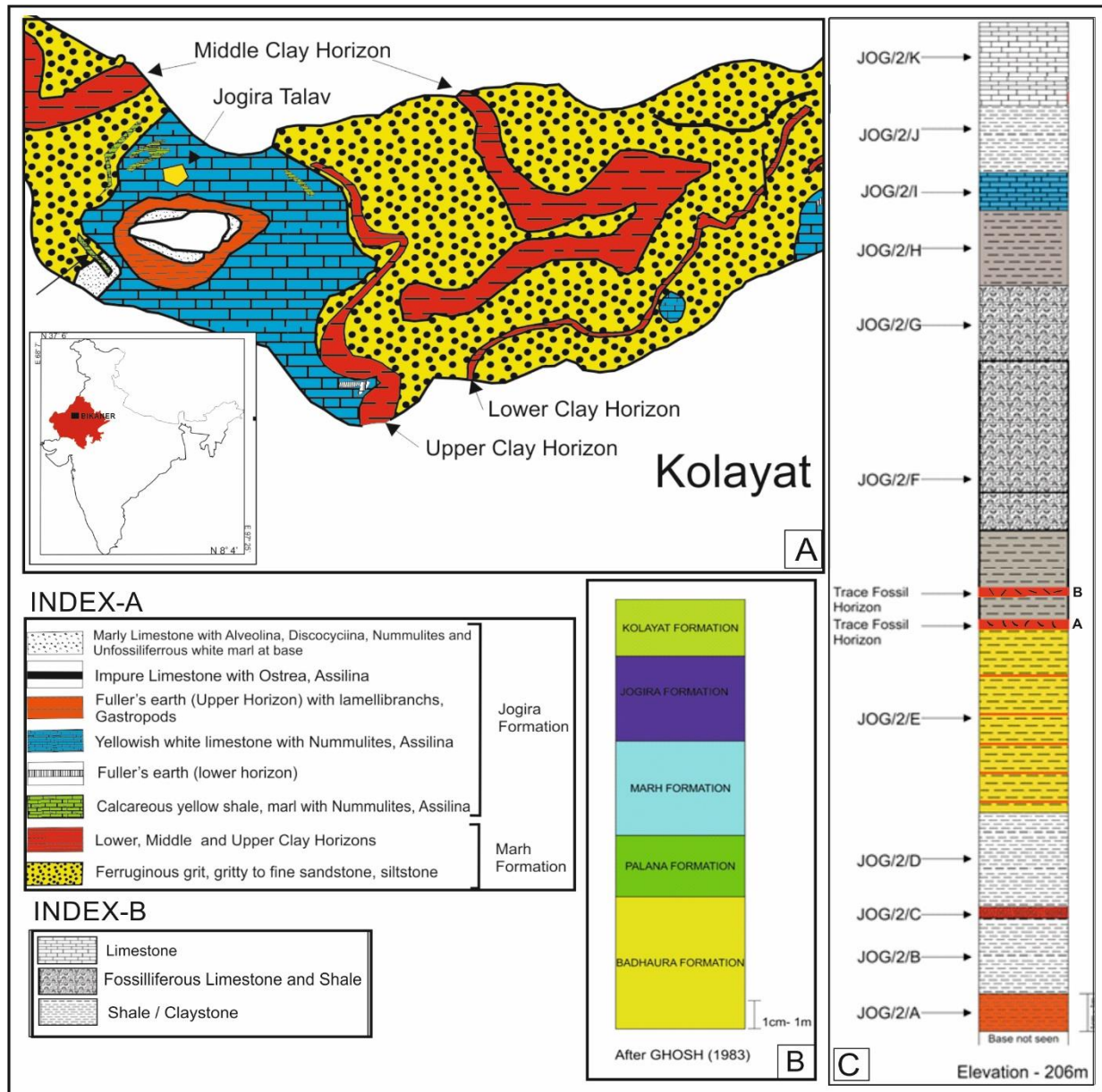


Figure 1: A. Geological map of the study area (After Ghosh, 1983), B. Litholog (After Ghosh, 1983) and C. Litholog of studied section

## Methodology

The sedimentological, ichnological variations and responses of ichnofossils to sediments have been studied from the present section in the field and accordingly lithocolumn was prepared. Total 11 representative samples (JOG/2/A to JOG /2/K) were collected from the section for laboratory studies. Thin sections of limestone were prepared and analyzed microscopically whereas sandstone, claystone and shale were studied megascopically. All the measurements of the ichnofossils were done in the field. All ichnological

interpretations are based on field observations and no type specimens were collected for repository. This study of palaeoichnology follows the Treatise on Invertebrate Palaeontology, (Haentschel, 1975), the morphological classification of Simpson (1975) and ethological classification of Seilacher (1964).

## Jogira Talab Section of Jogira Formation

A section of Jogira Formation (27 m thick) is exposed in a quarry SE of Jogira Talab (N 27°52'20.5"; E 72°54'28.5"; El. 206 ± 3) (Fig. 1C; Fig.2, A and B).

The bottom portion of the succession is marked by 1 m thick brown claystone horizon overlain by 1m thick off-white coloured claystone consisting of yellow and red bands enclosing ferruginous material. The off-white claystone is overlain by 30 cm thick gritty sandstone having angular fragments of quartz along with few iron oxide nodules, and showing red ferruginous cement. Gritty sandstone is overlain by 2.5 m thick claystone, showing yellow and red pockets of iron rich material. This claystone horizon is overlain by 5 m thick yellow claystone containing 5 bands of ferruginous material. Above it, 1 m bioturbated claystone / trace fossil horizon 'A' dominantly consisting of trace fossils belonging to ichnogenus *Psilonichnus*, is exposed. Above this horizon, 1.5 m thick brown coloured gritty sandstone is

exposed and on the top of it trace fossil horizon 'B' is exposed and shows dominant presence of ichnogenus *Planolites*. A 7 m thick horizon is overlain by the trace fossil horizon 'B', showing fine laminated shale (2.5 m thick) at the basal part which is followed by thick sequence of fossiliferous limestone (4.5 m) consisting of foraminifera viz., *Assilina* and *Discocyclina*. Fossiliferous limestone consisting of *Discocyclina* and few *Assilina* overlies the previous lithounit. Fossiliferous shale (2 m thick) consisting of *Discocyclina* and *Assilina* is exposed. This fossiliferous shale is overlain by whitish limestone (2 m thick) consisting mainly *Assilina*. Off-white to yellowish coloured claystone is exposed and overlain by limestone consisting of *Discocyclina* and *Assilina*.

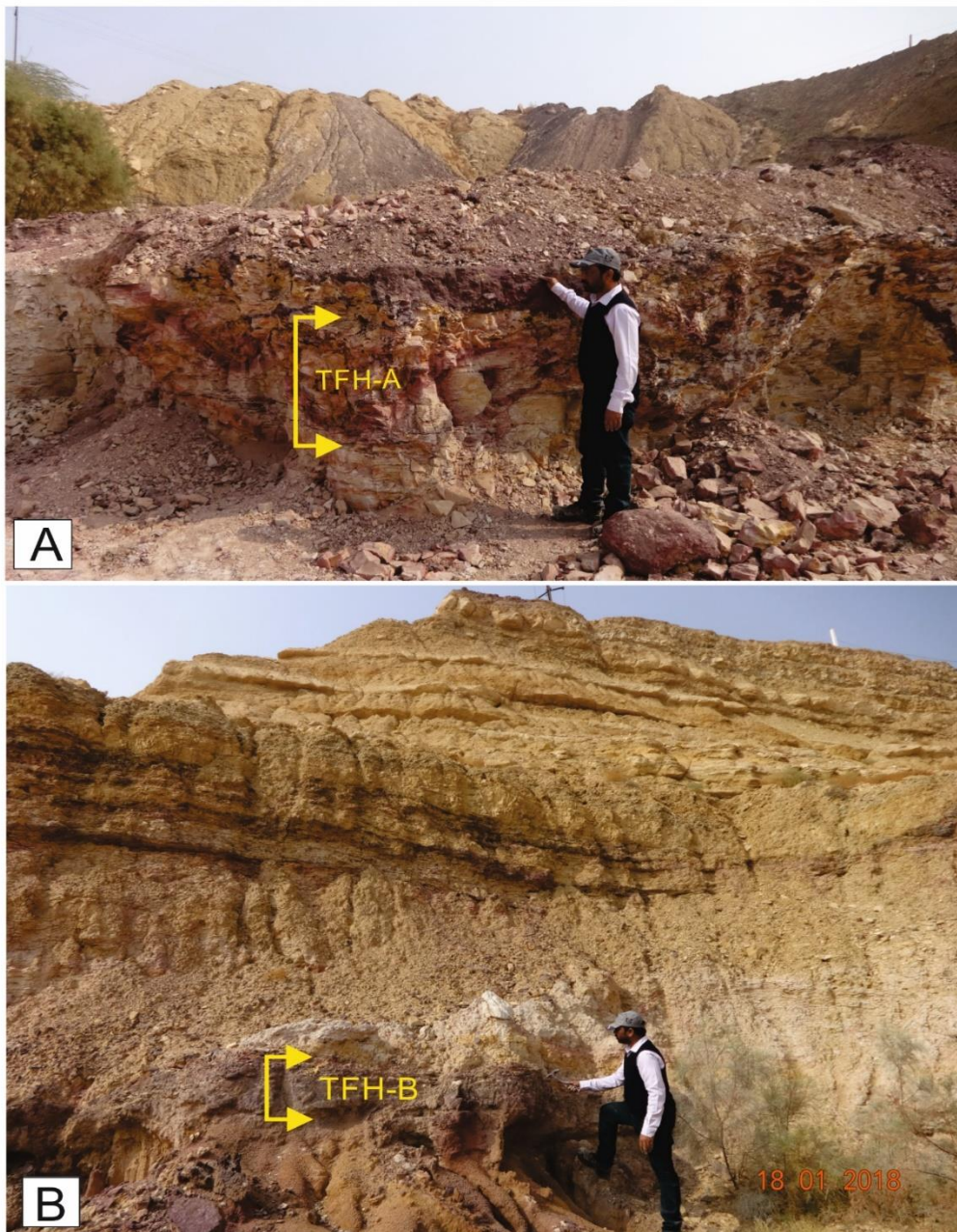


**Figure 2:** A. Trace fossil horizon- A exhibiting ichnogenus *Psilonichnus* and B. Trace fossil horizon- B exhibiting ichnogenus *Planolites*.

## Systematics of Trace Fossils

**Ichnogenus:** *Psilonichnus* Fürisch, 1981

**Ichnospecies:** *Psilonichnus* isp (Figs.3, A, B, C and D)

**Description:** Cylindrical, vertical to inclined burrows without lining are observed in the claystone horizon. 'J' and 'I' shaped burrows were dominant. The diameter of burrows ranges from 10 mm to 14mm.

**Remarks:** Vertically oriented cylindrical unlined burrows, exhibiting variation in the diameter of burrows at places. The present specimens show many similarities with ichnogenus *Psilonichnus* and thus it is described as *Psilonichnus* isp. These species are interpreted as domichnia which are suspension feeders.

**Horizon:** Claystone of the Jogira Formation near Jogira Talab, Bikaner, Rajasthan

**Ichnogenus:** - *Planolites* Nicholson, 1873

**Ichnospecies:** *Planolites montanus* (Figs.3, E and F)

**Description:** These burrows occur without lining and are straight to curved and occur parallel to the bedding planes. The burrow fill material is different from the host. Shape is circular to semi-circular in cross section. The diameter of these species varies from 4mm to 7mm.

**Remark:** Burrows are straight, unbranched and disposed parallel to the bedding plane. They are semicircular to circular in cross section. They are unlined burrows infilled with material different from that of host rock i.e. colour of burrow and host rock is different. The present burrows are considerably thin. Hence, they are placed under *Planolites montanus* (Pemberton and Frey, 1982). Morphologically they are interpreted as tunnel and ethologically as fodinichnia.

Badve and Ghare (1978, 1980); Sanganwar and Kundal (1997); Kundal and Sanganwar (1998, 2000) documented this ichnospecies from Bagh Group of Madhya Pradesh whereas Chiplonkar and Ghare (1979) recorded it from Trichinopoly Group, Tamil Nadu. Kundal et al., (2005) documented this from Babaguru Formation at Bhilod village, Broach district, Gujarat. Kundal and Dharashivkar (2006) reported this ichnospecies from Shankhodhar Sand Clay Member (Dwarka Formation) at Dingshwar Mahadev cliff.

**Occurrence:** Sandstone of the Jogira Formation near Jogira Talab, Bikaner, Rajasthan.

**Ichnospecies:** *Planolites beverleyensis* (Fig.3, F and G)

**Description:** These burrows occur without lining and are straight to curved. The burrow fill material is different from the host and occurs parallel to the bedding

plane. Shape is circular to semi-circular in cross section. The diameter of these species varies from 15mm to 24mm.

**Remark:** Burrows are straight and unbranched, and disposed parallel to the bedding plane. They are semicircular to circular in cross section. They are unlined burrows infilled with material different from that of host rock i.e. colour of burrow and host rock is different. The present burrows are considerably thick. Hence, they are placed under *Planolites beverleyensis* (Billings) (Pemberton and Frey, 1982). Morphologically they are interpreted as tunnel and ethologically as fodinichnia.

Borkar and Kulkarni (1992) and Kundal and Sanganwar (1998, 2000) recorded *Planolites beverleyensis* (Billings) from Wadhawan Formation of Gujarat and Bagh Group of Madhya Pradesh, respectively. Kundal et al., (2005) documented it from Babaguru Formation at Bhilod village, Broach district, Gujarat. Kundal and Dharashivkar (2006) recorded this species from Shankhodhar Sand-Clay Member Dwarka Formation. Recently, Mude et al. (2012) documented it from the Bhuj Formation, Kachchh. Further, Mude (2012a and b) documented it from Kand Formation and Babaguru Formation, Gujarat.

**Horizon:** Sandstone of the Jogira formation near Jogira Talab, Bikaner, Rajasthan.

## Discussion

The palaeoenvironmental study of marine sediments can be achieved by analysing lithology, associated primary structures and fossils. However, ichnofossils / ichnofossil assemblage are much significant in palaeoenvironmental investigations due to their autochthonous nature (Haentzschel, 1975). Ichnofossil assemblage helps to understand the depositional environment and to reconstruct palaeoenvironments and palaeobathymetry of the sedimentary horizon (Seilacher, 1967). There are various factors that control the behavioral responses of animals and these responses are controlled by energy conditions at a depositional interface, substrate type and availability of food. Thus, ichnofossils are very sensitive to environmental conditions and can be used as environmental indicators (Crimes, 1975). The ichnogenus *Psilonichnus* generally occur within shoreface to estuarine to fluvial settings (Nesbitt and Campbell, 2006). The ichnogenus *Planolites* represent the feeding trace of a mobile infaunal deposit feeder and generally associated with shallow marine sediments with low to moderate energy conditions (Pemberton and Frey, 1982).

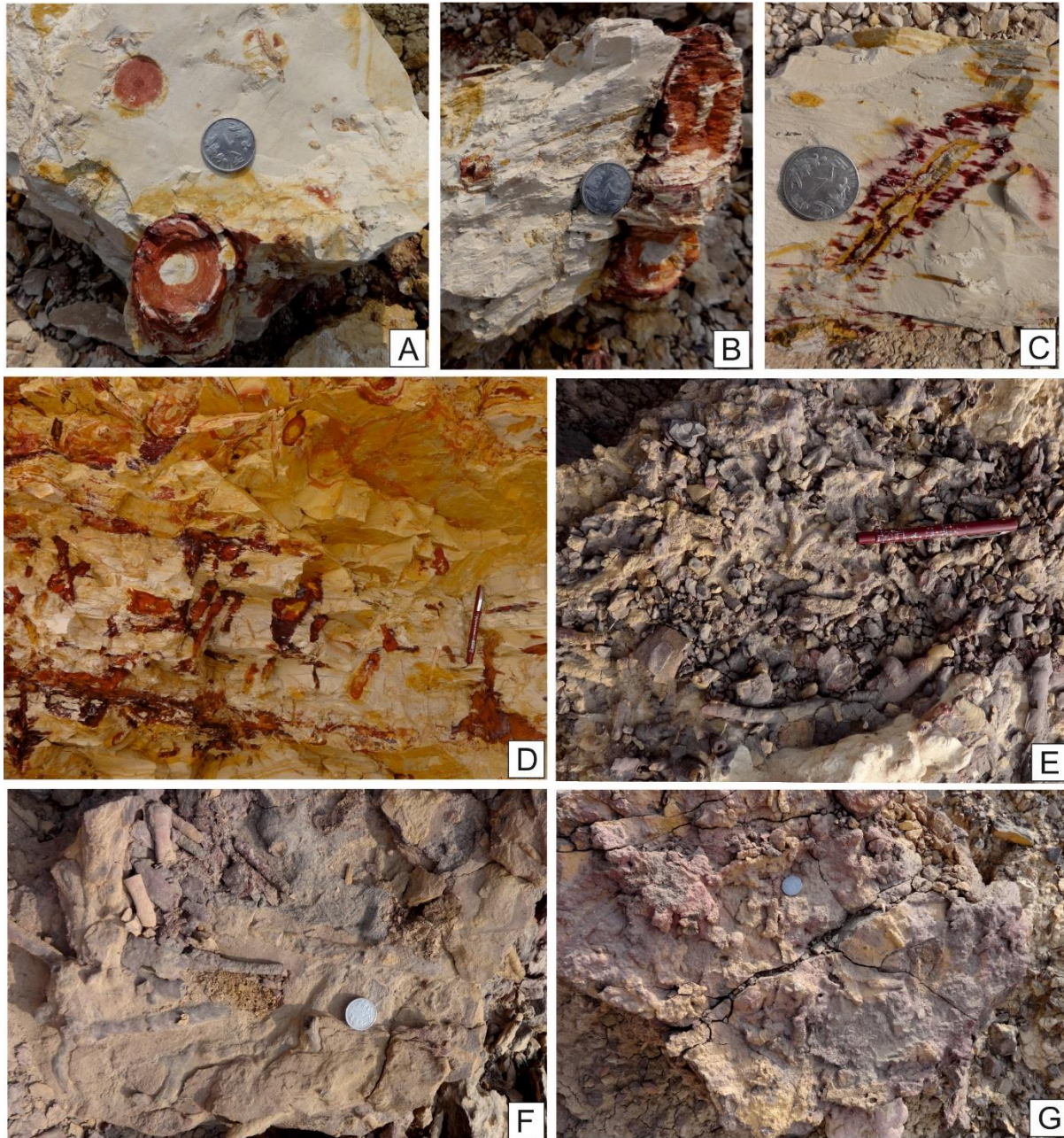


Fig. 3: A to D, field photographs of *Psilonichnus isp* and E & F, field photographs of *Planolites montanus* and F & G, field photographs of *Planolites beverleyensis*

### Conclusions

1. The present paper records ichnofossils viz., *Planolites montanus*, *P. beverleyensis* and *Psilonichnus isp* from Jogira Formation (Lower Middle Eocene) of Bikaner basin, Western India.

2. The present ichnofossil assemblage and sedimentological studies infer that the deposition of the Jogira Formation (exposed at Jogira Talab section) was initiated with lagoonal to backshore environment and subsequent transgression leading to deposition of shallow limestones.

### Acknowledgements

The author (RGP) is grateful to University Grants Commission, New Delhi (Western Region Pune) for financial assistance to carry out the present work under UGC Minor Research Scheme No. 47-1021/14(WRO). We are greatly indebted to anonymous reviewers for critical reviews of the manuscripts.

### References:

Badve, R. M. and Ghare, M. A., (1978), Jurassic Ichnofauna of Kutch-I, Biovigyanam, 4, 125-140.

- Badve, R. M. and Ghare, M. A., (1980), Ichnofauna of Bagh Beds from Deva river valley, south of Narmada, *Biovigyanam*, 6,121-130.
- Borkar V. D. and Kulkarni K. G., (1992), On the occurrence of *Planolites* Nicholson from the Bhaduka Limestone of the Wadhwan Formation (Cretaceous), Kathiawar, Gujarat, *Jour. Geol. Soc. India*, 40, 468-473.
- Chiplonkar, G. M. and Ghare, M.A., (1979), Trace fossils from Upper Cretaceous rocks of Trichinopoly district, Tamil Nadu, *Geol. Surv. India Misc. Publ.*, 45, 101-109.
- Ghosh, R.N., (1983), Tertiary clay deposits of Kolayat and adjacent areas in Bikaner district, Rajasthan, *Indian Minerals*, 37 (4), 56-69.
- Häntzschel, W., (1975), Trace fossils and problematica. In: C. Teichert (Ed.), *Treatise of Invertebrate Paleontology* (2nd Edition), part W, Miscellaneous, supp 1. University of Kansas and Geological Society of America, Boulder, Colorado, and Lawrence, Kansas, 269.
- Khosla, S. C., (1973), Stratigraphy and Microfauna of the Eocene Beds of Rajasthan, *Jour. Geol. Soc. India*, 14 (2), 142-152.
- Kundal, P. and Sanganwar, B.N., (1998), Stratigraphy and Palichnology of Nimar Sandstone, Bagh Beds of Jobat area, Jhabua district, M. P., *Jour. Geol. Soc. India*, 51(5), 619-634.
- Kundal, P. and Sanganwar, B. N., (2000), Ichnofossils from Nimar Sandstone Formation, Bagh Group of Manawar area, Dhar district, Madhya Pradesh, *Mem. Geol. Soc. India*, 46, 229-243.
- Kundal, P., Mude, S. N. and Humane, S., (2005), Ichnofossils from Late Eocene to Early Miocene of Narmada block of Cambay Basin Gujarat, India, *Jour. Palaent. Soc. India*, 50(2), 177-182.
- Kundal, P. and Dharashivkar, A.P., (2006), Ichnofossils from the Neogene and Quaternary deposits of Dwarka-Okha area, Jamnagar district, Gujarat, India, *Jour. Geol. Soc. India*, 68, 299-315.
- Mude, S. N., Jagtap, S. A., Kundal, P., Sarkar, P. K. and Kundal, M. P., (2012), Paleoenvironmental significance of ichnofossils from the Mesozoic Jaisalmer Basin, Rajasthan, north western India, *Proc. Inter. Acad. Ecol. and Env. Sci.*, 2(3), 150-167.
- Mude, S.N., (2012a), Paleoenvironmental significance of ichnofossils from the Kand Formation of the Cambay Basin, Gujarat, India. *Proc. Inter. Acad. Ecol. and Env. Sci.*, 2(1), 12-20.
- Mude, S. N., (2012b), Paleoenvironmental significance of ichnofossils from the Babaguru Formation of the Cambay Basin, Gujarat, India, *Univ. Jour. Env. Res. and Tech.*, 2(1), 52-57.
- Mude, S.N., Raut, S. D. and Wagh, R., (2012), Paleoenvironmental significance of ichnofossils from the Bhuj Formation (Gondwana Sediments) of the Kachchh region, Northwestern India. *World Jour. Env. Biosci.*, 1(1), 25-29.
- Nesbitt, E. A. and Campbell, K. A., (2006), The paleoenvironmental significance of *Psilonichnus*, *Palaios*, 21, 187-196.
- Nicholson, H. A., (1873), Contributions to the study of the errant annelids of the older Paleozoic rocks, *Procee. Royal Soc. London*, 21, 288-290.
- Pareek, H.S., (1984), Pre-Quaternary Geology and mineral resources of Northwestern Rajasthan, *Mem. Geol. Surv. India*, 115,1-95.
- Pemberton, R. K. and Frey, R. W., (1982), Trace fossils nomenclature and *Planolites Palaeophycus* dilemma. *Jour. Paleontol.*, 56 (2), 416-439.
- Seilacher A., (1964), Biogenic sedimentary structures. In: *Approaches to Palaeoecology* (Imbrie J, Newell ND, eds), John Willey and Sons, New York, USA, 246-316.
- Seilacher, A., (1967), Bathymetry of trace fossils: *Marine Geol.*, 5, 413-428.
- Simpson S., (1975), Classification of trace fossils. In: *The study of Trace Fossils* (Frey RW, ed), Springer Verlag, Berlin, Germany, 39-54.

(Received: 23 March 2021; Revised version accepted: 23 May 2021)

## Facies Architecture and Sedimentary Structures in the drill cores of Uranium Bearing Sediments of Banganapalle Formation of Palnad Sub-basin, Guntur District, Andhra Pradesh

Shekhar Gupta^{1*}, R. V. Singh¹, Rahul Banerjee^{1S} and M. B. Verma^{1S}

Atomic Minerals Directorate for Exploration and Research

¹Hyderabad – 500 016, ^SSuperannuated

*Corresponding author: [shekargupta.amd@gov.in](mailto:shekargupta.amd@gov.in)

### Abstract

The Banganapalle Formation, the lowest member of the Neoproterozoic Kurnool Group of rocks, resting over the Lower Proterozoic basement granitoids, has been identified as the host rock for uranium in Koppunuru area in the western part of Palnad sub-basin. Limited outcrops and sub horizontal dip of the Banganapalle Formation constrains the study of the sedimentological aspects but the drill cores of exploratory boreholes drilled for uranium exploration in Koppunuru and adjoining areas provide the sole access to study the structural and textural attributes of the different sub-lithounits of Banganapalle Formation in this area. Sedimentary structures recorded in the five distinct comparable lithofacies of Banganapalle Formation reported earlier viz., basal conglomerate facies, quartzite-shale intercalated facies, and two quartz arenite facies separated by a grey shale facies, were analysed. This study suggests deposition of the Banganapalle Formation sediments in Palnad Sub-basin commenced in fluvial, alluvial fan setting and culminated in a marginal marine (inter- to supra-tidal flat) environment.

**Keywords:** *Banganapalle Formation, Kurnool Group, Palnad sub-basin, drill core, Facies, sedimentary structures.*

### Introduction

The sedimentation of the Neoproterozoic Kurnool Group of rocks, is evidenced in two homotaxial sub-basins i.e. Kurnool in the west and Palnad in the northeastern part of Proterozoic intracratonic Cuddapah basin (Nagaraja Rao et al., 1987; Saha and Chakraborty, 2003; Ramakrishnan and Vaidyanadhan, 2008). The Banganapalle Formation, of Kurnool Group has been reported as potential target for unconformity-related uranium mineralization considering favourable time and space domains (Sinha et al., 1995, 1996). Intensive exploration efforts by Atomic Minerals Directorate for Exploration and Research (AMD) has brought the Palnad sub-basin into prominence after the discovery of a number of uranium occurrences in Banganapalle sediments and adjoining basement granites in the northern and western parts of the sub-basin (Jeyagopal et al., 1996; Roy et al., 2000; Singh et al., 2002; Nageswara Rao et al., 2005; Gupta et al., 2016). Sub-surface exploration activities have established a sizeable uranium deposit in Koppunuru–Chenchu Colony area where two sub-horizontal lodes of mineralization occur in the upper quartz arenite unit and one lode in the basal grit/conglomerate unit of Banganapalle Formation which at places transgresses below the unconformity in the basement granitoids (Verma et al., 2011). The Banganapalle Formation is thus, temporally and spatially regarded as a potential

host for Proterozoic unconformity-related uranium mineralization (Jeyagopal et al., 2011; Ramesh Babu et al., 2012).

Recent integrated studies on facies association and architectural element analysis of Banganapalle Formation in Kurnool basin have given a detailed insight of sedimentology and have led to the identification of fourteen facies types, grouped under four different facies associations, which record Palaeoenvironmental settings ranging between mid-alluvial fan to distal fluvial plain (Barkat et al., 2020). In Palnad sub-basin, five distinct comparable lithounits of Banganapalle Formation viz., basal conglomerate unit, quartzite-shale intercalated unit, and two quartz arenite units separated by a grey shale unit, were reported earlier (Gupta et al., 2010). In the present work, examination of drill core samples and down-hole lithological examination on course of exploratory drilling for uranium in Koppunuru area has provided exclusive access to study the structural/textural attributes of different sub-lithounits of Banganapalle Formation, as outcrops are scanty and dips of the Banganapalle Formation are sub horizontal. The scope of the present work is henceforth confined to documentation of the sedimentary facies and sedimentary structures in the drill cores of different lithounits of Banganapalle Formation from Koppunuru and adjoining areas and infer their depositional environments.

## Geological Setup

The Neoproterozoic Kurnool Group of rocks were deposited in two homotaxial sub-basins i.e. Kurnool in the west and Palnad in the northeastern part of Palaeo- to Meso-Proterozoic intracratonic Cuddapah basin which rest unconformably over the Archaean to Palaeoproterozoic peninsular gneisses with younger intrusive granitoids and mafic rocks (Nagaraja Rao et al., 1987; GSI, 1981, 2001, Chakraborti and Saha, 2006, Ramakrishnan and Vaidyanadhan, 2008). Cuddapah sediments predominantly consist of arenaceous and argillaceous rocks with subordinate calcareous units whereas the Kurnool sediments are dominated by calcareous rocks with minor arenaceous and argillaceous strata. In the Palnad sub-basin, spread over an aerial extent of ~ 3,400 sq km, Kurnool sediments unconformably overlie the older Cuddapah sediments in the eastern part whereas older granitoids form basement in the north and west of the basin. The Kurnool succession begins with Banganapalle Formation, followed by Narji, Auk shale, Paniam, Koilkuntla and the uppermost Nandyal Formation (Nagaraja Rao et al., 1987; Ramakrishnan and Vaidyanadhan, 2008) (Table-1). Sedimentological and geochemical aspects of the Banganapalle Formation were studied by various workers with special reference to incidence of diamond and uranium and shallow marine depositional environment with provenance comprising of granites in the north and west while older Cuddapah sediments in the south and east is envisaged (Vijayam and Reddy, 1976; Sivaji and Rao, 1989; Lakshminarayana et al., 1999; Gupta et al., 2010, 2012).

The study area falls in the westernmost part of the Palnad sub-basin. Palaeoproterozoic biotite granite exposed as an inlier, indicate basement highs (Fig. 1). Basement granites are also exposed to the south of the study area along the up-thrown block of WNW–ESE trending post Kurnool fault (Kandlagunta Fault). This fault is further offset by younger N–S trending faults. The basement granitoids are highly fractured and are profusely traversed by dolerite dykes and quartz veins. These granites are unconformably overlain by sub-horizontal beds of Palnad sediments. The overall thickness of the Palnad sediments varies from 10m to 140m and dips are gentle (3-7°). In the area around Koppunuru –Chenchu colony, five different lithofacies of Banganapalle Formation viz., basal conglomerate (LF-1), quartzite–shale intercalated unit (LF-2), lower quartz arenite (LF-3), dark grey shale dominated, siltstone intercalated unit (LF-4) and upper quartz arenite (LF-5) were identified from the borehole cores and study of borehole lithologs (Gupta et al., 2010). The overlying Narji Formation comprises of massive limestone and calcareous shale. The limonitised, yellowish Auk shale marks a gradational contact between the calcareous Narji Formation and the arenaceous Paniam Quartzite. The Paniam Quartzites occur as discontinuous ridges to the west of Koppunuru. The gentle dip of the Banganapalle sediments conceal the exposure of its lower lithounits and the exposed surface sections comprise only the upper quartz arenite (LF-5) which is monotonously extensive and conformably overlain by the Narji Limestone. This quartz arenite facies is characterized by light grey to white, medium grained, well sorted and uniformly rounded to sub rounded quartz clasts.

Table 1: Generalised lithostratigraphic succession of Cuddapah basin (modified after Ramakrishnan and Vaidyanadhan, 2008)

Super Gr / Group/ Sub Group		Formation	Thickness (m)
Kurnool Group	Kundair Sub-Group	Paniam Quartzite	10-35
	----- <i>Paraconformity</i> -----		
	Jamma-lamadgu Sub-Group	Auk (Owk) Shale	10-15
		Narji Limestone	100 -200
Banganapalle Quartzite		10 – 170*	
----- <i>Unconformity</i> -----			
Cuddapah Super Group	Srisailam Quartzite		300
----- <i>Unconformity</i> -----			
Archaean/ Dharwars	Intrusive Granite, Gneisses / Greenstones		

*Modified after Banerjee et al., 2012.

## Facies and Sedimentary structures

Scope of studying the sedimentary facies assemblages across different sections to characterise the facies architecture and infer the depositional

environment is restricted owing to sub horizontal dips and hence the absence of exposed stratigraphic lithocolumn lithocolumn” or “lithocolumn of the Banganapalle Formation. Hence, the depth-wise, down-hole drill core samples of ~52 mm diameter are

the exclusive window available for study of the structural and textural attributes of the sub-lithounits of Banganapalle Formation. Since, the size of the drill

cores cannot accommodate the lateral continuity of the bedform features viz., planar/trough cross-beds,

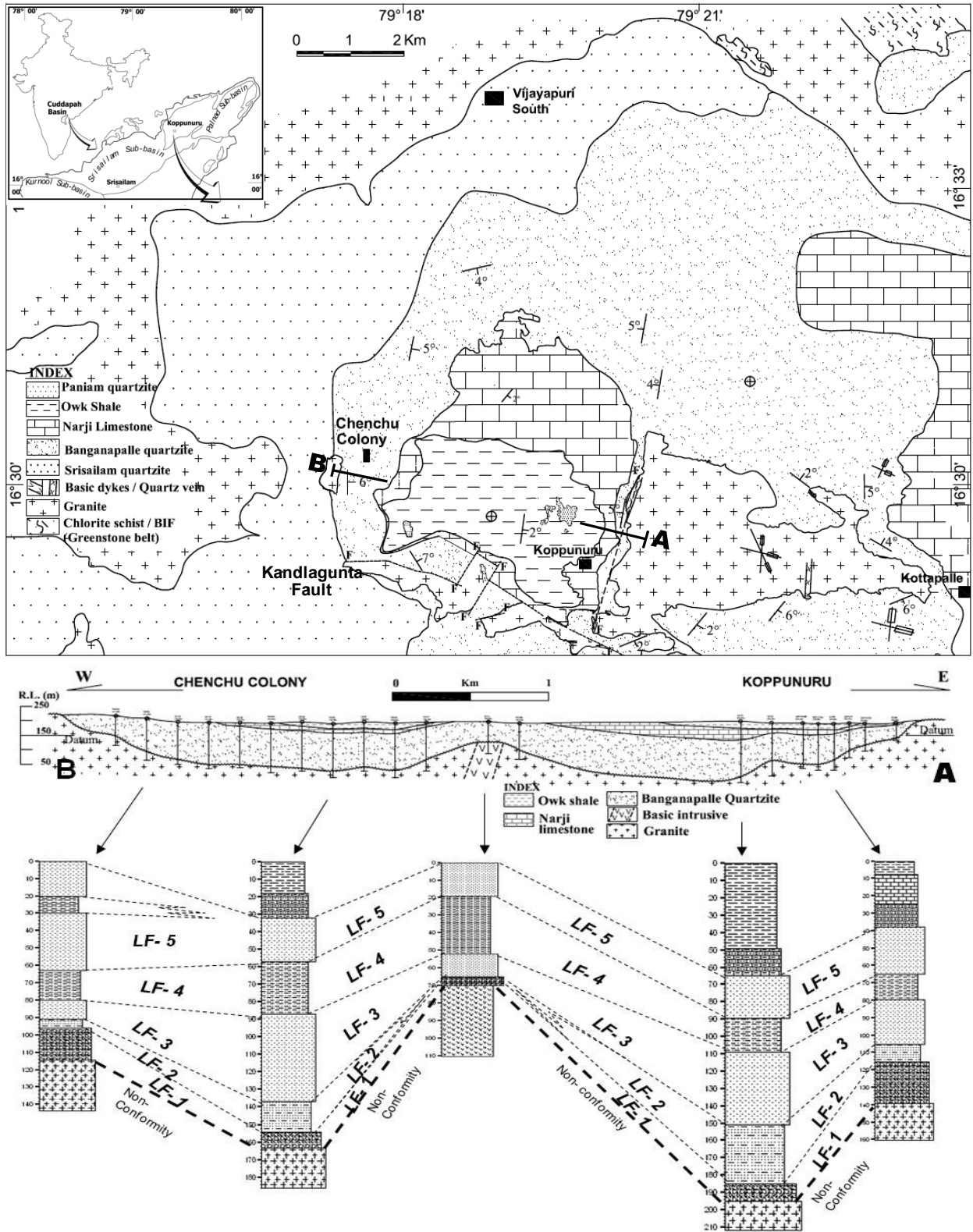


Fig.1 Geological map of the study area showing correlation of lithounits of Banganapalle Formation based on examination of drill cores (after Gupta et al., 2010).

ripples and channel geometry, the inferences on the sedimentation patterns and depositional environments are drawn solely based on the small scale sedimentary structures preserved in the cores and textural attributes limited to megascopic and microscopic observations in borehole core samples. However, observations recorded in the study area are compared with the architectural elements and facies associations of the Banganapalle Formation reported in the Kurnool Basin (Barkat et al., 2020).

**Basal conglomerate (LF-1):**

The basal unit of Banganapalle Formation is represented by a <1m to 38m thick polymictic conglomerate, with unsorted grit to pebble size clasts of granite, shale, quartzite, vein quartz and dolerite (Fig. 2a). This unit is deposited over basement granite along a visibly sharp non-conformity contact (Fig. 2b). Matrix is mainly composed of sericite and chlorite with minor pyrite as interstitial matrix, intergranular fracture fillings and as segregation along pebble margins (Fig. 2c). Petromineralogical studies have confirmed the presence of carbonaceous matter and colloform pyrite in matrix at places (Latha et al., 2009, 2011; Shobhita et

al., 2014). Nature of different clasts suggests their derivation from nearby granitoids traversed by quartz reef/basic dykes, and Upper Cuddapah sediments. The maximum thickness of this unit is seen along the slopes of the basement lows developed in proximity to the granite inliers (Fig. 1). The slopes of the basement highs have favourable conditions for alluvial-fan type sedimentation. Fining upward, planer, normal graded bedding observed at places along the non-conformity marks a flash flood like rapid depositional event (Fig. 2d).

This unit has been correlated to the similar conglomerate facies reported at the base of Banganapalle Formation in Kurnool Basin (Barkat et al., 2020). The comparable facies codes following the standard definitions (Miall, 1985) are- Gmm (clast-/matrix-supported, poorly sorted, ungraded, massive cobble-pebble conglomerate comprising of angular, pebble to cobble size clasts of quartzite, vein quartz and basic rock in crudely stratified sandy matrix), Gm (lenticular, clast-supported, massive conglomerate with boulder, cobbly clasts with intraclast voids filled by coarse granular sandstone) and Gsm (conglomerate-normal graded granular sandstone couplet).

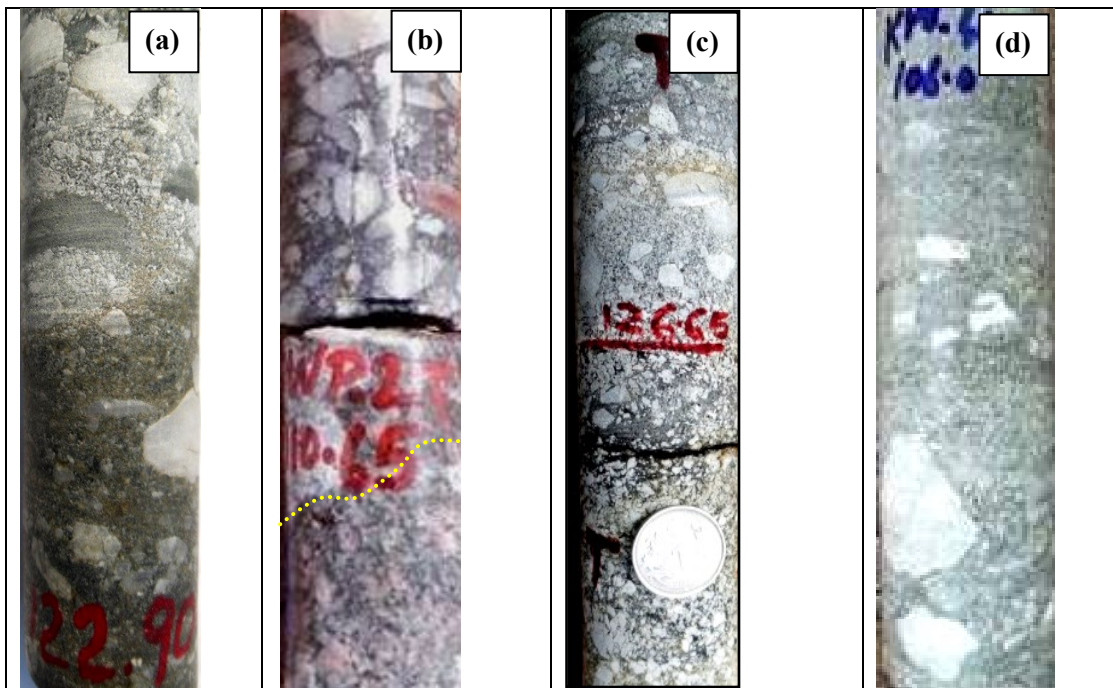


Fig. 2. Lithounit -1 (Basal Conglomerate):  
 a) Polymictic nature with subrounded to sub angular mixed clasts of shale, quartzite and vein quartz (KPU-438: 122.90m)  
 b) Sharp non-conformity contact between basement granite and LF-1 (DWP/21: 110.65m)  
 c) Unsorted clasts in matrix dominated by sericite and chlorite matrix (KPU-422: 126.65m)  
 d) Fining upward, planer, graded bedding (KPU-444:106.00m) in LF-1

**Quartzite-shale intercalation (LF-2)**

This lithounit was deposited immediately above the basal conglomerate unit in the deeper parts of

the basin. It is apparent from the borehole lithologs that quartzite–shale intercalated sequence is not developed in those parts where the overall thickness of the Banganapalle sediment column is below 25–30m. LF-2

is marked by rhythmic repetition of arenaceous (predominantly orthoquartzites) and argillaceous layers (grey to dark grey shales). Grey shale occurs as planar laminae with varying thickness from 2-3mm to 2cm and occasionally shows discontinuous/lenticular nature at places (Fig. 3a). Small scale cross stratification in the form of planar cross bedding is exhibited at places and the thickness of cross beds varies from 4 to 10cm (Fig. 3b). However, information on direction of current can't be derived since the directional drilling is not being carried out in this area to generate oriented borehole core. Presence of carbonaceous matter and pyrite specks/disseminations/lumps are common in this unit (Fig. 3c&d). Because of competency contrast between the arenaceous and argillaceous layers and occasional rapid sedimentation, soft-sedimentary deformation structures like convolute lamination, load and slump fault/fold structures are more prominent in LF-2 (Fig. 4a-d).

Convolute structures occur in the form of intrastratal crumpling and contortions of laminae (Fig.

4a). Folded laminae in this structure form upright cusps with broad U-shaped troughs and sharp crests. At places these contorted laminae form discrete lobes giving rise to load convolutions. The generally agreed mechanism for formation of convolute beddings is differential liquefaction and rapid internal readjustment of sediments as is evident from the confinement of convolutions within a single bed (Lowe, 1976; Nichols, 2009). Load structures occur as slight bulges and knobby bodies, a common feature observed in channels of muddy intertidal flats where arenaceous layers are deposited over argillaceous layers (Fig. 4b). At places, isolated lenticular arenaceous loads are also observed. These arenaceous load structures show contorted lamination. The contortion of lamination is more in the central part as compared to the periphery of the load structure. Such deformations generally occur before the deposition of overlying strata as evidenced by the presence of planar, non-contorted overlying beds.

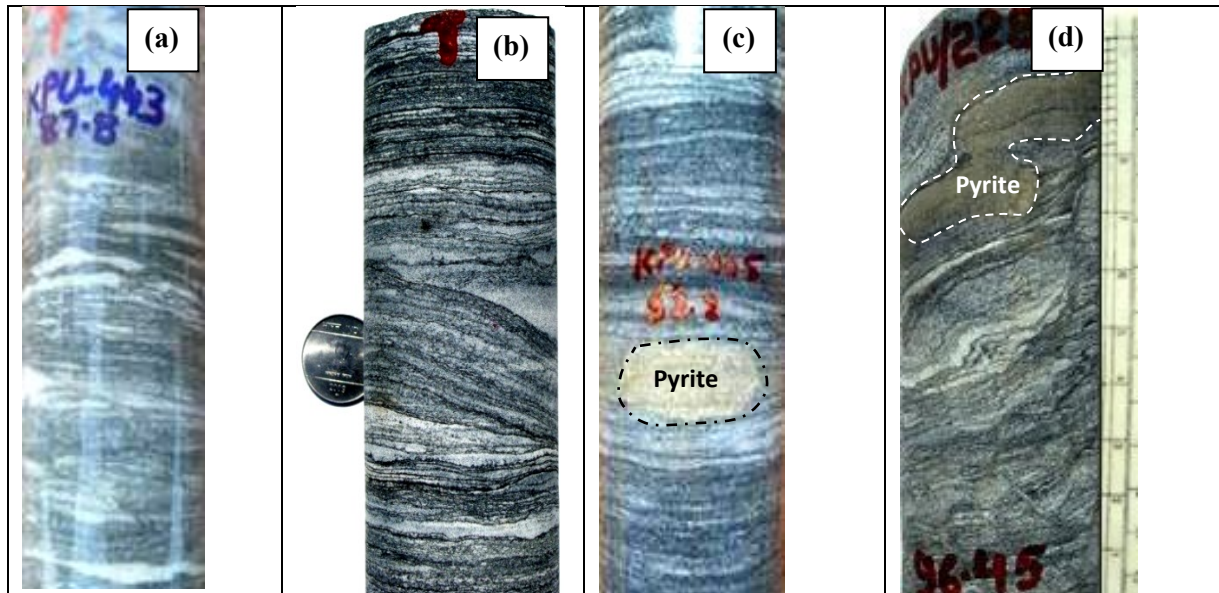


Fig. 3. Lithounit-2 (Quartzite-shale intercalation):

- a) Lenticular and wavy bedding / laminae in LF-2 (KPU-443: 87.80m)
- b) Cross bedding in LF-2 indicating change in current direction and intensity (KPU-310: 122.90m)
- c) Rhythmic sequence of quartzite-shale planer laminae with sub-rounded pyrite lump (KPU-445: 92.20m)
- d) Deformed wavy laminations with pyrite lump in LF-2 (KPU-228: 96.45m)

Small scale deformation structures, attributed to slumping are most commonly observed within the intercalated units. Such deformation zones are usually bounded by undisturbed beds and observed as offset of intercalated laminae along curvilinear fault planes (Fig. 4c), minor slippage of localized intercalated beddings along the inclined to sub-vertical planes (Fig. 4d) and hinge section of slump fold (Fig. 4e). Such rhythmic sand – shale sequence with synsedimentary deformation structures in this unit and its stratigraphic disposition over the basal conglomerate indicates regular changes in generation and transport of sediments and a

transgressive change from alluvial fan to inter-tidal flat environmental conditions of deposition.

#### **Lower and Upper quartz arenite (LF-3 & LF-5)**

The lower quartz arenite (LF-3) and upper quartz arenite (LF-5) lithounit are mineralogically and texturally mature and similar in nature. They are light grey in colour, medium to fine grained and saccharoidal in nature. Occasional grey shale lenses are also observed in these units (Fig. 5a). Previous works on petromineralogical characterization have shown that

these arenites are composed of moderate to well sorted, sub-rounded framework clasts (~90% of the rock by volume), which is dominated by quartz (~97%) with minor glauconite, chert and traces of carbonaceous matter. The quartz is mainly monocrystalline in nature with a few grains of polycrystalline quartz. The well indurated framework clasts are bounded by silica cement and matrix (Gupta et al., 2010).

The thickness of LF-5 unit varies from 10m to 26.50m and is recorded in all boreholes while LF-3 attains maximum thickness up to 45m and overly the quartzite–shale intercalated sequence in the deeper

parts. LF-5 is also exposed on surface and exhibit blanket type nature due to near horizontal beds of vast expanse. These arenites also exhibit various alteration features such as ferrugination, silicification, chloritization and kaolinization leading to formation of clay minerals viz., illite and kaolinite. Cross stratification observed at places suggests change in current direction and intensity (Fig. 5b). Numerous isolated mud streaks/lenses with streaks of pyrite are seen forming simple flaser beddings in these sand dominated units. The presence of flaser bedding also indicates the depositional environment more favourable

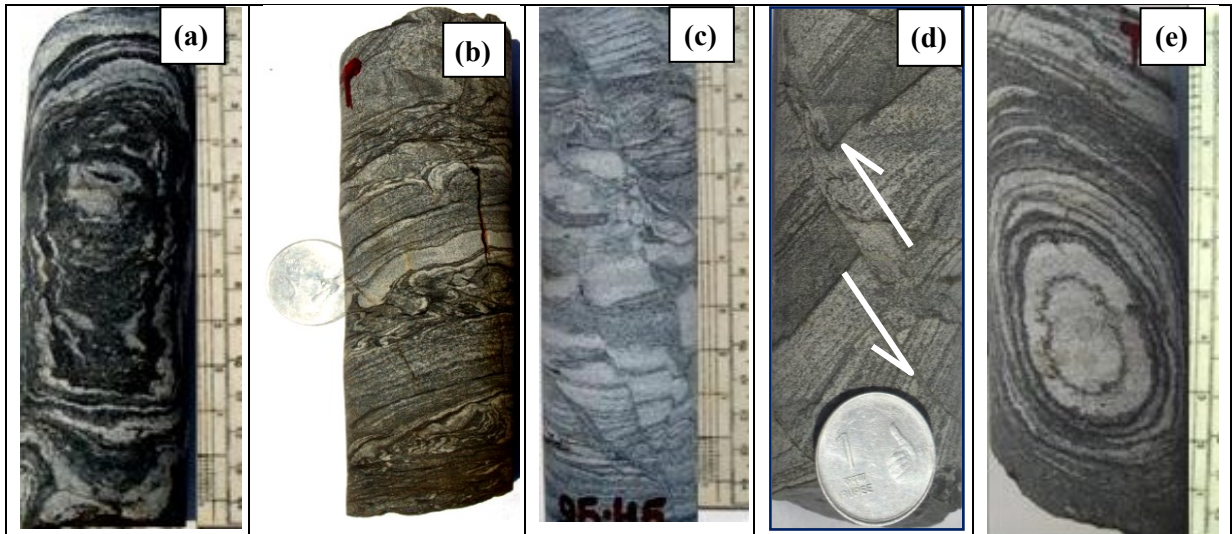


Fig. 4. Soft-sedimentary deformational structures in Lithounit -2:

- a) Convolute Lamination with broad U-shaped troughs and sharp crests (KPU-227: 158.30m)
- b) Lode Convolution structure; contorted laminae forms discrete lobes (KPU-271: 132.20m)
- c) Offset of laminae along sub-parallel vertical slip planes in LF-2 (KPU-302: 95.45m)
- d) Offset of laminae along oblique slip planes in LF-2 (KPU-310: 117.20m)
- e) Hinge section of slump fold (KPU-232: 122.10m)

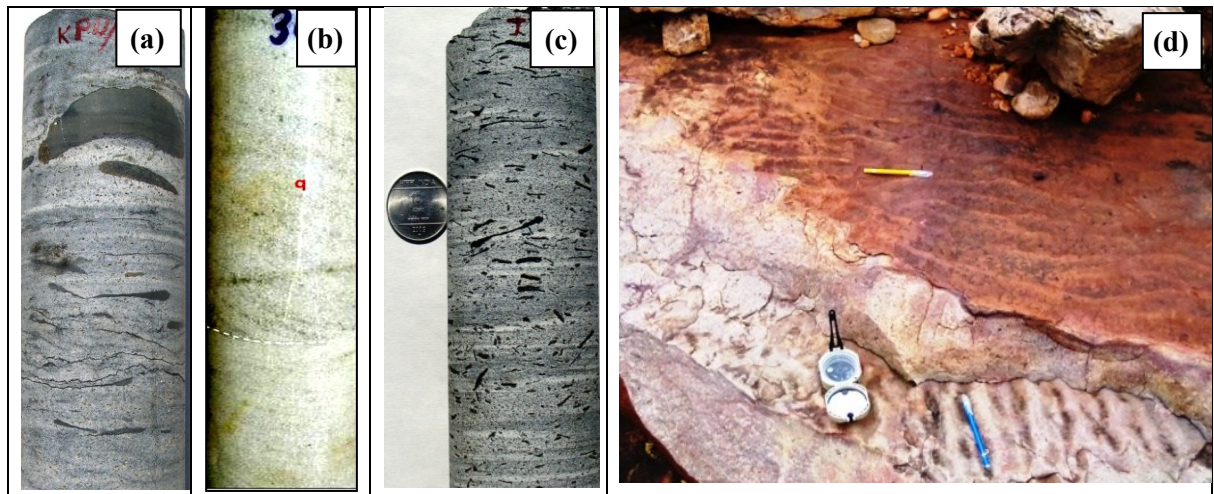


Fig. 5. Lower and upper quartz arenite, Lithounits -3 and 5:

- a) Isolated mud lenses in LF-5 (KPU-229: 64.30m)
- b) Cross stratification in LF-5 (DWI-28: 31.75m)
- c) Flaser bedding with numerous mud streaks in arenaceous LF-3 (KPU-226: 127.20m)
- d) Outcrop showing bi-directional, symmetrical ripples developed on the top of LF-5 (Dwarakapuri-Kottapalle area, southwest of Koppunuru).

environment more favourable for preservation of sands as compared to mud (Fig. 5c). Further, bi-directional symmetrical ripples recorded in outcrops of upper arenite unit suggest two different paleocurrent directions and points to dual provenance for the Banganapalle sediments. Geochemical studies on major element distribution patterns, alteration indices and discriminant function plots of these the different lithounits of Banganapalle Formation in the same area also suggest that Banganapalle Formation is mainly derived from two different sources i.e., basement granitoids and quartzose Cuddapah sediments in a passive margin setup (Gupta et al., 2012).

#### **Shale-siltstone intercalation (LF-4)**

This dominantly argillaceous unit (dark grey shale-siltstone intercalation) is sandwiched between the

upper and lower arenite units (LF- 3 and 5). The thickness of LF-4 ranges from 3m to 46m, and show thinning of the beds close to the basement granite inliers. Megascopically, this unit is characterized by higher argillaceous component as compared to LF-2. Shales are dark grey in colour, sub horizontally laminated and show fine intercalations of siltstone (Fig. 6). This unit is marked by the abundance of sulphides (mainly pyrite) occurring as fine disseminations, big nodules, thin stringers and veinlets. Sulphur isotope studies have indicated biogenic origin of these pyrites (Jeyagopal et al., 2008). Presence of glauconite with trashes of carbonaceous matter indicate mildly alkaline and reducing environment of deposition. Planer laminations, lenticular beddings and sand lenses embedded in argillaceous layers showing synsedimentary deformation structures are quite apparent in LF-4.

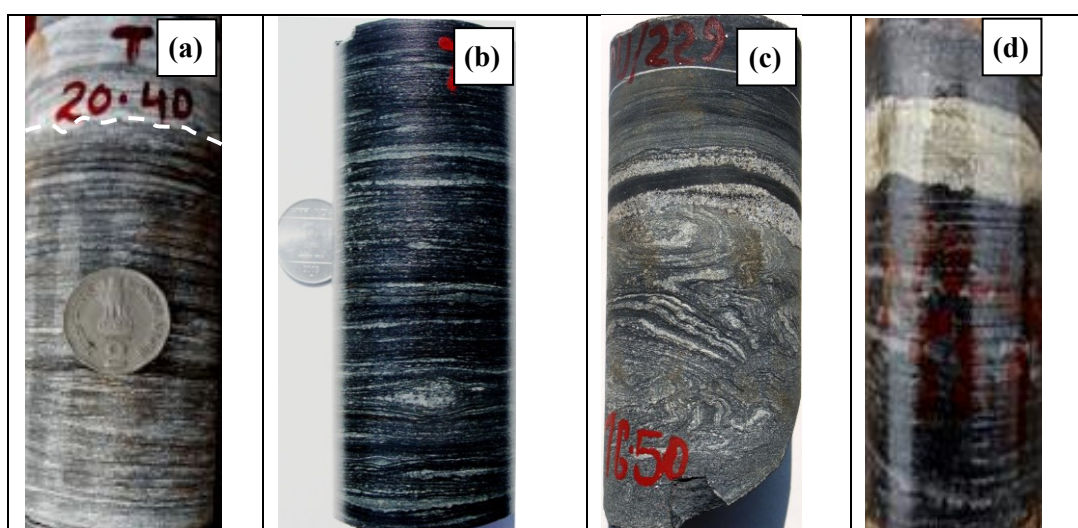


Fig. 6. Lithounit -4:

- a) Planer laminated shale along gradational contact of LF- 4 and 5 (KPU-420: 20.40m)
- b) Planer laminations and lenticular beddings in the form of sand lenses in argillaceous layers (KPU-229: 38.30m)
- c) Syn-sedimentary deformations in LF-4 (KPU-229: 46.50m)
- d) Dark grey shale with pyrite along bedding plane (KPU-444c: 52.10m)

#### **Discussion**

The basal conglomerate unit marks the non-conformity contact between the basement granite and the overlying Banganapalle Formation. Presence of carbonaceous matter and colloform pyrite are indicators of a reducing environment. The unsorted nature of the clasts and intragranular fractures also indicates high degree of porosity and permeability in this unit. The ungraded, angular, pebble to cobble size clasts of quartzite, vein quartz and basic rock in crudely stratified sandy matrix which points to their derivation from nearby granitoids traversed by quartz reef/basic dykes, and possibly, upper Cuddapah sediments. This is indicative of sub aerial rapidly freezed non-cohesive

hyper-concentrated flow (Sohn et al., 1999; Saula et al., 2002). The gradual fining upward, conglomerate-granular sandstone, normal graded bedding suggests a transformed cohesive flow. Overall, this facies marks a flash flood like rapid depositional event in an alluvial-fan type setting. The conglomerate is better preserved at places which were apex portions of fan (along the slopes) and could not be traced with similar thickness everywhere, as the thickness tapered as a conical wedge at the toe portions of the fan.

The overlying quartzite-shale intercalatory unit is marked by synsedimentary deformation structures like convolute beddings, load structures, lenticular and wavy beddings and slump structures. The rhythmic repetition of arenaceous and argillaceous layers

indicates regular changes in generation and transport of sediments in inter-tidal flat environment where sand layers get deposited in periods of flood and ebb current activity while the argillaceous/mud layers represent quiescent sedimentation phase. The planar cross beds are indicative of change in current direction and their intensity and suggest shallow water depositional environment. The disposition of this lithounit over the basal conglomerate indicate regular changes in generation and transport of the sediments and a transgressive change from alluvial fan to inter-tidal flat depositional environment.

The soft sedimentary deformation structures common in LF- 4 and LF-2 indicate submergence of the basin contemporaneous to the sedimentation. This is evidenced by the presence of deformed zones sandwiched between undisturbed beds. Convolute laminations commonly develop due to the deposition of sediments on sloping surfaces (Leeder, 1999; Collinson et al., 2006). Differential liquefaction and rapid internal readjustment of sediments are the accepted mechanism for formation of convolute beddings. In this study, it is evident from the confinement of convolutions within a single bed which indicates deposition of sediments under inter-tidal flats environment where sediments get compacted due to the expulsion of water during sub-aerial exposure at low tides. The development of load structures is attributed to the differential deposition and sinking of sandy bodies in underlying muddy layer in the channels of muddy inter-tidal flats. Development of the slump structures observed in the drill core are attributed to the mechanism of down slope movement of sediments under gravity due to elevated pore fluid pressure (Tucker, 2003; Collinson et al., 2006). Slump folds indicate compressive regime in the downslope position and the slippage along folded limbs are generally caused by syndimentary basinal tectonics. Slump structures observed in the study area indicate their deposition under inter-tidal flat tectono-sedimentary environment, particularly restricted to the over steepened segments. Formation of lenticular beddings in LF-4 is attributed to the fluctuating flows i.e., calm periods with a few short and strong currents allow incomplete sand ripple formation, which in turn is completely covered by argillaceous material. These are generally indicative of low energy depositional environments suitable for preservation of mud vis-à-vis low supply of the sand in the system. In contrast, flaser beddings in the arenaceous lithounits (LF-3&5) indicate strong current environment where both sand and mud were subjected alternatively to the periods of high current activity followed by intermittent short periods of quiescence.

High degree of mineralogical and textural maturity of arenites in LF-3 and LF-5 signify high current activity and deposition under high energy settings in shallow marine conditions. In contrast, the argillaceous facies LF-4 and LF-2 indicate deposition during standstill phase. Bi-directional symmetrical ripples in outcrops of upper arenite unit indicate that the

Banganapalle sediments were derived from the basement granitoids exposed to the north and upper Cuddapah sediments to its west.

Banganapalle Formation in western part of Palnad sub-basin has shown immense potential of uranium mineralisation (130-5,500ppm  $U_3O_8$ ; Jeyagopal et al., 1996) and intensive exploratory drilling by AMD has resulted in delineation of substantial uranium deposit in Koppunuru-Chenchu colony area, Guntur district, Andhra Pradesh. In this sector, comparable uranium mineralization has been intercepted in the upper quartz arenite facies and in the basal conglomerate facies occasionally transgressing to basement granitoids (Verma et al., 2011). Hydrothermally induced, fracture-controlled and epigenetic uranium mineralisation is postulated for this uranium mineralisation which was accentuated due to the presence of porous and permeable medium viz., quartz arenite and conglomerate facies which allowed free flow of mineralised solutions and the presence of suitable reductants like sulphides and carbonaceous matter favoured the precipitation and fixation of uranium mostly along the fractures, fine veins, intergranular cavities, intragranular fractures (Gupta et al., 2010, 2012; Jeyagopal et al., 2011). Various alteration features such as ferrugination, silicification, chloritization and kaolinisation substantiate hydrothermal activity in the system (Thomas et al., 2014).

## Conclusions

Based on observations of the disposition of the five distinct comparable facies of Banganapalle Formation, their lateral and depth continuity, sedimentary structures and textural attributes, it can be concluded that deposition of these sediments commenced in fluvial, alluvial fan setting and culminated in a marginal marine (inter to supra-tidal flat) environment. The transitional relationship of upper quartz arenite of Banganapalle Formation and overlying calcareous Narji Formation suggests shift from intertidal to supratidal regime where the detrital material became scarce and chemical milieu became suitable for carbonate precipitates. The porous and permeable lithounits viz., quartz arenite and conglomerate with available reductants in the form of sulphides and carbonaceous matter are the best suited loci for uranium mineralization.

## Acknowledgement

Authors are thankful to Director, Atomic Minerals Directorate for Exploration and Research (AMD) for kind permission to publish this paper.

## References

- Banerjee, Rahul, Bahukhandi, N.K., Rahman, M., Ramesh Babu, P.V., Umameswar. K. and Parihar, P.S. (2012). Lithostratigraphic and Radiometric Appraisal of deeper

- parts of Srisailam and Palnad Sub-basins in Kottapullareddipuram, Achchammagunta and Rachchamallepadu areas, Guntur district, Andhra Pradesh. *EARFAM*, v. 22, pp. 55-69.
- Barkat Rasikh, Chakraborty, Partha Pratim, Saha Subhojit and Das Kaushik (2020). Alluvial architecture, paleohydrology and provenance tracking from the Neoproterozoic Banganapalle formation, Kurnool Group, India: An example of continental sedimentation before land plants. *Precamb. Res.* v. 350, pp. 1-27. DOI: <https://doi.org/10.1016/j.precamres.2020.105930>
- Collinson, J.D., Mountney, N. and Thompson, D.B. (2006). *Sedimentary structures* (3rd Edition). Terra publishing, London, 292p.
- Gupta, Shekhar, Vimal, Rajiv, Banerjee, Rahul, Ramesh Babu, P.V. and Maithani, P.B. (2010). Sedimentation pattern and Depositional Environment of Banganapalle Formation in South Western Part of Palnad Sub-Basin, Guntur District, Andhra Pradesh. *Gond. Geol. Magz.*, spl. v.12, pp. 59-70.
- Gupta, Shekhar, Banerjee, Rahul, Ramesh Babu, P.V., Parihar, P.S. and Maithani, P.B. (2012). Geochemistry of Uraniferous Banganapalle Sediments in the Western Part of Palnad Sub-basin, Andhra Pradesh: Implications on Provenance and Paleo-weathering. *Gond. Geol. Magz.*, spl. v.13, pp. 1-14.
- Gupta Shekhar, Rajiv Vimal, Banerjee, R., Mary K. Kumar and Nayak, S. (2016). *Petromineralogy and Geochemistry of Uraniferous Banganapalle Quartzite around Chenchu Colony Area, Guntur District, Andhra Pradesh, India.* *Sp.Publ.Geol.Soc.Ind.*, v.4, pp. 23-37. DOI: 10.17491/cgsi/2016/95892
- GSI (1981). Explanatory brochure on Geological and Mineral Map of Cuddapah Basin (1:250000), pp. 1–21.
- GSI (2001). Geological and Mineral Map of Andhra Pradesh (1:500000). *Geol. Surv. India*, Hyderabad.
- Jeyagopal, A.V., Kumar, P. and Sinha, R.M. (1996). Uranium mineralization in the Palnad sub-basin, Cuddapah Basin, Andhra Pradesh, India. *Curr. Sci.*, v.71(2), pp.957–959.
- Jeyagopal, A.V., Umamaheswar, K. and Maithani, P.B. (2008). Sulphur Isotope studies on pyrite associated with the Koppunuru Uranium Deposit, Palnad sub-basin of Cuddapah basin, Guntur district, Andhra Pradesh. National Symposium “Significant Milestones in the growth of geochemistry in India during the 50 year period: 1958–2008”, Hyderabad, India, Abstract, pp. 31–32.
- Jeyagopal, A.V., Deshpande, M.S.M., Gupta, Shekhar, Ramesh Babu, P.V., Umamaheswar, K. and Maithani, P.B. (2011). Uranium mineralization and association of carbonaceous matter in Koppunuru Area, Palnad sub-basin, Cuddapah basin, Andhra Pradesh. *Ind. Mineral.*, v. 45(1), pp. 100–111.
- Latha, A., Umamaheswar, K., Gupta, Shekhar and Maithani, P.B. (2009). Presence of Coffinite and its implications at Koppunuru, Guntur District, Andhra Pradesh. National Symposium “Advances in Atomic Mineral Science in India during the 50 year period: 1959–2009”, Hyderabad, India, Abstract, pp. 96.
- Latha, A., Gupta, Shekhar, Umamaheswar, K. and Maithani, P. B. (2011) Pebbly Arenite Hosted Uranium Mineralization at Koppunuru, Guntur District, Andhra Pradesh – A Petrographic Introspection. *EARFAM*, v. 21, pp. 117-112.
- Lakshminarayana, G., Bhattacharjee, S. and Kumar, A. (1999). Palaeocurrents and depositional setting in the Banganapalle Formation, Kurnool sub-basin, Cuddapah basin, Andhra Pradesh. *Jour. Geol. Soc. India*, v. 53(2), pp. 255–259.
- Leeder, M. (1999). *Sedimentology and sedimentary basins: from turbulence to tectonics.* Blackwell Science Ltd., Oxford, 592p.
- Lowe, D.R. (1976). Subaqueous liquefied and fluidized sediment flows and their deposits. *Sedimentology*, v. 23, pp. 285–308.
- Miall, A.D. (1985) *Architectural-Element Analysis: A New Method of Facies Analysis Applied to Fluvial Deposits.* *Earth Sc. Rev.*, v.22, pp. 261-308.
- Nagaraja Rao, B.K., Rajurkar, S.T., Ramalinga Swamy, G and Ravindar Babu, B (1987). Stratigraphy, structure and evolution of the Cuddapah Basin. *Mem. Geol. Soc. India*, no.6, pp. 33–86.
- Nageswara Rao, P., Anjan Som, Perumal, T., Maithani, P.B., Saxena, V.P. and Sinha, R.M. (2005). Proterozoic unconformity related uranium occurrence around Rallavagu Tanda, Palnadu sub-basin, Andhra Pradesh. *Jour. Geol. Soc. India*, v.66, pp. 11–14.
- Nichols, G. (2009). *Sedimentology and stratigraphy* (2nd Edition). Wiley–Blackwell, U.K., 432p.
- Ramakrishnan, M. and Vaidyanadhan, R. (2008). *Geology of India* (Vol. 1). *Geol. Soc. India*, 556p.
- Ramesh Babu, P.V., Banerjee, R. and Achar, K.K. (2012). Srisailam and Palnad Sub-Basin: Potential Geological domains for Unconformity related Uranium mineralisation in India. *EARFAM*, v. 22, pp. 21-42.
- Roy, A.K., Saha, A., Singh, R.P. and Sinha, R.M. (2000). Application of soil radon and trace element geochemistry for uranium exploration of Kuchanapalle Uranium occurrence, Guntur district, A.P. (India). *Jour. Geol. Soc. India*, v. 56, pp. 89–96.
- Saha, D. and Chakraborty, S. (2003). Deformation pattern in the Kurnool and Nallamalai Groups in the northeastern part (Palnad area) of the Cuddapah basin, south India and its implication on Rodinia/Gondwana tectonics. *Gondwana Res.*, v. 6(4), pp. 573–583.
- Saula, E., Mato, E., Puigdefabregas, C., 2002. Catastrophic debris flow deposits from an inferred landslide-dam failure, the Eocene Berga Formation, eastern Pyrenees, Spain. In: Baker, V., Martini, I.P., Garzon, G. (Eds.), *Floods and Mega-floods Processes and Deposits.* International Association of Sedimentologists, Oxford, Special Publication 32, p. 195–209.
- Shobhita, K., Latha, A., Gupta, Shekhar, Banerjee, Rahul, Shivkumar, K. and Ramesh Babu, P.V. (2014). Petromineralogical studies of uranium mineralization in basement granites, Koppunuru, Guntur dist, A.P, India. *Ind. Mineral.*, v. 48(1), pp. 1–9.
- Singh, R.V., Sinha, R.M., Bisht, B.S. and Banerjee, D.C. (2002). Hydrogeochemical exploration for unconformity-related uranium mineralization: example from Palnad sub-basin, Cuddapah basin, Andhra Pradesh, India. *Jour. Geochem. Expl.*, v. 76, pp. 71–92.
- Sinha, R.M., Parthasarathy, T.N. and Dwivedy, K.K. (1996). On the possibility of identifying low cost, medium grade uranium deposits close to the Proterozoic unconformity in the Cuddapah basin, Andhra Pradesh, India. *IAEA–TECDOC–868*, pp. 35–55.
- Sinha, R.M., Srivastava, V.K., Sarma, G.V.G. and Parthasarthy, T.N.(1995). Geological favourability for unconformity related uranium deposits in the northern parts of the Cuddapah Basin: evidences from Lambapur uranium occurrences, Andhra Pradesh, Expl. Res. *Atomic. Miner.*, v.8, pp. 111–126.

- Sivaji, K. and Rao, K.R.P. (1989). Sedimentological studies of Banganapalle Conglomerate in connection with the assessment of diamond resources. *Rec. Geol. Surv. India*, v. 122(5), pp. 51–54.
- Sohn, Y.K., Rhee, C.W., Kim, B.C., 1999. Debris flow and hyperconcentrated flood flow deposits in an alluvial fan, northwestern part of the Cretaceous Yongdong Basin, Central Korea. *J. Geol.* 107, 111–132.
- Thomas, P.K., Thomas, T., Thomas, J., Pandian, M.S., Banerjee, Rahul, Ramesh Babu, P.V., Gupta, Shekhar and Vimal, Rajiv (2014). Role of hydrothermal activity in uranium mineralisation in Palnad Sub-basin, Cuddapah Basin, India. *Jour. Asian Earth Sci.*, v. 89, pp. 280-288 DOI: 10.1016/j.jseas.2014.02.013.
- Tucker, M.E. (2003). *Sedimentary rocks in the field* (3rd Edition). John Wiley & sons Ltd., U.S.A, 234 p.
- Verma, M.B., Gupta, Shekhar, Singh, R.V., Latha, A., Maithani, P.B. and Chaki, Anjan (2011). Ore body characterization of Koppunuru uranium deposit in Palnad sub-basin, Guntur district, Andhra Pradesh. *Ind. Mineral.*, v. 45(1), pp. 51–61.
- Vijayam, B.E. and Reddy, P.H. (1976). Tectonic framework of sedimentation in the western part of the Palnad basin, Andhra Pradesh. *Jour. Geol. Soc. India*, v. 17, pp. 439–448.

*(Received: 2 July 2020; Revised version accepted: 3 May 2021)*

## Investigation on Suitability of Argillaceous Rocks of Vindhyan Supergroup as Host Rock for Deep Geological Repository using Thermal Analysis

T. K. Pal^{1,*}, R. K. Bajpai¹, A. Acharya¹, R. S. Bhatia¹ and D. Datta²

¹Technology Development Division

²Radiological Physics and Advisory Division  
BARC, Mumbai-400085, India

*Email: [tkpal@barc.gov.in](mailto:tkpal@barc.gov.in)

### Abstract

Argillaceous rocks are being considered as a potential host rock for deep geological repository (DGR) for hosting vitrified high level radioactive waste canisters by many countries worldwide. Numerical simulation of thermal evolution in the repository environment is an important study for the long term safety performance assessment of a DGR. In this study, thermal dissipation in the near field area of a conceptual repository in Ganurgarh shales from Bhandar Group of Vindhyan Super Group, which is the thickest sedimentary succession of India, has been simulated using commercial software FLAC3D, which solves the governing heat diffusion equation using explicit and implicit finite difference methods. Model parameters like thermal conductivity, specific heat, density of the shales are generated in the laboratory. From the analysis of time dependent temperature profile it is observed that maximum temperature of 70.5°C is attained at canister surface after 22 years of heating for a heat loadings of 500 W/overpack. Since the maximum temperature is well below the permissible limit of temperature (100°C), the heat load of the source is increased to 700 W/overpack and in this case the simulated value of maximum temperature is 93°C. Maximum temperatures at other locations within the near field region are also within the permissible limit.

**Keywords:** *Argillaceous rock, Vindhyan Supergroup, deep geological repository, host rock, thermal analysis*

### Introduction

There is an international consensus that disposal of highly-active and/or long-lived radioactive waste generated during the various stages of nuclear fuel cycle in DGR is the most practical option available for long-term isolation of these radioactive materials from the biosphere. In India, vitrified products of high level radioactive waste in the form of canisters/ overpacks are being stored in engineered storage facilities and after a cooling period of about 30 years they are supposed to be disposed of in a suitable geological formation so called DGR at a depth of about 500-700m below the ground surface (Narayan et al., 2007). Countries across the world are working on various type of host rock, such as granite, basalt, argillite, tuff, etc., for assessing their suitability for DGR (Bajpai, 2004). Each rock type has its advantages and disadvantages when considered from the point of constructional, operational and post closure radiological safety aspects required for a DGR facility. In India, the choice of host rock is restricted largely to granite formations due to their very vast occurrence throughout the country and adequate thermo, mechanical and hydrological characteristics (Mathur et al., 1996).

Countries like France, Belgium, Switzerland are actively involved in assessing suitability of argillaceous/clay type rock formations for DGR (Kickmaier et al., 1997, Jacques et al., 2014). Though the strength of argillaceous rock is not as good as that of granite rock, low water permeability and high sorption capacity due to presence of clay minerals are two desirable features of this rock type make that it as a potential host rock for DGR. Since India also has a good coverage of sedimentary rock type, work on various argillaceous/clay type rock formation is taken up for assessing its suitability for hosting DGR (Bajpai, 2018). Claystones, mudstones, marls and shales, which belong to argillaceous rock types, have been identified as potential host rock for DGR. The sedimentary succession of the Vindhyan Supergroup is one of the thickest sedimentary successions in the world. In this study, the Ganurgarh shales from Bhandar Group are considered as host rock formation for a conceptual repository. Very good thermal conductivity of this rock is a favorable characteristic for smooth dissipation of heat. Numerical simulation of dissipation of heat generated by waste filled canisters

emplaced in DGR is an important study for the long term safety performance assessment of a DGR specially because design constrain posed by maximum allowable temperature of 100°C throughout the evolution of the facility to avoid water vaporization and resultant pressure build up which may eventually lead to release of radioactivity and its enhanced migration into geosphere. In order to achieve better radiological safety of a DGR by containing and isolating the radionuclides from the surface environment for a very long period, a multi-barrier design concept, where the disposed canisters are surrounded by clay barriers in disposal pit, is adopted worldwide (Narayan et al., 2007). Various authors have carried out numerical simulation of thermal conduction in such disposal mode (Goel et al., 2003, Zhao et al., 2014, Maheshwar et al., 2015a,b, Pal et al., 2016, 2019). Since the host rock considered in

loading of the source can be increased for the same design parameter, such as spacing between two disposal pits and two disposal tunnels while keeping the maximum temperature at any location of the of DGR within allowable temperature limit (100°C). Accordingly, the thermal heat source in this study is increased from the standard value for Indian scenario (500 W/overpack) to 700 W/overpack.

The simulation study is carried out using commercial software FLAC3D (Fast Lagrangian Analysis of Continua) which solves the governing heat diffusion equation using explicit and implicit finite difference methods. The rest of the paper is organized as follows.

### Mathematical Model and Numerical Framework

In general, heat transport through porous media occurs through conduction and convection processes. However, in low water permeable porous media, such as argillaceous rocks, convection can be neglected (Hokmark et al., 2003, Mathur et al., 1998). The general 3-Dimensional heat conduction equation in a homogeneous and isotropic medium is written as

$$\frac{\partial T(x,y,z,t)}{\partial t} = D \left( \frac{\partial^2 T(x,y,z,t)}{\partial x^2} + \frac{\partial^2 T(x,y,z,t)}{\partial y^2} + \frac{\partial^2 T(x,y,z,t)}{\partial z^2} \right) \dots (1)$$

where  $T(x,y,z,t)$  is the temperature at a location  $(x,y,z)$  at time  $(t)$ ,  $D = \frac{k}{\rho c}$  is thermal diffusion coefficient,  $k$  is thermal conductivity,  $\rho$  is material density and  $C$  represents specific heat of the material.

Ganurgarh rock samples were collected as per IS-9179-1979 (1979) in the form of rough blocks and marked to represent their position and orientation with respect to the parent rock mass. The samples were collected from upper Bhandar Group of Vindhyan Super Group from the town Damoh in the Sagar Division of north-eastern Madhya Pradesh. Geologically, two types of rocks, Rewa and Upper Bhandar groups of Vindhyan Super Group, are present in Damoh. There are thick successions of greyish-brownish coloured Ganurgarh shales with overlaid sandstones. Intense weathering in these shales has lead them to convert into clays. Shale samples were collected in medium to large lumps and cylindrical samples were prepared in accordance with the orientation and position of parent rock mass (Verma et al., 2016). The thermal properties  $k$ ,  $C$  and physical property  $\rho$  of rock were measured at the laboratory. The experimentally measured thermal and physical properties of Ganurgarh shales used in this study are given in Table 1 (Verma et al., 2016). Temperature dependent values of the parameters are not considered in our model.

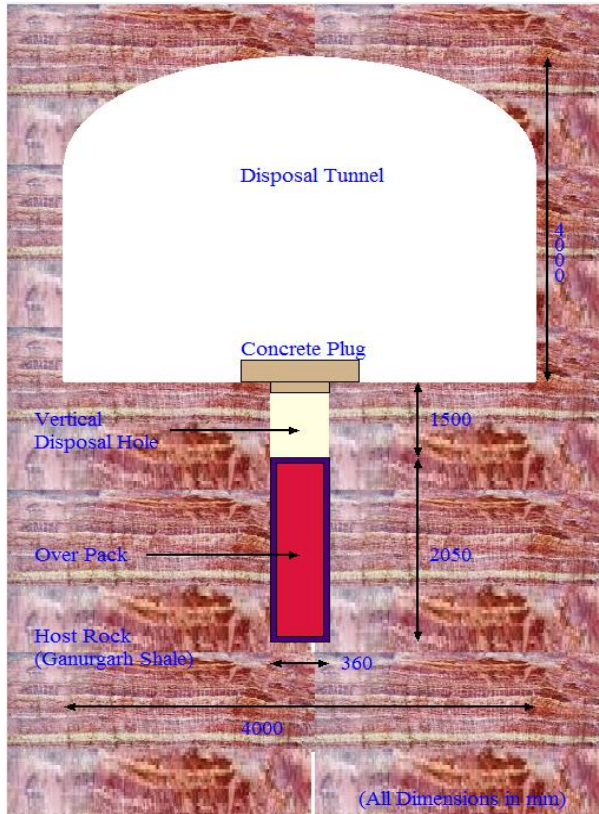


Fig 1. Schematic view of vertical disposal pit in shale rock

this study is argillaceous type, the thermal properties of the clay barrier such as thermal conductivity, specific heat are taken same as that of the host rock. So, the model geometry considered in this study, as schematically shown in Fig 1, does not consider clay barrier as a separate engineered barrier. The objective of the study is to see whether excluding the clay barrier, which has lower thermal conductivity than the host rock, heat

Table 1: Thermal and physical properties of the Ganugarh shales

Property	Value
Thermal conductivity (W/m/K)	3.36
Specific heat (W/Kg/K)	850.0
Density(Kg/m ³ )	2431.25

The radioactive waste disposal system considered in this study comprises a 2.05m long and 0.36m diameter overpack, containing heat emitting waste loaded SS canisters, emplaced in a 3.55m deep pit in Ganurgarh shale. As discussed in the introduction section, the concept of clay barrier surrounding the disposal pit is not taken as a separate engineered barrier. The separation between two disposal pits is 2.5m and spacing between two disposal tunnels is taken as 12m. These values of spacing between the two disposal pits and two disposal tunnels are kept same as used for granite host rock (Pal et al., 2016). The disposal facility with capacity to accommodate few thousands such canisters is normally located in the depth range of 500-700m depth in suitable sites. A quarter symmetry of the model geometry, comprising of one disposal pit and horseshoe shape disposal tunnel section of 4m × 4m, as shown in Figure 2, was created using FLAC3D software and was used for this study. The finite difference solver of FLAC3D is used to simulate the heat diffusion process governed by Eq. (1). Volumetric source term model is utilized to model the decaying heat source of the overpack.

## Results and Discussion

A geothermal gradient of 0.024°C/m was considered to calculate initial temperature of the shale at 500m depth. Considering temperature at the surface of earth as 35°C, the temperature at DGR depth is 47°C. No flux boundary condition is applied at all the symmetry planes (two XZ and two YZ planes) and constant temperature boundary condition was applied at the top and bottom surfaces. The value of the constant temperature at the top surface was 35°C and at 450m below DGR depth temperature was fixed at 57.8°C. The thermal flux of the source is modelled as an exponentially decaying term and is mathematically represented as

$$P(t) = P_0 \exp(-\lambda t)$$

where P(t) is thermal flux of each overpack at time t, P₀ is thermal flux of each overpack at the time of emplacement in disposal pit, λ is a constant parameter and its value is derived from the radiological properties such as half lives, isotopic compositions, Q values of the radionuclides present in the waste material. In this

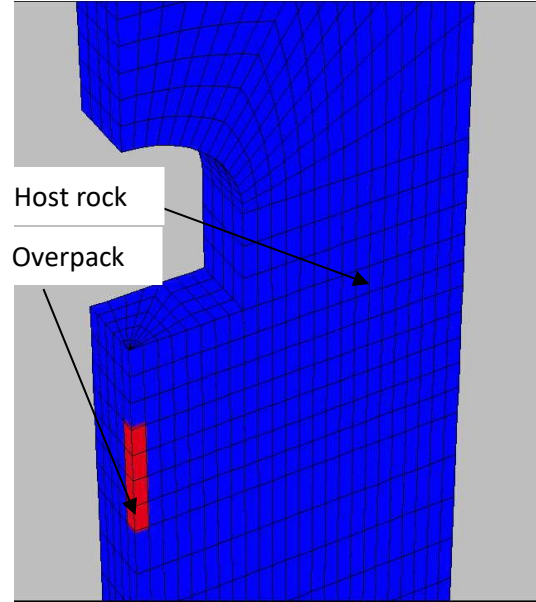


Fig. 2: FDM mesh for quarter symmetry model for near field study

study the value of λ is  $-7.32496 \times 10^{-10}/s$ , which is a standard value used for Indian scenario. Two simulation studies were carried out with different values of initial thermal source term.

### Case 1

In this case, the standard value of initial heat load of the Indian overpacks (500 W/overpack) was considered. The process was simulated for various heating periods of 1, 5 10, 20, 50 and 200 years. Results of the simulation in the form of contour plots of temperature are shown in Figs: 3.1-3.6. In order to find out maximum temperature and time required to attain that temperature, time dependent profile of temperature at various locations (canister surface, 1m, 2m, 3m, 4m, 5m and 6m away from the central canister's in a horizontal plane passing through the middle of canister's height) are plotted in Fig 3.7.

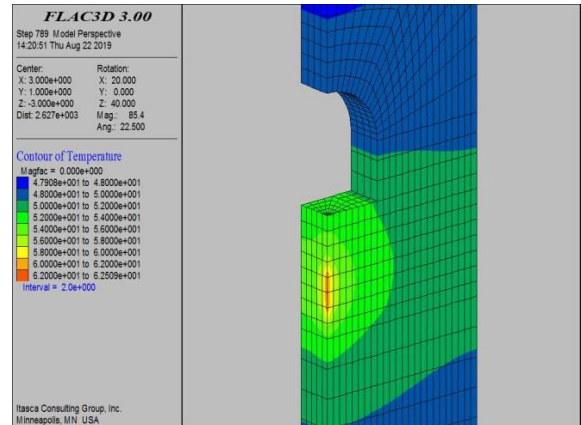


Fig 3.1. Temperature (°C) contour after 1 years of heating

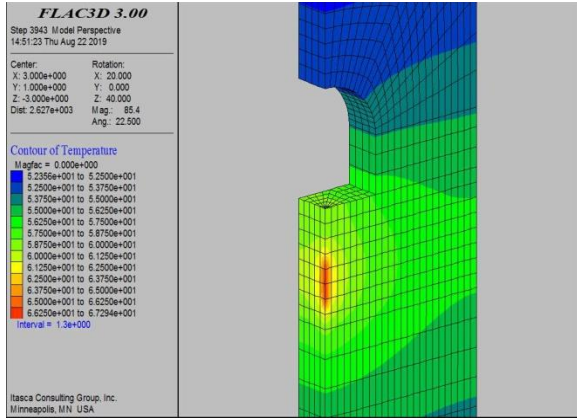


Fig 3.2. Temperature (°C) contour after 5 years of heating

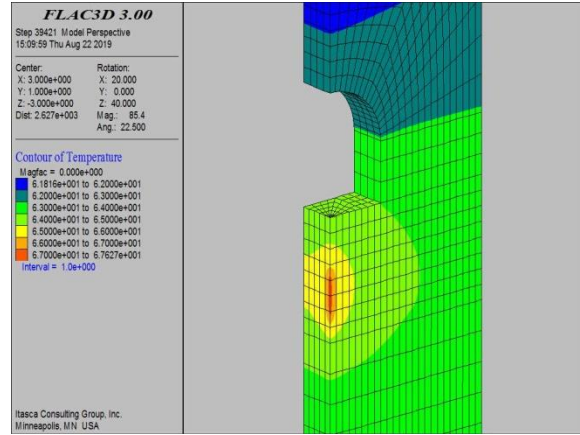


Fig 3.5. Temperature (°C) contour after 50 years of heating

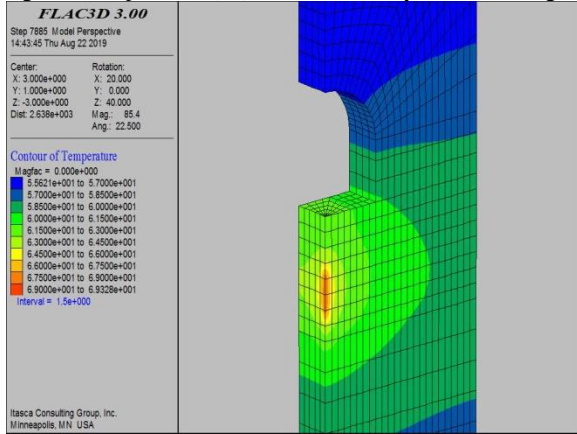


Fig 3.3. Temperature (°C) contour after 10 years of heating

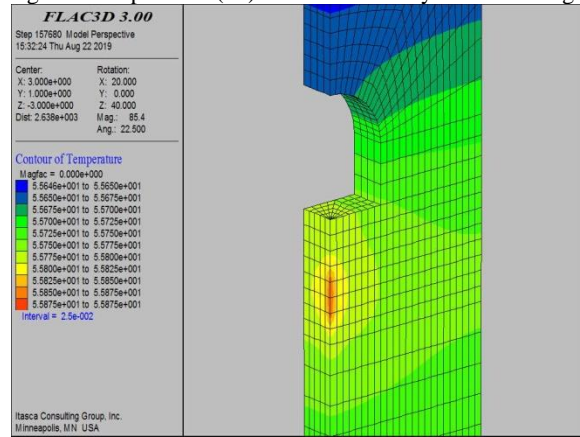


Fig 3.6. Temperature (°C) contour after 200 years of heating

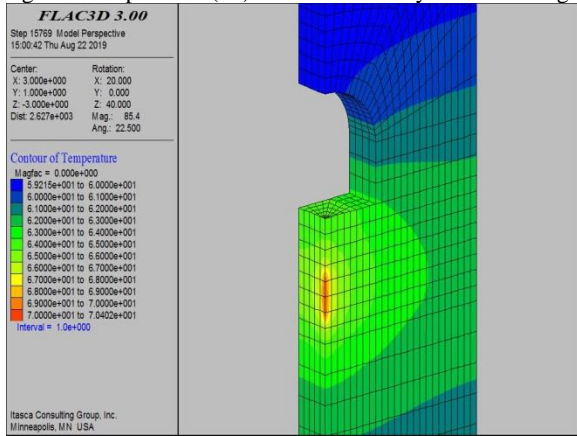


Fig 3.4. Temperature (°C) contour after 20 years of heating

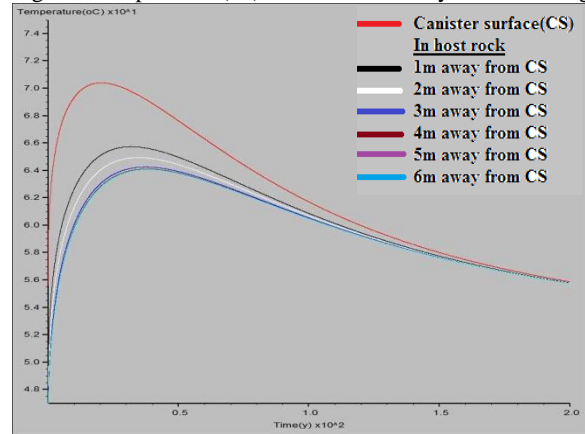


Fig 3.7. Time history of temperature at different locations in the repository.

## Case 2

In this case, the initial heat load of the overpack is increased to 700 W/overpack. This higher heat load value could represent the overpacks with a lower cooling period before disposal in DGR and/or overpacks having higher waste loading factor. Similar

to Case 1, this process is simulated for heating periods of 1, 5 10, 20, 50 and 200 years. Results of this simulation study in the form of contour plots of temperature are shown in Figs: 4.1-4.6 and time dependent temperature profiles are plotted in Fig 4.7

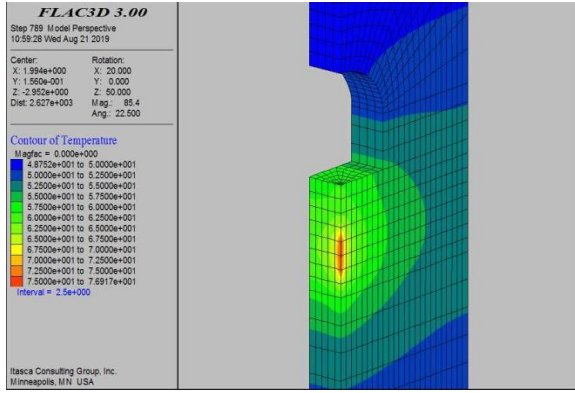


Fig 4.1. Temperature (°C) contour after 1 year of heating

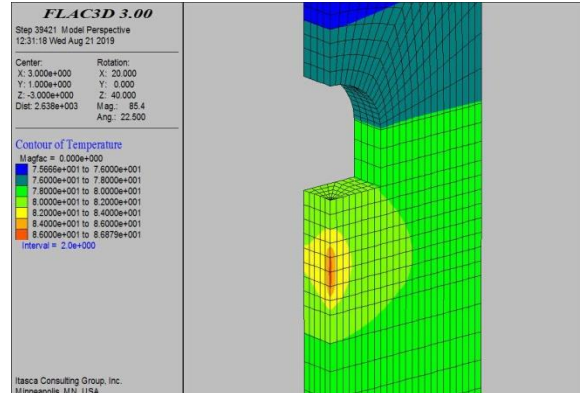


Fig 4.5. Temperature (°C) contour after 50 years of heating

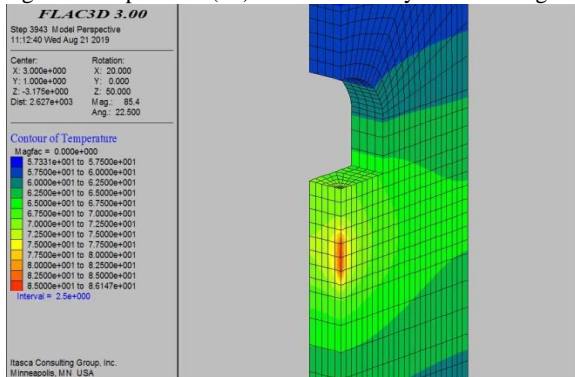


Fig 4.2. Temperature (°C) contour after 5 years of heating

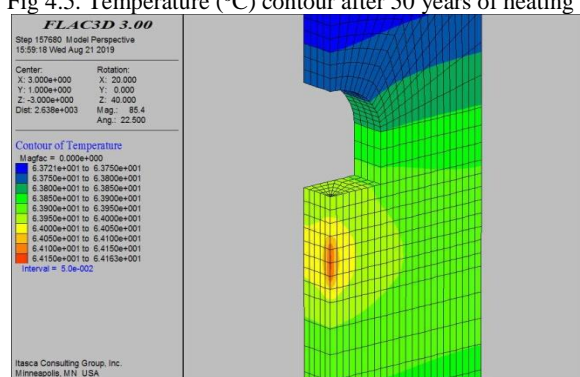


Fig 4.6. Temperature (°C) contour after 200 years of heating

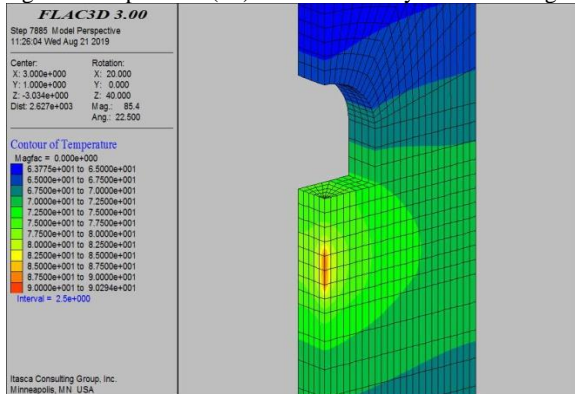


Fig 4.3. Temperature (°C) contour after 10 years of heating

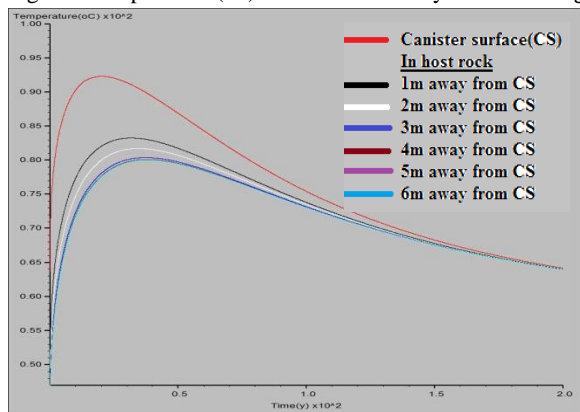


Fig 4.7. Time history of temperature at different locations in the repository

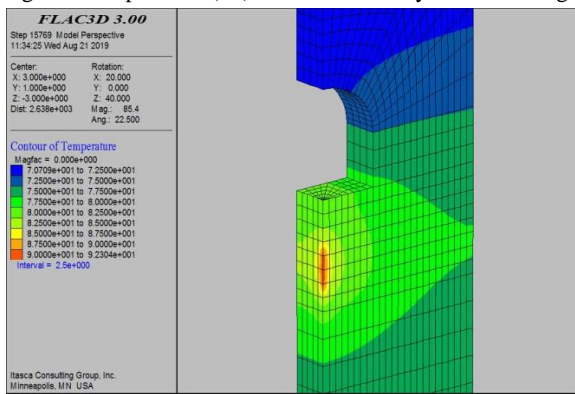


Fig 4.4. Temperature (°C) contour after 20 years of heating

From Fig 3.1 and 4.1 it can be observed that maximum temperature of 62.5°C and 76.92°C are observed at canister surface after 1 year of heating. From the other contour plots, it can be found that an increase in temperature is observed up to 20 years of heating and, for 50 and 200 years of heating, decrease in temperature is observed. The time dependent plots of temperature, as shown in Fig 3.7 and 4.7, indicate that maximum temperature of 70.5°C and 93°C are attained at canister surface after 22 years of heating for the first and second source, respectively. Maximum temperature

at other locations in the shales are observed with a slightly larger heating time periods and their values are also less than that observed at canister surface.

At a given temperature and pressure, thermal conductivity of a rock is highly dependent upon types of minerals composition and its micro and macro structural details, such as shape and size of the minerals, porosity, tortuosity, water saturation, etc. The thermal conductivity of Ganurgarh shales considered in this study is greater than other type of host rock and clay material used for such studies in India. For example, the thermal conductivities of the granite host rock and bentonite buffer used by Dutt et al. (2012) are 2.523 W/m/K and 1.47 W/m/K, respectively. The values are 2.30 W/m/K and 1.65 W/m/K as reported by Maheshwar et al. (2015b) for their studied granite host rock collected from near to Bhima basin of peninsular India. The higher thermal conductivity of the Ganurgarh shales than that of bentonite buffer material could be because of lower porosity of the shales compared to the bentonite materials reported in the above mentioned studies and for other properties which require further investigations. Bentonite buffer has less thermal conductivity than the host rock, so temperature build up occurs at the interface of canister and clay. But, since the rock studied here is argillaceous type, the concept of clay layer is not taken separately. This concept along with good thermal conductivity of the shales ensures smooth dissipation of heat in the near field of the repository.

## Conclusions

Temperature field at various locations in the near field of a conceptual DGR in Ganurgarh shales of Vindhyan Super Group for different time periods of heating were calculated for two different thermal sources and the resulting temperature contour plots show that maximum temperature at any location within the near field of the DGR is below 100°C, which is the maximum permissible limit of temperature. The results also indicate that initial heat flux of the overpack is an important parameter for the design of a DGR in terms of spacing between disposal pits and tunnels. The time dependent plots of temperature at various locations of the DGR show that maximum temperature of 70.5°C and 93°C are attained at canister surface after 22 years of heating for the two sources, respectively. These plots are important for estimating time period of thermal evolution of a DGR system. It can, therefore, be concluded from this thermal analysis that the studied Ganurgarh shales possess adequate thermal characteristics to ensure smooth dissipation of heat across the waste in the near field areas. Finally, it is worth to mention here that feasibility of the site for radioactive waste disposal can never be ascertained by doing thermal analysis only. Systematic steps for site

selection for DRG as recommended by international bodies, such as International Atomic Energy Agency (IAEA), Nuclear Energy Agency (NEA), World Health Organization (WHO) are needed to be followed before recommending any site for DGR. Nevertheless, the results of this thermal study show that the studied Ganurgarh shales can accommodate higher thermal load compared to the granite rocks studied in the Indian context. Therefore, from thermal point of view this type of rock having good thermal conductivity is more suitable than the granite rocks reported in Indian repository programme.

## References

- Raj, K., Prasad, K.K., Bansal and N.K. (2006). Radioactive waste management practices in India. *Nuclear Engineering and Design*, 236 (7–8), 914–930.
- Sengupta, P., Kaushik, C.P. and Dey, G.K. (2012). Immobilization of high-level nuclear wastes: the Indian scenario. In: Mu. Ramkumar (Ed.), *On the Sustenance of Earth's Resources*, Springer-Verlag.
- Narayan, P.K. and Bajpai, R.K. (2007). Deep Geological Repositories for Vitrified High Level Long Lived Wastes, *IANCAS Bulletin*, VI (3), 224–237.
- Bajpai, R.K. (2004). Recent Advances in the Geological Disposal of nuclear-Wastes Worldwide and Indian Scenario, *Jour. Geol. Soc. Ind.*, 63(3), 354–356.
- Mathur, R.K., Narayan, P.K. and Prasad A.N. (1996) Status of siting and host rock characterization programme for a geological repository in India, In *geological problems in Radioactive Waste Isolation, Second Worldwide Review*, P.A. Witherspoon, ed., LBNL-38915, Lawrence Berkley National Laboratory, Berkley, California, 125–131.
- Kickmaier, W. and McKinley, I. (1997) A review of research carried out in European rock laboratories. *Nuclear Engineering and Design*, 176, 75–81.
- Jacques Delay, Paul Bossart, Li Xiang Ling, Ingo Blechschmidt, Mats Ohlsson, Agnès Vinsot, Christophe Nussbaum and Norbert Maes, (2014) *Three decades of underground research laboratories: what have we learned?* Geological Society, London, Special Publications, 400, 7–32.
- Bajpai, R.K. (2018). Progress in implementing Deep Geological Repository in India. *International Atomic Energy Agency Technical Meeting on Global Progress on Geological Disposal of Radioactive Waste*, GCNEP New Delhi, 22–26 May 2018, (2018)
- Hokmark, H. and Falth, B. (2003). Thermal dimensioning of the deep repository. SKB TR-03-09, Sweden
- Mathur, R.K., Rakesh, R.R. et al. (1998). In-situ Multiheater Thermo-mechanical Experiment in Mysore Mines, Kolar Gold Fields. Rep. No. BARC/1998/I/015.
- Goel, R.K., Prasad, V.V.R. et al., (2003). Testing of rock samples and site-specific design of underground research laboratory. technical report, Central Mining Research Institute, Roorkee, India, GC/MT/R/1/2000-01.
- Zhao, H.G., Shao, H., Kunz, H., Wang, J., Su, R. and Liu, Y. M. (2014). Numerical analysis of thermal process in the near field around vertical disposal of high-level

- radioactive waste. *Journal of Rock Mechanics and Geotechnical Engineering*, 6(1), 55-60.
- Maheshwar, S., Verma, A.K., Singh, T.N. and Bajpai, R.K. (2015a) A numerical study of the thermal interferences between two nuclear waste canisters in a granite hosted repository, *International Journal of Earth Sciences and Engineering*, 8(3), 1089-1098.
- Maheshwar, S., Verma, A.K., Singh, T.N. and Bajpai, R.K. (2015b). Study of thermo-hydro-mechanical processes at a potential site of an Indian nuclear waste repository. *Journal of Earth System Science*, 124(8), 1693-1708.
- Pal, T.K., Bajpai, R.K., et al., (2016). Numerical Simulation of Heat Dissipation across Smectite Clay Buffer and Granite Host Rock in Near Field around High Level Radioactive Waste Canisters. Proc. Sixth Annual Rock Conference Indorock 2016, IIT Bombay, June 17-18, 2016.
- Pal, T.K., Bajpai, R.K., et al., (2019). Numerical Simulation of Heat Dissipation in Host Rock using In-house Developed GUI Tool. Proc. of international seminar on Innovations and Challenges in Radioactive Waste Management and Disposal (ICRWMD-2019), January 11-12, 2019, BARC, Mumbai.
- IS: 9179–1979 (1979) Indian standard method for preparation of rock specimen for laboratory testing. Bureau of Indian Standards, New Delhi
- Verma, A.K., Jha, M.K., Maheshwar, S., Singh, T. N. and Bajpai, R. K. (2016). Temperature-dependent thermophysical properties of Ganurgarh shales from Bhandar group, India. *Environmental Earth Sciences*, 75(4), 300.
- Dutt, A., Saini, M. S., Singh, T. N., Verma, A. K. and Bajpai, R. K. (2012) Analysis of thermo-hydrologic-mechanical impact of repository for high-level radioactive waste in clay host formation: an Indian reference disposal system. *Environmental Earth Sciences* 66(8), 2327-2341.

*(Received: 22 February 2021; Revised version accepted: 1 May 2021)*



## ACKNOWLEDGEMENTS

The Editorial Board of the Journal Indian Association of Sedimentologists (JIAS) gratefully acknowledges the cooperation given by the Reviewers and Editors in the review process of the current issue of JIAS, Volume 38 (1).

- 
1. A H M Ahmad, Aligarh Muslim University, Aligarh
  2. Armstrong Altrin John S, National Autonomous University of Mexico, Mexico
  3. Erfan Mondal, Aligarh Muslim University Aligarh
  4. Ganapati Narayan Nayak, Goa University
  5. G. M. Bhat, Jammu University, Jammu
  6. Kasturi Bhattacharyya, Indian Institute of Technology, Kharagpur, West Bengal
  7. Mateen Hafiz, MAM College, Jammu
  8. Mrinalinee Devi, Tezpur, Jorhat
  9. Nileash P. Bhat (late), Baroda University, Vadodara
  10. Omar Cruz, Universidad Nacional Autónoma de México, Ciudad del Carmen, México
  11. Pramod T Hanamgond G. C. College, Belgaum, Karnataka
  12. Rajeev Saraswat, National Institute of Oceanography, Goa
  13. R. Nagendra, Anna University, Chennai
  14. Rajeeva Guhey, Government NPG College of science, Raipur, Chhattisgarh
  15. Santanu Banerjee, IIT Bombay, Mumbai
  16. Shabnum Choudhary, Ministry of Earth Sciences, New Delhi
  17. Shabber Habib Alvi, Aligarh Muslim University Aligarh
  18. Shamim Ahmed, Birbal Sahni Institute of Palaeobotany, Lucknow
  19. S. K. Pandita, Jammu University, Jammu
  20. Subir Sarkar, Jadavpur University, Kolkata
- 

MANAGING EDITORS  
JIAS